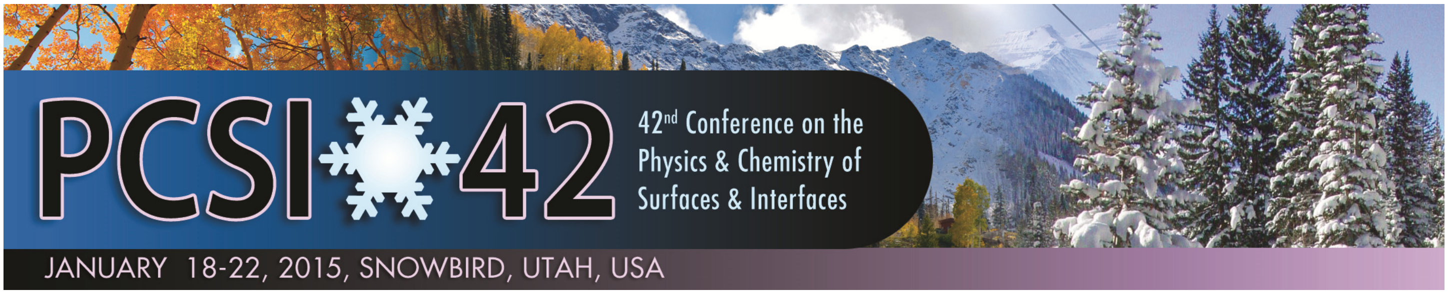

PCSI 42

42nd Conference on the Physics & Chemistry of Surfaces & Interfaces

JANUARY 18-22, 2015, SNOWBIRD, UTAH, USA

Abstract Book & Schedule

Gold Sponsor

SPECS™

Silver Sponsors

AMERICAN ELEMENTS	MANTIS MANTIS DEPOSITION INC
Kurt J. Lesker® Company	MDC Vacuum Products, LLC
OXFORD INSTRUMENTS *The Business of Science®*	STAIB INSTRUMENTS

UMC
UNITED MINERAL
& CHEMICAL CORP.

PCSI 42 General Information

Conference Hotel:

Snowbird Resort, Snowbird (Salt Lake City), Utah

Conference Website: www.pcsiconference.org

Chair:

Michael Flatté
Iowa State University
E-mail: michael_flatte@mailaps.org

General Chair:

Chris Palmstrøm
University of California, Santa Barbara
E-mail: cpalmstrom@ece.ucsb.edu

JVST Special Issue Editor:

Rudy Ludeke
E-mail: rudy_ludeke@msn.com

Registration:

Della Miller/Heather Korff
AVS, 110 Yellowstone Dr., Suite 120
Chico, CA 95973
E-mail: della@avs.org /heather@avs.org
Phone: 530-896-0477

Program Committee:

- Anand Bhattacharya, Argonne National Lab
- Leonard Brillson, The Ohio State University
- Alex Demkov, University of Texas, Austin
- Michael Flatté, University of Iowa
- Jessica Hilton, Mantis Deposition
- Harold Hwang, Stanford University
- Hisao Ishiii, Chiba University
- Karen Kavanagh, Simon Fraser University
- Roland Kawakami, University of California, Riverside
- William Lampert, Sustema Research LLC
- Lincoln Lauhon, Northwestern University
- Rudy Ludeke
- Chris McConville, Warwick University
- Anders Mikkelsen, Lund University
- Roberto Myers, Ohio State University
- Chris J. Palmstrøm, University of California, Santa Barbara
- Henning Riechert, Paul Drude Institute
- Jack Rowe
- Nitin Samarth, Penn State University
- Yuri Suzuki, Stanford University
- Alec Talin, Sandia National Labs
- Pani Varanasi, Army Research Office
- Jun Zhu, Penn State University

Presentation Formats:

Invited Talks—35 minute oral presentation, 5 minute discussion, plus poster
Upgraded Talks—17 minute oral presentation, 3 minute discussion, plus poster
Contributed Talks—4 minute oral presentation (max 3 slides, 1 minute discussion, plus poster)
Posters—Displayed all week (44 inches tall x 44 inches wide)

PCSI 42 Sponsors

Gold Sponsor
SPECS™

Silver Sponsors	
AMERICAN ELEMENTS	MANTIS MANTIS DEPOSITION INC
Kurt J. Lesker® Company	MDC Vacuum Products, LLC
OXFORD INSTRUMENTS *The Business of Science®*	STAIB INSTRUMENTS
UMC UNITED MINERAL & CHEMICAL CORP.	

NAP-XPS Solutions

NEAR AMBIENT PRESSURE IN SITU SURFACE ANALYSIS SYSTEMS

KEY FEATURES

- In Situ Analysis up to 100 mbar
- Backfilling or Reaction Cell
- PHOIBOS 150 NAP Electron Analyser
- NAP Laboratory X-ray and UV Sources
- Windowless Synchrotron Beam Entrance Stage

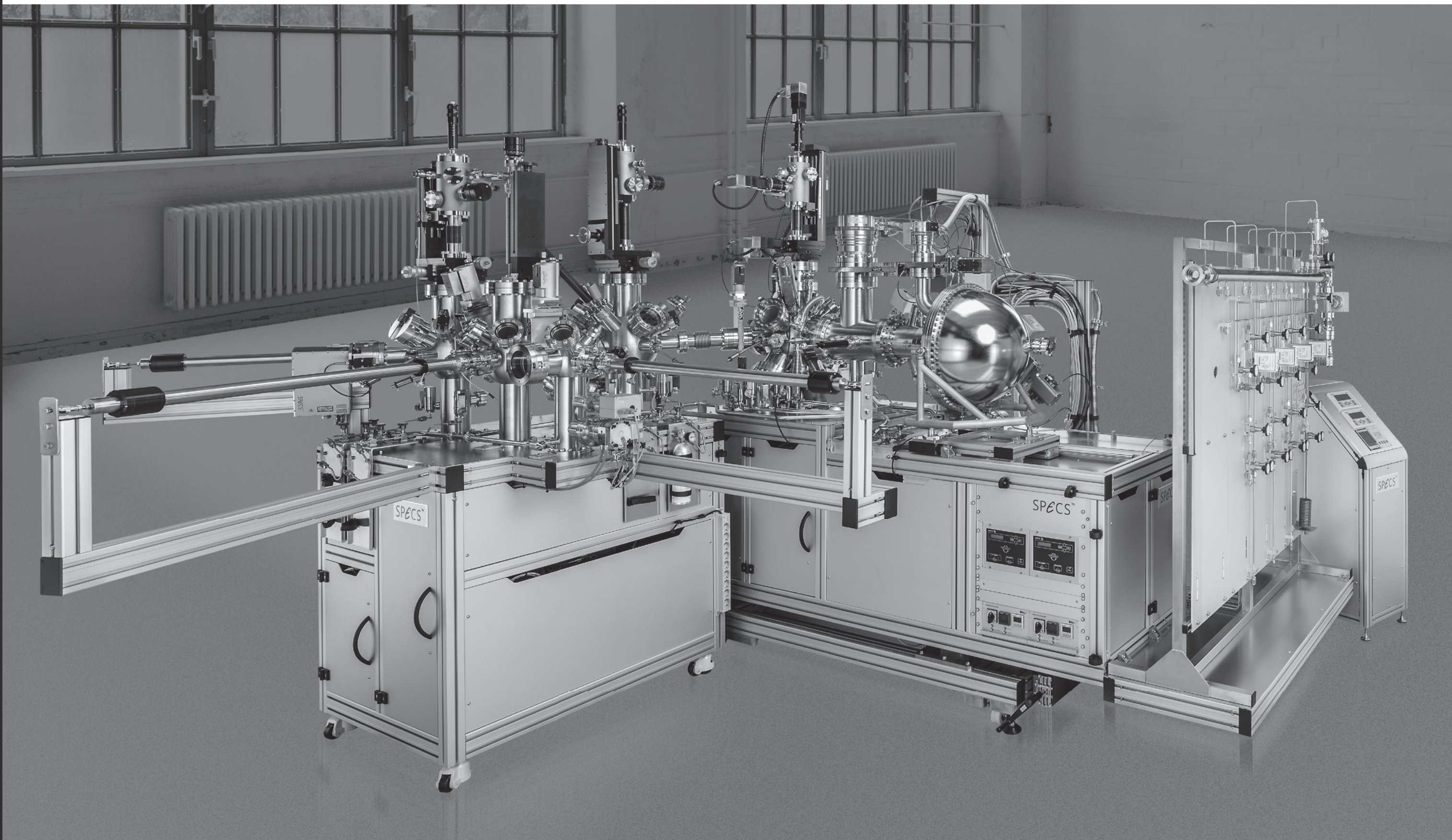

SPECS Surface Nano Analysis GmbH

T +49 30 46 78 24-0
E info@specs.com
H www.specs.com

SPECS™

strontium doped lanthanum III-IV nitride materials crystal growth nanofabri
organo-metallics regenerative medicine cerium polishing powder yttri
thin film dysprosium pellets atomic layer deposition scandium-aluminum
m materials aerospace ultra-light alloys iridium crucibles van m
solid green technology battery lithium gallium arsenide alt
zircon surface functionalized nanoparticles tantal
ite semiconductors palladium shot erme
catho anode
nucl iron
con liquid
galli

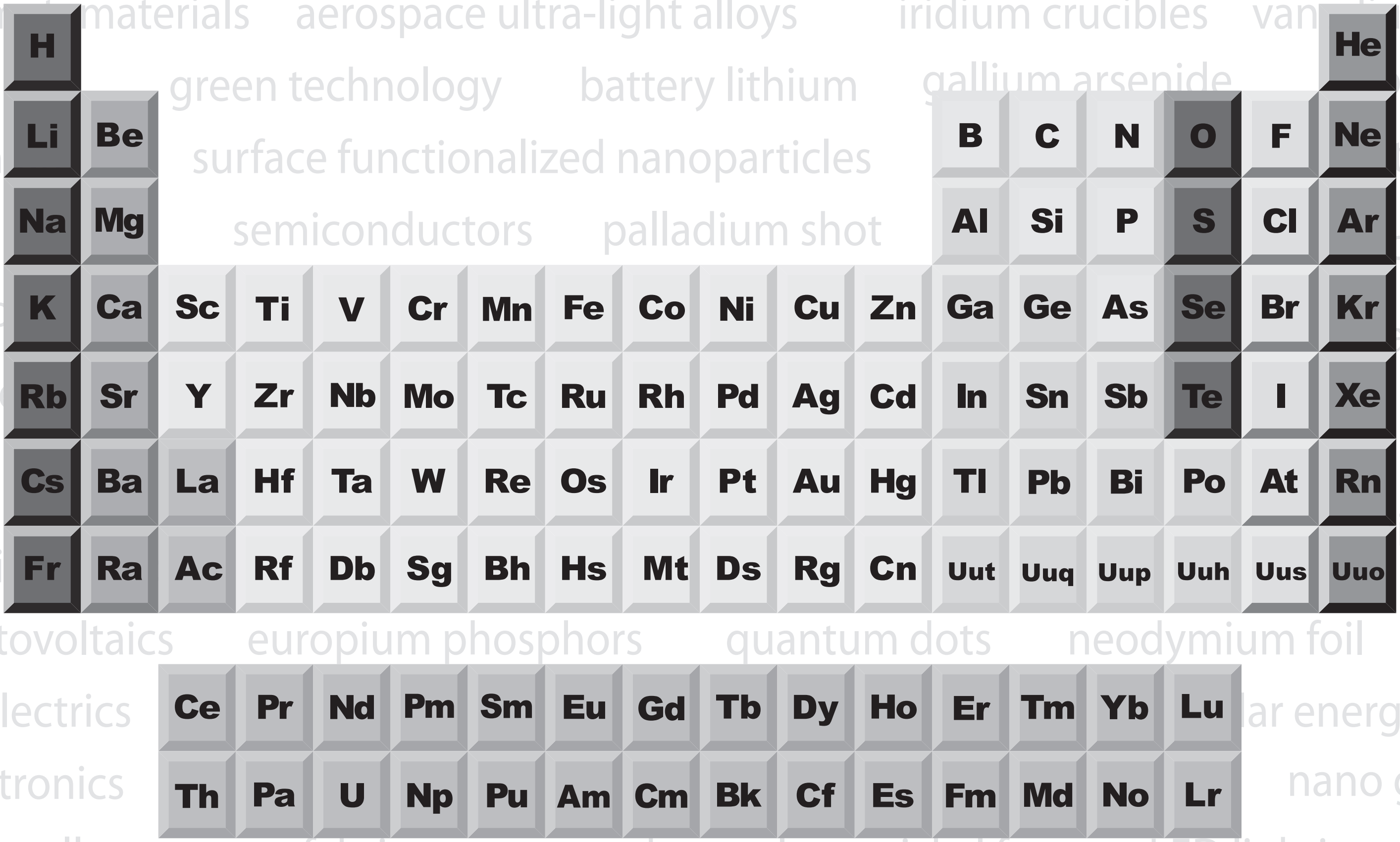

photovoltaics europium phosphors quantum dots neodymium foil ioni
dielectrics lar energy
spintronics nano gels
super alloys nanofabrics rare earth metals nickel foam LED lighting
rod platinum ink laser crystals titanium robotic parts tungsten carbide
CIGS stable isotopes carbon nanotubes gold nanoparticles optoelectro
optoelectroni mischmetal

Now Invent.™

es anti-ballistic ceramics fuel cell materials hafnium tubing Nd:YAG
biosynthetics germanium windows superconductors ultra high purity m
macromolecules 99.999% ruthenium spheres erbium doped fiber optics
sputtering targets gadolinium wire advanced polymers buckey balls
metalloids rhodium sponge shape memory alloys alternative energy
electrochemistry nanomedicine tellurium
te osmium

AMERICAN ELEMENTS
THE MATERIALS SCIENCE COMPANY®

catalog: americanelements.com

©2001-2014. American Elements is a U.S. Registered Trademark.

zirconium single crystal silicon diamond micropowder neodymium foil

PCSI 42 Schedule Overview

Sunday:

Su1400	Registration
Su1455	Welcome Remarks
Su1500	Sunday Afternoon Session: *Topological Insulators I*
Su1630	Poster Setup
Su1700	Welcome Reception
Su1930	Sunday Evening Session: *Epitaxial Oxide Heterostructures*

Monday:

Mo0745	Registration and Continental Breakfast
Mo0830	Monday Morning Session: *Semiconductors, Band Offsets, Dielectrics*
Mo1000	Coffee Break and Poster Viewing
Mo1100	Monday Morning Session: *Nanowires*
Mo1155	Lunch and Poster Viewing
Mo1400	Monday Afternoon Session: *Complex Oxides and Ferroelectrics I*
Mo1530	Coffee Break and Poster Viewing
Mo1630	Monday Afternoon Session: *2D Materials*
Mo1740	Monday Afternoon Session: *Late News*
Mo1800	Dinner
Mo1930	Monday Evening Session: *Energy Materials*

Tuesday:

Tu0745	Registration and Continental Breakfast
Tu0845	Tuesday Morning Session: *Characterization I*
Tu1000	Coffee Break and Poster Viewing
Tu1100	Tuesday Morning Session: *Characterization II*
Tu1150	Free Afternoon
Tu1930	Tuesday Evening Rump Session: *2D Materials and Heterostructures*

Wednesday:

We0745	Registration and Continental Breakfast
We0845	Wednesday Morning Session: *Complex Oxides and Ferroelectrics II*
We1005	Coffee Break and Poster Viewing
We1105	Wednesday Morning Session: *InAs Based Heterostructures*
We1155	Lunch and Poster Viewing
We1400	Wednesday Afternoon Session: *Novel Heterostructures*
We1510	Coffee Break and Poster Viewing
We1615	Wednesday Afternoon Session: *Graphene and Other 2D Materials*
We1800	Conference Banquet

Thursday:

Th0745	Continental Breakfast
Th0845	Thursday Morning Session: *Spintronics*
Th1000	Coffee Break and Poster Viewing
Th1045	Thursday Morning Session: *Topological Insulators II*
Th1130	Poster Viewing
Th1200	Conference Ends

PCSI 42 Schedule

Sunday Afternoon:				
Su1400	2:00 p.m.	Registration		
Su1455	2:55 p.m.	Welcome Remarks		
Topological Insulators I				Session Chair: N. Samarth
Su1500	3:00 p.m.	INVITED: Topological Insulators		Z.M. Hasan, Princeton Univ.
Su1540	3:40 p.m.	Surface and Electronic Structure of Half-Heusler PtLuSb (001) Thin-Films Grown by Molecular Beam Epitaxy		J.A. Logan, S.J. Patel, S.D. Harrington, J.K. Kawasaki, B.D. Schultz, Univ. of California, Santa Barbara; T. Balasubramanian, MAX IV Lab; A. Mikkelsen, Lund Univ.; C.J. Palmstrøm, Univ. of California, Santa Barbara
Su1545	3:45 p.m.	Epitaxial Growth and Electronic Structure of Half Heusler Co$_{1-x}$Ni$_x$TiSb		S.D. Harrington, J.A. Logan, S.J. Patel, J.K. Kawasaki, Univ. of California, Santa Barbara; T. Balasubramanian, A. Mikkelsen, Lund Univ.; C.J. Palmstrøm, Univ. of California, Santa Barbara
Su1550	3:50 p.m.	INVITED: Band Alignment of A$_{l2}$O$_3$/Ga$_2$O$_3$ Heterosturctures and their Application to Field-effect Transistors		M. Higashiwaki, T. Kamimura, National Institute of Information and Communications Technology, K. Sasaki, Tamura Corp. and National Institute of Information and Communications Technology; M.H. Wong, National Institute of Information and Communications Technology; A. Kuramata, S. Yamakoshi, Tamura Corp.
Su1630	4:30 p.m.	Poster Setup		
Su1700	5:00 p.m.	Welcome Reception		
Sunday Evening:				
Epitaxial Oxide Heterostructures				Session Chair: C. Leighton
Su1930	7:30 p.m.	INVITED: Transport Properties of Layered Perovskite Heterostructures: New Ideas and Insights from Theory and Simulation		N. Benedek, Univ. of Texas at Austin
Su2010	8:10 p.m.	INVITED: Room-Temperature Electronically Controlled Magnetism at the LaAlO$_3$/SrTiO$_3$ Interface		F. Bi, M. Huang, P. Irvin, J. Levy, Univ. of Pittsburgh; S. Ryu, H. Lee, C-W. Bark, C-B. Eom, Univ. of Wisconsin-Madison
Su2050	8:50 p.m.	Improvement of Characterization of Nonpolar M-plane ZnO on LiGaO$_2$ Substrate by Molecular Beam Epitaxy		C-Y. Lee, C. Chen, L. Chang, S-H. Yu, National Sun Yat-Sen Univ.
Su2055	8:55 p.m.	Epitaxial Growth and Optical Properties of (0002) Zn) Films on (001) LiGaO$_2$ Substrate by Chemical Vapor Deposition Method		C-Y. Lee, C. Chen, C-A. Li, M.M.C. Chou, S-H. Yu, National Sun Yat-Sen Univ.
Monday Morning:				
Mo0745	7:45 a.m.	Registration and Continental Breakfast		
Semiconductors, Band Offsets, Dielectrics				Session Chair: L. Brillson
Mo0830	8:30 a.m.	INVITED: Diffusion of Interstitial Defects in Semiconductors: The Case in CdTe		S-H. Wei, National Renewable Energy Lab
Mo0910	9:10 a.m.	New Approaches to Studying Band Offsets at Semiconductor Heterointerfaces		A. Zakutayev, V. Stevanovic, M. Young, G. Teeter, National Renewable Energy Lab
Mo0915	9:15 a.m.	Why Interfaces in Semiconductor Heteroepitaxy Cannot Be Atomically Abrupt		A. Beyer, A. Stegmüller, J. O. Oehlerich, K. Jandieri, K. Werner, W. Stolz, S. Baranovskii, R. Tonner, K. Volz, Philipps Univ. Marburg

Mo0920	9:20 a.m.	Correlation of Interface Characteristics and Dielectric Reliability with the Incorporation of Phosphorous in SiC Based Metal-insulator-semiconductor Devices		M.H. Weng, Raytheon UK/Newcastle Univ.; A.E. Murphy, D.A. Smith, D.T. Clark, R.A.R. Young, E.P. Ramsay, R.F. Thompson, Raytheon UK; A.B. Horsfall, Newcastle Univ.
Mo0925	9:25 a.m.	Oxidation States of Homoepitaxially Grown (001) and (110) Gaas Surfaces After Wet and Dry Surface Treatments		E. Cleveland, A. Podpirka, Naval Research Lab
Mo0930	9:30a.m.	Electronic Properties of Atomic-layer-deposited High-k Dielectrics on GaSb(001) with Hydrogen Plasma Pretreatment		L.B. Ruppalt, E.R. Cleveland, J.G. Champlain, B.R. Bennett, S.M. Prokes, Naval Research Lab
Mo0935	9:35 a.m.	Capacitance-voltage and Current-voltage Measurements of Epitaxial Thin Films of N-SrTiO3-δ on p-Si(100)		R. Cottier, D. Currie, N. Theodoropoulou, Texas State Univ.
Mo0940	9:40 a.m.	Atomic Layer Deposition of Crystalline $SrHf_xTi_{1-x}O_3$ directly on Ge (001) for High-k Dielectric Applications		M.D. McDaniel, C. Hu, A. Jiang, T.Q. Ngo, A. Posadas, A.A. Demkov, E.T. Yu, J.G. Ekerdt, The Univ. of Texas at Austin
Mo0945	9:45 a.m.	The Impact of Interface Characteristics on the 1/F Noise in SiC CMOS		L.C. Martin, H.K. Chan, M.H. Weng, Newcastle Univ.; R.F. Thompson, D.T. Clark, E.P. Ramsey, Raytheon UK; N.G. Wright, Newcastle Univ.
Mo0950	9:50 a.m.	Effect of -H, -F and -OH Surface Terminations on Optical Absorption Onset of 4H-SiC Quantum Dots		M. Rashid, A. Tiwari, P. Briddon, Newcastle Univ.; M. Rayson, Univ. of Surrey; J. Goss, A.Horsfall, Newcastle Univ.
Mo0955	9:55 a.m.	Characterisation of Interfaces in 4H-SiC High-κ MOS Structures		S. Roy, K. Vassilevski, N. Wright, A. Horsfall, Newcastle Univ.
Mo1000	10:00 a.m.	Coffee Break and Poster Viewing		
Nanowires				Session Chair: L. Lauhon
Mo1100	11:00 a.m.	INVITED: Vertically Aligned Semiconductor Nanowires and Their Applications		T. Fukui, E. Nakai, F. Ishizaka, K. Tomioka, Hokkaido Univ.
Mo1140	11:40 a.m.	Selective-area Growth of Wurtzite InP/AlGaP Core-shell Nanowires Toward Direct-band-gap Green Emission		F. Ishizaka, Y. Hiraya, K. Tomioka, T. Fukui, Hokkaido Univ.
Mo1145	11:45 a.m.	Scanning Tunneling Microscopy on Semiconductor Nanowire Surfaces and Devices		J. Knutsson, M. Hjort, J. Webb, O. Persson, S. Lehmann, L. Samuelson, K.A. Dick, R. Timm, Lund Univ.
Mo1150	11:50 a.m.	Orientation Dependent Luminescence of Nitride Nanowire Surfaces		D.F. Ogletree, S. Aloni, T. Kuykendall, V. Altoe, Lawrence Berkeley Lab
Mo1155	11:55 a.m.	Lunch and Poster Viewing		
Monday Afternoon:				
Complex Oxides and Ferroelectrics I				Session Chair: A. Demkov
Mo1400	2:00 p.m.	INVITED: Understanding Oxide Interfaces: From Microscopic Imaging to Electronic Phases		S. Ilani, Weizmann Institute of Science
Mo1440	2:40 p.m.	INVITED: Local Manipulation of Electronic Properties of Ferroelectric and Complex Oxides		P. Maksymovych, Oak Ridge National Lab
Mo1520	3:20 p.m.	Strain-Induced Energy Band Structure Changes inside $LaNiO_3/La_{2/3}Sr_{1/3}MnO_3/SrTiO_3$ Heterostructures		T. Asel, H. Gao, T. Heinl, The Ohio State Univ.; J. Hoffman, Argonne National Lab; A. Bhattacharya, Argon National Lab; L.J. Brillson, The Ohio State Univ.

Mo1525	3:25 p.m.	Carrier Density Modulation in Ge Heterostructure by Ferroelectric Switching		P Ponath, K Fredrickson, A B Posadas, Y Ren, X Wu, The Univ. of Texas at Austin; R K Vasudevan, M B Okatan, S Jesse, Oak Ridge National Lab; T Aoki, M R McCartney, D J Smith, Arizona State Univ.; S V Kalinin, Oak Ridge National Lab; K Lai, A.A. Demkov, The Univ. of Texas at Austin
Mo1530	3:30 p.m.	Coffee Break and Poster Viewing		
2D Materials				Session Chair: Z. Hasan
Mo1630	4:30 p.m.	UPGRADED: Investigation of Band-Offsets at Monolayer-Multilayer MoS_2 Junctions by Scanning Photocurrent Microscopy		S.L. Howell, D. Jariwala, C-C. Wu, V.K. Sangwan, T.J. Marks, M.C. Hersam, L.J. Lauhon, Northwestern Univ.
Mo1650	4:50 p.m.	UPGRADED: Interfaces Between Transferred, CVD-grown Graphene and MoS_2 Probed with STM and ARPES		M. Batzill, Univ. of South Florida
Mo1710	5:10 p.m.	Crystalline SrO(001) on Graphene: a Universal Buffer Layer for Oxide Integration		A. Ahmed, The Ohio State Univ.; H. Wen, Univ. of California, Riverside; I. Pinchuk, T. Zhu, The Ohio State Univ.; R. Kawakami, Ohio State and UCR
Mo1715	5:15 p.m.	Optically Probing 2D Materials at Length Scales that Matter: Correlating Nanoscale Charge Recombination Heterogeneity and Surface Potential		Wei Bao, Nicholas Borys, LBNL; Changhyun Ko, Sefaattin Tongay, Wen Fan, UC Berkeley; D. Frank Ogletree, Paul Ashby, Miquel Salmeron, Alex Weber-Bargioni, LBNL; Junqiao Wu, UC Berkeley;
Mo1720	5:20 p.m.	In Situ Study of Fluorine-Functionalized and TMA-dosed Epitaxial Graphene on SiC(0001)		Z.R. Robinson, G.G. Jernigan, V.D. Wheeler, S.C. Hernandez, R.L. Myers-Ward, D.K. Gaskill, Naval Research Lab; T. Mowl, E.W. Ong, C.A. Ventrice, Jr., College of Nanoscale Science and Engineering; H. Geisler, SUNY College at Oneonta; I. Pletikosic, T. Valla, Brookhaven National Lab; C.R. Eddy, Naval Research Lab
Mo1725	5:25 p.m.	In-situ Atomic Force Microscopy Study of Ion Intercalation into Two-dimensional Titanium Carbide		J. Come, N. Balke, J. Black, M. Naguib, Oak Ridge National Lab; M. Beidaghi, Drexel Univ.; S. Kalinin, Oak Ridge National Lab; Y. Gogotsi, Drexel Univ.
Mo1730	5:30 p.m.	First-principles Study of Structural and Catalytic Properties of Single-layer MoS_2 with Sulfur Vacancies		T.B. Rawal, D. Le, T.S. Rahman, Univ. of Central Florida
Mo1735	5:35 p.m.	Catalytic Reduction of Oxygen on Nitrogen-doped Graphene		A. Ichikawa, A. Akaishi, J. Nakamura, UEC-Tokyo (The Univ. of Electro-Communications)
Late News				Session Chair: Z. Hasan
Mo1740	5:40 p.m.	Enhancement of GaSb Tunnel Junctions with InAs Quantum Wells		S. Mack, M. P. Lumb, M. Gonzalez, K. J. Schmieder, R.J. Walters, Naval Research Lab
Mo1745	5:45 p.m.	Structural and Optical Characterization of AlN deposited by N_2/H_2 Plasma-Enhanced Atomic Layer Deposition		P. Motamedi, K.C. Cadien, Univ. of Alberta
Mo1800	6:00 p.m.	Dinner		
Monday Evening:				
Energy Materials				Session Chair: R. Myers
Mo1930	7:30 p.m.	INVITED: Nanostructured Interfaces for Efficient and Stable Photoelectrochemical Water Splitting		J. Ager, Lawrence Berkeley National Lab
Mo2010	8:10 p.m.	Improvement of Conversion Efficiency of Multicrystalline Silicon Solar Cell with Surface Pre-etching		W.H. Chen, National Cheng Kung Univ.

Mo2015	8:15 p.m.	The Origin of Crystallographic Orientation Dependence of SEM Contrast Revealed by the Difference in SiC Polytype and Polarity		K. Ashida, T. Kajino, Y. Kutsuma, N. Ohtani, T. Kaneko, Kwansei Gakuin Univ.
Mo2020	8:20 p.m.	III-V Semiconductor Nanowires on Silicon for Solar Fuel Generation		E. Alarcon-Llado, E. Frau, J. Vukajlovic, EPF Lausanne; K. Yasaroglu, EPF Lausanne, Fraunhofer Institute; G. Tutuncuoglu, F. Matteini, A. Fontcuberta i Morral, EPF Lausanne
Mo2025	8:25 p.m.	UPGRADED: Visualizing the Electric Double Layer of Ionic Liquids at Carbon Interfaces		J. Black, Oak Ridge National Lab; G. Feng, Vanderbilt Univ.; M. Baris Okatan, Oak Ridge National Lab; P. Cummings, Vanderbilt Univ.; S. Kalinin, N. Balke, Oak Ridge National Lab
Mo2045	8:45 p.m.	Nanoscale Variation of Physical Properties of $LiCoO_2$ After Li-ion Extraction		N. Balke, P. Maksymovych, A. Tselev, S. Jesse, S. Kalinin, Oak Ridge National Lab

Tuesday Morning:				
Tu0745	7:45 a.m.	Registration and Continental Breakfast		
Characterization I				Session Chair: J. Stangl
Tu0845	8:45 a.m.	INVITED: Ultrafast Terahertz Scanning Tunneling Microscopy		F. Hegmann, Univ. of Alberta
Tu0925	9:25 a.m.	XRD Transients During Capping of Different Sized InAs Quantum Dots on GaAs(001)		K. Shimomura, Toyota Technological Institute; H. Suzuki, Univ. of Miyazaki; T. Sasaki, M. Takahasi, Japan Atomic Energy Agency; Y. Ohshita, I. Kamiya, Toyota Technological Institute
Tu0930	9:30 a.m.	Atom Probe Tomography of GaAs-AlGaAs Core-shell Nanowire Heterostructures		N. Jeon, Northwestern Univ.; S.Morkötter, D. Rudolph, G. Koblmüller, TU Munich; L.J. Lauhon, Northwestern Univ.
Tu0935	9:35 a.m.	Measuring the Electronic Confinement of a Subsurface Metallic State		F. Mazzola, Norwegian Univ. of Science and Technology; M. Edmonds, Monash Univ.; K. Hoydalsvik, Norwegian Univ. of Science and Technology; D. Carter, N. Marks, Curtin Univ.; B. Cowie, L. Thomsen, Australian Synchrotron; J. Miwa, Aarhus Univ.; M. Simmons, Univ. of New South Wales; J. Wells, Norwegian Univ. of Science and Technology
Tu0940	9:40 a.m.	Growth, Morphology and Transport Properties of High Mobility (110) InAs Quantum Well Metamorphic Heterostructures		A. Podpirka, Naval Research Lab; J. Shabani, Univ. of California, Santa Barbara; M. Katz, S. Mack, M.E. Twigg, Naval Research Lab; C.J. Palmstrøm, Univ. of California, Santa Barbara; B.R. Bennett, Naval Research Lab
Tu0945	9:45 a.m.	*In Situ* Temporal Evolution of Plasma Enhanced Atomic Layer Epitaxy of Inn Growth Studied by Synchrotron X-ray Methods		N. Nepal, V.R Anderson, S.D Johnson, B.P. Downey, D.J Meyer, Naval Research Lab; A. DeMasi, K.F Ludwig, Boston Univ.; C.R. Eddy, Jr., Naval Research Lab
Tu0950	9:50 a.m.	Recent Advances In High Resolution Real And Reciprocal Space Photoelectron Emission Microscocopy		K. Winkler, Omicron NanoScience; N. Barrett, CEA/DSM/IRAMIS/SPCSI; N. Weber, M. Escher, FOCUS GmbH, Germany
Tu0955	9:55 a.m.	Polarity Dependent Pinning of a Surface State (note - GaN)		V. Portz, Forschungszentrum Juelich GmbH; H. Eisele, Technische Universitaet Berlin; R.E. Dunin-Borkowski, Ph. Ebert, Forschungszentrum Juelich GmbH
Tu1000	10:00 a.m.	Coffee Break and Poster Viewing		
Characterization II				Session Chair: F. Hegmann
Tu1100	11:00 a.m.	INVITED: In-situ Strain Monitoring of Suspended Nanowires Using Nano-focused X-ray Diffraction		J. Stangl, M. Keplinger, Johannes Kepler Universität Linz; R. Griphone, European Synchrotron Radiation Facility; J. Greil, A. Lugstein, Vienna Univ. of Technology
Tu1140	11:40 a.m.	Characterization of Aluminum Nitride Grown by Atomic Layer Epitaxy with in situ Grazing Incidence Small Angle X-ray Scattering		V.R. Anderson, N. Nepal, S.D. Johnson, Naval Research Lab; A. DeMasi, Boston Univ.; J.K. Hite, Naval Research Lab; K. Ludwig, Boston Univ.; C.R. Eddy, Jr., Naval Research Lab
Tu1145	11:45 a.m.	Partial Electron Yield NEXAFS Imaging Using Magnetic Collection Lens		C. Weiland, Synchrotron Research, Inc.; D.A. Fischer, C. Jaye, Z. Fu, National Institute of Standards and Technology; K. Scammon, Univ. of Central Florida; P. Sobol, E.L. Principe, Synchrotron Research, Inc.
Tu1150	Tu1150	Free Afternoon		
Tuesday Evening:				
Rump Session: 2D Materials and Heterostructure				Session Chair: J. Zhu
Tu1930	7:30 p.m.	Introduction INVITED: The Growth of 2D Heterostructures, J.A. Robinson, The Pennsylvania State Univ. INVITED: TBD, X. Duan, Univ. of California, Los Angeles		

Wednesday Morning:				
We0745	7:45a.m.	Registration and Continental Breakfast		
Complex Oxides and Ferroelectrics II				Session Chair: J. Levy
We0845	8:45 a.m.	INVITED: Engineering Transport and Magnetism at Perovskite Cobaltite Interfaces via Controlled Oxygen Vacancy Ordering		S. Bose, J. Walter, M. Sharma, M. Torija, Univ. of Minnesota; J. Gazquez, Oak Ridge National Lab and Universidad Complutense de Madrid, Spain; M. Varela, V. Lauter, H. Ambaye, R. Goyette, Oak Ridge National Lab; M. Fitzsimmons, Los Alamos National Lab; C. Leighton, Univ. of Minnesota
We0925	9:25 a.m.	UPGRADED: Two-dimensional Electron Gas at the Epitaxial Oxide/SrTiO$_3$ Interface: Tuning Oxygen Vacancies		K.J. Kormondy, A.B. Posadas, T.Q. Ngo, Univ. of Texas at Austin; S. Lu, Arizona State Univ.; N. Goble, X.P.A. Gao, Case Western Reserve Univ.; M.R. McCartney, D.J. Smith, Arizona State Univ.; J.G. Ekerdt, A.A. Demkov, Univ. of Texas at Austin
We0945	9:45 a.m.	Optical Properties of Transition Metal Oxide Quantum Wells		A.A. Demkov, The Univ. of Texas at Austin
We0950	9:50 a.m.	Influence of Structural Order on the Properties of ALD VO$_2$ Films		V. Wheeler, M. Tadjer, M. Currie, Z. Robinson, J. Greenlee, N. Nepal, Naval Research Lab; T. Nunney, ThermoFischer Scientific; F. Kub, C. Eddy Jr., Naval Research Lab
We0955	9:55 a.m.	Structural Variations of Epitaxial PbVO$_3$ Thin Films on LaAlO$_3$(001), SrTiO$_3$(001), and MgO(001) Crystal Substrates		S.H. Oh, H-J. Jin, H-Y. Shin, S. Yoon, Ewha Womans Univ.; S.J. Kang, M. Kim, Seoul National Univ.; J-S. Ahn, Pusan National Univ.; J. Cha, S. Hong, Sejong Univ.; S. Choi, National Renewable Energy Lab; W. Jo, Ewha Womans Univ.
We1000	10:00 a.m.	Atomic Structure and Intrinsic Electronic States of the In$_2$O$_3$(111) Surface		H. Eisele, R. Zielinski, A. Lenz, Technische Universität Berlin; Z. Galazka,Institut fürKristallzí_chtung Berlin; M. Dähne, Technische Universität t Berlin
We1005	10:05 a.m.	Coffee Break and Poster Viewing		
InAs Based Heterostructures				Session Chair: C. Palmstrøm
We1105	11:05 a.m.	INVITED: Engineering 2D Topological Insulators from InAs/GaSb Semiconductors		R-R. Du, Rice Univ.
We1145	11:45 a.m.	InAs Heterostructures with Superconducting Contacts		Javad Shabani, B. Shojaei, Univ. of California, Santa Barbara; S. Das Sarma, Univ. of Maryland; K. Shtengel, Univ. of California, Riverside; R. Lutchyn, C. Nayak, Microsoft; C.J. Palmstrøm, Univ. of California, Santa Barbara
We1150	11:50 a.m.	Tuning the Emission Wavelength from Self-assembled Inas Quantum Dots on Gaas(001) to over 1.55 µm by Controlling the Cap and Barrier Layers		K. Shimomura, I. Kamiya, Toyota Technological Institute
We1155	11:55 a.m.	Lunch and Poster Viewing		
Wednesday Afternoon:				
Novel Heterostructures				Session Chair: J. Hilton
We1400	2:00 p.m.	INVITED: Metal Oxides-Organic Semiconductor Interfaces		Z.H. Lu, Univ. of Toronto
We1440	2:40 p.m.	New Frontiers in Thin Film Organic-based Magnets		H. Yu, M. Harberts, R. Adur, I. Froning, Y. Lu, The Ohio State Univ.; G. Schmidt, Martin-Luther-Universitat Halle-Wittenberg; P. Chris Hammel, A.J. Epstein, E. Johnston-Halperin, The Ohio State Univ.
We1445	2:45p.m.	Growth of AlN/Pt Heterostructures on Amorphous Substrates at Low Temperatures Via Atomic Layer Epitaxy		N. Nepal, Sotera Defense Solutions; R. Goswami, S.B. Qadri, N.A. Mahadik, F.J. Kub, C.R. Eddy, Jr., Naval Research Lab

We1450	2:50 p.m.	Detection of Inhomogeneous Regions in Yttrium Iron Garnet Films Deposited by Aerosol Deposition		S.D. Johnson, E.R. Glaser, S-F. Cheng, J.K. Hite, F.J. Kub, C.R. Eddy Jr., Naval Research Lab
We1455	2:55 p.m.	The Study of Trapping States and Their Correlation to Gate Hysteresis and 1/f Noise on the Al_2O_3 and HfO_2 Atomic Layer Deposited Epitaxial Graphene Field Effect Transistor		H.K. Chan, Newcastle Univ.; D.K. Gaskill, C.R. Eddy Jr., Naval Research Lab; N.G. Wright, J.P. Goss, Newcastle Univ.; N.Y. Garces, R.L. Myers-Ward, L.O. Nyakiti, V.D. Wheeler, Naval Research Lab; A.B. Horsfall, Newcastle Univ.
We1500	3:00 p.m.	Interface Bonding Characteristics of Graphene with Metal and Dielectric Substrates		S. Das, Univ. of North Texas
We1505	3:05 p.m.	The Impact of GaN and AlN Nucleation by Metalorganic Chemical Vapor Deposition on Epitaxial Graphene		Z.Y. Al Balushi, The Pennsylvania State Univ.; T. Miyagi, Research Center, Asahi Glass Co., Ltd. Japan; Y. Lin, K. Wang, L. Calderin, G. Bhimanapati, J.M. Redwing, J.A. Robinson, The Pennsylvania State Univ.
We1510	3:10 p.m.	Coffee Break and Poster Viewing		
Graphene and Other 2D Materials				Session Chair: R. Kawakami
We1615	4:15 p.m.	INVITED: Probing the Valley Hall effect in MoS_2 Transistors		K.F. Mak, Pen State Univ.
We1655	4:55 p.m.	Band Structure, Band Gap Opening and Topological Edge States in Clean Bilayer Graphene		J. Li, K. Zou, J. Todd, Penn State Univ.; K. Watanabe, T. Taniguchi, NIMS, Japan; J. Zhu, Penn State Univ.
We1700	5:00 p.m.	Opto-electronic and Spin Dependent Properties of Transition Metal Dichalcogenides		Y. Luo, E. Bushong, The Ohio State Univ.; P. Odenthal, Univ. of California, Riverside; R. Kawakami, The Ohio State Univ.; Univ. of California, Riverside
We1705	5:05 p.m.	Impact of the Direct Growth of MoS_2 on Graphene for Tunneling Applications		C. Joiner, P. Campbell, E.M. Vogel, Georgia Institute of Technology
We1710	5:10 p.m.	UPGRADED: Conductance Fluctuations in Graphene Nanoribbons		B. Liu, R. Akis, D.K. Ferry, Arizona State Univ.
We1730	5:30 p.m.	Direct Growth of Hexagonal Boron Nitride on Epitaxial Graphene by High-vacuum-CVD		P.C. Mende, J. Li, R.M. Feenstra, Carnegie Mellon Univ.
We1735	5:35 p.m.	Large Area Transfer and Optoelectronic Properties of Multilayer Epitaxial Germanane		W. Amamou, P. Odenthal, D. O'Hara, Univ. of California, Riverside; E. Bushong, Y. Luo, The Ohio State Univ.; J. Van Baren, Univ. of California, Riverside; I. Pinchuk, The Ohio State Univ.; Y. Wu, M. Bockrath, Univ. of California, Riverside; H. Tom, Univ. of California Riverside; J. Goldberger, The Ohio State Univ.
We1740	5:40 p.m.	Computer Simulation Linear Defects in Graphene and Nanographene		I.D. Yadgarov, V.G. Stelmakh, Institute of Ion-Plasma and Laser Technologies; A.A. Dzhurakhalov, Univ. of Antwerp
We1745	5:45 p.m.	Step Flow Like Graphene Growth Controlled by Crystallographic Step Alignement During Thrermal Decomposition of 4H-SiC(000-1) C-face		Y. Kutsuma, D. Dojima, H. Shigemasa, K. Ashida, N. Ohtani, N. Tamai, T. Kaneko, Kwansei Gakuin Univ.
We1750	5:50 p.m.	Application of LEEM, PEEM and STM/ncAFM Techniques to Graphene on Metal Surfaces		T. Schulmeyer, SPECS Surface Nano Analysis, Inc.
We1800	6:00 p.m.	Conference Banquet		

Thursday Morning:				
Th0745	7:45 a.m.	Registration and Continental Breakfast		
Spintronics				Session Chair: M. Flatté
Th0845	8:45 a.m.	INVITED: Optically-Induced Persistent Magnetization in Strontium Titanate		W.D. Rice, Los Alamos National Lab; P. Ambwani, Univ. of Minnesota; J.D. Thompson, Los Alamos National Lab; G. Haugstad, Univ. of Minnesota, C. Leighton, Univ. of Minnesota; S.A. Crooker, Los Alamos National Lab
Th0925	9:25 a.m.	UPGRADED: Barrier Dependence of Spin-dependent Transport Accross FM/I/SrTiO$_3$		A.G Swartz, H. Inoue, S. Harashima, Stanford Univ.; T. Tachikawa, Univ. of Tokyo; Y. Xie, D. Lu, B. Kim, Stanford Univ.; C. Bell, Univ. of Bristol; Y. Hikita, SLAC National Accelerator Lab; H.Y. Hwang, Stanford Univ.
Th0945	9:45 a.m.	Optically Enhanced NMR Studies of Semiconductors		Z. Ma, M. Willmering, S. Hayes, Washington Univ.
Th0950	9:50 a.m.	Dynamic-nuclear-polarization-induced Anisotropic Spin Relaxation in n-GaAs		N.J. Harmon, Univ. of Iowa; T. Peterson, C. Geppert, Univ. of Minnesota; M.E. Flatté, Univ. of Iowa; P. Crowell, Univ. of Minnesota
Th0955	9:55 a.m.	Coffee Break and Poster Viewing		
Topological Insulators II				Session Chair: J. Shabani
Th1045	10:45 a.m.	INVITED: Direct Electrical Detection of Spin Momentum Locking in the Topological Insulator Bi$_2$Se$_3$		C.H. Li, O.M. J. van ’t Erve, J.T. Robinson, Y. Liu, L. Li, B.T. Jonker, Naval Research Lab
Th1125	11:25 a.m.	UPGRADED: Dirac Mass Generation and Unconventional Orbital Texture in Topological Crystalline Insulators		I. Zeljkovic, Boston College; Y. Okada, WPI-AIMR, Tohoku Univ.; C-Y. Huang, National Sun Yat-sen Univ.; R. Sankar, National Taiwan Univ.; D. Walkup, W. Zhou, Boston College; M. Serbyn, J. Liu, Massachusetts Institute of Technology; G. Chang, National Univ. of Singapore; Y.J. Wang, Northeastern Univ.; W-F. Tsai, National Sun Yat-sen Univ.; F. Chou, National Taiwan Univ.; M. Zahid Hasan, Princeton Univ.; H. Lin, National Univ. of Singapore; A. Bansil, Northeastern Univ.; L. Fu, Massachusetts Institute of Technology; V. Madhavan, Boston College
Th1130	11:30 a.m	Poster Viewing		
Th1200	12:00 p.m.	Conference Ends		

Sunday

Su1400	Registration
Su1455	Welcome Remarks
Su1500	Sunday Afternoon Session: *Topological Insulators I*
Su1630	Poster Setup
Su1700	Welcome Reception
Su1930	Sunday Evening Session: *Epitaxial Oxide Heterostructures*

Topological Insulators I

Surface and Electronic Structure of Half-Heusler PtLuSb (001) Thin-Films Grown by Molecular Beam Epitaxy

J. A. Logan[1], S. J. Patel[1], S. D. Harrington[1], J. K. Kawasaki[1],
B. D. Schultz[2], T. Balasubramanian[3], A. Mikkelsen[4], and C. J. Palmstrøm[1,2]

(1) Materials Department, University of California-Santa Barbara
(2) Department of Electrical and Computer Engineering, University of California-Santa Barbara
(3) MAX IV Laboratory, Lund University, Lund 221 00, Sweden
(4) Department of Physics, Lund University, Lund 221 00, Sweden

Three-dimensional topological insulators have opened up an entirely new avenue for fundamental physics research. These materials offer the unique combination of a bulk band gap and time-reversal protected cross-gap surface states. Recently, theoretical predictions have suggested that some 18-valence electron per formula unit half-Heusler compounds may also exhibit topologically insulating behavior that can be further tuned through the application of strain [1,2]. Unlike in two-dimensional topological insulators, where transport studies have been able to successfully reveal the topological edge states, the high bulk conduction in many three-dimensional topological insulators dominates transport measurements. In order to circumvent this complication, angle-resolved photoemission spectroscopy (ARPES) can be used. ARPES is ideal for this task since it is both extremely surface sensitive and capable of directly measuring both the energy and momentum of the photoemitted electrons.

Here, molecular beam epitaxy was used to grow epitaxial thin films of unstrained PtLuSb (001) for ARPES and angle-integrated photoemission spectroscopy at MAX-LAB beamline I4 in Lund, Sweden. In order to enable successful *ex-situ* transfer, PtLuSb was grown on a buffer stack of 5 monolayers of GdSb on beryllium doped p-type $Al_{0.1}In_{0.9}Sb$ on p+ GaAs (001) substrates and then capped with antimony. Rutherford backscattering spectroscopy was used for calibration of the beam fluxes for lutetium and antimony and a quartz crystal microbalance for platinum. The surface exhibits several reconstructions depending on antimony overpressure and substrate temperature. For low substrate temperatures and high antimony overpressures, the “antimony-rich” c(2x2) reconstruction appears, while for high substrate temperatures and low antimony overpressures the “antimony-poor” (1x3) reconstruction appears. The electronic structure of (1x3) PtLuSb is explored via ARPES and the results suggest the presence of surface states with linear dispersion with a projected crossing above the Fermi level that repeat with the surface Brillouin zone periodicity.

This work was funded in part by the Office of Naval Research and the Army Research Office.

[1] S. Chadov, X. Qi, J. Kübler, G. Fecher, C. Felser, and S.-C. Zhang, Nat. Mater. **9**, 541 (2010).

[2] H. Lin, L. A. Wray, Y. Xia, S. Xu, S. Jia, R. Cava, A. Bansil, and M. Hasan, Nat. Mater. **9**, 546 (2010).

Su1540

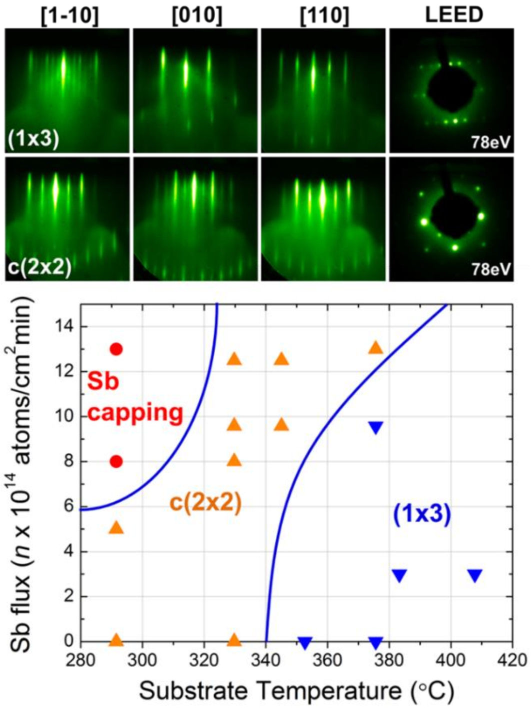

Figure 1. (a) RHEED and LEED of unstrained PtLuSb (001) showing streaky (1x3) and c(2x2) reconstructions. (b) Preliminary reconstruction phase map for unstrained PtLuSb showing three regions depending on substrate temperature and antimony overpressure.

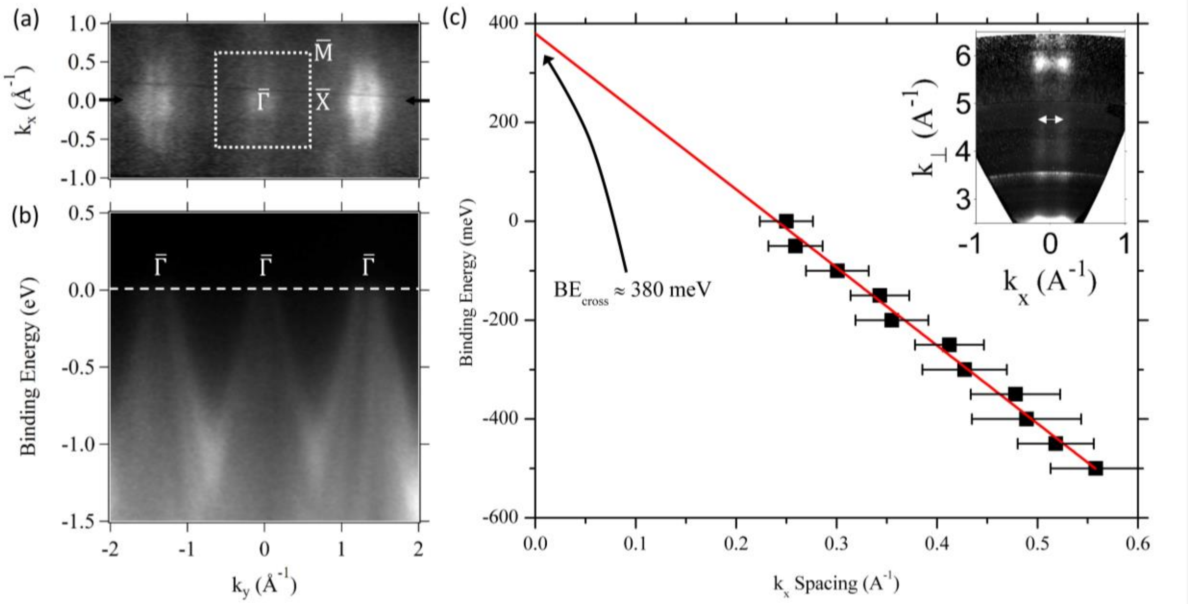

Figure 2. ARPES dispersion maps of unstrained PtLuSb (001). (a) Fermi surface slice (k_x vs k_y), 100 meV below the Fermi level, for a photon energy of 80 eV (near the bulk X point). (b) In-plane dispersion extraction for $k_x = 0$ showing surface states with linear dispersion. (c) Plot tracing the spacing between the two legs of the surface state as a function of binding energy. Extrapolating to higher energies, the crossover should occur ~380 meV above the Fermi level. The inset shows a $k_\perp$ (out-of-plane) vs $k_\parallel$ (in-plane) constant binding energy map, 100 meV below the Fermi level, showing an absence of out-of-plane dispersion.

Su1545

Epitaxial growth and electronic structure of half Heusler $Co_{1-x}Ni_xTiSb$

S. D. Harrington,[1] J. A. Logan,[1] S. J. Patel,[1] J. K. Kawasaki,[1]
T. Balasubramanian,[3] A. Mikkelsen,[4] and C. J. Palmstrøm[1,2]

[1]*Materials Department, University of California, Santa Barbara, CA*
[2]*Department of Electrical & Computer Engineering, University of California, Santa Barbara, CA*
[3]*MAX-lab, Lund University, Sweden*
[4]*Division of Synchrotron Radiation, Department of Physics, Lund University, Sweden*

Half Heusler compounds are an exciting class of intermetallics due to their multifarious electrical and magnetic properties, including semiconducting [1], half metallic [2], and thermoelectric [3]. Additionally, a number of the half Heusler compounds have been predicted to be topological insulators [4]. Their crystal structure and lattice parameters are closely related to III-V compound semiconductors, suggesting the possibility of half-Heusler/III-V semiconductor heterostructures with unique properties. Applications of epitaxial half-Heusler compound rely on a deeper experimental understanding of their electronic band structure. Most experimental studies of half Heusler compounds have been limited to bulk polycrystalline samples, which cannot be used for measurements of band dispersion and are not ideally suited for transport studies.

In this talk we demonstrate the epitaxial growth of the electron-doped half Heusler series $Co_{1-x}Ni_xTiSb$ by molecular beam epitaxy (MBE). CoTiSb has been extensively studied in the bulk and recently in MBE grown films where record high carrier mobilities were demonstrated [5]. In this presentation, the influence of the addition of Ni doping/alloying to CoTiSb epitaxial films is investigated. $Co_{1-x}Ni_xTiSb$ epitaxial films were grown on MBE-grown InAlAs (001) epitaxial layers grown on InP (001) substrates. The reflection high energy diffraction (RHEED) patterns were streaky indicating relatively flat surfaces and RHEED intensity oscillations were observed for all levels of nickel alloying investigated. This is consistent with a layer-by-layer growth mode. The temperature dependent electrical transport measurements suggest that films of composition $x \leq 0.1$ showed thermally activated transport. Using Sb-capping and decapping, ex-situ synchrotron based Angle-resolved photoemission spectroscopy (ARPES) experiments for determining the electronic band structure were performed to investigate the effects of nickel. The appearance of the conduction band minimum at the bulk X point below the Fermi level occurs for $x > 0.1$, suggesting a crossover from semiconductor to metallic behaviour. The effects of nickel alloying on the valence band, conduction band, and Fermi level positions will be discussed.

[1] H. Kandpal, C. Felser, and R. Seshadri, J. Phys. D. Appl. Phys. **39**, 776 (2006).
[2] M. Katsnelson, V. Irkhin, L. Chioncel, a. Lichtenstein, and R. de Groot, Rev. Mod. Phys. **80**, 315 (2008).
[3] S. Chen and Z. Ren, Mater. Today **16**, 387 (2013).
[4] H. Lin, L. A. Wray, Y. Xia, S. Xu, S. Jia, R. J. Cava, A. Bansil, and M. Z. Hasan, Nat. Mater. **9**, 546 (2010).
[5] J. K. Kawasaki, L. I. M. Johansson, B. D. Schultz, and C. J. Palmstrøm, Appl. Phys. Lett. **104**, (2014).

Su1545

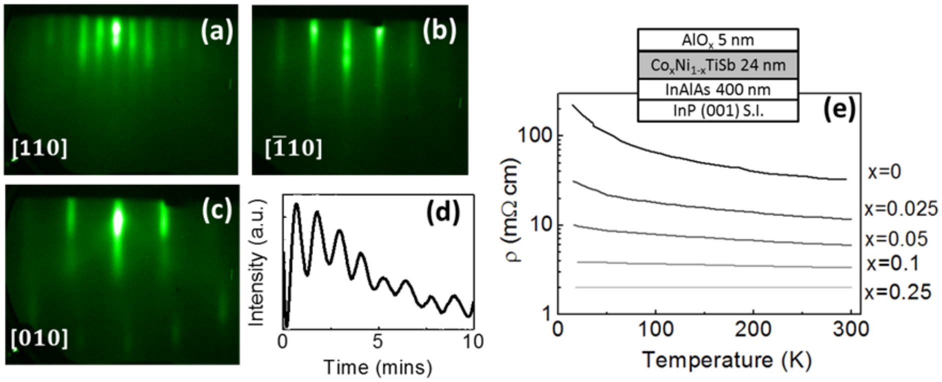

Figure 1. (a)-(c) RHEED patterns of $Co_{0.5}Ni_{0.5}TiSb$ along the [110], [$\bar{1}$10], and [010] azimuths. (d) RHEED oscillations demonstrating layer-by-layer growth. (e) Temperature dependent resistivity measurements for 24nm $Co_{1-x}Ni_xTiSb$ film on InAlAs/InP (001) for x=0, 0.025, 0.05, 0.1, and 0.25.

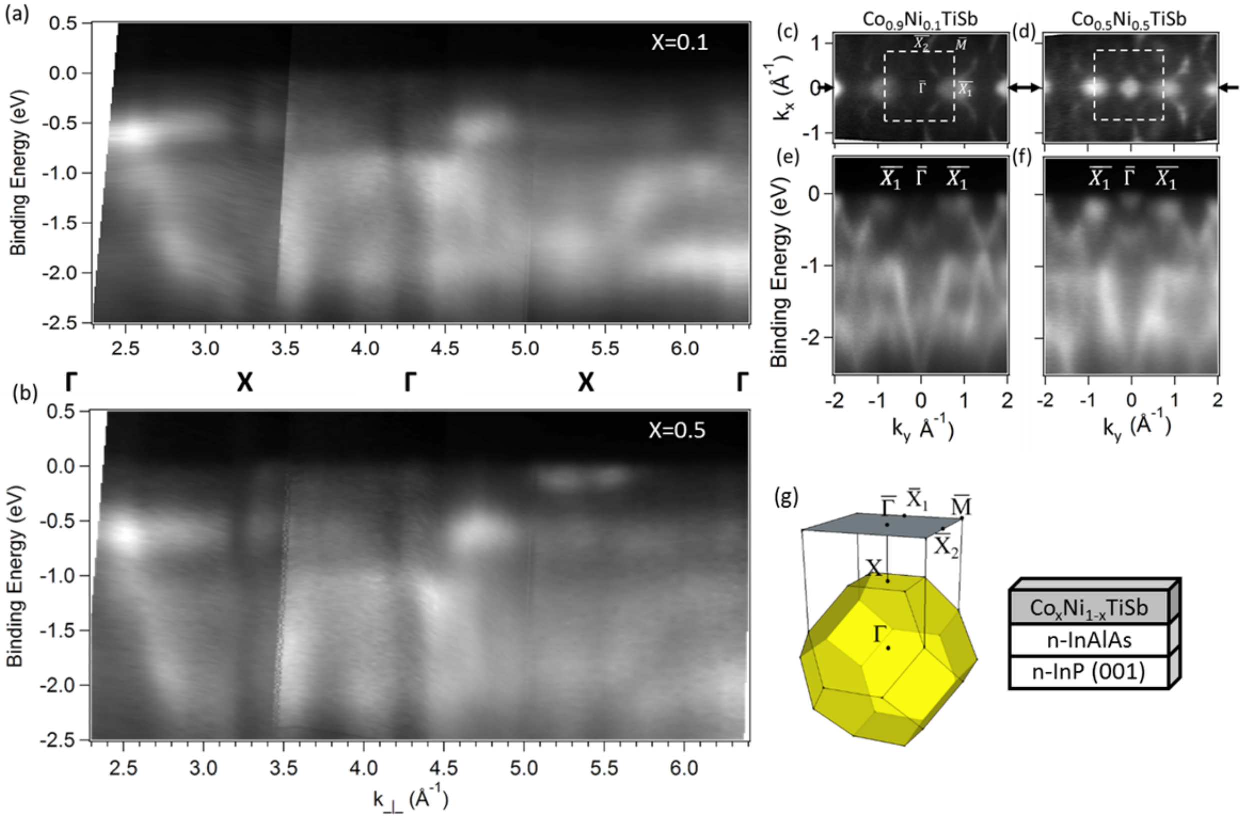

Figure 2. Normal emission measurement probing along Γ-X direction of the bulk Brillouin zone for (a) $Co_{0.9}Ni_{0.1}TiSb$ and (b) $Co_{0.5}Ni_{0.5}TiSb$. Fermi surface slice (k_x vs k_y) 80meV below the Fermi level for (c) $Co_{0.9}Ni_{0.1}TiSb$ and (d) $Co_{0.5}Ni_{0.5}TiSb$ (001) surfaces measured with 110 and 104 eV photon energies respectively which corresponds to the bulk X point. In-plane dispersions showing cuts at $k_x = 0$ indicated by the arrows for (e) $Co_{0.9}Ni_{0.1}TiSb$ and (f) $Co_{0.5}Ni_{0.5}TiSb$. (g) Bulk and surface Brillouin zones.

Su1550 Invited

Band alignment of Al_2O_3/Ga_2O_3 heterosturctures and their application to field-effect transistors

Masataka Higashiwaki[1], Takafumi Kamimura[1], Kohei Sasaki[2,1], Man Hoi Wong[1],
Akito Kuramata[2], and Shigenobu Yamakoshi[2]

[1]National Institute of Information and Communications Technology, Koganei, Tokyo 184–8795, Japan
[2]Tamura Corporation, Sayama, Saitama 350–1328, Japan

Tel : +81-42-327-6092, E-mail: mhigashi@nict.go.jp

A new widegap oxide compound semiconductor, gallium oxide (Ga_2O_3), has excellent material properties for power and high-temperature device applications mainly due to its large band gap of about 4.8 eV. Another important advantage of Ga_2O_3 over other widegap semiconductors such as SiC, GaN, and diamond is that large-area single-crystal wafers can be fabricated from a melt-grown bulk, which requires neither a high-temperature nor a high-pressure environment and uses less source material in its production process.

Here, after an introduction of material properties of single-crystal Ga_2O_3 and envisioned markets for Ga_2O_3 devices, we will first report a band alignment of $Al_2O_3/n\text{-}Ga_2O_3$ heterostructures investigated by using x-ray photoelectron spectroscopy and the Fowler-Nordheim tunneling current measured in $Au/Al_2O_3/n\text{-}Ga_2O_3$ diodes [1]. A schematic band diagram of the diode structure is shown in Fig. 1. With a measured band gap of 6.8 eV for the Al_2O_3 formed by atomic layer deposition (ALD), the conduction and valence band offsets at the Al_2O_3/Ga_2O_3 interface were estimated to be about 1.5~1.6 and 0.7 eV, respectively.

Next, we will introduce current status of research and development on Ga_2O_3 transistors mainly aiming for power device applications. We fabricated depletion-mode Ga_2O_3 metal-oxide-semiconductor field-effect transistors (MOSFETs) with an *n*-type channel layer fabricated by Si-ion (Si^+) implantation doping and an Al_2O_3 gate dielectric formed by ALD [2]. Figures 2(a) and (b) show room-temperature output and breakdown characteristics of the Ga_2O_3 MOSFET, respectively. The drain current (I_d) was effectively modulated by the gate voltage (V_g) with good saturation and sharp pinch-off characteristics. The maximum I_d was 65 mA/mm at $V_g = +6$ V. The three-terminal off-state breakdown voltage was as high as 415 V at $V_g = -30$ V. The off-state I_d remained below the detection limit (a few pA/mm) prior to device breakdown. At a drain voltage of 30 V, a high I_d on/off ratio of about ten orders of magnitude was achieved. No abrupt changes that might be indicative of breakdown events and/or permanent degradation were observed in a temperature range from 25 to 250°C. The device characteristics satisfied many of requirements from the viewpoints of practical power device applications.

This work was partially supported by Council for Science, Technology and Innovation (CSTI), Cross-ministerial Strategic Innovation Promotion Program (SIP), “Next-generation power electronics” (funding agency: NEDO).

[1] T. Kamimura et al., APL 104, 192104 (2014), [2] M. Higashiwaki et al., *IEDM Tech. Dig.*, pp. 707, 2013.

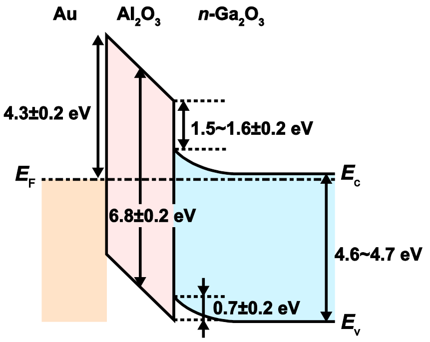

Fig. 1 Schematic band diagram of $Au/Al_2O_3/n\text{-}Ga_2O_3$ structure.

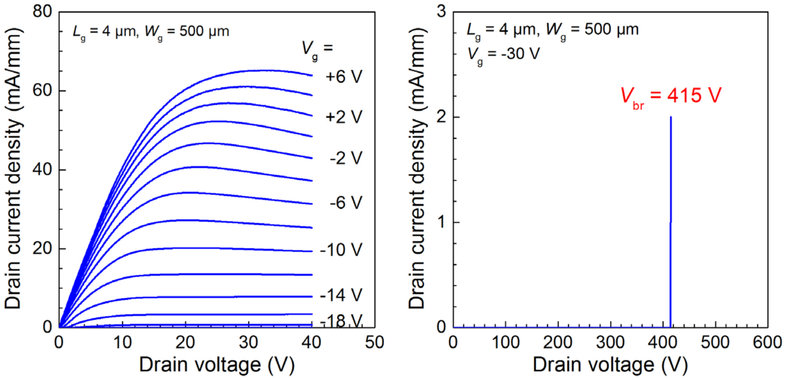

(a) (b)

Fig. 2 (a) Output and (b) breakdown characteristics of Ga_2O_3 MOSFET.

Epitaxial Oxide Heterostructures

Su1930 Invited

Transport Properties of Layered Perovskite Heterostructures: New Ideas and Insights from Theory and Simulation

Nicole A. Benedek
Materials Science and Engineering Program, The University of Texas at Austin

Complex oxides are one of the largest and most technologically important materials families. The ABO_3 perovskite oxides in particular display myriad fascinating electronic and magnetic properties. The details of the origin of these properties (how they arise from the structure of the material) are often complicated, but in many systems it is possible to identify simple guidelines or 'rules of thumb' that link structure and chemistry to the property of interest. Can we uncover a similar set of simple guidelines to yield new insights into the ionic transport properties of perovskites? I will discuss our recent work on the link between crystal structure and chemistry, soft lattice modes, epitaxial strain and ionic transport in a family of layered perovskite oxides. In particular, we seek ways to make new connections between known structure descriptors for perovskites (such as the tolerance factor) and transport properties and to identify new design principles. Our results suggest that it may indeed be possible to think about transport properties using simple rules of thumb.

Su2010 Invited

Room-Temperature Electronically Controlled Magnetism at the $LaAlO_3/SrTiO_3$ Interface

Feng Bi, Mengchen Huang, Patrick Irvin, and Jeremy Levy

Department of Physics & Astronomy, University of Pittsburgh, 3941 O'Hara Street, Pittsburgh, Pennsylvania 15260, USA

Pittsburgh Quantum Institute, Pittsburgh, Pennsylvania 15260, USA

Sangwoo Ryu, Hyungwoo Lee, Chung-Wung Bark, Chang-Beom Eom

Department of Materials Science and Engineering, University of Wisconsin-Madison, Madison, Wisconsin 53706, USA

Reports of emergent conductivity, superconductivity and magnetism have helped to fuel intense interest in the rich physics and technological potential of complex-oxide interfaces. Here we employ magnetic force microscopy to search for room-temperature magnetism in the well-studied $LaAlO_3/SrTiO_3$ system. Using electrical top gating to control the electron density at the oxide interface, we directly observe the emergence of an in-plane ferromagnetic phase as electrons are depleted from the interface. Itinerant electrons that are reintroduced into the interface align antiferromagnetically with the magnetization at first screening and then destabilizing it as the conductive regime is approached. Repeated cycling of the gate voltage results in new, uncorrelated magnetic patterns. This newfound control over emergent magnetism at the interface between two non-magnetic oxides portends a number of important technological applications.

Su2050

Improvement of characterization of nonpolar m-plane ZnO on $LiGaO_2$ substrate by Molecular Beam Epitaxy

Chun-Yu Lee, Chenlong Chen, Liuwen Chang, Shih-Hsun Yu, Mitch M.C. Chou*

Department of Materials and Optoelectronic Science,
National Sun Yat-Sen University, Kaohsiung, 80424, Taiwan, R.O.C.
MOST Taiwan Consortium of Emergent Crystalline Materials (TCECM)
E-Mail of corresponding author: mitch@faculty.nsysu.edu.tw

Nonpolar m-plane ZnO epitaxial films has successfully grown on (100) β-$LiGaO_2$ (LGO) substrates by plasma assisted molecular beam epitaxy (PAMBE). LGO is a suitable substrate for ZnO heteroepitaxy due to small lattice mismatch between ZnO and LGO (1.9-3.9%). However, C. J. et al. indicated that LGO will decompose to $LiGa_5O_8$ and Ga_2O_3 at high temperature [1]. Some experiments in our group also indicated that the damages from hydrogen atoms. In order to prevent decomposed of LGO substrate, we modified the pretreatment in MBE growth process. Here we set LGO substrates in load lock chamber of MBE system under specific hydrogen flow before heteroepitaxy. The structual properties characterized by high resolution X-ray diffraction (HRXRD) indicated that the ZnO epilayers were grown in the nonpolar $[1\bar{1}00]$ orientation and the FWHM of X-ray rocking curves has improved from 0.5° to 0.05° (Fig.1). The surface morphologies of ZnO films were investigated by scanning electron microscopy (SEM) and atomic force microscopy (AFM). Detailed structural characterization and defect analysis of nonpolar ZnO epilayer $LiGaO_2$ substrate was studied by transmission electron microscope (TEM). Optical properties of m-plane ZnO films were investigated by photoluminescence (PL) and cathodoluminescence (CL) analyses.

Reference:

[1] C.J. Rawna, J. Chaudhuri, J. Crystal Growth, 225 (2001) 214-220.

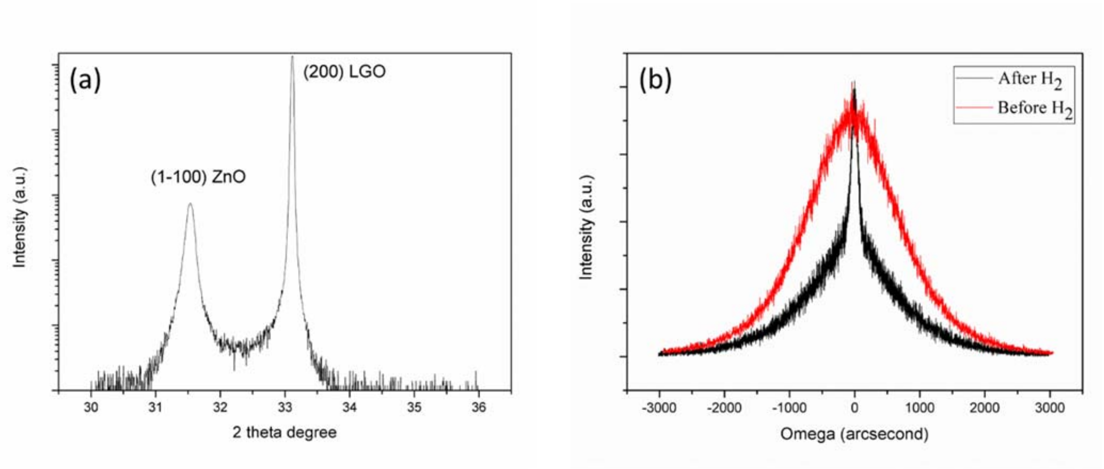

Fig. 1 (a) X-ray diffraction pattern of m-plane ZnO grown on $LiGaO_2$ substrate and (b) X-ray rocking curves before and after hydrogen flow.

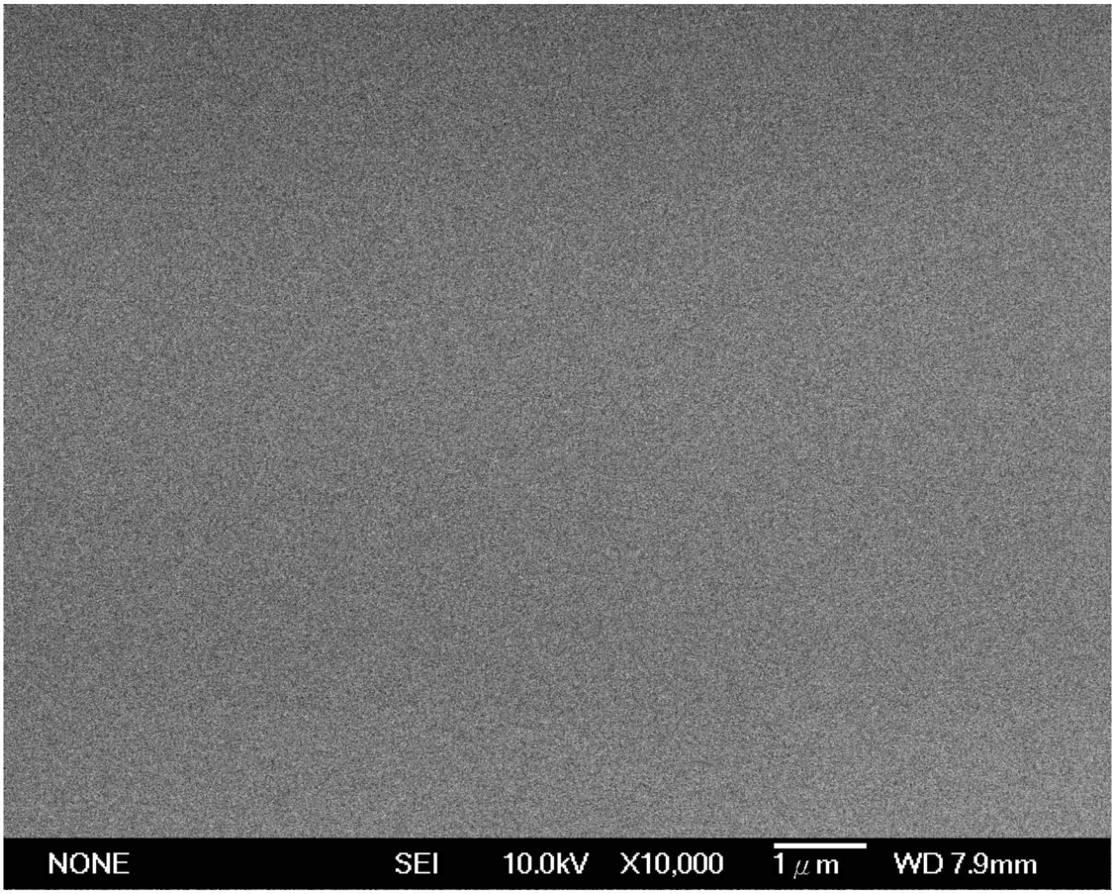

Fig.2 SEM image of m-plane ZnO grown on $LiGaO_2$ substrate after hydrgen flow.

Su2055

Epitaxial growth and optical properties of (0002) ZnO films on (001) $LiGaO_2$ substrate by chemical vapor deposition method

Shih-Hsun Yu [a,b], Chun-Yu Lee [a,b], Chenlong Chen [a,b], Chu-An Li [a,b], Mitch M.C. Chou [a,b]

[a] Department of Materials and Optoelectronic Science, National Sun Yat-Sen University, Kaohsiung 80424, Taiwan, ROC
[b] NSC Taiwan Consortium of Emergent Crystalline Materials (TCECM), Kaohsiung, Taiwan, ROC

Abstract

High quality c-plane ZnO epitaxial films have been successfully grown on closely lattice matched (001) $LiGaO_2$ (LGO) substrate by chemical vapor deposition (CVD) method. Zinc Acetylacetonate is used as zinc precursor. High purity oxygen and nitrogen are used as reaction gas and carrier gas, respectively. The dependence of growth characteristics on growth temperature, growth pressure and N_2/O_2 ratio are studied. The surface morphology demonstrates the very flat ZnO films with a surface root-mean-square roughness of 1.2nm. The high-resolution X-ray diffraction measurement reveals that high-quality crystalline ZnO films have been achieved on (001) $LiGaO_2$ (LGO) substrate by chemical vapor deposition. The cross-sectional transmission electron microscopy (TEM) images taken under a two beam contrast condition reveal that the major defects in ZnO epilayers are edge-type threading dislocations and intrinsic basal plane stacking fault. The high-resolution TEM image near the interface area clearly shows the $LiGaO_2$ substrate lattice was compliantly deformed, which is suggested to help to decrease the compressive strain in the ZnO epilayer and increase the quality of the ZnO. The strain state of the ZnO was elevated by XRD reciprocal space maps and Raman scattering analysis. Room temperature photoluminescence spectrum shows a strong UV emission peak at 3.3eV with a negligible green band emission. The low temperature spectrum at 12K was also taken to further reveal the luminescence characteristics. High optical transmittance value of ZnO films is observed over >85% in the visible light region which can also be determine the optical band gap of ZnO thin films.

Key words: epitaxy, ZnO, $LiGaO_2$, CVD,

Su2055

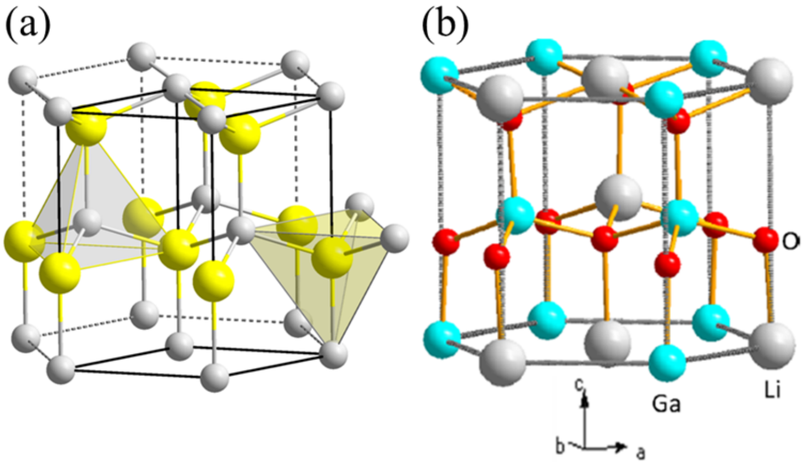

Fig. 1. Crystal structure of (a) ZnO, (b) LGO.

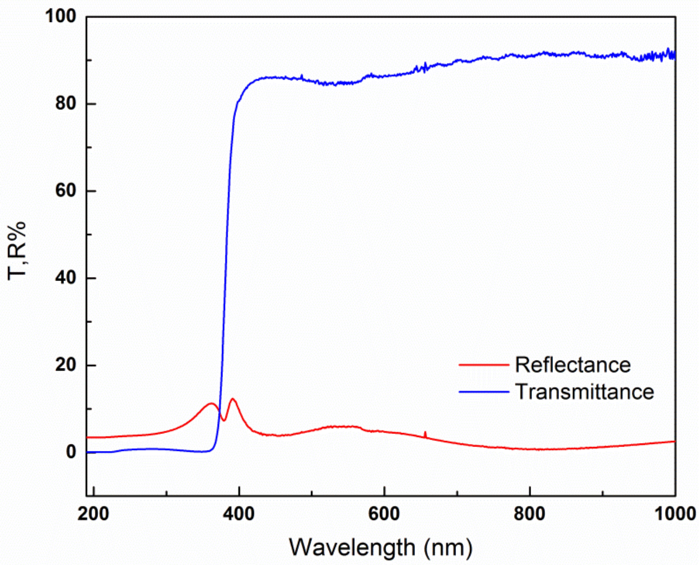

Fig. 2. Optical properties of ZnO films on LiGaO2 substrate.

Monday

Mo0745	Registration and Continental Breakfast
Mo0830	Monday Morning Session: *Semiconductors, Band Offsets, Dielectrics*
Mo1000	Coffee Break and Poster Viewing
Mo1100	Monday Morning Session: *Nanowires*
Mo1155	Lunch and Poster Viewing
Mo1400	Monday Afternoon Session: *Complex Oxides and Ferroelectrics I*
Mo1530	Coffee Break and Poster Viewing
Mo1630	Monday Afternoon Session: *2D Materials*
M01740	Monday Afternoon Session: *Late News*
Mo1800	Dinner
Mo1930	Monday Evening Session: *Energy Materials*

Semiconductors, Band Offsets, Dielectrics

Mo0830 Invited

Diffusion of Interstitial Defects in Semiconductors: The Case in CdTe

Su-Huai Wei

National Renewable Energy Laboratory, Golden, CO 80401, USA.

Atomic diffusion in semiconductors is an important issue because it can affect many material properties, such as doping, passivation, stability and performance of devices. For example, CdTe is one of the most promising candidates for thin-film photovoltaic applications and it is well known that Cu and Cl diffusions play critical roles in improving the CdTe solar cell efficiency. However, the diffusion behavior of these impurities as well as the host elements in CdTe has not been clearly understood. In this talk, using first-principles calculations, I will discuss the diffusion behaviors of the cation atoms (Cd and Cu) and the anion atoms (Te and Cl) at different charged states to establish the connection between the diffusion behavior and the electronic structure of the interstitial diffuser. We find that, due to different electronic level occupations and level splittings, the diffusions of the cation atoms and anion atoms are very different. We explaine why Cu can diffuse much faster than other elements and show that the diffusion speeds of the impurities can be controlled by tuning the Fermi level of CdTe. Moreover, with the help of Monte Carlo simulations, we have developed a general diffusion coefficient theory for multi-barrier diffusion. Our calculated diffusivity of the Cd interstitial agrees well with the experimental measurement.

The work was done in collaboration with Ji-Hui Yang, Jie Ma, and Joongoo Kang and is supported by US DOE.

Mo0910

New approaches to studying band offsets at semiconductor heterointerfaces

Andriy Zakutayev, Vladan Stevanovic, Matthew Young and Glenn Teeter

Band offsets at semiconductor interfaces are important for many electronic- and energy technologies. The energy band alignment between two perfectly lattice matched semiconducting materials like GaAs/AlAs depends largely on their intrinsic bulk properties. However, many technologically relevant interfaces (e.g. $CuInSe_2$/CdS) occur between materials with incommensurate crystal structures, leading to structural defects that modify the band alignment; such cases are referred to here as “heterointerfaces”. Scientific understanding the role that the defects and other non-idealities, such as elemental interdiffusion and chemical reactions, play in band alignment at heterointerfaces requires better experimental and theoretical approaches to determining band offsets.

Here we report on our progress towards developing and demonstrating two new research approaches, an experimental and a theoretical one, for studying band alignment at interfaces between materials with different crystal structures. The model materials system studies are the heterointerfaces of distorted rocksalt-like layered p-type SnS with a realtively narrow band gap, and wide-bandgap insulating zincblende ZnS and n-type wurtzite ZnO.

The new experimental approach leverages the ideas of combinatorial materials science to improve the throughput of photoelectron spectroscopy (PES) based layer-by-layer band offset measurements by parallelizing this process. For demonstration, a thickness wedge of ZnO deposited across a SnS under-layer is measured by spatially-resolved x-ray and ultraviolet PES (XPS/UPS), avoiding the need for repetitive vacuum transfer between the PES and growth chambers, and time-consuming heating/cooling of the sample. The preliminary results of the band alignment measurements confirm the expected cliff-type conduction band offset, and also suggest the presence of O/SnS reaction and Zn/Sn inter-diffusion at the SnS/ZnO interface.

The new theoretical approach extends the genetic algorithm based bulk structure prediction methods (GSGO) to create the structural models for the interfaces between two materials with incommensurate crystal structures. The band offsets for the resulting interfacial structural model is simulated using atom-projected local density of states calculated using first-principles DFT and NLEP methods. The initial results lead to conclusion that ZnS deposited on SnS forms an amorphous interface layer and causes the sheets in the SnS structure to sheer leading to appearance of electronic states in the band gap.

In summary, we demonstrated two new research approaches to determining band offsets at interfaces between two materials with different crystal structures. These new capabilities are expected to enhance our understanding and control of the interfaces for photovoltaics and other energy and electronic technologies.

Mo0915

Why Interfaces in Semiconductor Heteroepitaxy Cannot Be Atomically Abrupt

A. Beyer, A. Stegmüller, J. O. Oehlerich, K. Jandieri, K. Werner, W. Stolz,
S. Baranovskii, R. Tonner

Very often it is thought that interfaces in semiconductor heteroepitaxy can be atomically abrupt, if only growth conditions are chosen in an appropriate way. We will show with the example of GaP/Si (001) heteroepitaxy that this is for most material combinations not the case. The example of lattice matched integration of III/V semiconductors to Si-substrates has been chosen due to the high technological importance of this interface. Integration of active III/V devices on Silicon substrates would tremendously increase the functionality of this semiconductor material. In order to realize true monolithic integration, a defect-free nucleation layer is of outmost importance. As CMOS industry nowadays focuses on exactly oriented (001) Si substrates, the integration of a III/V semiconductor based device structure, employing either lattice relaxed III/V layers for high electron mobility devices or the pseudomorphically strained, active direct-band gap material Ga(NAsP) for optic devices, also has to be pursued on this substrate type. High-efficiency, Si-based solar cells can however also be deposited on off-cut substrates.

The III/V nucleation layer we use is GaP-based due to the similar lattice constants of GaP and Si. Besides the known challenges of III/V on IV heteroepitaxy, like charge neutrality of the interface, cross-diffusion of dopants and slight differences in lattice constant and thermal expansion coefficient, nucleation on Si furthermore poses the challenge of the formation of antiphase domains. These form as the Si surface is covered with monoatomar steps. Prior to the deposition of the heteroepitaxial III/V layer, a 500nm thick Si-buffer is grown by VPE using silane. The growth and post-growth annealing conditions of this layer are optimized to maximize the number of double steps on the Si-surface with respect to the monoatmar steps for exactly oriented as well as 2° and 6° offcut Si-substrates. The GaP layer is grown with triethylgallium (TEGa) and the more efficiently decomposing metal organic group-V-source tertiarybutyl phosphine (TBP). The MOVPE growth conditions of thin GaP layers on Si substrate have been varied systematically, e.g. growth temperature, TBP/TEG vapour phase ratio and sequence of the first III/V coverage layer.

Main investigation technique to address the interface structure between the GaP layers and the Si substrates was scanning transmission electron microscopy (STEM) in high-angle annular dark field (HAADF) mode, where atomic resolution can be obtained due to the use of an aberration-corrected microscope. Complementary simulations of HAADF intensities were carried out using “frozen phonon” as well as “absorptive potential” approach. Comparison of theoretical scattering simulation with experimental results allowed us to obtain the interface structure at an atomic scale. The interface morphology is – irrespective of growth conditions - several monolayers wide and has a very surprising – triangular – structure. To explain these experimental findings, kinetic Monte Carlo simulation of the GaP/Si growth as well as ab-initio calculations of stable interface structures have been carried out.

The presentation will summarize the atomic structure of the GaP/Si interface and explain mechanisms, which are concluded from experiment-theory comparison, which lead to the formation of interfaces in semiconductor heteroepitaxy.

Mo0920

Correlation of interface characteristics and dielectric reliability with the incorporation of phosphorous in SiC based metal-insulator-semiconductor devices

M.H. Weng[1, 2, a], A. E. Murphy[2], D. A. Smith[2], D.T. Clark[2], R. A. R. Young[2],
E. P. Ramsay[2], R. F. Thompson[2], A. B. Horsfall[1]

[1]School of Electrical and Electronic Engineering, Newcastle University, Newcastle, NE1 7RU, UK
[2]Raytheon UK, Queensway Industrial Estate, Glenrothes, KY7 5PY, UK
[a] Ming-Hung.Weng@newcastle.ac.uk

The possibility to thermally grow SiO_2 on silicon carbide gives a significant advantage over other wide band gap semiconductors. The realisation of high quality interfaces in terms of minimum hysteresis, high breakdown field and low interface state density in the metal-insulator-semiconductor structures to enable high performance practical SiC CMOS devices remains a significant challenge. Here we report on the effect of different process techniques for the gate dielectric on device characteristics. Three devices, each processed using different oxidation and annealing methods were studied. The fabrication details are outlined in [1] and the resulting device structure is shown schematically in Figure 1. The characteristics of the dielectric layer and the interfaces were extracted from photo-capacitance voltage measurements to identify fixed charge and interfacial traps in the gate stacks. The Constant Current (*ConI*) technique was used to determine the difference in breakdown characteristics and high temperature stress testing was also performed to investigate the stability of the dielectric stacks and interfaces.

The data in Figure 2 shows the flatband voltage shift extracted from photo CV data for typical n-type MOS capacitors for each of the three samples. The capacitors are similar in terms of their characteristics, with a well accumulated C_{OX} and showing evidence of a deep depletion region. After a sweep from accumulation to depletion, the device is exposed to UV whilst held in depletion. The subsequent sweep from depletion to accumulation allows charges tunnelling from the SiC valence band into the oxide to be identified [2]. All wafers show enhanced levels of positive charge after UV exposure; however the sample without phosphorous incorporation demonstrates the smallest shift, with a median voltage shift at flatband of 0.6V, in contrast to 3.3V and 3.0V for samples 2 and 3, respectively. It can be seen from the data in Figure 3 that both of the wafers treated with phosphorous have a $D_{IT} > 1x10^{12}\ eV^{-1}cm^{-2}$ within 0.5eV of the conduction band. In contrast the D_{IT} for sample 1 shows a 50% reduction, suggesting that the lack of phosphorous doping results in advantageous behaviour of the SiC/SiO_2 interface.

In order to determine the gate stack reliability, time-dependent constant voltage measurements were performed. A Weibull plot of the time to breakdown extracted from the *ConI* stresses for the different gate stacks is shown in Figure 4. The devices with and without phosphorous treatment show two significantly different observations. Firstly, for capacitors doped with phosphorous during fabrication, the Weibull distribution slopes are steeper in comparison to that of sample 1, where no phosphorous doping was present. The deviation of the statistic failure rate between 0 to -3 in sample 1 also indicates a significantly less uniform distribution of the breakdown characteristic. Secondly, both samples 2 and 3 show repeatable distributions of the breakdown strengths. This indicates that the process used for samples 2 and 3 offers a more manufacturable process, where the reproducibility of the device characteristics is higher than the non-phosphorous doped structure. Although devices fabricated without phosphorous doping show lower D_{IT} and reduced positive charge in the dielectric in comparison to those with phosphorous inclusion, the overall breakdown field is lower and shows a lower uniformity in time to breakdown. The data in Figure 5 shows the change in flatband voltage for capacitors held at a gate bias of +15V for 120 seconds at 200°C to simulate the operation of CMOS devices at high temperatures. The data shows that in common with the photo CV data, the inclusion of phosphorous doping in the dielectric layer results in an unstable interface between the SiC and the SiO_2. A further investigation in to the metal – semiconductor barrier height in all samples extracted from DC characteristics to identify the nature of the defects in the dielectric layer will be reported.

These initial findings indicate that although the inclusion of phosphorous at the silicon carbide – silicon dioxide interface is detrimental to the device performance, the enhanced reliability and manufacturability makes this approach viable in volume manufacturing.

[1] D.T. Clark, *et al*, Proceedings of the Materials Research Symposium, San Fransisco, 2014.
[2] M.-H. Weng, *et al*, Mater. Sci. Forum, Vols. 679-680 (2011) pp. 350-353

Mo0920

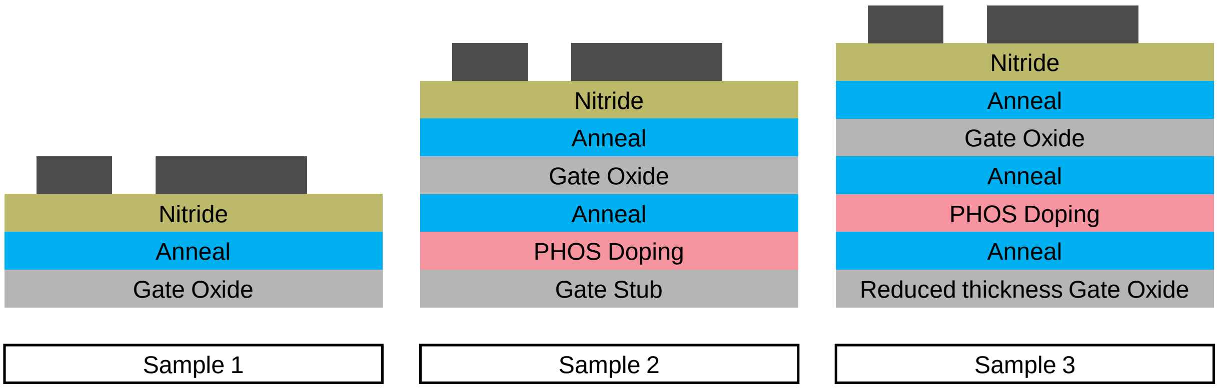

Figure 1 : Schematic cross section and fabrication of the SiC MOS capacitors

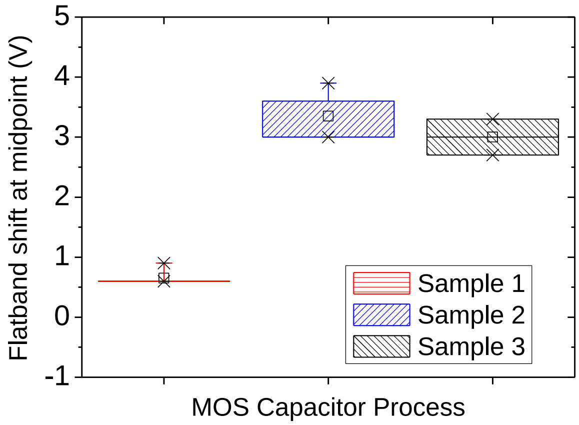

Figure 2 : Statistic plot of flatband voltage shift at midpoint with open squares show median values

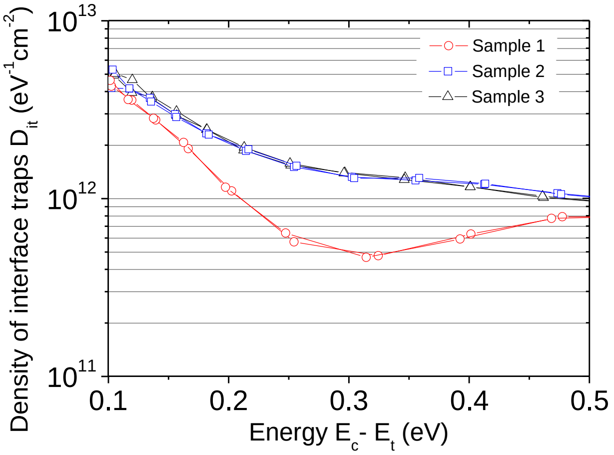

Figure 3 : Density of interface traps D_{IT} as a function of the energy position in the 4H-SiC bandgap

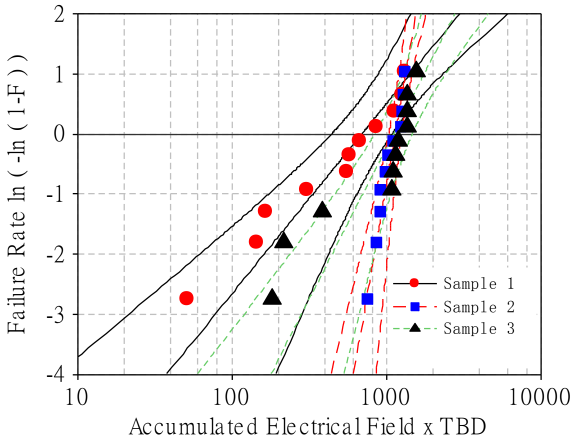

Figure 4 : Weibull plot of Constant Current (*ConI*) in comparison of breakdown oxide field strength and elapsed time

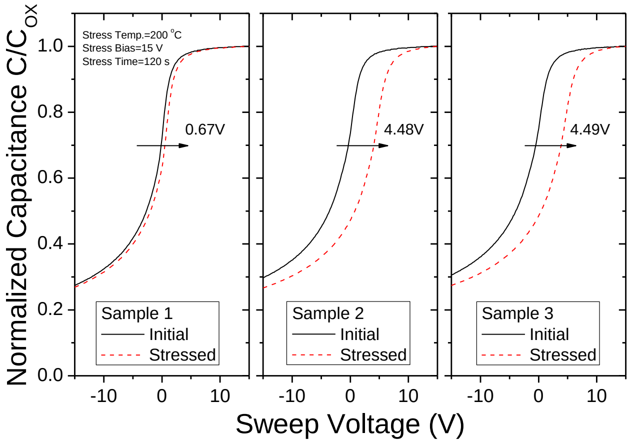

Figure 5 : High temperature stress C-V plots

Mo0925

Oxidation States of homoepitaxially grown (001) and (110) GaAs Surfaces after Wet and Dry Surface Treatments

Erin Cleveland and Adrian Podpirka
Electronic Science and Technology Division, U.S. Naval Research Laboratory, Washington D.C.

Silicon-based complementary metal oxide semiconductor (CMOS) devices are approaching the performance limits achievable by conventional scaling. In order to continue improving device speed and density, new materials and geometries must be utilized in order to go beyond the fundamental limits set by Si. An increasing amount of work has been performed on III-V metal-oxide-semiconductor field effect transistors (MOSFETs), which show promise due to their excellent on/off state characteristics and high carrier mobilities. Of particular interest, (110)-oriented III-V heterostructures show great potential due to their non-polar surface and the ability to integrate onto group IV surfaces. The (110) III-V zinc blende surface has been proposed as a preferred orientation for epitaxial growth on zinc blende group IV surfaces due to the absence of interface charge imbalance. For devices such as finFETs, the (110) surface would be the dominant surface of vertically aligned III-V (001) based transistors and with proper passivation technology, an ideal interface with the gate oxide.

Of particular importance in MOSFET devices is the interface between the gate dielectric and the III-V semiconductor. The removal of natively-occurring oxides, passivation of the surface, and growth of an ideal high-k dielectric layer on GaAs remain of great concern. Current approaches for native oxide removal typically rely upon wet-chemical etches, such as HCl, HF, and NH_4OH; however, due to rapid re-oxidation, potential contamination, and lack of reproducibility a better means of interface cleaning is needed. Several studies have shown the effective use of atomic layer deposition (ALD) for integration of device-quality oxides on GaAs(001); however to date, few have reported on the GaAs(110) surface, with little being known of the structural and chemical nature of the interface. In this paper, we compare homoepitaxially grown atomically-smooth (001) and (110) GaAs surfaces and their native oxide compositions while investigating the effectiveness of both wet and dry surface treatments. We first evaluated the effectiveness of trimethyaluminum (TMA), the metal containing ALD precursor, as a “self-cleaning” process by investigating the removal of native oxides from both the (001) and the (110) GaAs surfaces and those dipped in HCl prior to TMA exposure. Furthermore, we examined the use of an *in situ* H_2 plasma treatment as a means to obtain a suitable electrical interface prior to the deposition of high-*k* Al_2O_3 films.

Mo0930

Electronic Properties of Atomic-Layer-Deposited High-k Dielectrics on GaSb(001) with Hydrogen Plasma Pretreatment

Laura B. Ruppalt, Erin R. Cleveland, James G. Champlain, Brian R. Bennett, and Sharka M. Prokes
Electronics Science and Technology Division, Naval Research Laboratory, Washington, DC 20375, USA

Increasingly, III-V materials are being seriously considered for use in high-speed, low-power complementary metal-oxide-semiconductor (CMOS) logic devices. In particular, InGaAs- and InSb-based alloys, with their high electron mobilities and saturation velocities, have emerged as promising alternatives for n-channel devices, with Ge and GaSb the leading contenders for p-channel devices. A formidable hurdle to MOS implementation in GaSb, however, is the development of a suitable dielectric/semiconductor interface. The ideal interface would employ a high-k dielectric in order to limit leakage current while supporting low gate-voltage operation, but must also possess few defects to prevent Fermi-level pinning and carrier mobility degradation. A variety of methods for GaSb surface preparation prior to oxide deposition have been reported, including wet chemical treatments,[1, 2] in-situ capping with a passivating layer,[3, 4] and in-situ H_2 plasma exposure.[5, 6] In particular, H_2-plasma exposure has shown promise as it avoids wet-chemical processing, which often leaves detrimental surface residue and can be difficult to reproduce, and does not require the inclusion of a non-active interface layer. Mild in-situ H_2-plasma treatments, performed immediately prior to atomic layer deposition (ALD) of Al_2O_3 layers, are found to preferentially remove Sb-oxides, resulting in a dramatically improved electrical interface, with interface defect densities as low as $<10^{12}$ $cm^{-2}eV^{-1}$.

In this work we examine the application of H_2-plasma exposure to composite and high-k dielectric stacks on GaSb, as well as to ex-situ processing. MBE-grown GaSb(001) surfaces were subjected to a 30 minute H_2/Ar plasma treatment and subsequently removed to air. High-k Al_2O_3/HfO_2 and HfO_2-only insulating films were then deposited via ALD and samples were processed into standard metal-oxide-semiconductor (MOS) capacitors. In both cases, the leakage current across the dielectric layer (Fig. 1) is low, with the composite dielectric stack exhibiting roughly an order of magnitude lower leakage, suggesting that inclusion of an Al_2O_3 layer may enhance the current blocking properties of the insulating film. Low temperature, frequency-resolved capacitance and conductance measurements (Fig. 2) indicate a relatively constant D_{it}~$1x10^{13}$ $cm^{-2}eV^{-1}$ across the sampled energy range for both samples (Fig. 3), a level comparable to other literature reports[1-6] and approximately two-orders-of-magnitude less than that found on untreated interfaces. The similarity of the D_{it} values for the two cases suggests that the dominant traps in these systems exist at the interface between the GaSb surface and the thin Ga-oxide remaining after the H_2-plasma treatment[5, 6] and may be independent of the dielectric composition.

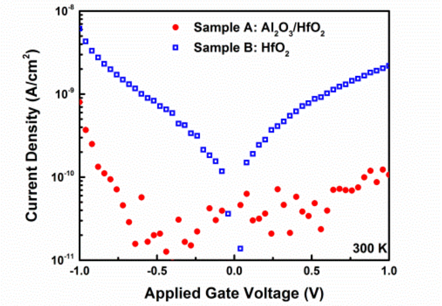

Fig. 1: Leakage current

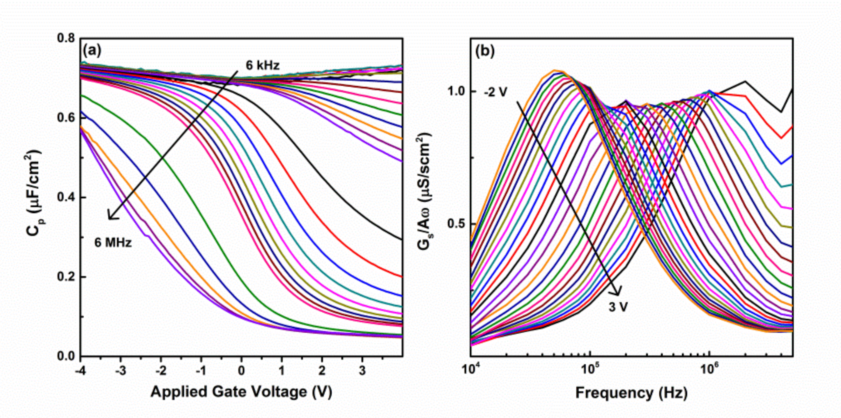

Fig. 2: Frequency-resolved (a) capacitance and (b) conductance of a HfO_2/GaSb device measured at 250K

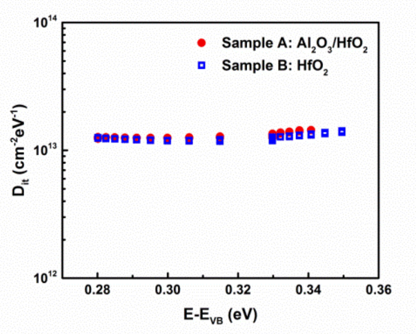

Fig. 3: Estimated D_{it}

[1] A. Ali, et al., *Appl. Phys. Lett.* **97**, 143502 (2010).
[2] A. Nainani, et al., *IEEE Trans. on Electron Devices* **58**, 3407 (2011).
[3] A. Greene, et al., *Solid-State Electronics* **78**, 56 (2012).
[4] V. Tokranov, et al., *J. of Crystal Growth* **378**, 631 (2013).
[5] L. B. Ruppalt, et al., *Appl. Phys. Lett.* **101**, 231601 (2012).
[6] E. R. Cleveland, et al., *Appl. Surf. Sci.* **277**, 167 (2013)

Mo0935

Capacitance-voltage and current-voltage measurements of epitaxial thin films of n-$SrTiO_{3-\delta}$ on p-Si(100)

Ryan Cottier, Daniel A. Currie, and Nikoleta Theodoropoulou
Texas State University, Physics Department, San Marcos, TX 78666

Epitaxial growth of $SrTiO_3$ (STO) thin films on Si can be achieved through MBE (Molecular Beam Epitaxy) techniques that suppress the formation of a SiO_2 interfacial layer. STO thin films on Si (STO/Si) can provide a buffer layer for growth of other oxides, allowing oxide integration with Si technology. Epitaxial (STO) films were considered as a replacement dielectric material for MOS technology due to their high dielectric constant but were never implemented mainly because of the small conduction band offset. STO/Si are strained compressively because of the lattice mismatch and can induce ferroelectric order. Additionally, interface dipole, interface states, and band bending complicate further the characterization of devices.

A series of n-p (n-STO/p-Si) junctions were grown by MBE with the thickness of the STO layer varying from 3.6 to 30 nm and were characterized using capacitance-voltage (C-V) and current-voltage (I-V) measurements. Oxygen vacancies were introduced by controlling the oxygen pressure during growth resulting in oxygen deficient $SrTiO_{3-\delta}$ with δ up to 0.4%. The low oxygen pressure during growth was advantageous for the growth of high quality films, and at the same time, oxygen vacancies acted as donors for STO. The single phase STO/Si films were of high crystalline quality as verified by x-ray diffraction (XRD), transmission electron microscopy (TEM), and had a surface roughness of < 0.5 nm (RMS) as measured by atomic force microscopy (AFM). Transport measurements of the STO thin films in a Van der Pauw configuration showed carrier concentrations on the order of 10^{20} cm^{-3} at RT due to the induced oxygen vacancies, and all films were semiconducting at low temperatures. We fabricated capacitor structures by contacting the STO side of the films with Cr (area of 0.04 cm^2) and the Si backside with Al. I-V measurements taken from 5-300K showed characteristics of an n-p junction, consistent with the transport measurements on the STO/Si films. At a temperature range of 5-20K, the IVs show a negative slope at a forward bias around 0.5 V. C-V measurements at 300 K for a frequency range of 1 kHz to 1 MHz show depletion layer capacitance behavior for reverse bias. When the junctions are forward biased, both the built-in potential (V_{bi}, 1.8 to 0.5 V) and the dielectric constant decrease with increasing thickness. The capacitance under forward bias has a clear peak for voltages higher than V_{bi} at low frequencies, but this effect disappear at frequencies of 10 kHz and up. The origin of the observed behavior is considered in terms of strain, interface states, charged defects, ferroelectricity, an interface dipole, band bending and an inversion layer at the interface.

Project Funded by NSF Career Award DMR-1255629

Mo0940

Atomic layer deposition of crystalline $SrHf_xTi_{1-x}O_3$ directly on Ge (001) for high-*k* dielectric applications

Martin D. McDaniel[a,*], Chengqing Hu[b], Aiting Jiang[b], Thong Q. Ngo[a], Agham Posadas[c],
Alexander A. Demkov[c], Edward T. Yu[b], and John G. Ekerdt[a]

[a]The University of Texas at Austin, Department of Chemical Engineering, Austin, TX 78712, USA
[b]The University of Texas at Austin, Department of Electrical and Computer Engineering, Austin, TX 78758, USA
[b]The University of Texas at Austin, Department of Physics, Austin, TX 78712, USA
*Presenter's e-mail: mcdanimd@utexas.edu

We demonstrate the growth of crystalline strontium titanate, $SrTiO_3$ (STO), and strontium hafnate, $SrHfO_3$ (SHO), directly on Ge via atomic layer deposition (ALD). Both STO (a ~ 3.905 Å) and SHO (a ~ 4.069 Å) have good lattice match to the Ge (001) surface ($a/\sqrt{2}$ ~ 3.992 Å), yielding a ~2.2% tensile and ~1.9% compressive strain in the epitaxial film, respectively. After thermal deoxidation, the 2×1 reconstructed, clean Ge substrate is transferred *in vacuo* to the deposition chamber where a thin film of STO / SHO is deposited by ALD. Following a post-deposition anneal, the perovskite film becomes crystalline with epitaxial registry to the underlying Ge (001) substrate. The STO and SHO films exhibit excellent crystallinity, as shown by x-ray diffraction and transmission electron microscopy.

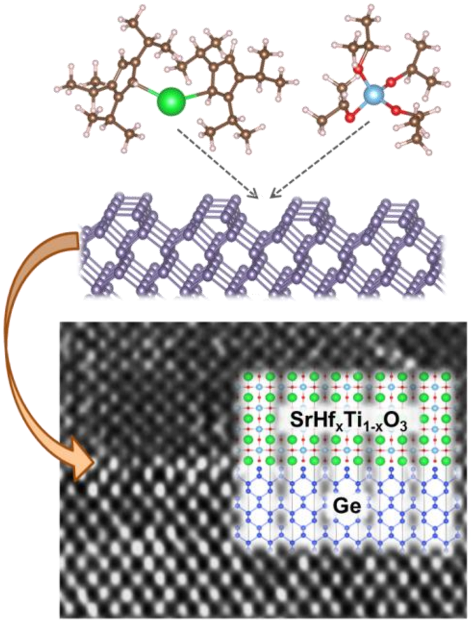

Capacitor structures using the crystalline STO dielectric show a high permittivity (k~90), but also high leakage current (~10 A/cm^2 at +1 eV). The unfavorable conduction band offset (and high leakage current) of STO on Ge is circumvented by growing the Hf-based perovskite, SHO. The SHO films have favorable electronic properties, with satisfactory band offsets with Ge (> 2 eV), low leakage current (< 10^{-5} A/cm^2 at an applied field of 1 MV/cm) at an equivalent oxide thickness of 1 nm, and a reasonable dielectric constant (k~15). The interface trap density (D_{it}) is estimated to be ~2-5 × 10^{12} cm^{-2} eV^{-1} under the current growth and anneal conditions. Some interfacial reaction is observed between SHO and Ge at temperatures above ~650 °C, which may contribute to the observed D_{it} value.

In efforts to improve electrical performance of the crystalline perovskite dielectric, including leakage current, permittivity, and D_{it}, we have recently studied crystalline $SrHf_xTi_{1-x}O_3$ (SHTO) grown directly on Ge by ALD. SHTO benefits from a reduced leakage current over STO and a higher permittivity than SHO. The SHTO films crystallize at a relatively lower temperature than SHO (600 °C vs. 650 °C), which limits the formation of hafnium germanide. In addition, the lattice constant of SHTO (x~0.5) is estimated to be 4.014 Å, yielding minimal (~0.6%) compressive strain in the epitaxial film. By minimizing the epitaxial strain and maintaining an abrupt interface, the SHTO films are expected to reduce D_{it} at the oxide-Ge interface. We will report our recent results on the growth, characterization, and electrical performance of epitaxial SHTO films on Ge for next-generation high-*k* dielectric applications.

Mo0945

The impact of interface characteristics on the 1/f noise in SiC CMOS

L.C. Martin[1], H.K. Chan[1], M.H. Weng[1,2], R.F. Thompson[2],
D.T. Clark[2], E.P. Ramsey[2], N.G. Wright[1], and A. B. Horsfall[1]

[1]School of Electrical and Electronic Engineering, Newcastle University, Newcastle, NE1 7RU, UK
[2]Raytheon UK, Queensway Industrial Estate, Glenrothes, KY7 5PY, UK

The superlative material properties of silicon carbide have made it the technology of choice for electronic circuits in hostile environments. However, the challenge of realising a high quality interface between the metal-insulator-semiconductor (MIS) interfaces to enable practical SiC CMOS devices is significant. Here we report on the effect of different process techniques for the dielectric layer on the device characteristics. Three devices, each processed using different oxidation method were studied. Here, HV06 was based on thermally annealed oxide, CR25 a chemical vapour deposited oxide after a sacrificial thermal oxide and CV27 a thermally stub grown oxide with CVD enhancement. The remainder of the fabrication details are given in [1] and the resulting device structure is illustrated schematically in Figure 1. In addition to parametric characterisation using a Keithley 4200 SCS, the low frequency (1/f) noise at frequencies up to 100kHz was measured using the system shown in Figure 2.

The data in Figures 3, 4 and 5 show the transconductance plot of n-type MOS devices for each of the three samples. The data shows that the transistors are similar in terms of their DC characteristics, with a threshold voltage of around 4V and a drain current of 4mA at V_{GS}=15V. The figures also show the variation in the current normalised noise spectral density (NNPSD or S_I/I^2) at 10Hz with gate voltage. In all cases it can be seen from the data that the magnitude of the NNPSD decreases significantly and converge to a value of -110 dB Hz^{-1} once the transistor is operating in strong inversion.

The origin of the low noise characteristic in CR27 has been considered in terms of the mechanisms that limit the carrier mobility in the channel of the device. At low gate bias (weak inversion), carrier scattering from charge trapped at the SiC/SiO_2 interface dominates the mobility, whereas at high gate bias, the surface roughness of the interface is the limiting factor. The data in Figure 6 shows the extracted surface roughness mobility and this shows that the characteristic for sample CR25 is distinct from the others shown here. Considering the functional form of the surface roughness scattering indicates that the surface roughness of CR25 is significantly lower than either HV06 or CR27 [2]. However, as shown by the data in Figure 7, the value of D_{IT} for CR25 extracted from the sub-threshold slope show a significant increase at room temperature in comparison to both HV06 and CR27. A similar trend is observed for D_{IT} values extracted using the Terman technique on monolithically fabricated test structures. The reduction in the low field mobility due to the increase in D_{IT} results in the maximum field effect mobility being comparable between the three different devices.

The 1/f noise characteristics shown by the data in Figures 3, 4 and 5 indicate that under the strong inversion operating regime, where the surface roughness dominates the channel mobility; the 1/f noise behaviour is dictated by the SiC/SiO_2 interface. In such a system, where the carriers are constrained to the inversion layer, the noise origin is described by means of the McWhorter model [3], whereas in the low gate bias region, the bulk noise behaviour of the semiconductor dominates and so the Hooge model may be employed to investigate the crystal quality of the bulk silicon carbide [4].

These observations indicate that in order to maximise the performance of SiC MOSFETs, research is needed to address the surface roughness of the SiC/SiO_2 interface and the 1/f noise technique can be used to understand both the characteristics of the bulk silicon carbide and the characteristics of the SiC/SiO_2 interface.

1. D.T. Clark, et al, Proceedings of the Materials Research Symposium, San Fransisco, 2014.
2. J.V. Varzgar, PhD Thesis, Newcastle University, 2010.
3. A. L. McWhorter, Research Laboratory of Electronics, Technical Report No.295, M.I.T., 1955.
4. F. N. Hooge, *IEEE Trans. Electron Devices*, vol. 41, no. 11, pp. 1926–1935, 1994.

Mo0945

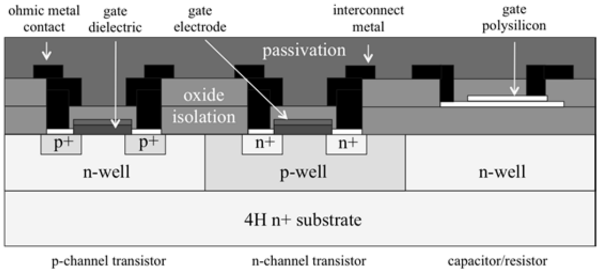

Figure 1 : Schematic cross section of the SiC CMOS devices

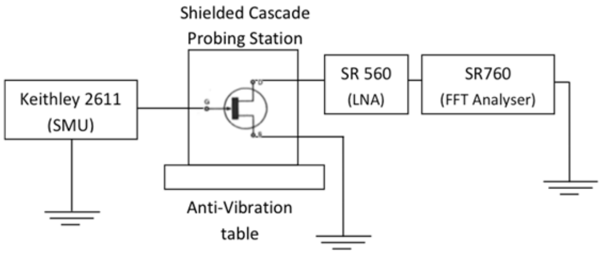

Figure 2 : Schematic of the 1/f noise measurement system

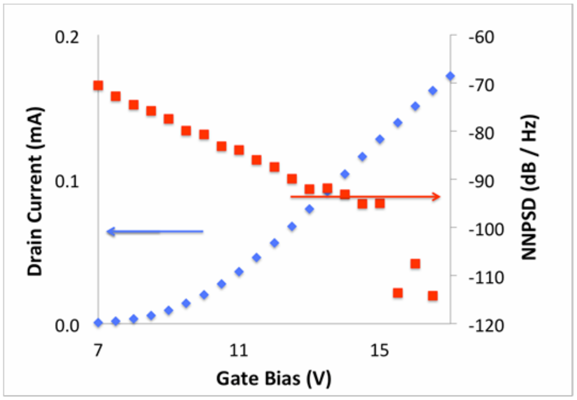

Figure 3 : Noise and I-V characteristics for HV06

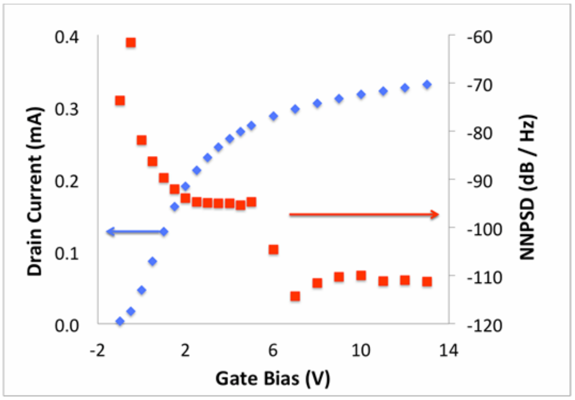

Figure 4 : Noise and I-V characteristics for CR25

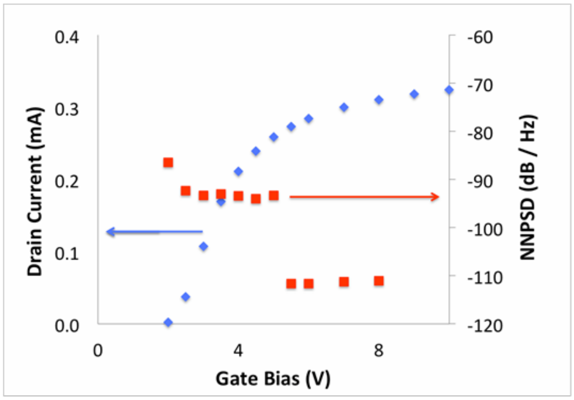

Figure 5 : Noise and I-V characteristics for CR27

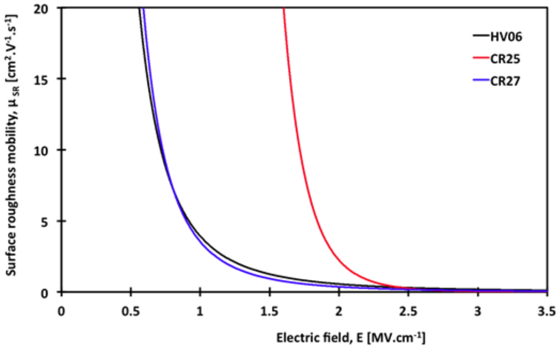

Figure 6 : Surface roughness mobility comparison

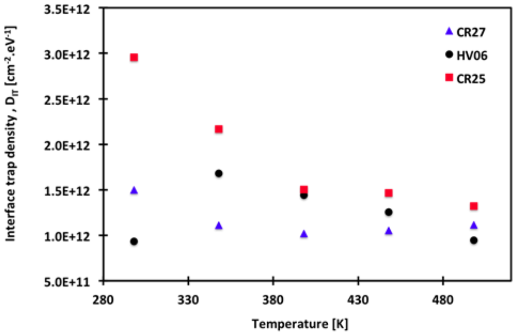

Figure 7 : D_{IT} extracted from the sub-threshold slope characteristics

Mo0950

Effect of –H, –F and –OH Surface Terminations on Optical Absorption Onset of 4H-SiC Quantum Dots

Marzaini Rashid[1,2*], A.K. Tiwari[1], P. Briddon[1], M. Rayson[3], J.P. Goss[1], A.B. Horsfall[1]
[1]School of EEE, Newcastle University, Newcastle Upon Tyne, NE1 7RU, UK.
[2]School of Physics, Universiti Sains Malaysia, 11800, USM, Penang, Malaysia.
[3]Department of Chemistry, University of Surrey, Guildford GU2 7XH, UK.
*E-mail: m.m.b.m.rashid@ncl.ac.uk

Functionalised semiconductor quantum dots (QDs), which have the potential of tuning the electronic bandgap, are of particular interest for optoelectronic applications [1]. However, suitable passivation of QD surfaces with either organic or inorganic capping groups is understood to be a prerequisite in order to achieve the high quantum yields and to suppress the non-radiative charge recombination on the surface. Previous studies have mainly focussed upon the use of semiconductors, such as CdS and PbS, using the alkyl and carboxylic groups [1,2]. Such materials exhibit superior optoelectronic properties but these are highly toxic in nature, which has necessitated the exploration of more environmentally friendly options. SiC, a wide bandgap biologically inert material, is a superb choice in this context. While 3C-SiC-based QDs show promising operation in the blue to ultraviolet spectrum range and enhance the optical absorption in solar cells [3,4], 4H-SiC-based QDs exhibit the potential of accessing even higher energy UV spectrum when compared to other SiC-polytypes or Si and Ge counterparts.

In this work, the effect of –OH, –F and –H surface termination on the optical absorption onsets of 4H-SiC QDs is investigated using density functional calculations, as implemented in the AIMPRO code [5]. Pseudo-spherical 4H-SiC QDs with 10, 16 and 22 Å diameters, are geometrically relaxed using the conjugate gradients scheme, with the optimised structures having forces on atoms $<10^{-3}$ atomic units, and the final structural optimisation step is required to result in a reduction in the total energy of less than 10^{-5} Ha.

Fig. 1 shows the geometrically relaxed 22 Å diameter QD terminated with –OH, –F and –H functional groups. Calculated average bond lengths for bulk and suface Si-C (1.87 and 1.88 Å) bonds and Si-F (1.60 Å), Si-H (1.50 Å), Si-O (1.67 Å), C-F (1.41 Å), C-H (1.10 Å) and C-O (1.44 Å) bonds are comparable to those found in single bond systems [6]. Comparison between the joint density of states (JDoS) and the absorption cross sections (ACS) with varying QD size are used to identify the optical absorption onsets and to assess the interband optical transitions. Fig. 2 illustrates the size dependent JDoS and ACS for –OH, –F and –H. The size dependent blue shift in absorption onset is clearly distinguishable between different surface terminations, with –H termination showing the largest energy shift, followed by –F and –OH, respectively. This implies that in the examined diameter range, the surface termination is highly influential in terms of enhancing the size dependent quantum confinement which in turn governs the QDs' optical absorption onsets.

The electronic density of states at 0.1 polynomial broadening and the sum of the squared wave functions are examined to observe the changes in energy and spatial distribution, particularly, for the highest occupied molecular orbital (HOMO) energy level. Fig. 3 shows the DoS, where the observed blue shift in the optical absorption onsets can be attributed to HOMO energy shift. For all terminations, the change in the LUMO energy level with size is relatively small. The wave function probability density for energy levels within 0.25 eV of HOMO indicates that for both –OH and –F, the electron densities are predominantly localised on the QD surface groups and for –H the electrons are localised within the QD core. Therefore, it can be concluded that the weak quantum confinement seen for –OH and –F terminations are due to the surface states, while the strong quantum confinement for –H termination is because of the HOMO being localised to the QD core rendering the confining potential more dominant.

Based upon our calculations, we propose that –H surface termination though technologically challenging is highly promising for those applications which require a wide range of absorption onsets tunable by QD size whereas –OH and –F terminations would produce predictable lower energy absorption onsets that are less sensitive to variation of QD size.

References

[1] P.V. Kamat, J. Phys. Chem. Lett. Vol. 4, No. 6, pp. 908-918 (2013)

Mo0950

[2] H.L. Chou *et al.*, J.Phys.Chem Vol. 115, pp. 20856-20863 (2011)
[3] S.Saha *et al.,* Chem. Phys. Lett., Vol. 536, pp. 118-122 (2012)
[4] B. Parida *et al.,* Journal of Nanomaterials, Vol. 143, pp. 1-10 (2013)
[5] P.R. Briddon *et al.*, Phys. Status Solidi B, Vol. 217, No. 1, pp. 131-171 (2000)
[6] D.R. Lide, CRC Handbook of Chemistry and Physics, 87th ed, Taylor & Francis, NY, p. 9-46 (2006)

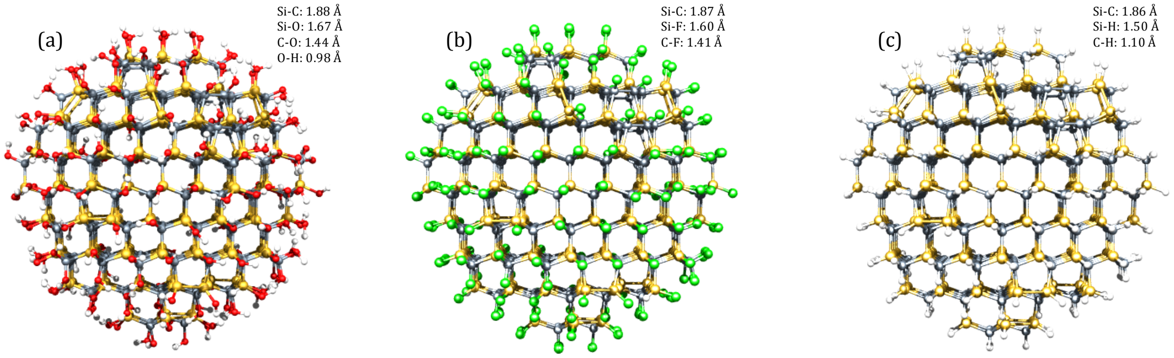

Fig. 1 Geometrically relaxed 22 Å diameter structures and bond lengths of 4H-SiC QDs (a) with OH termination, (b) with F termination and (c) with H termination. Color code as follows yellow: Si, gray: C, white: H, red: O, green: F.

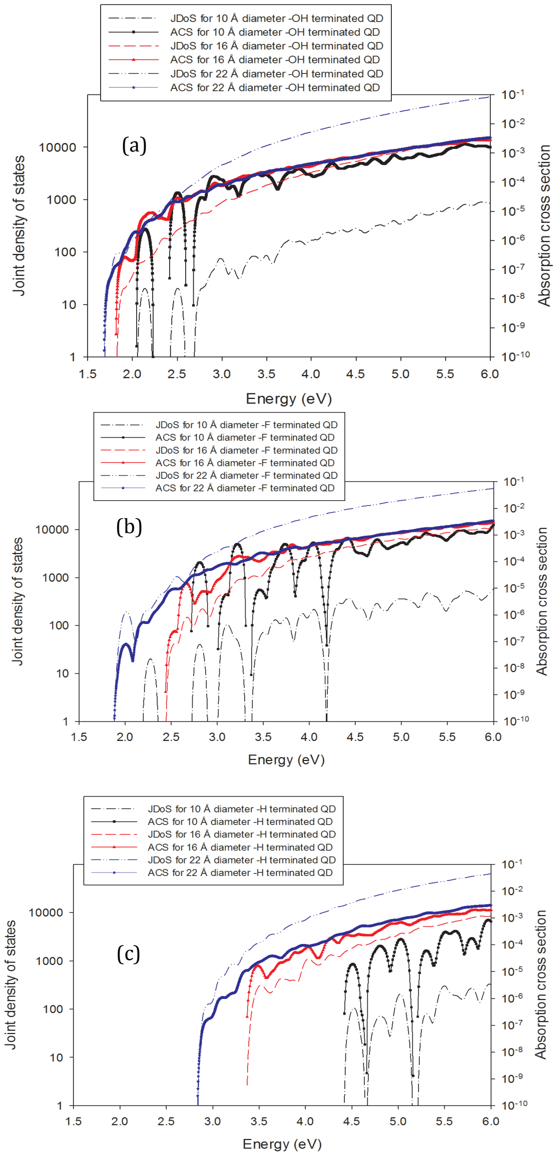

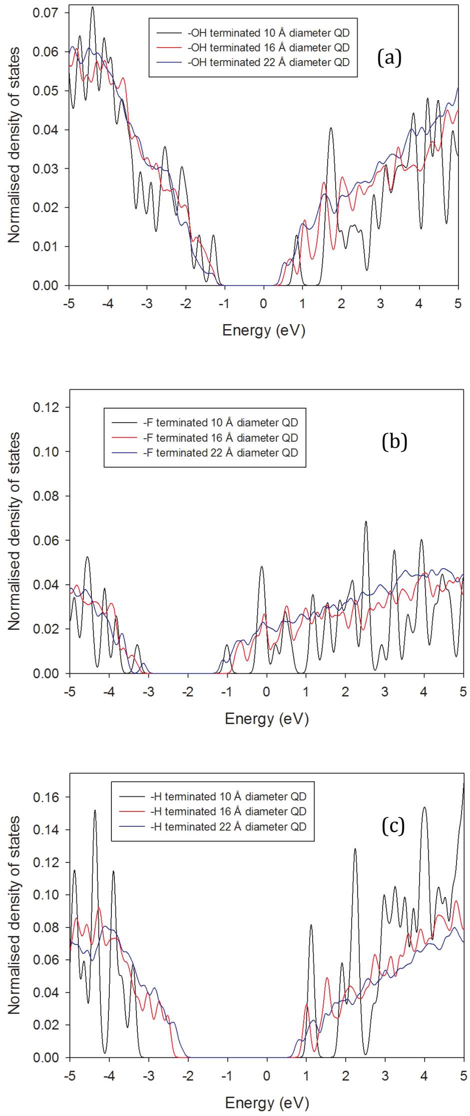

Fig.2 QD size dependent joint density of states (JDoS) and absorption cross section (ACS) for (a) OH termination, (b) F termination and (c) H termination.

Fig.3 QD size dependent density of states (DoS) for (a) OH termination, (b) F termination and (c) H termination.

Mo0955

Characterisation of Interfaces in 4H-SiC High-κ MOS Structures

S. K. Roy[1)], K. V. Vassilevski[1)], N. G. Wright[1)], A. B. Horsfall[1)]
[1)] School of Electrical and Electronic Engineering, Merz Court, Newcastle University,
Newcastle Upon Tyne, NE1 7RU, United Kingdom
E-mail: s.k.roy@ncl.ac.uk

Silicon carbide (SiC) is a suitable semiconductor for the realization of micro and nano scale electronic devices that operate in high-power, high frequency, and/or high-temperature environments [1]. Thermal oxidation of the SiC surface leads to a higher interface states density (D_{it}) than is observed in equivalent SiO_2/Si structures [1], although successful routes to reduce D_{it} have been demonstrated, such as thermal treatments involving NO and N_2O [2]. The integration of high-κ gate oxides in SiC based MOS devices has attracted a great deal of attention due to the possibility of enhanced electrical strength and stability [3]. In addition to the application in MOSFETs, high-κ dielectrics on SiC are a popular structure for monitoring environmental conditions within hazardous ambients. The SiC-based Metal-Insulator-Semiconductor (MIS) capacitor, which uses a catalytic gate contact such as Pt, Pd and dielectric layer such as TiO_2, HfO_2 has been shown to act as a suitable means to discriminate between different gases in a mixture at extreme temperatures [4]. Data has shown that selectivity of the sensors to different gases is dominated by the behaviour of defects at the interface between the dielectric film and the underlying SiC [4]. A monolithic SiC-based gas sensor array comprising capacitor structures which are compatible with CMOS processing and capable of discriminating between the constituents of mixed gas species under harsh environments has been studied to understand the behaviour of the SiC/dielectric and dielectric/metal interfaces. This monolithic device comprises capacitors fabricated with HfO_2 and TiO_2 based enhancement layers in the dielectric and Pt and Pd as contact metals.

SiC-based monolithic MOS capacitor structures have been fabricated on the silicon face of 4H-SiC epilayers with a nitrogen concentration of 1×10^{17}cm^{-3}. A 25nm thermal oxide layer high-κ dielectric layers comprising 50nm of HfO_2 and 57nm of $TiO_{2,}$ grown using a method similar to that described in [3]. The top contact was formed from 70nm of e-beam evaporated Pt or Pd with a 5nm Ti adhesion layer, to form a MIS structure, as shown schematically in Fig. 1. The characteristics of the monolithic MOS capacitors have been evaluated between 289K and 698K. The data shows that the D_{it} values extracted using the Terman technique reduces with increasing temperature due to the difference of bond energy between C–H and Si–H in n type 4H-SiC.

The data in Fig. 2 shows values of oxide capacitance (C_{ox}) extracted from the accumulation region of the C-V characteristics. The data indicates a high level of dielectric stability over the temperature range studied. Fig. 3 shows the variation of flat band voltage with temperature. The data given in Fig. 4 shows the variation of D_{it} at the mid gap as a function of temperature, which have been extracted by using the Hill-Coleman technique. Macfarlane *et al* reported the observation of dangling bonds of C atoms at the SiO_2 /SiC interface by electron paramagnetic resonance [5], results that there are dangling bonds of both Si and C atoms at the SiO_2 /n-type 4H–SiC interface, which is the origin of the interface states. The reduction in D_{it} occurs cause of the bond energy of C–H which is higher than that of Si–H. Devices utilising a HfO_2 dielectric have a lower D_{it} than those based on TiO_2 for both contact metals, probably because of superior interface quality of HfO_2.

The data in Fig. 5 shows the temperature dependence of the DC leakage characteristics of the capacitor structures. Curves have been fitted, by modifying the C_1 and φ_A parameters [6]. Where the parameters used were φ_A= 0.4eV or 0.5eV and $C_1 = 1\text{x}10^{-8}\text{cm}\Omega^{-1}$ or $2.1\text{x}10^{-6}\text{cm}\Omega^{-1}$ for the devices utilising a Pd and Pt gate contact respectively [7]. This result suggests that the bulk properties of the dielectric layer are constant, suggesting that the TiO_2 and HfO_2 layers are stable across the temperature range. TiO_2 high-*κ* dielectric layer have a leakage current larger than for those with HfO_2, due to the wider bandgap of HfO_2 (5.7eV) producing larger band offsets than TiO_2 (3.5eV) [8]. The data shows that the leakage through the TiO_2 MOS structure is catalytic material dependent, whilst HfO_2 show negligible dependency on choice in contact material.

For the surface characterisation of the TiO_2 and HfO_2, XPS and AFM analysis have been performed. The data in Figs. 6 and 7 show the high-resolution XPS spectra of TiO_2 and HfO_2 respectively. The Ti $2p_{1/2}$ and Ti $2p_{3/2}$ spin-orbital splitting photoelectrons for the sample are located at binding energies of 458.3eV and 464.19eV, respectively, which is in agreement with the reported literature values [9], showing the presence of Ti^4+. The Hf $4d_{5/2}$ and $4d_{3/2}$ peaks are at 211.2 eV and 222.0 eV respectively showing the presence of Hf [10]. Fig. 8 shows the 3 μm × 3 μm AFM images for the TiO_2 and HfO_2 surface. TiO2 has surface roughness (*rms*) 0.974 nm and HfO_2 has 0.544 nm. The data in the figure shows a significant difference in surface roughness between TiO_2 and HfO_2. Related to the increase in grain size after oxidation, resulting in a higher roughness for TiO_2. The higher leakage current for the TiO_2 devices is due the higher surface roughness and non-stoichiometric sturctures.

[1] J. B. Cassady *et al.,* Soli State Electronics, vol. 39, (1996), p. 1409 n
[2] V. V. Afanas'ev, *et al*., Appl. Phys. Lett., vol. 82, (2003), p. 568
[3] R. Mahapatra, *et al*., Appl. Phys. Lett., vol. 92, (2008), p. 042904
[4] S.K. Roy, *et al*., Proceedings of IEEE Sensors Conference 2013, pp 250

Mo0955

[5] P. J. Macfarlane *et al.,* Mater. Res. Soc. Symp. Proc. Vol. 51 (1991), p.572
[6] P. Fiorenza *et al.,* Journal of Appl. Phys. Vol. 98, (2005), p. 044312
[7] M.H. Weng *et al*., Sensors Journal, IEEE, vol. 7, (2007), p. 1395
[7] G. D. Wilk et al., Journal of Appl. Phys., vol. 89, (2001), p. 5243
[8] H.M. Liu *et al.,* Langmuir, vol. 19**,** (2003), p. 3001
[9] R. Nyholm *et al.,* J. Phys. C: Solid St. Phys., vol 13, (1980), p. L1091

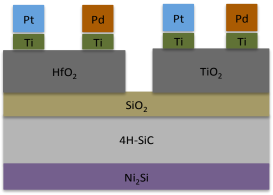

Fig. 1: Schematic cross section of monolithic MOS capacitor

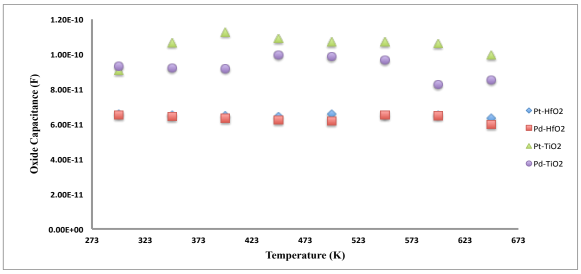

Fig. 2: C_{ox} as a function of temperature of monolithic MOS capacitors

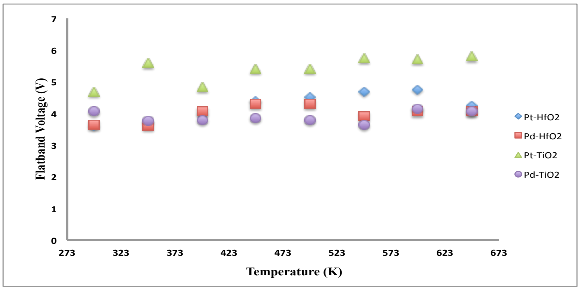

Fig. 3: V_{fb} as a function of temperature of monolithic MOS capacitors

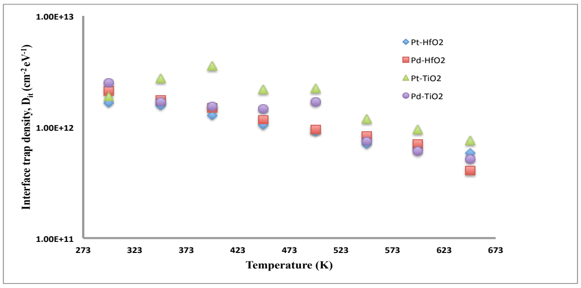

Fig. 4: D_{it} as a function of temperature of monolithic MOS capacitors

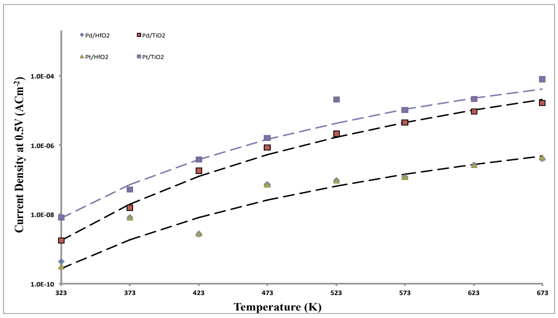

Fig. 5: J as a function of temperature of monolithic MOS capacitors

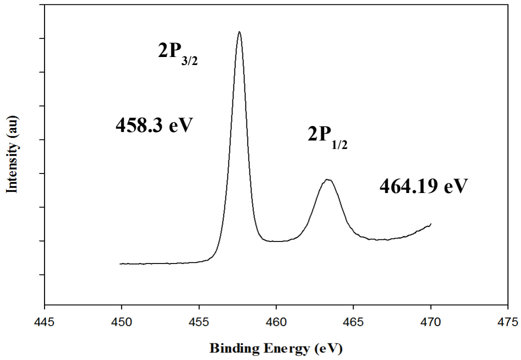

Fig. 6: High resolution XPS spectra of Ti 2p

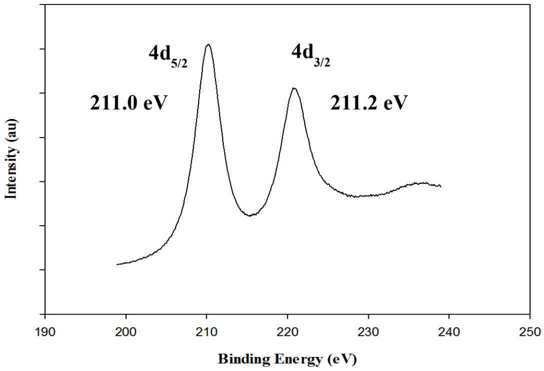

Fig. 7: High resolution XPS spectra of Hf 4d

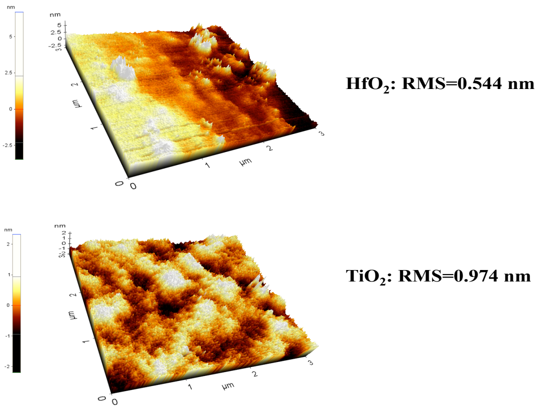

Fig. 8: 3D AFM images of TiO_2 and HfO_2 Surface

Nanowires

Vertically aligned semiconductor nanowires and their applications

T. Fukui[1*], E. Nakai[1], F. Ishizaka[1] and K. Tomioka[1,2]
[1]RCIQE, Hokkaido University, Kita 13, Nishi 8, Sapporo 060-8628, Japan,
[2]Japan Science and Technology Agency-PRESTO, Kawaguchi, Saitama 332-0012, Japan,
*fukui@rciqe.hokudai.ac.jp

We report on the systematically controlled growth of GaAs and InP and related III-V compound semiconductor nanowire arrays by catalyst-free selective area metalorganic vapor phase epitaxy on partially masked (111) oriented substrates. First, we discuss selective area growth mechanism including hetero-epitaxy on silicon, poly-siricon and graphene. Vertically alined nanowire array was grown uniformly on non-polar silicon substrates[1-3]. We also grow InAs nanowire on sigle layer graphene uising van der Waals epitaxy mode.

Next, we demonstrate photovoltaic and electron device applications. We fabricated photovoltaic devices using the core–shell pn junction InP nanowire array on the p-type InP (111)A substrates with and without AlInP window layer [4,5]. After nanowire growth, the space between nanowires was filled with a resin, and an ITO film electrode was then sputtered onto the nanowire array. The device with window layer has the short-circuit current density, J_{SC} of 23.4 mA cm^{-2}, open-circuit voltage V_{OC} of 0.457 V, and fill factor FF of 0.596 for an overall conversion efficiency of 6.35%, which are higher than those without window layer (3.59%). The J_{SC} of the CMS NWSCs is close to 80% that of the best InP planar solar cell reported even though their absorption volume is only 8% for the total epitaxial layer thickness of the best planar cell (3.5 micron). Similar surface passivation effect was also observed for GaAs/InGaP CMS NWSCs. Conversion efficiency improved from 0.71% to 4.01% by introducing InGaP layer. We also discuss a posibility of ‘flexible nanowire array’ without the substrates. It is easy to remove the wire part after all the device processes, and the substrate can be reproducibly used. This flexible device has the advantage in that it needs two orders less of semiconducting materials.

Finally, we demonstrate nanowire FETs on silicon. We fabricate surrounding-gate transistors using InGaAs nanowires and InGaAs/InP/InAlAs/InGaAs core–multishell nanowires as channels. Surrounding-gate transistors using core–multishell nanowire channels with a six-sided, high-electron-mobility transistor structure greatly enhance the on-state current and transconductance while keeping good gate controllability [1,6]. These devices provide a route to making vertically oriented transistors for the next generation of field-effect transistors and may be useful as building blocks for wireless networks on silicon platforms. We also fabricate tunneling field-effect transistors (TFETs) using III-V nanowire/Si heterojunctions and experimentally demonstrate steep-slope switching behaviors using InAs NW/Si heterojunction TFET with surrounding-gate architecture and high-k dielectrics. Control of resistances in this device structure is important for achieving steep-slope switching. A minimum subthreshold slope (SS) of the TFET is 21 mV/dec at VDS of 0.10 – 1.00 V [7].

References

[1] K.Tomioka, et. al., *Nature* **488**, 189(2012)
[2] K. Ikejiri, et. al., *Nanotechnology*, **24** 115304 (2013)
[3] Y. J. Hong, J.W.Yang, et. al., Advanced Materials **25**, 6847 (2013)
[4] T. Fukui et. al. *AMBIO* **41** Suppl.2 119(2012)
[5] M. Yoshimura et. al. *APEX* **6** 052301(2013)
[6] K.Tomioka, et. al., Nano Letters **13**, 5822 (2013)
[7] K.Tomioka, et. al., J. Phys. D: Appl. Phys. Vol.47, 394001 (2014).

Mo1140

Selective-area Growth of Wurtzite InP/AlGaP Core-shell Nanowires Toward Direct-band-gap Green Emission

Fumiya Ishizaka[1], Yoshihiro Hiraya[1], Katsuhiro Tomioka[1, 2], and Takashi Fukui[1]

[1]Graduate School of Information Science and Technology, and Research Center for Integrated Quantum Electronics (RCIQE), Hokkaido University, Sapporo, Japan
[2]Japan Science and Technology Agency (JST) – PRESTO, Kawaguchi, Japan
Phone: +81-11-706-7173, E-mail: ishizaka@rciqe.hokudai.ac.jp

Semiconductor nanowires (NWs) have attracted considerable interest in the last decade because the crystal structure can be controlled by appropriately adjusting growth conditions [1]. Interestingly, band structure calculations for GaP and AlP predict that when their crystal phases are changed from zinc blende (ZB) to wurtzite (WZ), their band gaps also change from indirect to direct [2]. Recently, these predictions are experimentally confirmed by the WZ GaP nanowires, suggesting the direct-band-gap transition at 2.09 eV [3]. This direct-band-gap WZ GaP may increase the efficiency of green light-emitting diodes and close the green gap issue. However, further understanding of WZ AlGaP is necessary to obtain pure green emission. Here, we report on the selective-area growth of WZ InP/AlGaP core-shell nanowires and their structural and optical characterization.

First, a 20-nm-thick SiO_2 film was deposited on an InP (111)A substrate by plasma sputtering, and hexagonal-opening patterns were defined by electron beam (EB) lithography and wet chemical etching. Selective-area growth of InP nanowires were performed at 660 °C with a V/III ratio of 18, which is the typical condition for growing WZ structures [1]. Low temperature AlGaP interlayer was then grown at 600 °C to prevent InP nanowires from P desorptions, followed by AlGaP shell growth at 700–750 °C. Quantum well stuctures were fabricated in the AlGaP shell by changing the Al composition.

Figure 1(a) shows a scanning electron microscopy (SEM) image of InP/AlGaP core-shell nanowires, showing a high uniformity despite the large lattice mismatch of InP/AlGaP. Transmission electron microscopy (TEM) and the corresponding fast Fourier transform (FFT) images of the AlGaP shell grown on the top and side of the InP core are shown in Figs. 1(b) and (c), respectively. These images reveal that ZB AlGaP was grown on the top and WZ AlGaP was grown on the side. This is because the ABAB... stacking sequence of the WZ phase is strongly fixed in the lateral direction, while both the WZ and ZB phases are geometrically possible in the axial direction. Figure 1(d) shows a cross-sectional STEM image of an InP/AlGaP core-shell nanowire, indicating that the quantum well structure was successfully fabricated in the AlGaP shell. The Al composition of barrier layers and quantum well layer were respetively 50% and 20%, which were determined by energy-dispersive X-ray spectroscopy (EDX) measurements. Cathode luminescence (CL) spectrum of the core-shell nanowire is shown in Fig. 1(e). The CL emission from the AlGaP shell was observed at 2.37 eV, showing a possibility of the direct-band-gap green emission.

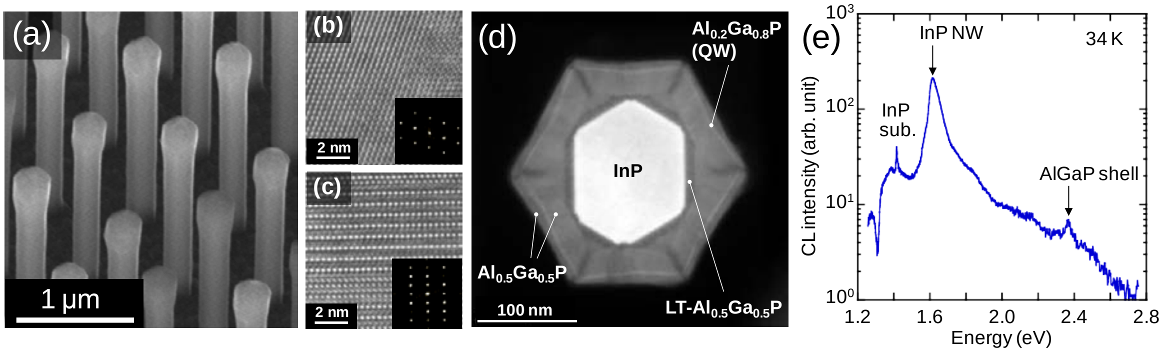

Fig. 1 (a) SEM image of InP/AlGaP core-shell NWs. TEM and FFT (inset) images of AlGaP shell grown on (b) top and (c) side of the InP NW. (c) Cross-sectional STEM image. (e) Cathode luminescence spectrum.

References: [1] Y. Kitauchi *et al.*, Nano Lett. **10**, 1699 (2010). [2] A. De *et al.*, Phys. Rev. B, **81**, 155210 (2010). [3] S. Assali *et al.*, Nano Lett., **13**, 1559 (2013).

Mo1145

Scanning Tunneling Microscopy on Semiconductor Nanowire Surfaces and Devices

J. Knutsson[1], M. Hjort[1], J. Webb[1], O. Persson[1], S. Lehmann[1], L. Samuelson[1], K.A. Dick[1], R. Timm[1],and A. Mikkelsen[1*]

[1] *Department of Physics, Nanometer Structure Consortium (nmC@LU), Lund University, Box 118, 221 00 Lund, Sweden*

III-V semiconductor nanowires (NWs) offer exciting possibilities for device application in solid-state lightning, energy conversion, and information technology [1]. With their small diameter and their very large surface-to-volume ratio, the NW device behavior is strongly influenced by their surface structure. Thus, it is very relevant (but challenging) to image their atomic scale surface structure and to combine this information with electrical measurements on individual NWs.

Recently, we have managed to remove the native oxide from several types of III-V NWs and image the atomic arrangement of the clean sidewall surfaces with scanning tunneling microscopy (STM). Here, we present STM images of various III-V NW surfaces of both wurtzite (Wz) and zincblende (Zb) crystal structure [2], focusing on the InAs and GaAs materials. While all non-polar III-V nanowire surfaces observed until now have appeared unreconstructed and unpinned, we find that polar NW surfaces exhibit reconstructions not found on planer substrates. This was investigated by studying specially tailored InAs Nws wires which consisted of segments with both {10-10} and {11-20} Wz facets and twinned superlattices in zincblende, with overgrowth transforming {111}A/B-type facets to non-polar {110}-type.

By combining STM imaging with scanning tunneling spectroscopy (STS) measurements, we simultaneously study the surface structure and local electronic properties across the interfaces of NW heterostructures, both at room temperature [3] and now at 5K. We find that the non-polar facets are unreconstructed and that STS data of defect free surfaces will correspond to the bulk electronic properties, allowing for determination of valence and conduction band edges as well as band alignments. We were also able to study individual defects such as atomic steps and stacking faults and their influence on the local electronic structure.

For correlating local structural and electronic characterization with transport measurements of NW devices, we have developed a novel device setup for direct STM measurements on NW devices that can be Hydrogen cleaned to more than 400C without deteriorating device performance. We show initial results of this unique approach on InAs NWs demonstrating atomic resolution on the NW during device operation. Using this approach, we can observe defect migration on the NW surfaces. In a reverse experiment, we have used our combined STM/AFM tip as local gate and then measured the resulting I(V) behavior through Esaki diode NWs as a function of tip position achieving a resolution of ~5nm[4].

To measure the electrical behavior of the individual as-grown NWs in an upright-standing configuration without any sample processing we have developed an alternative setup where the STM tip is used to first image free-standing NWs from the top and then form a point contact [5,6]. We will demonstrate how this method is used to establish low-resistive Ohmic contacts to individual InAs NWs [6], with the aim to understand the effect of the surface Oxide removal on NW performance.

[1] J. Wallentin *et al.*, Science **339**, 1057 (2013)

[2] M. Hjort *et al.*, Nano Lett. **13**, 4492 (2013)

[3] M. Hjort *et al.*, ACS Nano **6**, 9679 (2012)

[4] J. L. Webb *et al.*, Nano Res., **7**, 877 (2014)

[5] D. B. Suyatin *et al.*, Nature Commun. **5**, 3221 (2013)

[6] R. Timm *et al.*, Nano Lett. **13**, 5182 (2013)

---

* Corresponding author email: anders.mikkelsen@sljus.lu.se

Mo1145

Scanning Tunneling Microscopy on Semiconductor Nanowire Surfaces and Devices

J. Knutsson[1], M. Hjort[1], J. Webb[1], O. Persson[1], S. Lehmann[1], L. Samuelson[1], K.A. Dick[1], R. Timm[1],and A. Mikkelsen[1*]

[1]*Department of Physics, Nanometer Structure Consortium (nmC@LU), Lund University, Box 118, 221 00 Lund, Sweden*

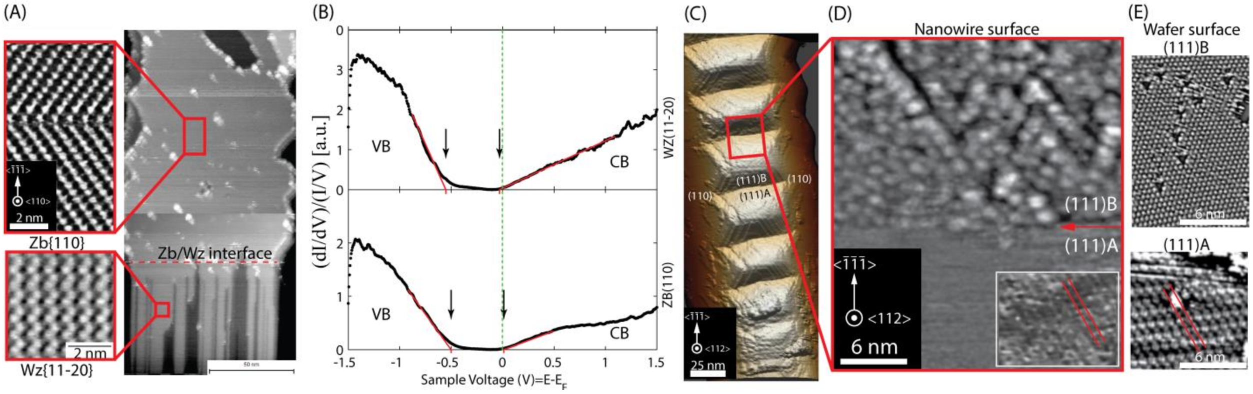

Figure 1. *STM results on InAs NWs. All images were obtained at negative sample bias. (A) STM image of interface between Zb {110} (top) and Wz {11-20} (bottom). Inset shows atomic structure of each facet. (B) STS data obtained on two neighbouring Wz and Zb facets in a single NW, depicting the local density of states.(C) Overview STM image of Zb twinned superlattice. (D) High resolution image of {111}A/B facet of NW TSL showing a highly reconstructed {111}B. Inset shows {111}A. (E) {111}A/B surfaces of substrate wafers for comparison.*

---

* Corresponding author email: anders.mikkelsen@sljus.lu.se

Mo1150

Orientation Dependent Luminescence of Nitride Nanowire Surfaces

D. Frank Ogletree, Shaul Aloni, Tevye Kuykendall and Virginia Altoe
Molecular Foundry, Lawrence Berkeley National Lab,
Berkeley, California 94720 USA

GaN nanowires and related heterostructures are highly luminescent and have potential applications ranging from solid-state lighting to photocatalysis. The local optical properties of nanoscale structures can be investigated by cathodoluminescence spectroscopy. A focused electron beam is used for excitation, and the resulting luminescence is collected in the far field, allowing deep sub-wavelength characterization of various optical processes including band-edge and defect-controlled recombination of excited carriers. The excitation volume depends on the composition of the nanowire and the kinetic energy of the incident electron beam, and lateral spatial resolution of 20 nm can be obtained. The excitation depth also depends on kinetic energy. When a 1 kV electron beam is incident on GaN, the excitation depth is only ~ 10 nm, while at 10 kV the excitation depth is ~ 50 times greater, allowing the full volume of the nanowire to be excited. In this way surface and "bulk" contributions to nanowire luminescence can be separated.

The nanowires used in this study were grown by MOCVD and have a triangular cross-section oriented perpendicular to the a- or m- crystal planes.[1] The nanowire cross sections are close to an equilateral triangle, with each orientation terminated by with two equivalent crystal planes and the GaN basal plane. Under certain growth conditions, the nanowire growth direction can change, and a nanowire originally growing along the a-axis can change direction to m-axis growth. TEM studies show such wires are continuous single crystals without stacking faults or grain boundaries. The figure shows excitation-energy dependent CL spectra from the a-axis base (red) and m-axis tip (blue), along with spectrally-filtered CL maps showing near band-edge (370 nm) and defect (410, 510 nm) contributions. Even though the volume of the m-axis tip is smaller, the CL intensity is greater than for the a-axis base. At the lowest (1 kV) energy, band-edge luminescence from the a-axis region is completely quenched, showing the influence of surface crystal plane termination. The influence of surface orientation on surface recombination will be discussed.

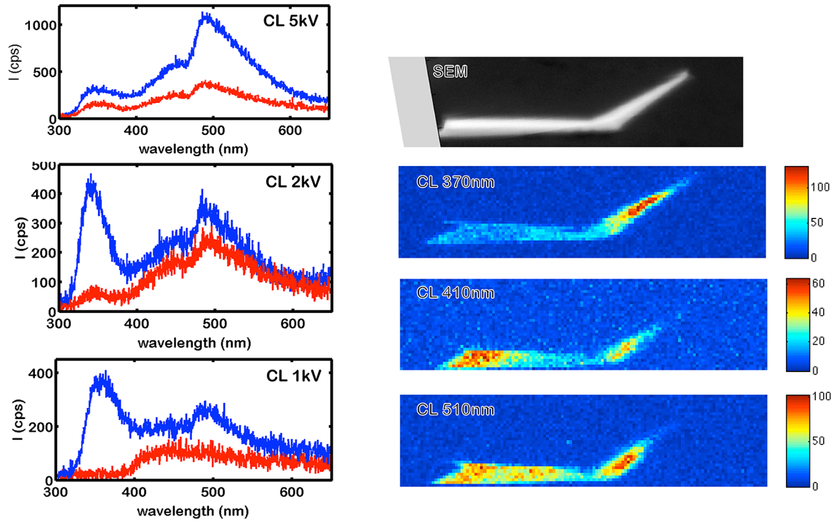

This work was performed at the Molecular Foundry and the National Center for Electron Microscopy, Lawrence Berkeley National Laboratory, with support from the U.S. Department of Energy Office of Science, Office of Basic Energy Sciences under Contract DE-AC02-05CH1123.

1) "Catalyst Directed Crystallographic Orientation Control in GaN Nanowires", T.R. Kuykendall, M.V.P. Altoe, D.F. Ogletree and S. Aloni, (submitted).

Complex Oxides & Ferroelectrics I

Mo1400 Invited

Understanding oxide interfaces: From microscopic imaging to electronic phases

Shahal Ilani

Department of Condensed Matter Physics, Weizmann Institute of Science.

In the last decade, the advent of complex oxide interfaces has unleashed a wealth of new possibilities to create materials with unexpected functionalities. A notable example is the two-dimensional electron system formed at the interface between $LaAlO_3$ and $SrTiO_3$ (LAO/STO), which exhibits ferromagnetism, superconductivity, and a wide range of unique magneto-transport properties. A key challenge is to find the microscopic mechanisms that underlie these emergent phenomena. While there is a growing understanding that these phenomena might reflect rich structures at the micro-scale, experimental progress toward microscopic imaging of this system has been so far rather limited due to the buried nature of its interface. In this talk I will discuss our experiments that study this system on microscopic and macroscopic scales. Using a newly-developed nanotube-based scanning electrometer we image on the nanoscale the electrostatics and mechanics of this buried interface. We reveal the dynamics of structural domains in STO, their role in generating the contested anomalous piezoelectricity of this substrate, and their direct effects on the physics of the interface electrons. Using macroscopic magneto-transport experiments we demonstrate that a universal Lifshitz transition between the population of d-orbitals with different symmetries underlies many of the transport phenomena observed to date. We further show that the interactions between the itinerant electrons and localized spins leads to an unusual, gate-tunable magnetic phase diagram. These measurements highlight the unique physical settings that can be realized within this new class of low dimensional systems.

Local Manipulation of Electronic Transport in Ferroelectric and Complex Oxides

Petro Maksymovych
Center for Nanophase Materials Sciences
Oak Ridge National Laboratory, Oak Ridge, TN, 37831, USA

Transport measurements typically aim to identify electronic ground states, thus avoiding large electric fields, hysteresis, chemical reactions and hot electrons. In this talk, I will discuss the opposite regime where a complex oxide surface is subjected to strong local field and/or force gradients and new transport properties emerge, often intertwined with intrinsic phase transitions or electrochemistry within the oxide lattice. I will present a generalized view of resistive switching phenomena induced by polarization switching in ferroelectric lead zirconate and bismuth ferrite, including the paradigmatic conductivity of ferroelectric domain walls. Our quest to improve and control the conductivity of domain walls has led to discovery of an insulator-metal transition in lead zirconate [1], which locally increases the electronic conductance of a nominally insulating oxide by 7-10 orders. This effect is observed any time a ferroelectric nanodomain (with the raidus of < 10 nm) is created by localized electric fields. We surmised that the conductance is controlled by tilted and charged walls of ferroelectric nanodomains. Moreover, it appears that a metal-insulator transition can be caused *within* a domain wall itself, with the insulating state behaving as a small polaron hopping conductor and still much more conducting that the parent insulating matrix. The basic underlying motif of carrier accumulation on charged domain walls also explains the conductivity of as-grown domain walls in bismuth ferrite, which need to be viewed as dynamic and hysteretic conductors [2]. On the other hand, local transport measurements on the surfaces of nominally conducting surfaces (such as manganites and nickel oxide) often induce an insulating state, the effect we refer to as 'piezochemistry' and assign to strain-induced redistribution of oxygen vacancies [3,4]. Curiously, strain and field control can be combined in these materials, allowing for facile patterning of surface and bulk regions of thin films, much like the established way to pattern domains in ferroelectrics. Overall, the coupling of local electrochemistry and transport or ferroic properties of complex oxides appears to be fundamentally important and may eventually develop into a deterministic methodology to control electronic phases. Finally, I will discuss our recent developments toward a quantitative methodology to differentiate between ferroelectric, piezoelectric, electret and ionic effects through a combination of local transport and strain measurements with scanning probe microscopy [5].

Experiments were conducted at the Center for Nanophase Materials Sciences, sponsored at Oak Ridge National Laboratory by the Division of Scientific User Facilities, U.S. Department of Energy. Work was also supported by the U.S. Department of Energy, Basic Energy Sciences, Materials Sciences and Engineering Division.

[1] P. Maksymovych, A. N. Morozovska, P. Yu, E. A. Eliseev, Y.-H. Chu, R. Ramesh, A. P. Baddorf, S. V. Kalinin, *Nano Lett.*,12, 209 (2012).

[2] P. Maksymovych, J. Seidel, Y. H. Chu, P. Wu, A. P. Baddorf, L.-Q. Chen, S. V. Kalinin, R. Ramesh, *Nano Lett.*, *11*, 1906 (2011).

[3] Y. Kim, S. Kelly, E. Strelcov, A. Morozovska, E. Eliseev, S. Jesse, N. Balke, I. Hwang, T. Choi, B. Ho Park, P. Maksymovych, S. V. Kalinin, *Nano Lett.* 2013, 13, 4068−4074 (2013).

[4] S. Kelly, Y. Kim, E. Strelcov, A. Morozovska, E. Eliseev, S. Jesse, N. Balke, I. Hwang, T. Choi, B. Ho Park, S. V. Kalinin, P. Maksymovych, *Nanotechnology* in press (2014).

[5] N. Balke, P. Maksymovych, S. Jesse, I. Kravchenko, Q. Li, S. V. Kalinin, *ACS Nano* (2014), 10.1021/nn505176a

Mo1520

Strain-Induced Energy Band Structure Changes inside $LaNiO_3/La_{2/3}Sr_{1/3}MnO_3/SrTiO_3$ Heterostructures

T. Asel,[1] H. Gao,[1] T. Heinl,[2] J. Hoffman,[3] A. Bhattacharya,[3] and L.J. Brillson[1,2†]

[1] The Ohio State University, Department of Physics, The Ohio State University, 191 West Woodruff Ave., Columbus, OH 43210 USA
[2] Department of Electrical & Computer Engineering, The Ohio State University, 205 Dreese Lab, 2015 Neil Ave., Columbus, OH 43210 USA
[3] Materials Science Division, Argonne National Laboratory, Argonne, Illinois 60439

We have used a differential form of depth-resolved cathodoluminescence spectroscopy (DRCLS)[1] to measure the optical transitions between unoccupied and highest occupied energy levels inside $LaNiO_3/La_{2/3}Sr_{1/3}MnO_3/SrTiO_3$ heterostructures,[2] the energy level changes at their interfaces, and the energy level shifts induced by applied mechanical strain. This differential technique enhances DRCLS depth resolution even further and enables direct measurements of energy level separations inside each of the epilayers and at their interfaces on a nanometer scale. A key goal of complex oxide research is the creation and control of spin states in heterojunctions and their superlattices using charge transfer, proximity effects, and locally broken symmetries. Biaxial strain using lattice mismatch can affect these processes by altering band alignments and local symmetries. Our work shows that uniaxial strain applied externally produces analogous changes that can be controlled without growing films on different lattice mismatched substrates.

Here we applied differential DRCLS to 30 nm $LaNiO_3$/ 30 nm $La_{2/3}Sr_{1/3}MnO_3$/ $SrTiO_3$ substrates as a function of incident beam energy $E_B = 0.5 – 5$ keV and applied uniaxial bending strain up to 2%. For $SrTiO_3$, the energy level diagram based on both theory and experiment[3] enables optical identification of the 3.2 eV indirect band gap (E_G), the 3.7 eV direct band gap (Γ-Γ), the 4.13 eV A_1, 4.64 eV A_2, and 5.05 eV A_3 transitions between the O *2p* valence band and Ti *3d* t_{2g} states as well as 1.57 eV Ti^{3+}, 1.9 eV V_{Sr}, and 2.97 eV V_O [4]defect states. For the $LaNiO_3$ epilayer, transitions from empty to highest filled states appear at 2.37, 3.03, 3.71, and 4.27 eV. For the $La_{2/3}Sr_{1/3}MnO_3$ epilayer, corresponding transitions appear at 4.17, 4.43 and 5.10 eV. With applied uniaxial strain, both energies and intensities of these transitions change. For $LaNiO_3$, the 2.37 and 3.03 eV transitions attributed to Ni 3d e_g orbitals shift up in energy by 20 and 50 meV, respectively. Higher lying orbital transitions also shift upward by 50-60 meV. These changes may also reflect expected Ni valence state shifts.[2] For $La_{2/3}Sr_{1/3}MnO_3$, the 4.43 and 5.10 eV transitions attributed to Mn 3d $e_g t_{2g}$ orbitals shift downward by 10 meV. Upward vs. downward shifts can be related to tensile strain and lattice distortion along d_{3z2-r2} vs. d_{x2-y2} orbitals, respectively. For $SrTiO_3$, the Γ-Γ direct gap shifts upward by 70 meV, the 3 eV V_O transition shifts upward by 30 meV while a 2.4 eV V_{Sr}-related defect transition shifts downward by 40 meV. These results show that strain-induced changes in energy level/band structure can be identified with specific layers and their interfaces within a heterostructure and their impact on charge transfer and local symmetry. Argonne National Laboratory work was supported by the U.S. Department of Energy, Office of Basic Energy Sciences.

[1] L. J. Brillson, *J. Phys. D: Appl. Phys.* **45**, 183001 (2012).

[2] J. Hoffman, B.J. Kirby, J. Kwon, J.W. Freeland, I. Martin,O.G. Heinonen, P. Steadman, H. Zhou, C. Schlepütz, S.G.E te Velhuis, J.-M. Zuo, and A. Bhattacharya, unpublished.

[3] K. Van Bentham, C. Elsässer, and R.H. French, *J. Appl. Phys.* **90**, 6156 (2001).

4 M.M.Rutkowski, K. McNicholas, Z. Q. Zeng, F. Tuomisto, and L. J. Brillson, *J. Phys. D: Appl. Phys.* **47**, 255303 (2014).

Mo1520

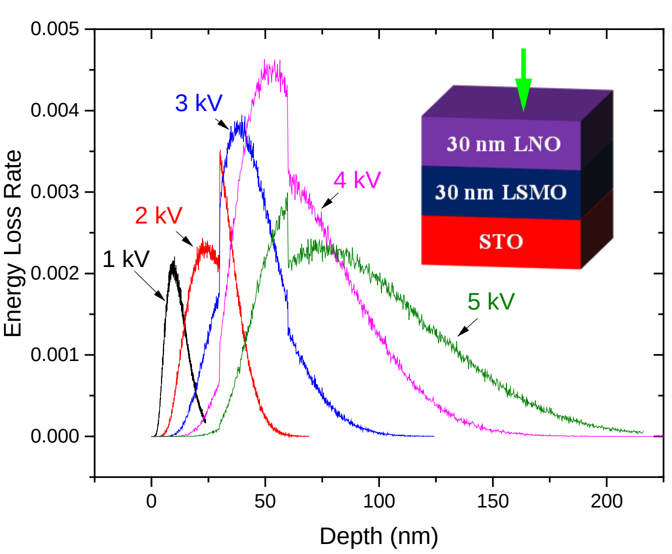

Fig. 1. Monte Carlo simulation of energy loss rate vs. depth for 30 nm $LaNiO_3$/30 nm $La_{2/3}Sr_{1/3}MnO_3$ on $SrTiO_3$. LNO/LSMO transition occurs at ~1.25 kV. LSMO/STO transition occurs at 2.5 kV.

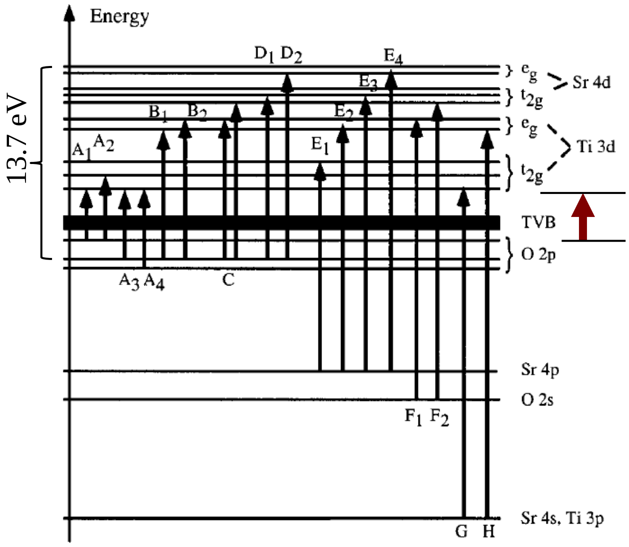

Fig. 2. Interband transitions determined from UV experiment and theory.[Bentham *et al.*, *J.Appl.Phys*. **90**, 6156 (2001).

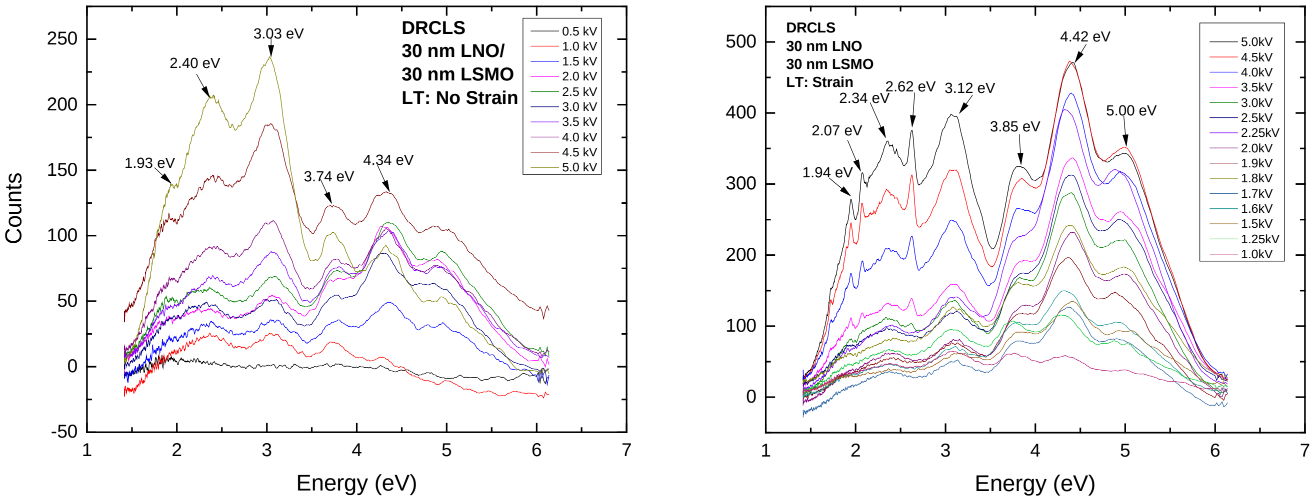

Fig. 3. DRCLS of 30 nm LNO/30 nm LSMO/STO at 80 K showing changes at ~1.5 and 3 kV before (left) and during (right) uniaxial strain.

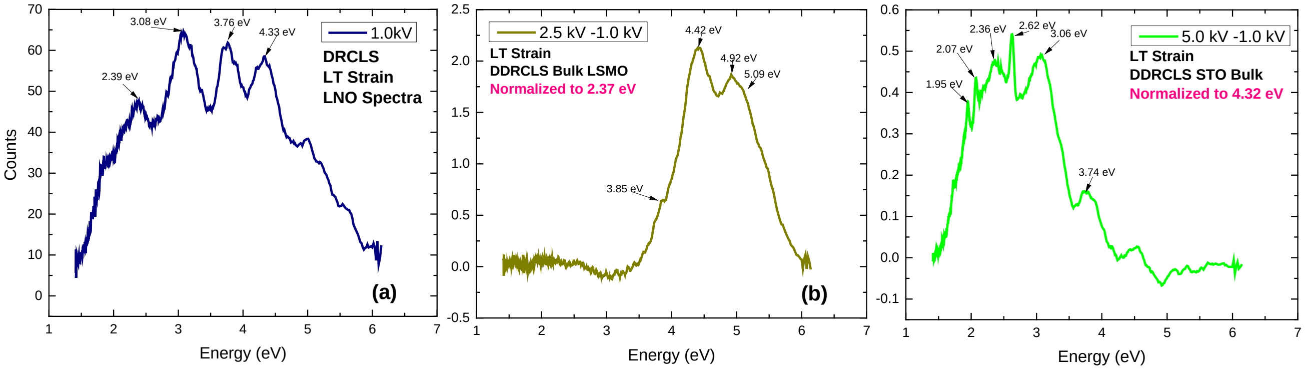

Fig. 4. Layer-specific LNO (a), LSMO (b), and STO (c) spectra. Sharp peaks in (c) are Fe defects in STO.

Mo1525

Carrier Density Modulation in Ge Heterostructure by Ferroelectric Switching

Patrick Ponath[a], Kurt Fredrickson[a], Agham B. Posadas[a], Yuan Ren[a], Xiaoyu Wu[a] , Rama K. Vasudevan[b],
M. Baris Okatan[b], S. Jesse[b], Toshihiro Aoki[c], Martha R. McCartney[d], David J. Smith[d], Sergei V. Kalinin[b],
Keji Lai[a], and Alexander A. Demkov[a]

[a]Department of Physics, The University of Texas at Austin, Austin, TX 78712, USA
[b]Center for Nanophase Materials Sciences, Oak Ridge National Laboratory, Oak Ridge, TN 37831, USA
[c]Center for Solid State Sciences, Arizona State University, Tempe, AZ 85287, USA
[d]Department of Physics, Arizona State University, Tempe, AZ 85287, USA

Germanium with its higher hole and electron mobility than silicon is an attractive candidate to realize a ferroelectric FET [1,2]. Here we report a true ferroelectric field effect – carrier density modulation in an underlying Ge(001) substrate by switching of the ferroelectric polarization in the epitaxial *c*-axis-oriented $BaTiO_3$ (BTO) grown by molecular beam epitaxy (MBE) on Ge.

The Ge surface was prepared using the method described in Ref. [3]. Prior to BTO growth, 5 unit cells of STO are deposited at 200°C. After increasing the temperature to 600°C to crystallize the STO, BTO is co-deposited on the STO/Ge template at a temperature of 650°C. Fig. S1a shows symmetric 2θ-θ scans of a 160-Å-thick BTO film grown on Ge, both with and without a 20-Å-thick STO buffer layer. The BTO peaks correspond to a single orientation with an out-of-plane spacing of 4.06 Å for the film with the STO buffer, and 3.98 Å for the film without the buffer, which clearly demonstrates the *c*-axis orientation for the STO-buffered sample.

Individual Ti, Ge, Sr and Ba atomic column locations can be identified in both bright-field and high-angle annular-dark-field images, while Fourier transforms of these images also confirm the tetragonality of the BTO with the longer *c*-axis pointing out of the plane (Fig. S2).

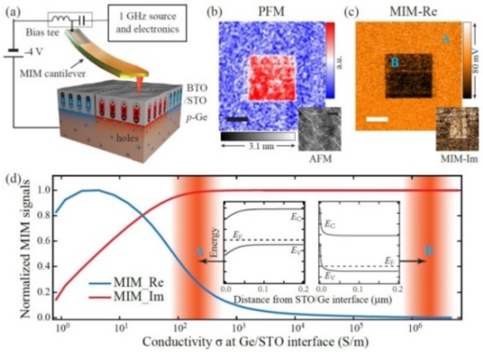

Figure 1: Ferroelectric switching and electrical detection using microwave impedance microscopy (MIM). (a) Schematic diagram illustrating the measurement setup and configuration of samples. PFM (b), AFM (bottom right corner in b), MIM real part (c) and MIM imaginary part (bottom right corner in c). (d) Simulated MIM-Re (blue line) and MIM-Im (red line) signals as a function of conductivity at the BTO/Ge interface. Left and right insets, respectively, show band diagrams of Ge in regions A and B in panel (c).

The ferroelectric properties of the BTO layer were tested using Band-Excitation Piezoresponse Force Microscopy (BE-PFM). Results from a typical BE-PFM switching experiment are shown in Figs. S3(a-c).

We demonstrate the ferroelectric field effect in the BTO/STO-Ge heterostructures using microwave impedance microscopy (MIM). After a 20×20 μm^2 square was written, the DC bias was removed and a larger region concentric with the previous scan was then imaged by the same tip using PFM and MIM, both of which show clear contrast between the written and unwritten areas (Fig 1b). In Fig. 1c, the poled area shows substantially lower MIM-Re and slightly higher MIM-Im signals than the intact region. Since neither the conductivity ($\sigma_{BTO} = 0$) nor the first-order dielectric constant (ε_{BTO}) of the BTO is affected by the polarization reversal, the MIM contrast must come solely from the underlying Ge layer accompanied by the poling process.

In conclusion, we clearly demonstrate the ferroelectric field effect for highly crystalline *c*-axis-oriented $BaTiO_3$, epitaxially grown on Ge(100) substrates using molecular beam epitaxy *via* a thin (20 Å) $SrTiO_3$ buffer layer. The ferroelectric properties of the BTO layer are confirmed using piezoelectric force microscopy and microwave impedance microscopy.

References: [1] Kamata, Y. *et al.* High-k/Ge MOSFETs for future nanodevices. Mater Today **11**, 30-38 (2008); [2] Fredrickson, K. D. *et al.* Atomic and electronic structure of the ferroelectric $BaTiO_3$/Ge(001) interface. Appl. Phys. Lett. **104**, 242908 (2014); [3] Ponath, P. *et al.* Preparation of clean Ge(100) surface using oxygen plasma cleaning. J. Vac. Sc. Technol. B **31**, 031201 (2013).

Mo1525

Supplement:

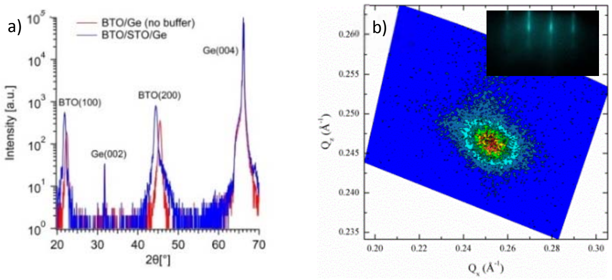

Figure S1: (a) X-ray diffraction 2θ-θ scan of 16 nm $BaTiO_3$ epitaxially grown on Ge(001) substrate, with and without a 2 nm $SrTiO_3$ buffer layer. With the STO buffer, the *c*-axis of BTO is directed out of plane. (b) Reciprocal space map of the (103) Bragg reflection for BTO/STO/Ge. Inset: RHEED of a 15 nm thick BTO/STO/Ge sample along the [110] direction

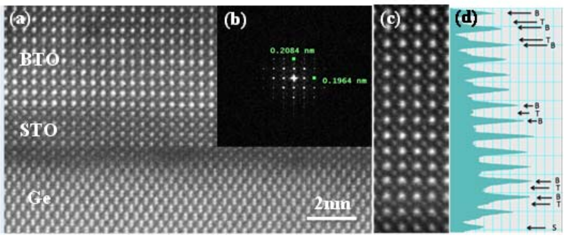

Figure S2: Aberration-corrected electron microscopy, (a) High-angle annular-dark-field (ADF) image of BTO/STO/Ge(001). (b) Fourier transform of ADF image confirming tetragonality of BTO layer; (c) Enlargement of ADF image showing region of BTO film; (d) Corresponding line profile from (c) showing shifts in Ti atomic-column positions.

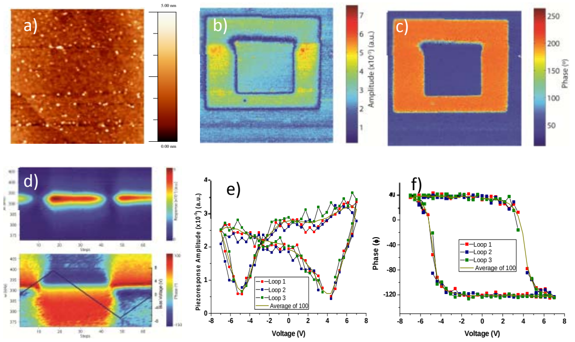

Figure S3: PFM and Voltage Spectroscopy of BTO heterostructures: (a) Topography, (b) BE-PFM amplitude and (c) associated phase image on the BTO heterostructure, showing clear ferroelectric switching. 100 hysteresis loops were then captured on the same film using BE spectroscopy. The average response is shown in the spectrograms in (d) for amplitude (above) and phase (below), with the applied DC waveform shown in blue. Selected amplitude and phase loops are shown in (e,f), respectively.

2D Materials

Mo1630 Upgraded

Sarah Howell
Abstract – PCSI 2015

Investigation of Band-Offsets at Monolayer-Multilayer MoS_2 Junctions by Scanning Photocurrent Microscopy

Sarah L. Howell,[1,4] Deep Jariwala,[1,4] Chung-Chiang Wu,[1,4] Vinod K. Sangwan,[1,4] Tobin J. Marks,[1,2,4] Mark C. Hersam,[1,2,3,4] and Lincoln J. Lauhon[1]
[1] *Department of Materials Science and Engineering, Northwestern University, USA*
[2] *Department of Chemistry, Northwestern University, USA.*
[3] *Department of Medicine, Northwestern University, USA*
[4] *Materials Research Center, Northwestern University, USA*

Transition metal dichalcogenides (TMDCs) such as MoS_2 consist of discrete two-dimensional (2D) layers bound together by van der Waals forces, with important consequences for both physical and electronic structure of these ultrathin semiconducting crystals. First, flakes exhibit discrete thickness-dependent variations in physical properties that are readily detected by optical microscopy. Second, the band structure varies with multilayer thickness, transitioning from a direct bandgap in single layer (1L) MoS_2 to an indirect bandgap in two-layer (2L) and multilayer materials. Finally, the large optical absorption cross-section of single layers motivates applications in photodetection and energy conversion.

The thickness-dependent band structure suggests the intriguing possibility of a semiconductor heterojunction in which discontinuities in the energy bands arise from abrupt discontinuities in physical thickness. While photovoltaic effects in 2D semiconductors have been exploited using asymmetric metal-semiconductor junctions and vertical heterojunctions, lateral semiconductor-semiconductor junctions are just beginning to be explored. Indeed, there has been recent significant progress in the controlled formation of lateral semiconductor heterojunctions in 2-D materials, however no report exists on the electrical properties of any lateral heterojunctions in TMDCs. Here we report the formation of abrupt, rectifying junctions at the interfaces of monolayer and multilayer MoS_2 films, and investigate the mechanisms of rectification and photocurrent generation using scanning photocurrent microscopy (SPCM) and finite element modeling. We explain the photocurrent generation under applied bias using a model incorporating a type II band alignment, and conclude that hot carriers contribute to energy conversion at zero applied bias. The utility of these junctions in photodetection and energy conversion applications is discussed.

Mo1630 Upgraded

Sarah Howell
Abstract – PCSI 2015

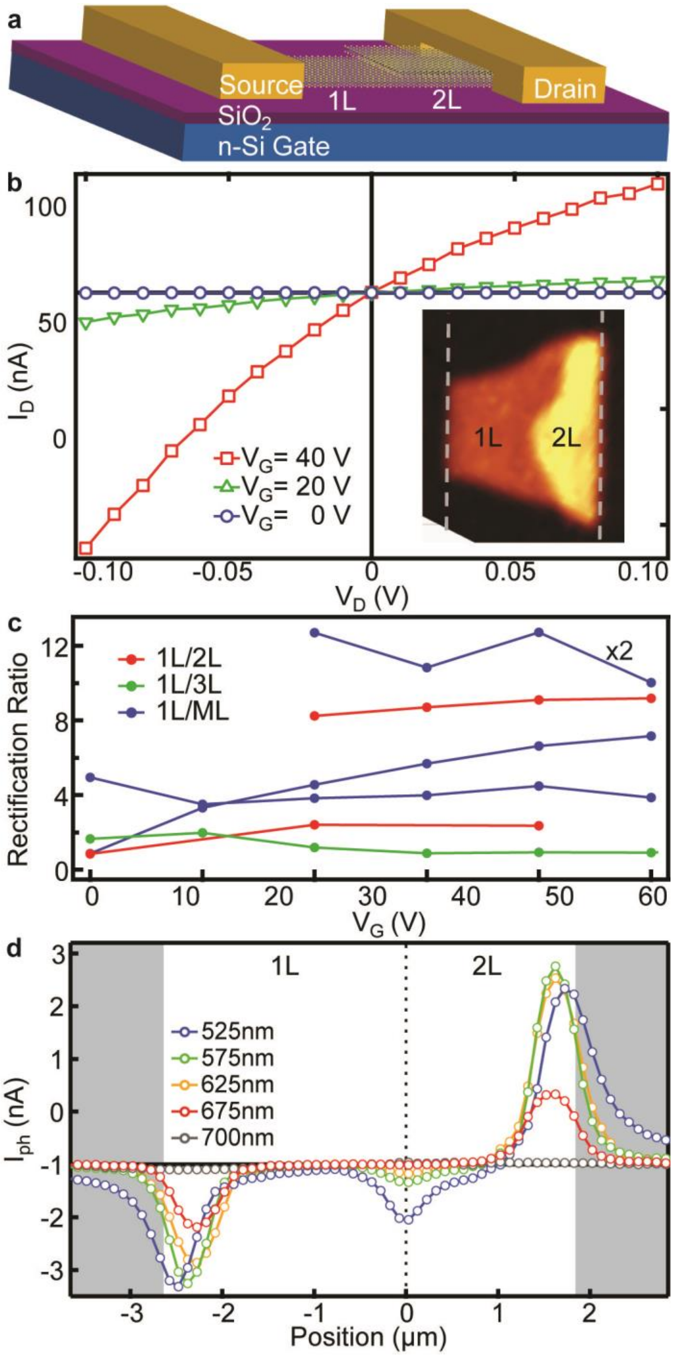

Figure 1: (a) Schematic side view of a 1L/2L MoS_2 junction FET. (b) Drain-source output curves under gate biases V_G= 0 V, 20 V, and 40 V. Inset of (b): Raman map of integrated intensity between 382 and 385 cm^{-1}. The dotted lines indicate source and drain contacts separated by 4.4 μm. (c) Rectification ratio of 1L/ML devices as a function of gate bias. (d) Zero-bias experimental SPCM profiles of a 1L/2L device at different excitation wavelengths. Gray areas indicate contact regions.

Mo1630 Upgraded

Sarah Howell
Abstract – PCSI 2015

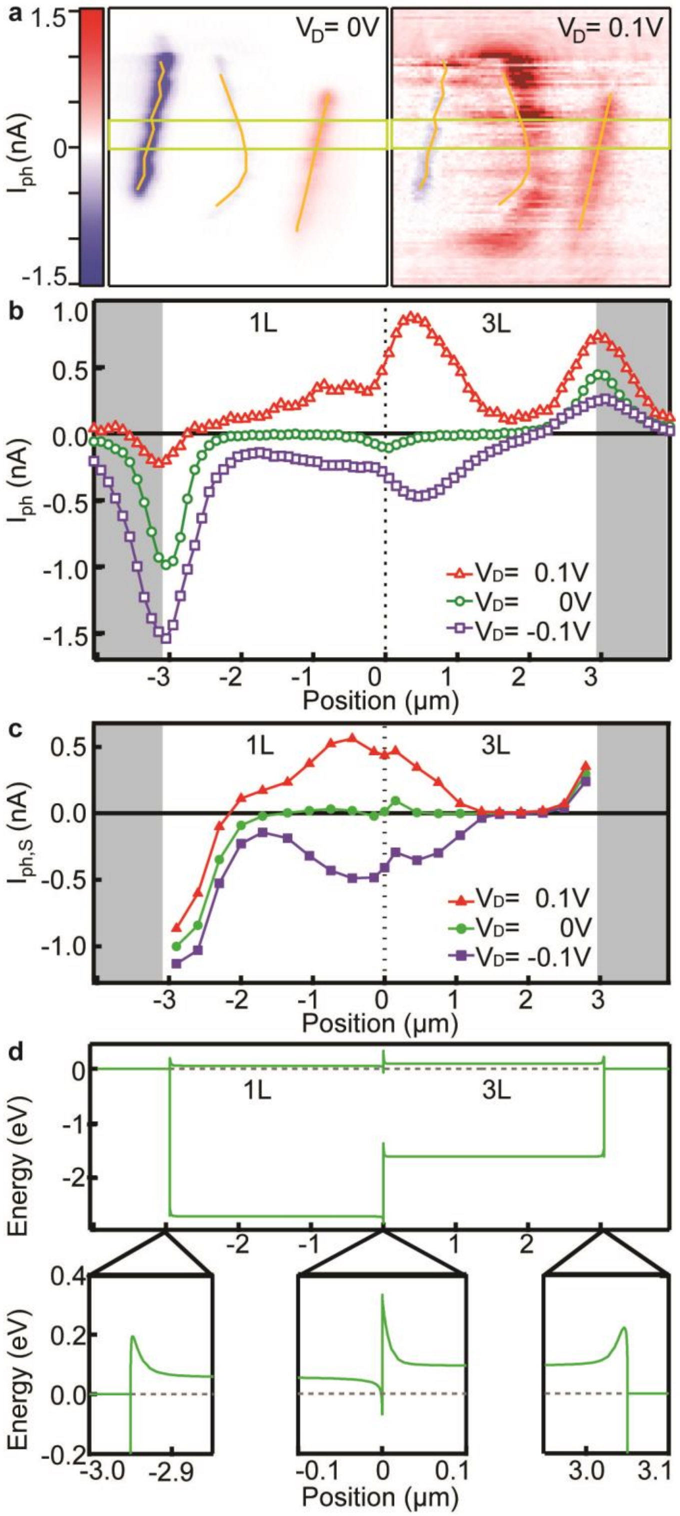

Figure 2: (a) Spatial photocurrent mapping of a 1L/3L device at V_{DS}= 0V and 0.1V (V_G=0, λ=525 nm). Yellow lines indicate approximate positions of the contacts and 1L/3L junction. (b) Photocurrent profiles at different biases averaged along the green boxes in (a). The gray areas and dotted line indicate contact locations and 1L/3L junction, respectively. (c) Simulated photocurrent generation. (d) Simulated band diagram.

Mo1650 Upgraded

Interfaces between transferred, CVD-grown graphene and MoS$_2$ probed with STM and ARPES

Horacio Coy Diaz1, Jose Avila2, Rafik Addou1, Maria Carmen Asensio2, Matthias Batzill1

[1]*Department of Physics, University of South Florida, Tampa, FL 33620, USA*
Email:mbatzill@usf.edu

[2]*Synchrotron Soleil, Orme des Merisiers - Saint Aubin, BP 48 - 91192 - GIF SUR YVETTE Cedex, France*

Heterostructures made of different van der Waals materials are of increasing interest because of potential applications in energy harvesting and combination of spin- and valley-tronics. However, the interface properties of these materials are not yet well characterized. One challenge for their characterization is the preparation of large-area high quality materials that enable employment of surface characterization techniques such as scanning probe microscopy and photoemission spectroscopy. Here we demonstrate the transfer of CVD-grown graphene to bulk MoS$_2$ substrates and report the first STM and ARPES studies of such a system. As expected for weakly interacting materials STM studies only exhibit a very weak moire-superstructure and (nano) ARPES measurements show that the Dirac cone of graphene is maintained. However, (nano) ARPES also shows the formation of band-gaps in the pi-band of graphene where the out-of-plane molecular orbitals of MoS$_2$ intersect with the electronic-states of graphene, as shown in Fig.1. This modification of the electronic structure of graphene in the graphene/MoS$_2$ heterostructure is contrary to expectations of simple van-der Waals stacked materials. The high quality of the samples will enable further studies of the spin state of the graphene and MoS$_2$ substrate as well as enable preparation of other heterostructure materials and thus will give a detailed description of the interaction in these heterostructure systems.

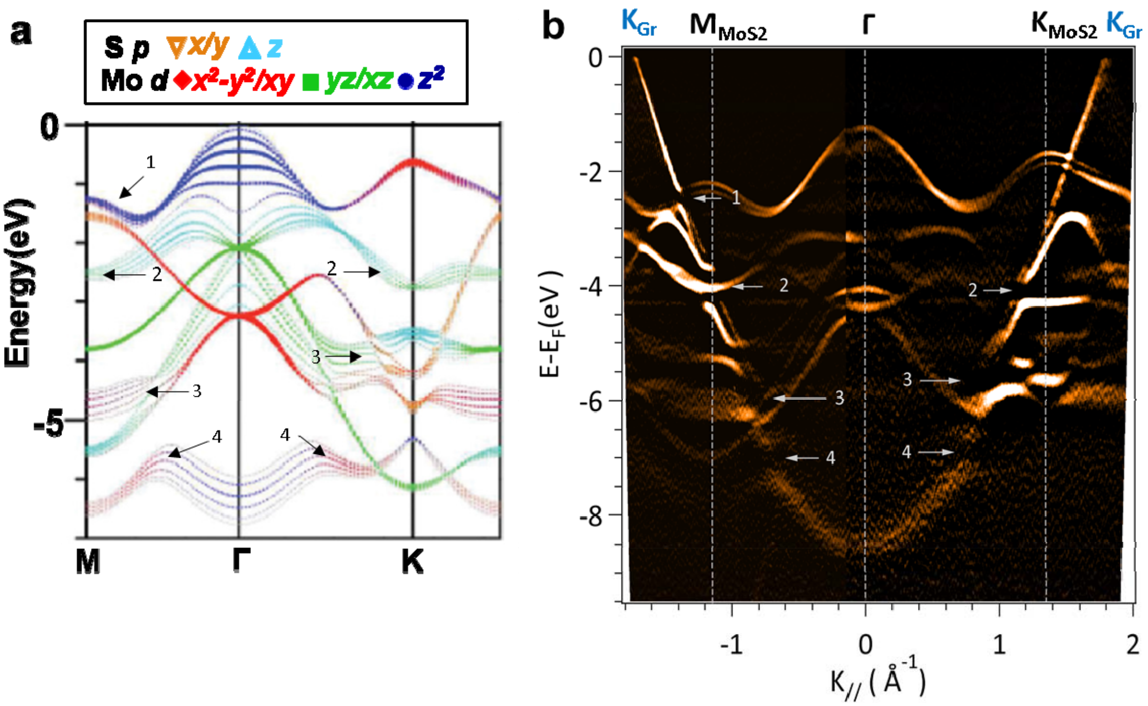

Fig. 1. (a) Calculated band structure of MoS2 with the orbital character of the individual bands color coded. Data reproduced from: Han, S.W., Cha, G.-B., Frantzeskakis, E., Razado-Colambo, I., Avila, J., Park, Y.S., Kim, D., Hwang, J., Kang, J.S., Ryu, S., Yu, W.S., Hong, S.C., Asensio, M.C. Band-gap expansion in the surface-localized electronic structure of MoS$_2$ (0002). Phys. Rev. B 86, 115105 (2012). (b) 2nd derivative of E-k ARPES spectrum of graphene/MoS$_2$. The observed band gaps in the graphene π-band are labeled and their position with respect to the MoS$_2$ band structure are indicated in (a). This illustrates that the band-gaps in graphene open where there π-band overlaps in energy and momentum with MoS$_2$ states that exhibit out-of plane orbital character.

Mo1710

Crystalline SrO(001) on graphene: a universal buffer layer for oxide integration

Adam Ahmed[1]*, Hua Wen*[2]*, Igor Pinchuk*[1]*, Tiancong Zhu*[1]*, Roland Kawakami*[1,2,*]
[1]Department of Physics, The Ohio State University, Columbus, Ohio 43210
[2]Department of Physics and Astronomy, University of California, Riverside, California 92521

Oxides are known for their multitude of electronic phases and interface chemistry. Particularly, transition metal oxides (TMO) are well known for their strong electron-electron (*e-e*) correlations and competing order between the Coulomb and exchange interactions in the presence of crystal field splitting. From these competing energies it is known that oxide materials have been shown to exhibit a wide range of thermodynamic and/or quantum phase transitions: magnetic ordering, ferroelectricity, colossal magnetoresistance, metal-insulator transitions, and high temperature superconductivity. In addition, the extreme sensitivity to crystalline distortions and chemical compositions offers a great deal of tunability of electronic and optical properties.

Our goal is to integrate TMOs with 2D materials such as graphene and merge the parameter space between the 2D Dirac-like properties of graphene and strongly correlated electron physics. However, epitaxial thin film growth on graphene has been challenging due to its weakly interacting van der Waals surface, and the growth of smooth, crystalline overlayers has been extremely limited. Our strategy is to develop a universal buffer layer on graphene. This approach was highly successful for integration of complex oxides onto silicon. High-κ dielectric $SrTiO_3$ was first grown on Si(001) using a Sr flux to desorb SiO_2 from the surface, followed by silicide formation with Sr to facilitate the growth of SrO and, subsequently, $SrTiO_3$.

Here, we demonstrate the molecular beam epitaxy (MBE) growth of crystalline SrO(001) on highly-ordered pyrolytic graphite (HOPG) and single-layer graphene as a universal buffer layer for oxide integration. From our growth study, we find that the optimal conditions are for room temperature growth with a relatively high growth rate of 100 Å/min. Atomic force microscopy (AFM) shows an rms roughness of ~1.2 Å for SrO/HOPG (Figure 1), and x-ray diffraction (XRD) shows out-of-plane orientation in the (001) direction. Since HOPG has in-plane rotational disorder, the epitaxial relationship between SrO and HOPG still remains unknown. Electrical measurement of SrO/graphene devices show that the Dirac point and mobility can be altered with post-oxidation of the SrO layer. Because many complex oxides have been grown on SrO-terminated surfaces, this can be regarded as a universal buffer layer for oxide integration. We demonstrate the proof-of-principle by successfully growing $SrTiO_3$ (001) on a SrO buffer layer on HOPG. This opens the door to integration of many other complex oxides to explore novel correlated electron physics in graphene.

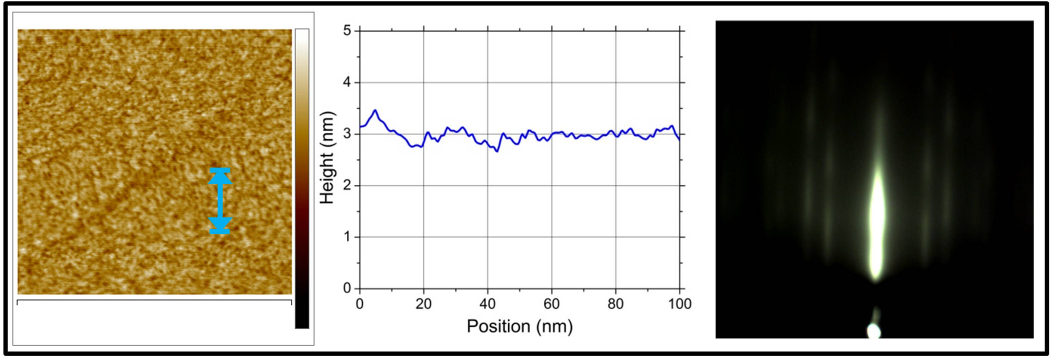

Figure 1. AFM image and RHEED pattern for a 3 nm SrO film on HOPG.

This work was supported by C-SPIN/STARnet sponsored by MARCO and DARPA, ONR (N00014-14-1-0350), ENCOMM, and NRI-NSF (DMR-1124601).

Optically Probing 2D Materials at Length Scales that Matter: Correlating Nanoscale Charge Recombination Heterogeneity and Surface Potential

Wei Bao[1,2]*, Nicholas Borys*[1]*, Changhyun Ko*[2]*, Sefaattin Tongay*[2]*, Wen Fan*[2]*,*
D. Frank Ogletree[1]*, Paul Ashby*[1]*, Miquel Salmeron*[1,2]*, Alex Weber-Bargioni*[1]*, Junqiao Wu*[2]*,*
P. James Schuck[1]

[1] *Molecular Foundry, Lawrence Berkeley National Laboratory, Berkeley, CA, United States.*
[2] *Department of Materials Science and Engineering, UC Berkeley, Berkeley, CA, United States.*
wbao@lbl.gov

The functionality of novel nanostructures depends strongly on local physical and electronic properties, increasing the importance of optically probing matter with true nanoscale spatial resolution. In previous work [1], we proposed a novel photonic-plasmonic hybrid Scanning Near-field Optical Microscopy (SNOM) probe called the "campanile" tip. These campanile tips couple the photonic to the plasmonic mode, then adiabatically compress the plasmon mode, over a broad bandwidth. Using these probes, we mapped carrier radiative recombination within individual CVD grown Molybdenum disulfide (MoS_2) flake, observing optoelectronic heterogeneity with deep subwavelength length scale. It had been previously shown that grain boundary and point defects will significantly change the photoluminescence (PL) emission property of these materials. Here, by combining near-field campanile hyperspectral imaging, scanning electron microscopy and high resolution AFM, we have mapped both local PL emission properties and local morphology with nanoscale resolution. We show for the first time on such a small length scale how local morphology of MoS_2 changes it's the local PL emission properties.

[1] W. Bao *et al.*, *Science*. **338**, 1317 (2012).

Mo1720

In Situ Study of TMA-dosed Fluorine Functionalized Epitaxial Graphene on SiC(0001)

Z. R. Robinson[1], G. G. Jernigan[1], R. L. Myers-Ward[1], V. D. Wheeler[1], D. K. Gaskill[1], S.C. Hernandez[1], T. Mowl[2], E.W. Ong[2], C. A. Ventrice Jr.[2], H. Geisler[3], I. Pletikosic[4], T. Valla[4], C.R. Eddy, Jr.[1]

[1] U.S. Naval Research Laboratory, Washington, DC
[2]College of Nanoscale Science and Engineering at SUNY Albany, Albany, NY
[3]SUNY College at Oneonta, Oneonta, NY
[4]Brookhaven National Laboratory, Upton, NY

Graphene growth on Si-face SiC is epitaxial, and results in a single rotational orientation film with single-layer thickness control when performed in an argon environment. In order to use the graphene in electronic applications, it is often required that a gate dielectric be deposited on top of the graphene. Al_2O_3 is one material that has been widely used as a gate dielectric, and can commonly be deposited by a thermally activated atomic layer deposition process. In this process, trimethylaluminum (TMA) is used as the aluminum precursor, and H_2O is used as the oxygen source. On graphene, growth of Al_2O_3 by this technique is inhibited by the inertness of the graphene surface, which manifests itself in a low sticking coefficient for both the TMA and H_2O. In order to enable Al_2O_3 growth, a fluorine functionalization process was developed that increases the sticking coefficient for both of the precursor molecules [1].

Key to fully understanding the fluorine-functionalization process is determining whether it affects the electronic structure of the graphene. To study this, angle resolved photoelectron spectroscopy (ARPES) was performed on single and bilayer graphene with a functionalization dose previously shown to enable AL_2O_3 deposition. ARPES and LEED on hydrogen intercalated, fluorine functionalized graphene is shown in Figure 1 (upper plots), where bilayer electronic structure and p-type doping can be seen. This sample was annealed *in situ* to desorb both the fluorine functional groups and the intercalated hydrogen. Following the anneal, the graphene regains its single-layer electronic structure and the n-type doping typically seen for single layer films on SiC(0001) (Figure 1, lower plots) [2]. Comparison with an as-grown hydrogen intercalated sample shows that the functionalization process negligibly affects the electronic structure of the graphene.

Similar experiments were performed on single layer films, whereby the *in situ* anneal desorbed the fluorine with no measurable effect on the doping level. Additionally, TMA dosing experiments were performed in a second UHV chamber equipped with XPS to measure the uptake as a function of dose. This was performed on both fluorine functionalized and as-grown single layer graphene. Recent results will be discussed.

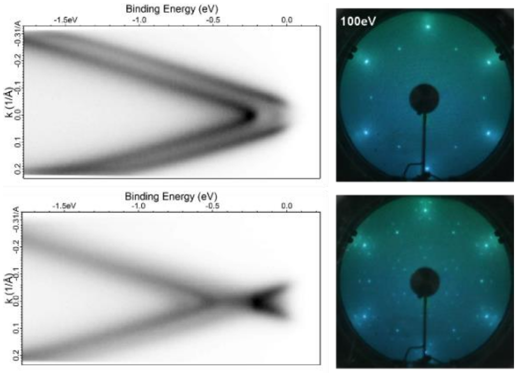

Figure 1: (will be updated) ARPES and LEED for (upper) hydrogen intercalated, fluorine functionalized graphene on SiC(0001). An in situ anneal was performed to desorb the F and H_2, resulting in (lower) single layer graphene.

[1] Wheeler, Virginia, et al. "Fluorine functionalization of epitaxial graphene for uniform deposition of thin high-κ dielectrics." Carbon 50.6 (2012): 2307-2314.

[2] Riedl, C., et al. "Quasi-free-standing epitaxial graphene on SiC obtained by hydrogen intercalation." Physical review letters 103.24 (2009): 246804.

Mo1725

In situ Atomic Force Microscopy Study of Ion Intercalation into Two-dimensional Titanium Carbide

Jérémy Come,[a] Jennifer M. Black,[a] Michael A. Naguib,[b] Majid Beidaghi,[c] Sergei V. Kalinin,[a] Yury Gogotsi,[c] and Nina Balke[a]

[a]Center for Nanophase Materials Sciences, Oak Ridge National Laboratory, Oak Ridge, TN, 37831, USA
[b]Materials Science and Technology Division, Oak Ridge National Laboratory, Oak Ridge, TN, 37831, USA
[c]Department of Materials Science and Engineering & A. J. Drexel Nanotechnology Institute, Drexel University, Philadelphia, PA, 19104, USA

Titanium carbide Ti_3C_2 is a member of the recently discovered family of two-dimensional materials known as MXenes. This material demonstrates a high storage capacity related to the rapid intercalation of ions within the structure, making this a promising electrode material for supercapacitors. In this work, *in-situ* Atomic Force Microscopy is used to monitor the strain developed in a Ti_3C_2 electrode during intercalation/extraction of monovalent and divalent cations in a variety of aqueous electrolytes. The actuation mechanism was found to be strongly dependent on the cation charge and ionic radius. When small cations such as Li^+ or Mg^{2+} are inserted, electrostatic attraction between layers dominates, whereas intercalation of larger cations such as K^+ or Ba^{2+} can lead to a lattice expansion as large as 20%. By using AFM as a high resolution probe, the strain measurements clearly evidenced a 2-steps electrochemical intercalation in Ti_3C_2, corresponding to the charge storage in the shallow or the deep sites of the layered structure (Figure 1a,b). Faster intercalation kinetics were observed for larger cations, as the increase in the interlayer spaces gives more room for the ionic transport within the 2D channels (Figure 1c,d). Various counter-ions were used, and their effects on the capacitance and strain behavior were also investigated.

These results are exciting because they shed light on the cation intercalation mechanism in the 2D structure of the carbide, and show that the actuation of Ti_3C_2 can be electrochemically tuned by a proper electrolyte selection. Moreover, the interactions between cations and the layers can be efficiently probed with an AFM tip. Since a variety of 2D transition metal carbides can be synthesized, MXenes offer the promise of exciting discoveries for electrochemical capacitors and actuators.

The work was supported by the Fluid Interface Reactions, Structures and Transport (FIRST), an Energy Frontier Research Center funded by the U.S. Department of Energy, Office of Science, Office of Basic Energy Sciences. . The facilities to perform the experiments were provided by the Center for Nanophase Materials Sciences, which is sponsored at Oak Ridge National Laboratory by the Scientific User Facilities Division, Office of Basic Energy Sciences, U.S. Department of Energy.

Mo1730

First-principles Study of Structural and Catalytic Properties of Single-layer MoS_2 with Sulfur Vacancies

T.B. Rawal, D. Le, T.S. Rahman, University of Central Florida

Single-layer MoS_2, a promising transition-metal dichalcogenide(TMD) material, is of great interest owing to its wide variety of applications. Creating sulfur vacancy, on single-layer MoS_2 without its destabilization, is regarded as a prudent way for making MoS_2 basal plane catalytically active. In this talk, we shall show, on the basis of our density functional theory simulations, that the formation energy per sulfur vacancy on one side of the layer is the lowest (energetically favorable) when the vacancies form a row and that the formation energy gets lowered when row becomes longer, indicating a tendency of elongating the sulfur-vacancy row. In addition, we shall show that the lowest energetic barrier for spoiling these row structures by exchanging a vacancy with a nearby sulfur atom is 0.79 eV, and the barrier increases as the row elongates. At the end, we shall reveal that the alcohol synthesis from syngas is found to be energetically more favorable for the layer with sulfur-vacancy patch as compared to that on the layer with sulfur-vacancy row.

Work supported in part by DOE grant DE-FG02-07ER15842.

Catalytic reduction of oxygen on nitrogen-doped graphene

Akihide Ichikawa[1,2], Akira Akaishi[1,2], and *Jun Nakamura[1,2]
[1]*The University of Electro-Communications (UEC-Tokyo), Tokyo, Japan*
[2]*JST-CREST, Saitama, Japan*
E-mail: junj@ee.uec.ac.jp

Recently, several groups have reported high oxygen reduction reaction (ORR) activities in nitrogen-doped carbon nanomaterials which are candidates of metal-free catalysts for ORR [1]. Lee et al. have successfully fabricated nitrogen-doped graphene with the high ORR activity in acid media [2]. It has been confirmed that local atomic configurations of dopants in nitrogen-doped graphene are classified into three functional groups (pyrrole-like, pyridine-like, and graphite-like configurations) [3]. However, the mechanism of the ORR on the nitrogen-doped graphene has not fully understood.

In this work, we examine the ORR on the nitrogen-doped graphene containing the graphite-like N in a basal plane using first-principles calculations. In general, the ORR occurs mainly two pathways: The two-electron pathway ($2e^-$) that is reduced to hydrogen peroxide (H_2O_2), and the direct four-electron pathway ($4e^-$) that reduces to water (H_2O). Thermodynamic electrode potentials of each process at standard conditions are about 0.68V ($2e^-$) and 1.23V ($4e^-$), respectively. In case of the associative mechanism for the two- and four- electron reduction pathways, the electrocatalytic activity is governed by the stability of reaction intermediates like OOH*, OH*, and O* (where "*" refers to a surface site). Free energies of the reaction intermediates have been calculated based on the computational hydrogen electrode model suggested by Norskov et al. [4]. We have taken account of effects of electrode potential, pH of a solution, a local electric field in double layer, and water environment.

We have constructed energy diagrams at several electrode potentials on the basis of the first-principles calculations. It has been shown that the $2e^-$ and $4e^-$ reduction processes proceed at potentials up to about 0.5V and 0.8V, respectively. This means that we can control the reduction pathway for the nitrogen-doped graphene with the graphite-like N. Proton-electron transfer to OOH* (the $2e^-$ pathway), and the formation of OOH* (the $4e^-$ pathway) are confirmed to be the rate-limiting steps, respectively. The effects of electric field and water environment will also be discussed in the presentation.

[1] J. Ozaki, N. Kimura, T. Anahara, and A. Oya, Carbon **45**, 1847 (2007).
[2] K. R. Lee et al., Electrochem. Commun. **12**, 1052 (2010).
[3] H. Niwa et al., J. Power Sources **187**, 93 (2009).
[4] J. K. Norskov, J. Rossmeisl, A. Logadottir, and L. Lindqvist, J. Phys. Chem. B **108**, 17886 (2004).

Late News

Mo1740

Enhancement of GaSb Tunnel Junctions with InAs Quantum Wells

S. Mack, M. P. Lumb, M. Gonzalez, K. J. Schmieder, R. J. Walters
Naval Research Laboratory, Washington, DC, USA

Tunnel junctions (TJs) enable series connections between subcells of multi-junction solar cells. Desired characteristics are low resistance and low absorption below the bandgap of the preceding subcell. (Thermo)photovoltaics based on GaSb presently lack a TJ design that meets these requirements because: (1) n-type GaSb has a relatively small maximum free carrier concentration, so GaSb homojunctions are resistive, and (2) p+GaSb / n+InAs heterojunctions absorb photons below the GaSb bandgap in the InAs layer.

Here, we report GaSb TJs with InAs broken-gap quantum wells (BGQWs) at the tunnel interface. The p+GaSb / n+InAs(BGQW) / nGaSb TJ, or BGQW TJ, is designed to optimize the tradeoffs between resistivity and absorption. The thin InAs QW retains the broken gap GaSb / InAs interfaces of the bulk heterojunction, significantly increasing the tunnel probability through the forbidden GaSb gap. This increases the tunnel current relative to a homojunction while reducing the volume of absorbing material compared to a bulk heterojunction. We describe the performance of the BGQW TJs as a function of InAs QW thickness.

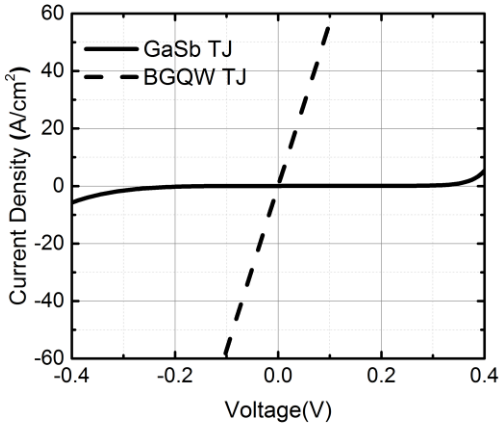

Fig. 1: Dark I-V characteristics of a GaSb TJ with(out) an n+InAs BGQW.

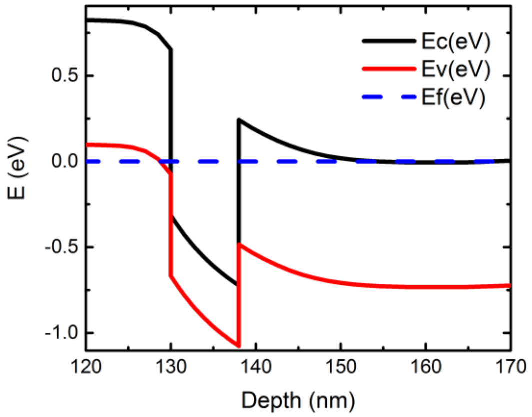

Fig. 2: Band diagram of a GaSb TJ with an n+InAs BGQW.

Mo1745

Structural and Optical Characterization of AlN deposited by N_2/H_2 Plasma-Enhanced Atomic Layer Deposition

Pouyan Motamedi and Kenneth C. Cadien

Chemical and Materials Engineering Department, University of Alberta, Edmonton, Alberta, Canada T6G 2V4, email: p.motamedi@ualberta.ca

AlN thin films deposited using a novel PE-ALD approach have been analyzed through several surface characterization methods to investigate their elemental analysis, chemical stability, crystal structure and optical properties. The films were deposited on Si (111) and sapphire substrates, using nitrogen plasma and TMA as the two precursors. The use of nitrogen plasma eliminates many drawbacks associated with the commonly-employed methods involving halides and NH_3 plasma. High-resolution XPS was used to measure film stoichiometry and to determine the oxidation states and bond energies. Chemical stability of the films deposited at different temperatures was investigated by monitoring the chemical and electronic state of Al, N, and O atoms before and after exposure to air. Results showed that complete chemical stability can be achieved at 250°C deposition temperature, at which the only Al2p peak present corresponds to the Al-N bond, as distinguished from would-be neighboring peaks related to Al-O and Al-Al bonds. GAXRD showed the films have Wurtzite hexagonal crystal structure with preferential orientation along the (100) direction. Spectroscopic ellipsometry was used to analyze the optical properties of the films. The results indicated a refractive index of 2.06 at the wavelength of 632.8 nm. This value is in line with other reports of ultra-thin AlN films. In addition, the absorption edge of 6.1 eV was extracted from the optical data, which is close to the values corresponding to bulk crystalline AlN.

Energy Materials

Mo1930 Invited

Nanostructured interfaces for efficient and stable photoelectrochemical water splitting

Joel W. Ager
JWAger@lbl.gov, Joint Center for Artificial Photosynthesis and Materials Sciences Division,
Lawrence Berkeley National Laboratory, USA.

Solar photoelectrochemical (PEC) water splitting is potential future carbon-neutral energy source which could dramatically change the landscape of global energy generation and storage. The cathodic and anodic electrochemical half reactions for water splitting are as follows:

$$2H^{+} + 2\,e^{-} \Leftrightarrow H_2 \qquad (1)$$

$$H_2O \Leftrightarrow 2e^{-} + 2H^{+} + 1/2O_2. \qquad (2)$$

The free energy change for the overall reaction, $H_2O \rightarrow H_2 + 1/2O_2$ is, at standard conditions, +237 kJ/mol, which corresponds to 1.23 eV per electron transferred. The most commonly used approach for integrated solar water splitting employs photocathodes (H_2 or hydrocarbon producing) and photoanodes (O_2 producing) linked in a tandem geometry, as shown in Fig. 1. The minimum potential required from the photovoltaic elements is 1.23 V. In actuality, the required amount is somewhat higher, >1.5 V, in order to overcome kinetic limitations, particularly for the oxygen evolution reaction (OER), Eqn (2).

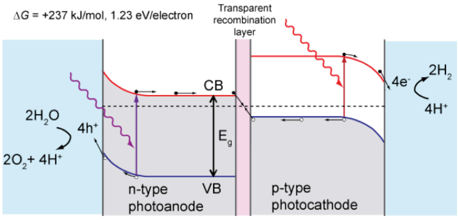

Fig 1. Schematic of a tandem-coupled photoanode and photocathode driving overall water splitting. The dotted line depicts the Fermi level at equilibrium conditions.

The interface challenges required to demonstrate a practical system which is both efficient and stable under operation are substantial and severe. In addition to constructing interfaces, either solid-solid or solid liquid, which achieve the desired photovoltaic charge separation, the surfaces of these photoelectrodes can be a failure point under sustained operation due to corrosion. We have found that the use of nanoscale conformal oxide layers can greatly reduce corrosion rates. Moreover, it is possible to achieve both high performance and lifetime by the use of protection layers which are also tuned for selective carrier contact. Examples of such a strategy will be shown for photocathodes [3,4] and for photoanodes [5]. Recent work on p-type transparent oxides used as selective hole contacts for photoanodes (Fig. 2) will be presented.

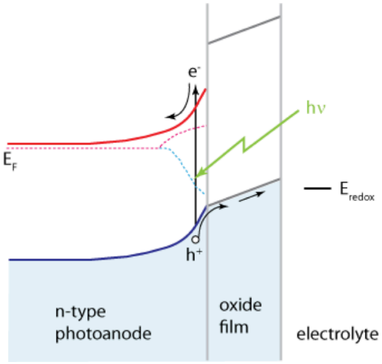

Fig 2. Use of a p-type transparent oxide as a selective hole contact and protection layer for an n-type photoanode.

Acknowledgements. This material is based upon work performed by the Joint Center for Artificial Photosynthesis, a DOE Energy Innovation Hub, supported through the Office of Science of the U.S. Department of Energy under Award Number DE-SC0004993.

References.

1. M. H. Lee *et al.*, *Angewandte Chemie International Edition* **51** 10760 (2012).
2. Y. Lin *et al.*, *Nano Letters* **13** 5615 11 (2013)
3. J. Yang *et al.*, *J. Amer. Chem. Soc.* **136** 6191 (2014)

Mo2010

Improvement of Conversion Efficiency of Multicrystalline Silicon Solar Cells Using Reactive Ion Etching with Surface Pre-etching

Wen-Hua Chen[2], Hsin-Han Lin[2], and Franklin C.-N. Hong[1,2,3]
[1]Department of Chemical Engineering, National Cheng Kung University
[2]Institute of Nanotechnology and Microsystems Engineering, National Cheng Kung University
[3] Micro-Nano Imprinting Technology and Device Center, National Cheng Kung University
Tel: (06)2757575 ext. 62662, Email: hong@mail.ncku.edu.tw

ABSTRACT

In solar cell manufacturing, surface texturing plays quite an important role in light trapping. Besides optical performance, surface texturing is revealed to be also critical for passivation performance of solar cells in this study. After deposition with PECVD SiN_x:H films, the acid HNO_3 textured wafers showed the highest bulk lifetime, while the wafers textured with alkaline KOH chemicals showed the lowest surface recombination velocity (SRV). With the advantage of bulk lifetime improvement from acid textured surface, an additional passivation process via the template of acid textured surface prior to KOH or KOH+IPA texturing can obviously enhance the performance of bulk lifetime and SRV. Besides the results of bulk lifetime and SRV shown in this study, CV measurement also indicates the density of interface trap D_{it} shows the same correlation with the passivation performance revealed by SRV.

INTRODUCTION

Due to the use of thinner wafers and the goal to achieve higher conversion efficiencies efficiencies, future industrial solar cell concepts are mainly based on the use of reactive ion etching(RIE) concepts to achieve it. RIE processing has proven its potential to effectively texture multicrystalline silicon wafers by many authors in the past resulting in surface structures more or less suitable for solar cell fabrication. Therefore,texturing of mc-Si wafers as a relevant industrial process step has been adopted by PV industry only in wet chemical acidic isotropic etching solutions so far. Depending on the actual process scheme, wafer pre-clean should be a critical stage in cell manufacture. Within this paper different pre-clean approaches for the solar cells, either acid or alkaline method, have been investigated in terms of resulting surface clean, and, combined with double-side PECVD stack passivation, in terms of surface recombination velocity and optical performance. Correlations between surface reflectance, surface recombination velocity and final Voc and Jsc potential have been taken.

EXPERIMENTAL DETAILS

In this work, 3-5 Ωcm B-doped p-type Cz wafers were used and followed by three kinds of texturing process, isotropic, shiny-polished and pyramid texturing with chemicals of HNO_3, KOH and KOH+IPA, respectively. These textured wafers were then cleaned by diluted HF chemicals and subsequently passivated with amorphous hydrogenated-nitride film SiN_x:H deposited by plasma-enhanced chemical vapor deposition (PECVD). In order to understand different passivation effects of these wafers, the measurements of bulk lifetime and SRV were achieved with the QSSPC lifetime tester of Sinton WCT-120. All samples prepared for lifetime measurement were textured with various chemicals described above and then deposited with bifacial PECVD SiN_x:H passivation layers. Besides, the structure of metal-dielectrics-silicon was also used to acquire the information of capacitance-voltage curves with extracted results of density of interface trap D_{it}, a reference of interface quality between dielectric film and silicon wafer.

RESULTS AND DISCUSSION

Texturing dependent passivation performance

As shown in Fig.1, with hydrogenated SiN_x:H film as a passivation layer, the hydrogen passivation via acid textured surface showed higher bulk lifetime as being compared with KOH texturing, while KOH+IPA texturing showed the worst performance. As for the SRV results shown in Fig.2, SRV of the KOH textured wafer was the lowest, while that of the KOH+IPA textured wafer was the highest and still the worst.

Mo2010

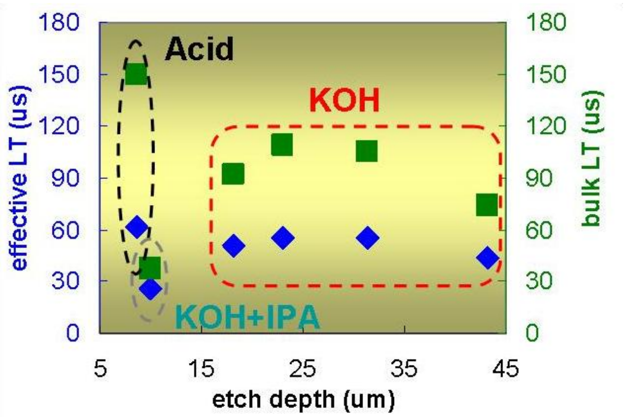

Figure 1 Effective lifetime and bulk lifetime versus etching depth of the three kinds of textured surface passivated with SiN_x:H film.

To explain why acid texturing (HNO_3) can achieve higher bulk lifetime than alkaline texturing (KOH or KOH+IPA), the different chemical reactions of silicon etching process could be probably addressed. For acid texturing process, the process of silicon oxidation by HNO_3 occurs first and is then followed by the oxide etching via diluted HF chemicals. The alkaline process, however, employs a much more intense etching to directly break the silicon inter-bonding and remove the atomic silicon layer by layer. With the addition of IPA solution into KOH alkaline etching process, much more silicon-etching reaction happens than KOH-only process. As we know, IPA can take the hydrogen gas away during the process and then proceeds the etching process for the formation of pyramid shape with silicon surface orientation of [111]. As a result, in terms of silicon-etching intensity, HNO_3 texturing process shows much milder than alkaline process resulting to a speculation that less damage formation of silicon surface could be beneficial for the hydrogen movement from dielectrics into bulk silicon.

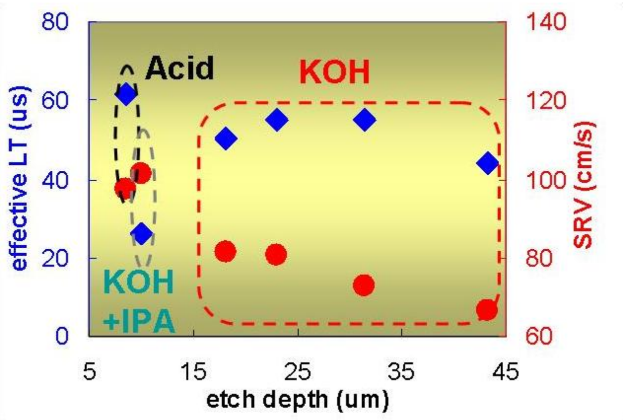

Figure 2 Effective lifetime and surface recombination velocity versus etching depth of the three kinds of textured surface passivated with SiN_x:H film.

As for the mechanism discussion why KOH-only process showed better SRV performance than others, an observation of density of interface trap D_{it} was introduced to investigate the silicon interfacial quality after the deposition of passivated amorphous silicon nitride films. As depicted in Fig.3, Dit showed the same correlation to various textured silicon surface as SRV shown in Fig.2. The lower SRV reveals correspondence to the lower density of interface trap. The textured silicon orientation, therefore, can be speculated to affect the deposition performance. For orientation [100] of KOH textured surface, the deposition of dielectrics can achieve better interfacial quality leading to less formation of interface traps. On the other hand, the formation of surface orientation [111] in KOH+IPA process will relatively perform the worst interfacial quality during the deposition of dielectrics. The isotropic texturing process with HNO_3 chemicals, however, will achieve a medium performance of interfacial quality between KOH-only and KOH+IPA.

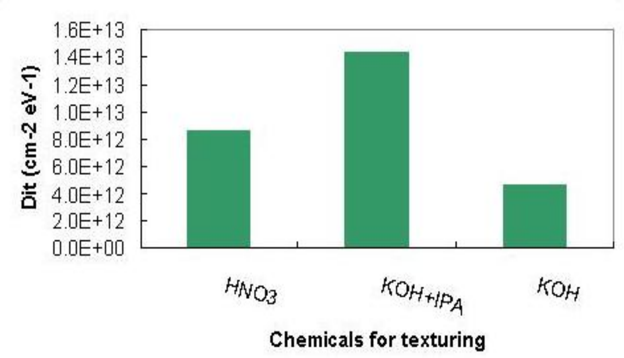

Figure 3 Measurements of density of interface trap for dielectrics deposition onto various textured silicon surface.

Additional passivation via template of acid texturing

Since acid texturing can derive better passivation performance with higher bulk lifetime, a concept of additional SiN_x:H passivation process prior to KOH texturing and KOH+IPA texturing process is addressed in this study. To verify this idea, several groups of samples were prepared and listed as below.

#1: Normal acid textured surface

#2: Deeper acid textured surface

#3: Normal KOH+IPA textured surface

#4: Single side deposited SiN_x:H passivation via the template of acid texturing prior to KOH+IPA texturing

#5: Bifacial-deposited SiN_x:H passivation via the template of acid texturing prior to KOH+IPA texturing

Firstly, to reveal the correlation between etching depth of acid texturing and passivation performance is of interest.

As illustrated in Fig.4 and Fig.5, deeper acid texturing showed better passivation performance of both bulk lifetime and SRV. According to the earlier disng witcussion, the results can be implied that deeper acid texturih more reaction of silicon oxidation will have less surface damage and thus result to better hydrogen passivation within the bulk silicon. Secondly, to verify the advantage of SiN_x:H passivation via acid textured surface, it was combined with KOH+IPA texturing, which was widely used for mono-crystalline cells. Prior to the process of KOH+IPA texturing, the raw wafer was textured with acid chemicals and then followed by SiN_x:H passivation. Later on, the SiN_x:H layers were removed by dilute HF solution and then subsequently textured with KOH+IPA chemicals. Improvement of both bulk lifetime and SRV can be achieved on samples with KOH+IPA texturing, as shown in Fig.4 and Fig.5. However, since SiN_x:H passivation was applied on only single side, the improvement showed only a little bit.

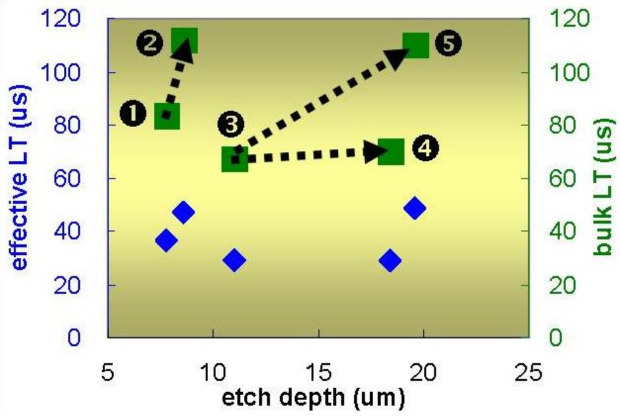

Figure 4 Bulk lifetime improvement compared between normal and deeper acid texturing (indicated as #1 and #2); besides, additional SiN_x:H passivation on the template of acid textured surface prior to KOH+IPA texturing can also improve bulk lifetime (compared between #3 and #5).

The effects using a template acid textured surface followed by the hydrogen passivation prior to the passivated structure of KOH+IPA texturing indicate that the pre-passivation of hydrogen happens within the bulk silicon and such pre-deposited film can generate a less-trap interface even though it will be removed later.

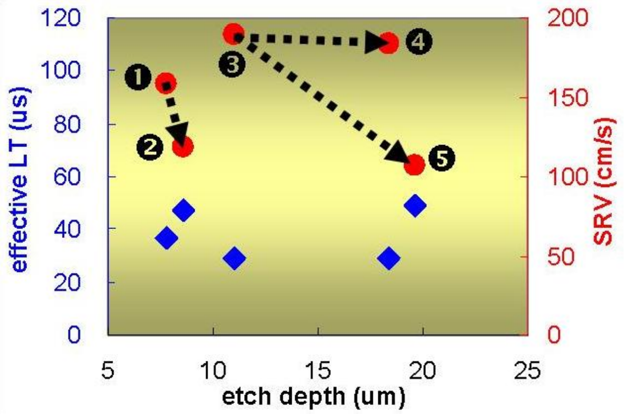

Figure 5 SRV improvement compared between normal and deeper acid texturing (indicated as #1 and #2); besides, additional SiN_x:H passivation on the template of acid textured surface prior to KOH+IPA texturing can also improve SRV (compared between #3 and #5).

The same process of additional SiN_x:H passivation via the acid textured template applied on wafers prior to KOH texturing can result in longer bulk lifetime and comparable SRV as shown in Fig.6. The surface pre-formation with less damage indeed brings the benefit of better hydrogen passivation toward the bulk silicon and such pre-handling still remains its intrinsic better performance of interface quality.

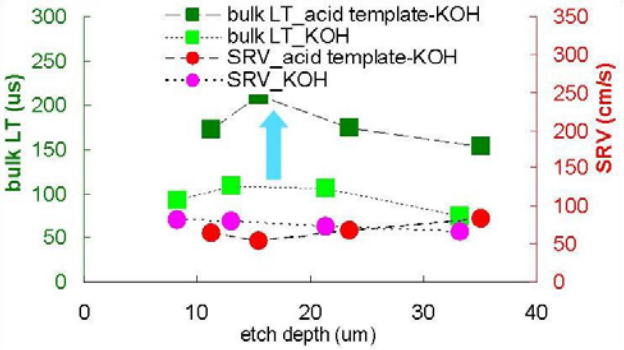

Figure 6 Additional SiN_x:H passivation on acid textured surface prior to KOH texturing obviously showed bulk lifetime improvement and comparable SRV results.

We use different pre-clean method and combine with RIE process as cell process. It was shown in table.1. The surface pre-formation with less damage indeed brings the benefit and get high current density(Jsc). But, we also find that higher bulk lifetime will induce higher open circuit voltage(Voc).

Table 1 Cell efficiency in different pre-clean condition

Process	V_{oc} (V)	J_{sc} (mA/cm^2)	FF (%)	Efficiency (%)
Wet texturing	0.623	34.09	78.49	16.67
Alkaline pre-etching/RIE texturing	0.622	35.17	78.86	17.25
Acid pre-etching/RIE texturing	0.624	35.38	78.41	17.31
RIE texturing (No pre-etching)	0.618	33.81	77.79	16.25

CONCLUSIONS

The texturing dependence on passivation performance was discussed in this study. The acid HNO_3 textured wafers showed the highest bulk lifetime, while the wafers textured with alkaline KOH chemicals showed the lowest surface recombination velocity. The surface damage formation during the texturing of silicon surface is speculated to correlate with the performance of hydrogen passivation within the bulk silicon. The orientation of textured surface reveals a correlation to the formation of interface traps during the deposition of dielectrics on the textured silicon surface. Higher bulk lifetime and lower SRV can be achieved using the template of acid textured surface to additionally combine of effects of hydrogen pre-passivation and less-trap interface.

REFERENCES

[1] Sanden, W.M.M. Kessels: “Surface passivation of highefficiency silicon solar cells by atomic-layer-deposited Al2O3“, *Prog. Photovolt. Res. Appl.* **16**, 2008, pp. 461-466

[2] Mack et al., Fraunhofer ISE“Towards 19% Efficient Industrial PERC Devices Using Simultaneous Front Emitter and Rear Surface Passivation by Thermal Oxidation “, *Proc. 35th IEEE* ,2010

[3] I. Cesar, E. E. Bende, G. Galbiati, L. jansen, A. A. Mewe, P. Manshanden, A. W. Weeber, and J. H.Bultman, "Parasitic shunt losses in all-side SiNx passivated mc-Si solar cells" *Proc. 24th EUPVSEC* ,2009.

Mo2015

The origin of crystallographic orientation dependence of SEM contrast revealed by the difference in SiC polytype and polarity

K. Ashida, T. Kajino, Y. Kutsuma, N. Ohtani, and T. Kaneko
Gakuen 2-1, Sanda, Hyogo, 669-1337, Japan, E-mail: Kaneko@kwansei.ac.jp

Recently, the contrast mechanisms in SEM imaging in low-voltage regime have been eagerly investigated in order to exploit the information about the local crystalline structure. However, the relevant phyisical model is still under discussion [1]. In order to investigate the contrast mechanism in low-voltage regime, the preparation of the homogeneous and well-ordered sample is the most critical issue. The sample inhomogenity induces various contrast mechanisms, which complicates the interpretation of the obtained data. In this perspective, single crystal is more sensitive compared with alloy or poly-crystal. By considering backscattered electrons (BSEs) or secondary electrons (SEs) which are generated from the different depth and atomic species, the use of single crystalline compound material with definitive marker layers with different depth is useful. In this study, in order to fulfill all the requirements as described above, cubic 3C-SiC (111) and hexagonal 4H- and 6H-SiC {0001} single crystals were used as standard samples. 3C-SiC has a zincblende structure in which Si-C bilayers (BLs) are stacked in the identical crystallographic orientation. On the other hand, 4H- (6H-) SiC has a hexagonal structure in which the stacking orientation of the Si-C BLs turns over at every hexagonal site at the half stacking period of each unit-cell along the *c*-axis (2BL or 0.5nm for 4H-, 3BL or 0.75nm for 6H-SiC)[2]. The difference in the depth of the hexagonal sites from the surface acts as the depth sensitive marker layer. In addition, (0001) and (000-1) planes are terminated with Si- and C-atoms, respectively, so that the chemical information can be also acquired to be distinguished. By utilizing these standard samples, we evaluated the structure and material effect on the SEM contrast independently by measuring the polar angle and azimuthal angle dependent BSE and SE signals with a FE-SEM (Zeiss SUPRA40) below 2kV.

As the result, the crystallographic orientation dependent BSE and SE signals were obtained via the SEM image. By comparing the images obtained from the various SiC samples, the signals obtained are found to be quite sensitive to the difference in the structural and chemical properties of the sample. The intensity of the signals reaches the maximum when the direction of the incident PEs is parallel to the close-packed atomic-chain direction. It is revealed that that the origin of the SEM contrast comes from the difference in the direction of the atomic-chains and in the atomic species which terminate the surface. These results can be explained by the multiple scattering cluster theory.

Acknowledgement

This research was financially supported by Strategic Innovation Program for Energy Conservation Technologies under New Energy and Industrial Technology Development Organization (NEDO). Authers are thankful to Dr. T. Matsushita of Japan Syncrotron Radiation Research Institute (JASRI) for theoretical discussions.

References

[1] J. Cazaux, N. Kuwano, and K. Sato, Ultramicroscopy, **135** (2013) 43-49.

[2] U. Starke, J. Schardt, and M. Franke, Applied Physics A, **65** (1997) 587-596.

Mo2020

III-V Semiconductor Nanowires on Silicon for Solar Fuel Generation

E. Alarcon-Llado, E. Frau, J. Vukajlovic, K. Yasaroglu, G. Tutuncuoglu, F. Matteini, and A. Fontcuberta-i-Morral

Ecole Polytechnique Fédérale de Lausanne, Lausanne, Switzerland

At present, lack of reliable sources of renewable and energy global warming are one of the biggest environmental threats. While the sun is one of the major renewable sources of energy, its energy can be directly converted into fuel (hydrogen, hydrocarbons or alcohols) from water and/or CO_2 through a photo-electrochemical (PEC) cell. Due to the constraints in the working principles of PEC cells, there is yet no simple, cheap, efficient and reliable solution.

Semiconductor nanowires are filamentary crystals with new properties from their bulk counterparts. Their main advantages comprise (i) large surface-to-volume ratio (ii) relative ease of fabrication (iii) large variety of material combinations and geometries and (iv) high compatibility with standard industrial fabrication technologies. The versatility of nanowires makes them not only best candidates as building blocks for nanoelectronics, but also for contributing to the energy problem in the near future. The fabrication of systems that convert solar energy directly into chemical fuels highly benefits from such properties particular to nanowires. In this work we discuss the different properties inherent to semiconductor nanowires homo and heterostructures with potential interest for efficient solar water splitting. From the optical point of view, III-V semiconductors such as GaAs, are the most suitable for solar energy harvesting. What's best, when in the form of nanowires, light resonances occur giving rise to effective absorption cross-sections that are much larger than the geometrical one (Fig. 1). By appropriate designing of a nanowire array, maximal absorption efficiency can be obtained with photo-carrier generation along large surface areas. Furthermore, we optimize carrier extraction through fabrication of core-shell hetero-structures.

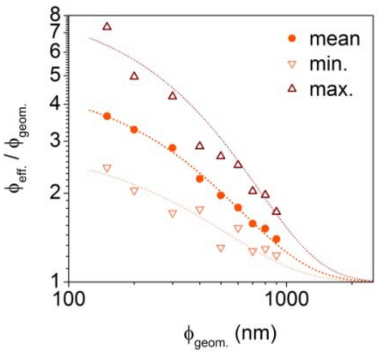

Figure 1. Effective absorption cross-section diameter of a single GaAs nanowire as a function of the geometrical diameter. The values have been calculated by FDTD for wavelengths in 300-900nm range. The minimum, maximum and mean values within this wavelenght range are represented.

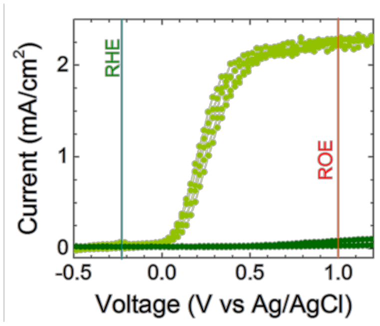

Figure 2. Electrochemical performance of a GaAs nanowires-based photoanode in aqueous solution

The drawback of using such kind of material is its lack of stability in aqueous environments. Fortunately, nowadays technology offers the possibility of fabricating nm-thin conformal layers than can both protect and allow charge transport towards the electrolyte. In this work, we show how we are able to protect GaAs-based nanowires by using two fabrication methods of TiO_2 and Al_2O_3 protective coatings. The performance of the nanowires as photo-anodes for water oxidation in terms of photo-voltage generation is extremely promising as component in a Z-scheme photoelectrochemical cell (Fig. 2).

Finally, in this work we will also address different surface treatments to Silicon in order to improve its performance as photo-cathode for hydrogen generation and discuss the main remaining challenges for fabricating the full Z-scheme device.

Visualizing the electric double layer of ionic liquids at carbon interfaces

Jennifer Black,[1] Guang Feng,[2] M. Baris Okatan,[1] Peter T. Cummings, [2] Sergei V. Kalinin[1] and Nina Balke[1]

[1]Oak Ridge National Laboratory, Oak Ridge, TN, USA 37831
[2]Vanderbilt University, Nashville, TN, USA 37235

Ionic liquids are attractive electrolytes for electrochemical capacitors due to the large operational voltage windows thereby providing an increased energy density in these systems. The structure and properties of the electrical double layer in ionic liquids is of interest in to a wide range of areas including energy storage, catalysis, lubrication, and many more. Theories describing the electrical double layer for ionic liquids have been proposed, however a full molecular level description of the double layer is lacking. To date, studies have been predominantly focused on ion distributions normal to the surface, however the 3D nature of the electrical double layer in ionic liquids requires a full picture of the double layer structure not only normal to the surface, but also in plane.

Here we utilize 3D force mapping to probe the in plane structure of an ionic liquid at a graphite interface and report the direct observation of structure and properties of topological defects. We will explain in depth the use of atomic force microscopy (AFM) to study the layering of ionic liquids and introduce a statistical approach to identify ion layer positions as function of distance from the carbon surface. In this study, we will focus on the room temperature ionic liquid 1-ethyl-3methyl-imidazolium bis(trifluoromethanesulfonyl)imide (Emim$^+$Tf$_2$N$^-$) at a highly oriented pyrolytic graphite surface. Distinct steps are observed during the approach of the AFM tip due to interaction with ion layers present at the interface. The experimental data shows an excellent agreement with predicted ion layer positions from molecular dynamics.

Spatially resolved studies reveal that structural defects, such as step edges, were found to result only in short range changes in ionic liquid ordering, with the changes in 3D force fields consistent with rigid shift of the layers with narrow disordered region between the two, consistent with MD simulations. At the same time, formation of serendipitous dislocation-type topological defects were observed on planar surfaces. The decrease in the ordering was observed within the defect, consistent with behaviour expected for classical liquid crystals. This is the first time, dislocations in liquid crystal like systems could be directly visualized with a lateral resolution of down to 20 nm.

The experimental, modeling, and sample preparation efforts of JB, GF, PTC, PCH, and SD, was supported by the Fluid Interface Reactions, Structures and Transport (FIRST), an Energy Frontier Research Center funded by the U.S. Department of Energy, Office of Science, Office of Basic Energy Sciences. Additional support was provided by the U.S. Department of Energy, Basic Energy Sciences, Materials Sciences and Engineering Division through the Office of Science Early Career Research Program (NB) and the Center for Nanophase Materials Sciences, which is sponsored at Oak Ridge National Laboratory by the Scientific User Facilities Division, Office of Basic Energy Sciences, U.S. Department of Energy (MBO and SVK).

Mo2045

Nanoscale variation of physical properties of $LiCoO_2$ after Li-ion extraction

Nina Balke, Petro Maksymovych, Alexander Tselev, Stephen Jesse, and Sergei V. Kalinin
Oak Ridge National Laboratory Oak Ridge, TN 37831

Lithium ion batteries are an essential element to modern life. Recent efforts are pushing this technology towards electrical vehicles and other large scale applications. While the development of full Li-ion batteries made tremendous progress in the last 40 years for various applications, our understanding of the basic processes within a battery are still lacking. This includes especially the transport path of Li-ions through the electrodes and electrolytes and across the electrode-electrolyte interface and the role of the microstructure. The reason for this knowledge gap is the limited amount of characterization techniques available to address the necessary length scales of below 1μm. In recent years, more and more characterization techniques are adapted to work with Li-ion batteries, including transmission electron microscopy (TEM), scanning probe microscopy (SPM), Raman, and X-Ray to expand our knowledge of ionic transport below the μm range. Here, we want to focus on AFM-based characterization techniques which allow for lateral resolutions of down to 20 nm and address the question how homogeneously Li-ions are extracted from a $LiCoO_2$ cathode during the charging process.

Ionic transport in energy storage materials results in a variety of physical changes in the sample properties which can be detected using SPM. First, there is a significant volume change associated with a change in ionic concentration as described by the Vegard law. This strain can be quite significant and can lead to cracking and performance degradation. In addition, electronic properties, such as polarizability, will also change when the ionic concentration is altered within the cathode. In this talk, we will summarize the different physical materials changes and discuss ways to measure those using SPM-based methods. We will especially focus on measurement artifacts and how to identify them.

We will investigate $LiCoO_2$ cathode materials with different Li-content after they have been charged and discharged. The electrochemical cells are disassembled inside a glove box and be prepared for SPM by drying the electrodes. The information about the spatial variation of physical sample properties are compared with the microstructure and conclusion about the Li-ion extraction from the cathode during charging will be drawn. We will discuss the future direction and challenges of the presented experimental capabilities.

Support was provided by the U.S. Department of Energy, Basic Energy Sciences, Materials Sciences and Engineering Division through the Office of Science Early Career Research Program, and by the Center for Nanophase Materials Sciences, which is sponsored at Oak Ridge National Laboratory by the Scientific User Facilities Division, Office of Basic Energy Sciences, U.S. Department of Energy.

Tuesday

Tu0745	Registration and Continental Breakfast
Tu0845	Tuesday Morning Session: *Characterization I*
Tu1000	Coffee Break and Poster Viewing
Tu1100	Tuesday Morning Session: *Characterization II*
Tu1150	Free Afternoon
Tu1930	Tuesday Evening Rump Session: *2D Materials & Heterostructures*

Characterization I

Tu0845 Invited

Ultrafast terahertz scanning tunneling microscopy

Frank A. Hegmann

Department of Physics, University of Alberta, Edmonton, Alberta T6G 2E1, Canada

The ability to directly probe ultrafast phenomena on the nanoscale is essential to our understanding of excitation dynamics on surfaces and in nanomaterials. The scanning tunneling microscope (STM) can image surfaces with atomic resolution, but the time resolution is typically limited to a few tens of microseconds by the bandwidth of the amplifier electronics. To achieve picosecond or sub-picosecond time resolution, various ultrafast STM techniques that integrate femtosecond lasers have been developed [1-8]. Recently, a new ultrafast STM technique that couples terahertz (THz) pulses to the scanning probe tip of an STM was demonstrated (THz-STM), providing simultaneous 0.5 ps time resolution and 2 nm spatial resolution under ambient laboratory conditions [9,10]. THz-STM imaging of ultrafast carrier capture into a single InAs nanodot on GaAs photoexcited with 800 nm pump pulses was also shown.

This talk will provide an introduction to terahertz pulse spectroscopy [11,12], an overview of ultrafast STM techniques, and a description of THz-STM. Recent THz-STM experiments performed in UHV and the potential for probing ultrafast dynamics on surfaces with atomic resolution will be discussed.

References:

[1] D. A. Yarotski et al., “Ultrafast carrier-relaxation dynamics in self-assembled InAs/GaAs quantum dots,” *J. Opt. Soc. Am. B* **19**, 1480 (2002).

[2] R. H. M. Groeneveld and H. van Kempen, “The capacitive origin of the picosecond electrical transients detected by a photoconductively gated scanning tunneling microscope,” *Appl. Phys. Lett*. **69**, 2294-2296 (1996).

[3] G. M. Steeves, A. Y. Elezzabi, and M. R. Freeman, “Nanometer-scale imaging with an ultrafast scanning tunneling microscope,” *Appl. Phys. Lett.* **72**, 504-506 (1998).

[4] N. N. Khusnatdinov, T. J. Nagle, and G. Nunes, Jr, “Ultrafast scanning tunneling microscopy with 1 nm resolution,” *Appl. Phys. Lett*. **69**, 2294-2296 (1996).

[5] S. Grafström, “Photoassisted scanning tunneling microscopy,” *J. App. Phys*. **91**, 171-1753 (2002).

[6] A. Dolocan et al., “Two-color ultrafast photoexcited scanning tunneling microscopy,” *J. Phys. Chem*. C **115**, 10033-10043 (2011).

[7] Y. Terada, S. Yoshida, O. Takeuchi, and H. Shigekawa, “Real-space imaging of transient carrier dynamics by nanoscale pump-probe microscopy,” *Nature Photon*. **4**, 869-874 (2010).

[8] S. Yoshida, Y. Aizawa, Z. Wang, R. Oshima, Y. Mera, E. Matsuyama, H. Oigawa, O. Takeuchi, and H. Shigekawa, “Probing ultrafast spin dynamics with optical pump-probe scanning tunneling microscopy,” *Nature Nanotech*. **9**, 588 (2014).

[9] T. L. Cocker, V. Jelic, M. Gupta, S. J. Molesky, J. A. J. Burgess, G. De Los Reyes, L. V. Titova, Y. Y. Tsui, M. R. Freeman, and F. A. Hegmann, “An ultrafast terahertz scanning tunnelling microscope,” *Nature Photon*. **7**, 620-625 (2013).

[10] V. Jelic, T. L. Cocker, J. R. Hoffman, M. Gupta, R. Miller, S. J. Molesky, J. A. J. Burgess, G. De Los Reyes, L. V. Titova, Y. Y. Tsui, M. R. Freeman, and F. A. Hegmann, “Ultrafast THz-pulse-induced tunneling dynamics in an STM,” *Proc. SPIE* **8984**, 898412 (2014).

[11] P. U. Jepsen, D. G. Cooke, and M. Koch, “Terahertz spectroscopy and imaging – Modern techniques and applications,” *Laser Photon. Rev.* **5**, 124-166 (2011).

[12] L. V. Titova, T. L. Cocker, D. G. Cooke, X. Wang, A. Meldrum, and F. A. Hegmann, "Ultrafast percolative transport dynamics in silicon nanocrystal films," *Phys. Rev. B* **83**, 085403 (2011)

XRD transients during capping of different sized InAs quantum dots on GaAs(001)

K. Shimomura[1], H. Suzuki[2], T. Sasaki[3], M. Takahasi[3], Y. Ohshita[1], and I. Kamiya[1]*

[1] Toyota Technological Institute, 2-12-1 Hisakata, Tempaku, Nagoya 468-8511, Japan

Phone: +81-52-809-1854 E-mail: sd12502@toyota-ti.ac.jp, *Corresponding author: kamiya@toyota-ti.ac.jp

[2] Faculty of Engineering, University of Miyazaki, Miyazaki 889-2192, Japan

[3] Japan Atomic Energy Agency, Hyogo 679-5148, Japan

Strain engineering is imperative to tune the emission wavelength of InAs quantum dots (QDs) on GaAs(001) for telecommunication applications. The emission wavelength of InAs QDs is redshifted when capped with InGaAs instead of GaAs [1]. While it is known that the QD lattice constants vary and larger lattices appear with increasing QD size [2], the influence of such lattice constants of the embedded QDs on strain between the QDs and cap layer has not been well studied. X-ray diffraction (XRD) is one of the very few techniques that can observe lattice strain on the nm scale, and has been successfully employed for the study of strain during GaAs capping on InAs QDs [3]. In this study, we report the XRD intensity transient during capping of different sized QDs and discuss the development of the strain in the system.

The experiments were performed at SPring-8 (BL11XU), Japan, using a molecular beam epitaxy - X-ray diffractometer (MBE-XRD) system. The InAs QD layer is grown on GaAs(001) at a substrate temperature of 470°C after buffer layer growth. The InAs growth rate is 0.017 ML/s. The X-rays 10 keV in energy with incident angle of 0.2° were reflected by the (220) planes and monitored by a CCD detector during the InAs QD and cap layer growth. The total amount of InAs deposition for the QDs was either 2.2 or 2.9 ML, and the 30-nm thick GaAs and $In_{0.09}Ga_{0.91}As$ cap layers were grown.

Figure 1 shows typical X-ray CCD images of InAs QDs with total deposition of 2.2 ML (a) before and after capping by (b) 4 nm, (c) 16 nm, or (d) 30 nm GaAs. The vertical axis represents the in-plane lattice constant normalized by that of the GaAs substrate. The horizontal axis shows the outgoing angle α normalized by the critical angle for total reflection of X-ray α_c. The XRD intensities from almost all lattice constants decrease monotonously with increasing cap thickness. In contrast, the XRD intensity from large lattice constant components (around 1.05) decreases with cap thickness, while that from small lattice constant (around 1.01) first decreases, then increases, and decreases again when capped by InGaAs. In the case of larger QD size, the trend of the XRD intensity transient is similar, whereas the rate of intensity variation is different. From these results, the development of the lattice strain during capping of different sized QDs will be discussed in detail.

This work was supported by the Strategic Research Infrastructure Project, MEXT, Japan. The synchrotron radiation experiments were performed at BL11XU of JAEA in Spring-8 with approval of Nanotechnology Platform project supported by MEXT, Japan.

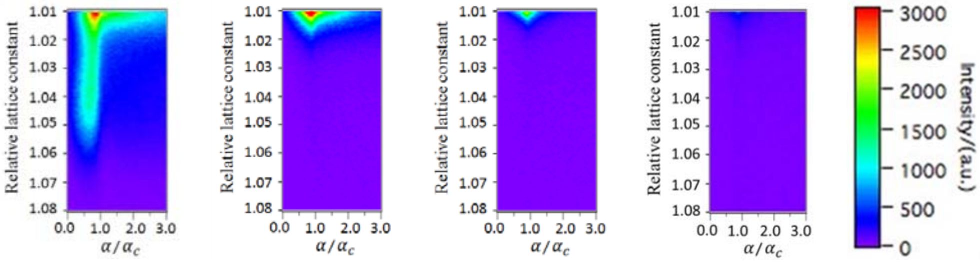

Figure 1. XRD images showing distribution of lattice constant of InAs QDs with total deposition of 2.2 ML (a) before and after capping by (b) 4 nm, (c) 16 nm, or (d) 30 nm GaAs.

[1] W. H. Chang, *et al.*, Appl. Phys. Lett. **86** (2005) 131917.

[2] M. Takahasi, *et al.*, Appl. Phys. Lett. **88** (2006) 101917.

[3] M. Takahasi and J. Mizuki, J. Cryst. Growth **275** (2005) e2201.

Atom Probe Tomography of GaAs-AlGaAs Core-Shell Nanowire Heterostructures

Nari Jeon[1], Stefanie Morkötter[2], Daniel Rudolph[2], Gregor Koblmüller[2], Lincoln J. Lauhon[1]
[1] *Department of Materials Science and Engineering, Northwestern University, USA*
[2] *Walter Schottky Institut and Physik Department, TU Munich, Germany*

Nonplanar heterostructures have been adopted in CMOS technology, have recently been commercialized in light emitting diode technologies, and are being considered in new generations of photovoltaics. However, analysis of the structure and properties of interfaces between semiconductors and metals, dielectrics, and other semiconductors becomes significantly more challenging when the interfaces are not planar. The increasing prevalence of nonplanar heterostructures motivates efforts to advance the three-dimensional characterization of interfaces. This contribution focuses on atom probe tomography (APT) characterization of nanowire heterostructures and 2D materials with an emphasis on correlated characterization of properties.

Nanowire radial core-shell heterostructures show promise in applications such as high-speed transistors, solar cells, and photodetectors. As in planar heterostructures, modulation doped nanowire heterostructures offer the potential to realize high carrier density without compromising mobility. However, the radial geometry presents significant challenges to the measurement of dopant distribution. We have analyzed the composition of modulation doped GaAs–$Al_xGa_{1-x}As$ core-shell nanowire heterostructures in three dimensions by atom probe tomography. Correlated analysis by electrical transport, optical spectroscopy, and high resolution electron microscopy reveals a rich set of features and properties unique to these nonplanar heterostructures, including 1-D quantum wires that arise due to the tendency of aluminum to segregate. To better understand the origins of these features, and control their morphology and distribution, a three-dimensional perspective is highly desirable. The nanowire heterostructures were grown by molecular beam epitaxy at TU Munich and analyzed by APT at Northwestern University. APT analysis of the Al enrichment at {110} facet vertices within the shells reveals frequent rotations of the threefold symmetric composition plots due to the introduction of stacking faults. These unusual heterostructures thereby provide the opportunity to examine simultaneous growth on adjacent facets of opposite polarity, and explore the impact on III-V alloy composition and growth rate. For the first time, the distribution of Si dopants within the AlGaAs shell is also revealed, facilitating analysis of the relationship between Al and Si diffusion and interpretation of transport measurements. Correlated studies of modulation doped planar heterostructures enable direct comparisons of intentional modulations in composition (e.g. doping) and unintentional modulations (e.g. segregation) in both planar and nonplanar geometries. Correlated atom probe tomography and photoluminescence analyses will also be presented.

Finally, recent efforts to analyze 2-D transition metal dichalcogenides by atom probe tomography will be presented.

Tu0930

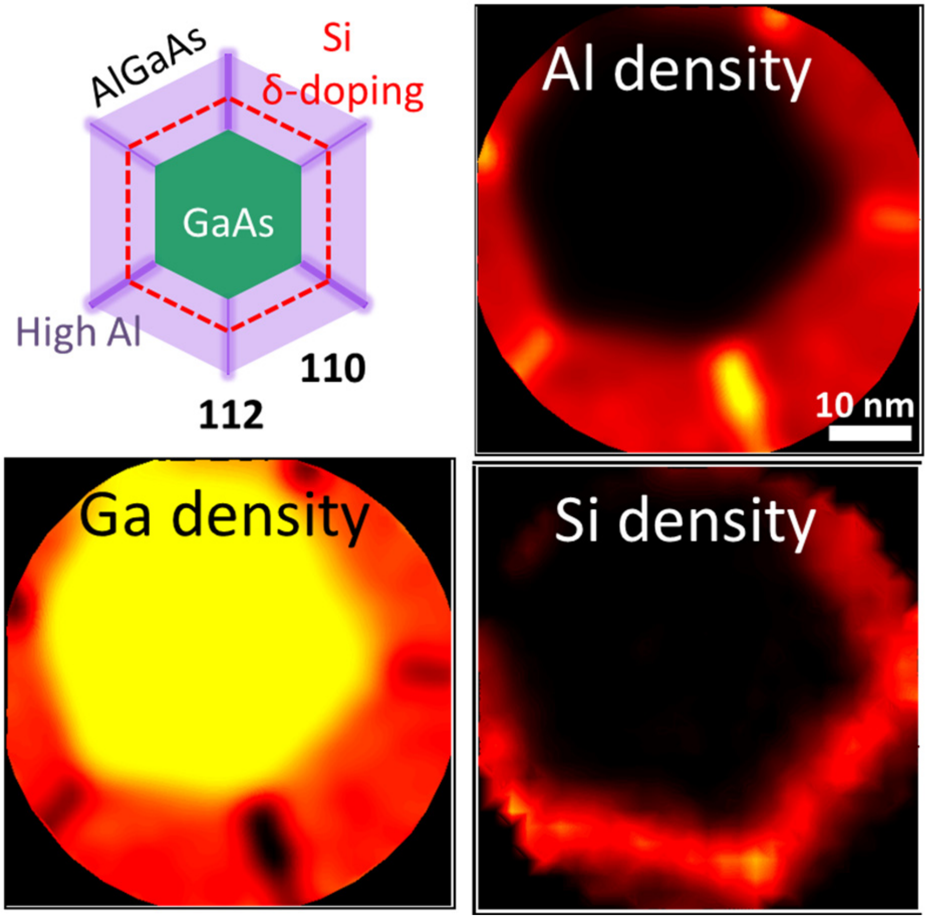

End view of atom probe tomography reconstruction of a GaAs-AlGaAs core-shell heterostructure nanowire revealing aluminum enrichment at {110} facet vertices and the distribution of Si dopant atoms.

Tu0935

Measuring the Electronic Confinement of a Subsurface Metallic State

Federico Mazzola[1], Mark T. Edmonds[2], Kristin Høydalsvik[1], Damien Carter[3], Nigel A. Marks[3], Bruce C. C. Cowie[4], Lars Thomsen[4], Jill Miwa[5], Michelle Yvonne Simmons[6] and **Justin W. Wells**[1]

1: Norwegian University of Science and Technology (NTNU), Trondheim, Norway,
2: School of Physics, Monash University, Clayton, Victoria 3800, Australia,
3: Nanochemistry Research Institute, Curtin University, Perth, WA 6845 Australia,
4: Australian Synchrotron, Clayton, Victoria 3168, Australia,
5: University of Aarhus, 8000 Aarhus C, Denmark, and
6: University of New South Wales, Sydney, NSW 2052, Australia

Dopant profiles in semiconductors are important for understand- ing nanoscale electronics. Highly conductive and extremely confined phosphorus doping profiles in silicon, known as Si:P δ-layers, are of particular interest for quantum computer applications, yet a quantitative measure of their electronic profile has been lacking. Using resonantly enhanced photoemission spectroscopy, we reveal the real-space breadth of the Si:P δ-layer occupied states and gain a rare view into the nature of the confined orbitals. We find that the occupied valley-split states of the δ-layer, the so-called 1Γ and 2Γ, are exceptionally confined with an electronic profile of a mere 0.40 to 0.52 nm at full width at half-maximum, a result that is in excellent agreement with density functional theory calculations. Furthermore, the bulk-like Si $3p_z$ orbital from which the occupied states are derived is sufficiently confined to lose most of its p_z-like character, explaining the strikingly large valley splitting observed for the 1Γ and 2Γ states.

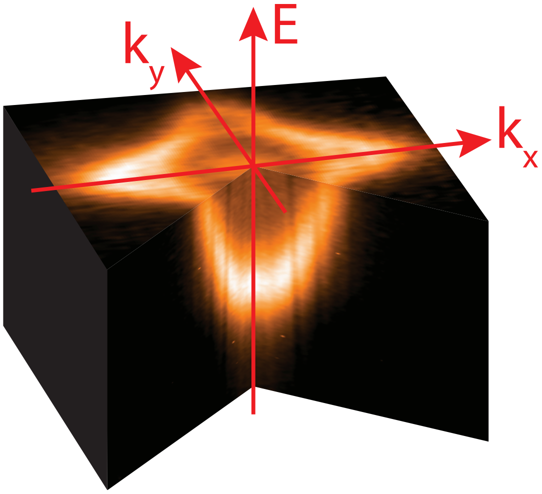

Figure: resonant ARPES measurement of a 2D electron gas buried >1 nm beneath the surface of Si(001), formed due to an atomically thin layer of dopants which has been placed there.

Tu0940

Growth, morphology and transport properties of high mobility (110) InAs quantum well metamorphic heterostructures

Adrian Podpirka[1*], Javad Shabani[2], Michael B. Katz[1], Shawn Mack[1], Mark E. Twigg[1], Chris J. Palmstrom[2] and Brian R. Bennett[1]

1. U.S. Naval Research Laboratory, Washington, DC 20375
2. University of California – Santa Barbara, Santa Barbara, CA 93106

One of the major challenges facing the semiconductor industry is to sustain the remarkable growth of the last few decades. The end of traditional Moore's law scaling is projected to occur in less than a decade leading to the need for the development of new technologies that overcome the fundamental limits of current devices. A promising route to complement current CMOS technology is the use of III-V materials with tunable spin orbit interaction in spin-field-effect transistors (SpinFETs). Among III-V semiconductor heterostructures, symmetric quantum wells grown in the (110) direction are of particular interest because of long spin relaxation times that could be achieved due to the (110) crystal symmetry. The (110) oriented quantum wells exhibit longer spin relaxation times due to the D'yakonov-Perel spin relaxation mechanism being suppressed. A key requirement of spinFETs is the high-mobility transport of carriers in the channel to allow for coherent propagation. InAs, with its large electron g-factor (~15), low electron mass and suitable buffer layers makes it a promising candidate for future spinFET devices.

In this work, we report on the growth and characterization of high mobility InAs quantum wells grown on highly mismatched (110) GaAs. Growth conditions for the AlGaSb buffer and the InAs QW were varied to maximize the two-dimensional electron gas mobility. Dislocation propagation and layer tilting was characterized using X-ray diffraction and transmission electron microscopy to determine the role it plays in growth and mobility (Figure 1A). A mobility of nearly 10,000 cm^2/Vs was obtained at room temperature through optimization of the buffer layer growth temperature (Figure 1B). Variations in buffer layer thickness and quantum well thickness led to mobilities of over 16,000 cm^2/Vs. Low temperature transport measurements exhibited Shubnikov - de Haas oscillations in the presence of a strong magnetic field. We show that the high temperature deposition of the buffer and the quantum well improve the electron mobility and that even with a similar surface roughness, significant variations in mobility are observed.

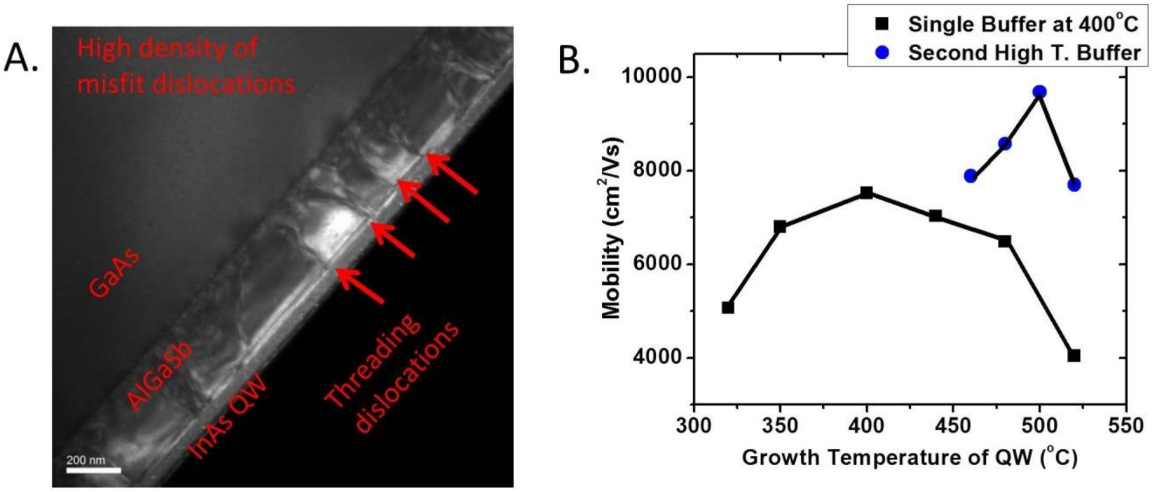

Figure1: (A) Cross-sectional TEM image of InAs QW grown on GaAs with thick AlGaSb buffer layer. (B) Room temperature mobility as a function of growth temperature for different buffer layer structure.

* presenting author: adrian.podpirka.ctr@nrl.navy.mil

Tu0945

In Situ Temporal Evolution of Plasma Enhanced Atomic Layer Epitaxy of InN Growth Studied by Synchrotron X-ray Methods

N. Nepal[1], V.R. Anderson[1], S.D. Johnson[1], B.P. Downey[1],
D.J. Meyer[1], A. DeMasi[2], K.F. Ludwig[2], and C.R. Eddy, Jr.[1]
[1]*U.S. Naval Research Laboratory, Washington, DC 20375, USA*
[2]*Physics Department, Boston University, Boston, Massachusetts 02215, USA*
*Email: neeraj.nepal.ctr@nrl.navy.mil

Atomic layer epitaxy (ALE) is a layer-by-layer materials growth method achieved by separating the reaction for growth into two surface-mediated half reactions at relatively low temperatures. Recently, plasma enhanced ALE (PA-ALE) has been used to grow epitaxial III-nitride films at temperatures from 180-500 °C [1-2]. At these growth temperatures, the ad-atom mobility is low and the growth process is significantly influenced by the nature of the substrate surface. Thus, the mechanism of nucleation and growth kinetics are very important to understand for improved material quality for technological applications. To monitor nucleation and growth mechanisms, ultra high vacuum *in situ* monitoring systems are hard to use during growth as the standard growth chamber pressure for ALE is in the order of 1-500 mTorr. Therefore high intensity coherent x-rays, such as from synchrotron light source, offer an effective method to monitor the ALE nucleation and growth process. Such methods can provide details of the stacking of atoms, nucleation and two dimensional (2D) growth mechanism, and strain development in the PA-ALE films during growth.

Here we present *in situ* studies on the temporal evolution of high quality InN growth on a-plane sapphire at 200-250 °C probed by synchrotron x-rays. The growth was carried out in thin film growth facility installed at beamline X21 of the National Synchrotron Light Source (NSLS) at Brookhaven National Laboratory (BNL). The surface pretreatment, nucleation and growth process were monitored using glancing incidence small angle x-ray scattering (GISAXS), x-ray fluorescence (XRF) and x-ray reflectivity (XRR) measurements. *Ex situ* Atomic force microscopy (AFM), x-ray photoelectron spectroscopy (XPS), x-ray diffraction (XRD) and Hall measurements were used for the post growth characterization.

In situ GISAXS measurement at the x-ray incidence angle of 0.8 degrees shows that H_2 plasma cleaning roughens the sapphire substrate surface, but this same surface is recovered completely during subsequent N_2 plasma pretreatment, which also reveals InN growth steps for each PA-ALE cycle at the optimal growth conditions. During the initial cycles (~1 nm growth) the specular peak broadens slightly indicating roughening of the surface during homogenous nucleation. At about 1.3 nm of growth Yoneda Wings start to evolve indicating surface roughening at a correlated length scale of 10 nm. After 3 nm of InN growth, the area in between these features fills in forming a 2D layer. *In situ* XRR measurement shows that for indium precursor (trimethylindium, TMI) and purge time of 30 seconds, the InN growth was self-limited with growth rate of 0.35 nm/cycle between 200-250 $^{\circ}$C. *Ex situ* AFM measurement shows that the root mean square surface roughness after 5 nm of ALE growth was 0.12 nm, which is lower than the resolution of AFM. Hall measurements show electron sheet carrier density and resistance of $3.5\mathrm{x}10^{13}$ cm^{-2} and 3.59 kΩ/sq, respectively. An electron mobility of 50 cm^2/V-s is measured, which is higher than the reported value of 30 cm^2/V-s for 1300 nm thick InN grown by MBE directly on sapphire [3]. *In situ* synchrotron x-ray study of the epitaxial growth kinetics of InN films is one of the most powerful methods to understand nucleation and growth mechanism to improve material quality and broaden material applications.

References:[1] Nepal et al., Cryst. Growth and Des. **13**, 1485 (2013). [2] Nepal et al., Appl. Phys. Lett. **103**, 082110 (2013). [3] Kuo et al., Diamond & Related Materials **20**, 1188 (2011).

Tu0950

Recent Advances In High Resolution Real And Reciprocal Space Photoelectron Emission Microscocopy

Konrad WINKLER[1], Nicholas BARRETT[2], Nils Weber[3], Matthias Escher[3]

Email: k.winkler@omicron.oxinst.com

[1]*Omicron NanoScience, Germany*, [2]*CEA/DSM/IRAMIS/SPCSI, F-91191 Gif-sur-Yvette, France,*
[3]FOCUS GmbH, *Germany*

Conventional electron spectroscopy methods are limited in providing simultaneous real and reciprocal or k-space information from small areas under laboratory conditions. Therefore, the characterization of materials with only micron scale sample homogeneity requires new instrumentation. Recent improvements in aberration compensated energy-filtered photoelectron emission microscopy (PEEM) can overcome the known limitations in both synchrotron and laboratory environments.

We present first results from real and reciprocal space photoelectron emission microscopy (PEEM) e.g. on Ag (111) showing high k and high energy resolution using a laboratory based He I and II radiation at room temperature and temperatures below 40K. The combination of a recently developed LHe cooled sample stage with an improved aberration compensated energy-filter allows 30 meV energy resolution while a new type of event counting detector improves the signal to noise ratio of the detector.

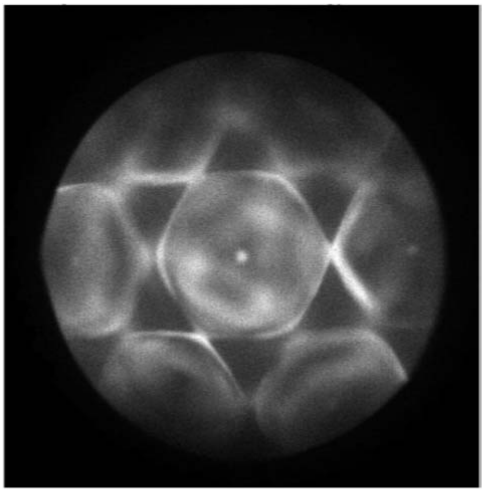

Figure 1: Photoemission data excited by a laboratory VUV light source (He II) from a Ag(111) surface at room temperature. The photoemission horizon (±90°start angles) corresponds to 6.0 (±0.1) Å^{-1}. The surface state visible in the centre of the image surrounded by six neighboring surface states defines a circle with a diameter of 5.02 Å^{-1} used to scale this image.

Tu0955

Polarity dependent pinning of a surface state

M. Schnedler,[1] V. Porz,[1] H. Eisele,[2] R.E. Dunin-Borkowski,[1] and Ph. Ebert[1]

[1]Peter Grünberg Institut, Forschungszentrum Jülich GmbH, 52425 Jülich, Germany
[2]Institut für Festkörperphysik, Technische Universität Berlin, Hardenbergstraße 36, 10623 Berlin, Germany

Chargeable electronic states at semiconductor surfaces and interfaces, with energies inside the fundamental band gap, commonly induce a phenomenon known as Fermi level pinning. These states can either arise from the interface bonding structure of the semiconductor with, e.g., a metal (so-called metal-induced gap states), or originate from the interruption of periodicity and broken (dangling) bonds at a semiconductor-vacuum surface. At high densities these surface states may accommodate large quantities of surface charges, which effectively shield the underlying semiconductor bulk from electric potentials applied at the surface or interface, respectively, e.g, by metal contacts. The screening shifts the semiconductor's bands and aligns the Fermi level with the energy of the surface or interface states (so-called Fermi level pinning). This effect influences the charge transport across the surface or interface and thus the Fermi level pinning phenomenon is of critical importance for semiconductor-based devices.

In this contribution we illustrate a polarity dependent Fermi level pinning on semiconductor surfaces with chargeable surface states within the fundamental band gap. Scanning tunneling spectroscopy of the GaN($10\underline{1}0$) surface shows that the intrinsic surface state in the band gap pins the Fermi energy at positive voltages only, but not at negative. This polarity dependence is attributed to low rates of electron transfer from the conduction band to the surface state due to quantum mechanically prohibited transitions. Thus, a chargeable intrinsic surface state in the band gap may not pin the Fermi level or only at one polarity, depending on the band to surface state transition rates under the experimental conditions. This leads to a one sided, polarity dependent Fermi level pinning and by itself can create rectifying behavior.

Characterization II

In-situ strain monitoring of suspended nanowires using nano-focused x-ray diffraction

J. Stangl[1], M. Keplinger[1], R. Griphone[2], J. Greil[3], A. Lugstein[3],

[1] *Institut für Halbleiter- und Festkörperphysik, Johannes Kepler Universität Linz, Altenbergerstraße 69, 4040 Linz, Austria*

[2] *European Synchrotron Radiation Facility, Rue Jules Horowitz 6, 38043 Grenoble, France*

[3] *Institute of solid state electronics, Vienna University of Technology, Floragasse 7, 1040 Vienna, Austria*

The search for optoelectronic building blocks compatible with state of the art silicon CMOS technology drives research on group IV-based direct band-gap semiconductor materials. Among several routes, strain engineering is promising, especially for germanium, which is theoretically predicted to become direct under sufficient tensile strain [1]. The practical realization of the required several percent of uniaxial strain along the crystallographic [111] direction is, however, rather challenging. Nanowires have been shown to be able to resist high tensile strains strain [2].

Here, high strain values have been achieved using complex straining devices to elongate suspended Ge or Si nanowires (NWs) [3,4]. For monitoring the strain values we use nanofocused synchrotron radiation. With focus sizes in the order of 150 nm, diffraction experiments on single nanowires are possible, and the strain variation along the wires can be investigated with a real space resolution of around 300 nm.

We found a complex strain state in the investigated Ge NWs, due to tapering and an amorphous shell covering part of the wires. In addition, we have measured the strain perpendicular as well as along growth direction for Si NWs in a device where we could change the strain in-situ. This allowed to measure the Poisson ratio of Si at nanoscale dimensions.

[1] F. Zhang, V. H. Crespi, and P. Zhang, Phys. Rev. Lett., **102**, 156401, (2009).

[2] D. A. Smith, V. C. Holmberg, and B. A. Korgel, ACSNano, **4**, 2356–2362, (2010).

[3] J. Greil, A. Lugstein, C. Zeiner, G. Strasser, and E. Bertagnolli, Nano Letters, **12**, 6230–6234, (2012).

[4] A. Lugstein, M. Steinmair, A. Steiger, H. Kosina, and E. Bertagnolli, Nano Letters, **10**, 3204–3208, (2010).

Corresponding author email: Julian.stangl@jku.at

Characterization of Aluminum Nitride Grown by Atomic Layer Epitaxy with *in situ* Grazing Incidence Small Angle X-ray Scattering

V.R. Anderson*, N. Nepal, S.D. Johnson, A. DeMasi, J.K. Hite, K.F. Ludwig, and C.R. Eddy, Jr.
*Email: Virginia.Anderson.ctr.@nrl.navy.mil

Semiconductors in the III-V nitride family have high breakdown fields and direct band gaps, properties that make them attractive for photovoltaics, transistors, and photonics. Recent research on III-nitrides suggests there may be an alternative to the current primary methods of growth, which are molecular beam epitaxy and chemical vapor deposition. Atomic layer epitaxy (ALE) of the III-nitrides would add more possible structures and devices by allowing thinner films and lower growth temperatures for these semiconductors. Films of GaN, AlN, and InN have been deposited in a plasma capable Ultratech/Cambridge Nanotech atomic layer deposition system. The deposition temperatures and film purities are lower than the GaN, AlN, and InN deposited by molecular beam epitaxy (MBE) and metalorganic chemical vapor deposition (MOCVD), and improving the understanding of the film deposition process remains the subject of ongoing research.[1] Epitaxial AlN on GaN was seen at 500 °C, rather than the >1000°C used for MOCVD. In addition, indium nitride was as low as 183 °C, as opposed to the 450 °C generally required for MOCVD, and a previously unreported crystal phase was the result.[2] In order for epitaxial quality film, the substrates and surface preparation are important, both *in situ* and *ex situ*.

Using a custom reactor at the Brookhaven synchrotron, *in situ* glancing incidence small angle X-ray scattering (GISAXS) was used to examine substrate preparation and ALE AlN film growth. The deposition was performed using trimethylaluminum and a hydrogen/nitrogen plasma. The substrates were MOCVD gallium nitride on sapphire.

Ideal growth of ALE is layer-by-layer, and since that is difficult to achieve, *in situ* observation is important for tuning growth conditions. The scattering from the surface during the plasma cleaning steps before depositing AlN showed that the substrate GaN was roughened during H_2 plasma. The roughening of the surface during AlN deposition suggests formation of AlN islands during early deposition, and comparison of various growth conditions will be done in future synchrotron studies. After the GISAXS monitored films were grown, they were examined *ex situ* with X-ray photoelectron spectroscopy and atomic force microscopy, and the information on the chemistry and morphology will be reported.

The GISAXS method of probing surface changes during atomic layer epitaxy of AlN provided information on the film interface. Continuing characterization of the films could lead to advances in high mobility transistors and optoelectronic devices by leading to improvements in the film quality.

References:

---

[1] N. Nepal et al., *Appl. Phys. Lett.* **103** 082110 (2013).
[2] N. Nepal et al., *Cryst. Growth Des.* **13**1485 (2013).

Tu1140

Characterization of Aluminum Nitride Grown by Atomic Layer Epitaxy with *in situ* Grazing Incidence Small Angle X-ray Scattering

[1]V.R. Anderson*, [1]N. Nepal, [1]S.D. Johnson, [2]A. DeMasi, [1]J.K. Hite, [2]K.F. Ludwig, [1]C.R. Eddy, Jr.

[1]US Naval Research Laboratory, [2]Department of Physics, Boston University

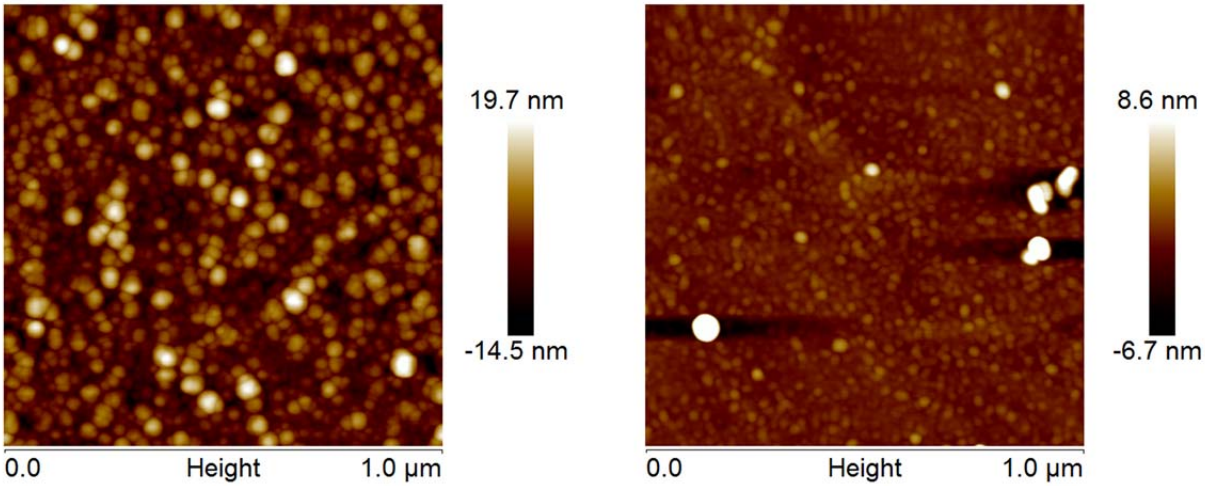

AFM images of (left) AlN with surface roughness of 3.9 nm deposited on plasma treated MOCVD GaN, and (right) a starting MOCVD GaN surface with 1.5 nm roughness.

Partial Electron Yield NEXAFS Imaging Using Magnetic Collection Lens

Conan Weiland,[*],[†] Daniel A. Fischer,[‡] Cherno Jaye,[‡] Zugen Fu,[‡] Kirk Scammon,[¶] Peter Sobol,[†] and Edward L. Principe[†]

Synchrotron Research, Inc., National Institute of Standards and Technology, and University of Central Florida

E-mail: cweiland@synchres.com

Chemical spectral imaging with simultaneously a high througput, a large depth of field, large field of view, and fine imaging resolution is difficult to achieve using traditional imaging methods. The large area rapid imaging analysis tool, or LARIAT, achieves all of these in partial electron yield near-edge x-ray absorption fine structure imaging through the use of a magnetic lens. The magnetic lens imaging permits the collection of all eletrons emitted within the field of view, leading to rapid data collection times. With the use of a high-temperature superconducting magnet, resolutions on the order of 5 μm are achieved, with sufficiently homogeneous magnetic field to provide a 2x2 cm^2 filed of view and depth of field of a few mm. We will present features of the design of the LARIAT microscopes and experimental results demonstrating the instrumental capabilities.

---

[*] To whom correspondence should be addressed

[†] Synchrotron Research, Inc.

[‡] National Institute of Standards and Technology

[¶] University of Central Florida

Rump Session:

2D Materials & Heterostructures

Tu1930 Invited

The Growth of 2D Heterostructures

Joshua A. Robinson
Materials Science and Engineering
The Center for 2D and Layered Materials
The Pennsylvania State University

Since 2004, the overwhelming majority of electronic transport of 2D materials has been reported using mechanically exfoliated flakes. Recently, there has been a concerted effort to directly synthesize layered transition-metal dichalcogenides (TMDs), with powder vaporization synthesis paving the way for direct growth of atomically thin structures. Beyond monolayer TMDs, van der Waals heterostructures (heterogeneous stacks of dissimilar atomic layers) have been predicted to lead to novel electronic properties not found in their constituent layers, where their realization has primarily come from mechanical exfoliation and stacking. Manual stacking has provided experimental verification of electronic bandgap modulations and strong interlayer coupling, but it can also lead to interface contamination that introduces additional scattering mechanisms and inhibits electronic coupling between the layers. I will discuss synthetic routes to achieve van der Waals (vdW) heterostructures and alloys with pristine interfaces, and provide evidence that direct synthesis, rather than mechanical stacking, will be the critical step in the advancement of the field.

Wednesday

We0745	Registration and Continental Breakfast
We0845	Wednesday Morning Session: *Complex Oxides and Ferroelectrics II*
We1005	Coffee Break and Poster Viewing
We1105	Wednesday Morning Session: *InAs Based Heterostructures*
We1155	Lunch and Poster Viewing
We1400	Wednesday Afternoon Session: *Novel Heterostructures*
We1510	Coffee Break and Poster Viewing
We1615	Wednesday Afternoon Session: *Graphene and Other 2D Materials*
We1800	Conference Banquet

Complex Oxides & Ferroelectrics II

We0845 Invited

Engineering Transport and Magnetism at Perovskite Cobaltite Interfaces *via* Controlled Oxygen Vacancy Ordering

S. Bose[1], J. Walter[1], M. Sharma[1], M. Torija[1], J. Gazquez[2,3], M. Varela[2], V. Lauter[4],
H. Ambaye[4], R. Goyette[4], M. Fitzsimmons[5], and C. Leighton[1]

[1] *Dept. of Chemical Engineering and Materials Science, University of Minnesota, USA*
[2] *Materials Science and Technology Division, Oak Ridge National Laboratory, USA*
[3] *Universidad Complutense de Madrid, Spain*
[4] *Spallation Neutron Source, Oak Ridge National Laboratory, USA*
[5] *Los Alamos Neutron Science Center, Los Alamos National Laboratory, USA*

The formation of electronic and magnetic “dead layers” at interfaces in complex oxide heterostructures is a general issue of considerable fundamental interest, with important implications for devices. In our recent work we have employed epitaxial thin films of the perovskite cobaltite $La_{1-x}Sr_xCoO_3$ (LSCO) [1] (a material of interest for solid oxide fuel cells, catalysis, gas separation mebranes, oxide spintronics, *etc.*), as a model system to probe the origins of electronic and magnetic property degradation at oxide interfaces. In $SrTiO_3$(001)/LSCO the dramatic suppression in magnetization and conductivity in the very thin film limit was found to occur due to interface-induced magnetic phase separation, nanoscopic ferromagnetic metallic clusters forming in a non-ferromagnetic insulating matrix [2]. This is driven by O vacancy formation near the interface, related to a novel mechanism of strain relaxation based on O vacancy ordering [2]. With this understood, in the current work we demonstrate how this defect ordering can be controlled *via* strain and crystallographic orientation, using various substrates [3]. Then, by combining cross-sectional STEM/EELS, magnetometry, neutron reflectometry, transport, and magnetotransport we demonstrate this as a novel means to control interface transport and magnetism. Specific results include dramatic suppression of the dead layer thickness under optimized conditions (we obtain bulk-like magnetic and transport properties down to 6-7 unit cell thickness on $LaAlO_3$(001) [4]), highly anisotropic transport on $SrTiO_3$(110) [4], and strongly enhanced magnetic anisotropy and anisotropic magnetoresistance due to symmetry-lowering from oxygen vacancy ordering [5]. Controlled oxygen vacancy ordering appears to be an attractive general approach to tailoring the physical properties of such materials.

Work supported by NSF and DoE (specifically neutron scattering).

[1] Torija, Sharma, Fitzsimmons, Varela, Wu and Leighton, *J. Appl. Phys.* **104,** 023901 (2008); Sharma, Gazquez, Varela, Schmitt and Leighton, *J. Vac. Sci. Technol.* **29,** 051511 (2011).

[2] Torija, Sharma, Gazquez, Varela, He, Schmitt, Borchers, Laver, El-Khatib and Leighton, *Adv. Mater.* **23,** 2711 (2011).

[3] Gazquez, Bose, Sharma, Torija, Pennycook, Leighton and Varela, *APL Mater.* **1**, 012105 (2013).

[4] Bose, Sharma, Torija, Gazquez, Varela, Ambaye, Goyette, Lauter, Zhernenkov, Fitzsimonns, Hovorka, Berger, Schmitt and Leighton, unpublished.

[5] Walter, Gazquez, Varela and Leighton, unpublished.

We0925 Upgraded

Two-dimensional electron gas at the epitaxial oxide/SrTiO₃ interface: tuning oxygen vacancies

Kristy J. Kormondy,[1] Agham B. Posadas,[1] Thong Q. Ngo, [2] Sirong Lu,[3] Nicholas Goble,[4] Xuan P. A. Gao,[4] Martha R. McCartney,[3] David J. Smith,[3] John G. Ekerdt,[2] and Alexander A. Demkov[1]
[1]Department of Physics, University of Texas at Austin, Austin, Texas, 78712; [2]Department of Chemical Engineering, University of Texas at Austin, Austin, Texas 78712; [3]Department of Physics, Arizona State University, Tempe, Arizona, 85287; [4]Department of Physics, Case Western Reserve University, Cleveland, Ohio 44106

In recent studies of the two-dimensional electron gas (2DEG) at the oxide/oxide interface where one of the oxides is $SrTiO_3$ (STO), no matter whether the mechanism is oxygen vacancies, cation substitution, or polar catastrophe, confined conduction in STO is a common thread. Simultaneously, a growing body of work has developed particularly investigating formation of oxygen vacancies in STO and their properties [1]. One approach involves heteroepitaxy of aluminum-based oxides to stabilize an ultra-thin oxygen-deficient STO layer that demonstrates confined conduction [2-3].

In order to study methods for controlling this conducting layer, molecular beam epitaxy (MBE) was employed to fabricate well-ordered heterostructures with atomic layer-by-layer control. Thin (0.1-7.0 nm) γ-alumina films were deposited on single-crystal STO (001) at substrate temperatures ranging from 400-800°C. Crystallinity of alumina was monitored during deposition with reflection high-energy electron diffraction. X-ray diffraction and negative spherical aberration corrected high-resolution transmission electron microscopy imaging reveal an abrupt interface with highly crystalline epitaxial alumina on the STO substrate (Fig. 1).

The properties of the resulting conducting interfacial layer depend on growth parameters, particularly substrate temperature during film depostition. *In-situ* x-ray photoelectron spectroscopy (XPS) of the Ti 2*p* core level provides quantification of the oxygen vacancy concentration on the STO side of the interface (Fig. 2). This analysis of reduced titanium was repeated for samples of different film thickness and substrate temperature (Fig. 3).

Furthermore, conductivity measurements as a function of temperature reveal metallic behavior for the interface between the two insulators (Fig. 4). Comparison between two samples (one deposited at a substrate temperature of 400°C and the other at 600°C) indicates a decrease in sheet resistance for increased deposition temperature. A maximum electron Hall mobility of 3100 $cm^2V^{-1}s^{-1}$ measured for the heterostructure at 3.2 K, with a room temperature mobility of 22 $cm^2V^{-1}s^{-1}$. Conduction ceases following oxygen anneal, confirming STO oxygen vacancies as the mechanism of conduction.

These results indicate that MBE-grown γ-alumina on STO (001) offers a controlled method for formation of a conducting oxygen-deficient STO layer near the interface. This tunability lends itself to both the development of sensors and the investigation of novel physical phenomena.

[1] C. Lin and A.A. Demkov, Phys. Rev. Lett. 111, 217601 (2013).
[2] Y.Z. Chen, N. Bovet, T. Kasama, W.W. Gao, S. Yazdi, C. Ma, N. Pryds, and S. Linderoth, Adv. Mater. 26, 1462 (2014).
[3] S.W. Lee, Y. Liu, J. Heo, and R.G. Gordon, Nano Lett. (2012).

We0925 Upgraded

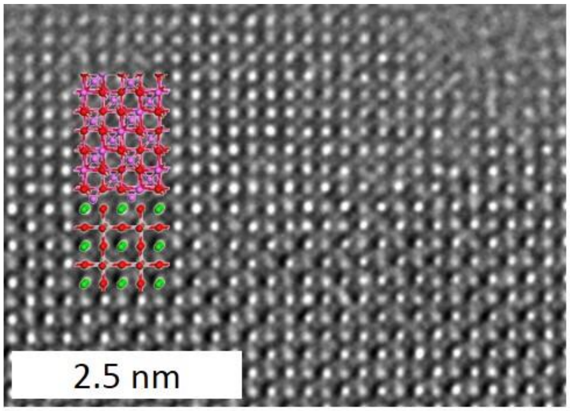

Figure 1: Negative spherical aberration high-resolution transmission electron microscopy imaging reveals an abrupt interface with highly crystalline epitaxial alumina on the STO substrate.

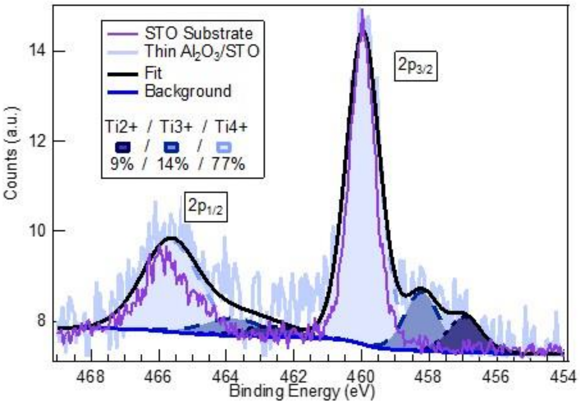

Figure 2: Peak decomposition of the Ti 2*p* core level in STO allows a comparison of intensities from Ti in different oxidation states.

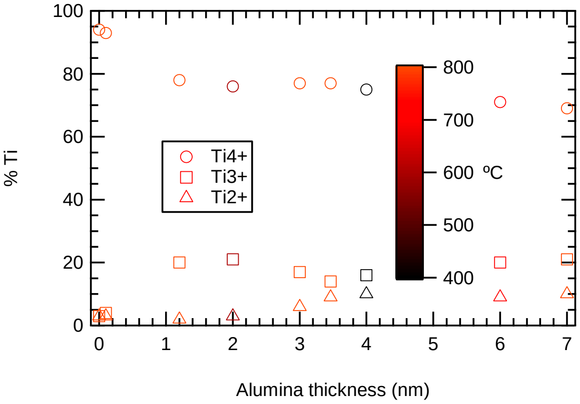

Figure 3: Analysis of reduced titanium based on XPS Ti 2*p* spectra for samples of varied thickness (0-7 nm) and substrate temperature during deposition (400-800°C).

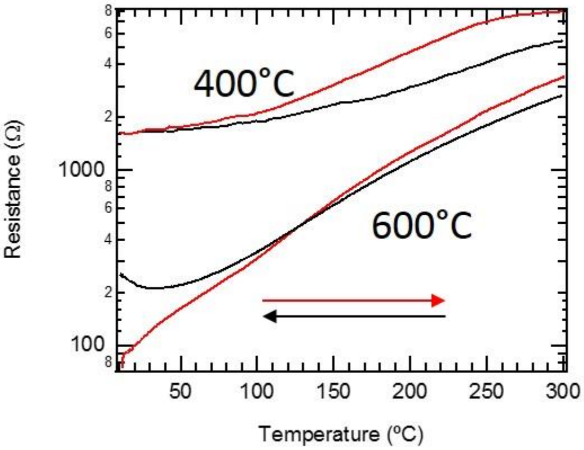

Figure 4: Resistance as a function of temperature for 4nm and 6 nm alumina/STO deposited at 400C (top two curves) and 600C (bottom two curves). The black and red colored data were collected during cool down and warm up respectively, and measured with current along two perpendicular directions in a square shaped sample using the van der Pauw method.

We0945

Optical properties of transition metal oxide quantum wells

Alexander A. Demkov[a], Miri Choi[a], Chungwei Lin[a], Matthew Butcher[a], Cesar Rodriguez[b], Qian He[c], Agham B. Posadas[a], Albina Y. Borisevich[c], and Stefan Zollner[b]

[a]Department of Physics, The University of Texas at Austin, Austin, TX 78712, USA
[b]New Mexico State University, Department of Physics, Las Cruces, NM 88003, USA
[c]Materials Science and Technology Division, Oak Ridge National Laboratory, Oak Ridge, TN 37831, USA

We report on the investigation of $SrTiO_3$ (STO) quantum wells (QWs) grown by molecular beam epitaxy. The QW structure consists of $LaAlO_3$ (LAO) and STO layers grown on LAO substrate. Structures with different QW thicknesses ranging from two to ten unit cells were grown and characterized. Optical properties were measured by spectroscopic ellipsometry (SE) in the range of 1.0 eV to 6.0 eV at room temperature. We observed that the absorption edge was blue-shifted by approximately 0.39 eV as the STO quantum well thickness was reduced to two unit cells (uc). This demonstrates that the energy level of the first subband can be controlled by the QW thickness in a complex oxide material.

Owing to advances in layer-by-layer growth techniques, it has become possible to fabricate artificial structures based on high quality transition metal oxide (TMO) films. This in turn has enabled band engineering, interface manipulation and dimensional control in oxide heterostructures. Compared to semiconductor heterostructures, where constituent materials typically have band gaps on the order of 1.0 eV thus limiting the band offset, TMOs can have rather large band discontinuities. STO has a 3.2 eV band gap and LAO has a 5.6 eV band gap, and as the valence band maxima have similar energy levels (the valence band offset is only 0.2 eV), the conduction band offset between the two materials is expected to be about 2.3 eV. This makes the system attractive for short wavelength (visible to near UV) inter-sub-band (ISB) devices. The conduction band bottom of STO is formed by the Ti t_{2g} orbitals and in the bulk is triply degenerate. At the interface with LAO the degeneracy of Ti t_{2g} orbitals is lifted, with the d_{xy} band shifting to lower energy. When the STO QW thickness is decreased, the entire conduction band starts feeling the effects of confinement. This confinement causes the band structure to develop sub-bands corresponding to the quantum well levels. By controlling the QW thickness, one can manipulate the number of quantized energy levels in the well and the energy separation between them. STO films can be readily n-type doped making STO/LAO QW heterostructures a natural candidate for unipolar ISB devices. Finally, these structures can be readily integrated with conventional semiconductors thus opening a route for hybrid systems involving *e.g.*, silicon nano-photonics.

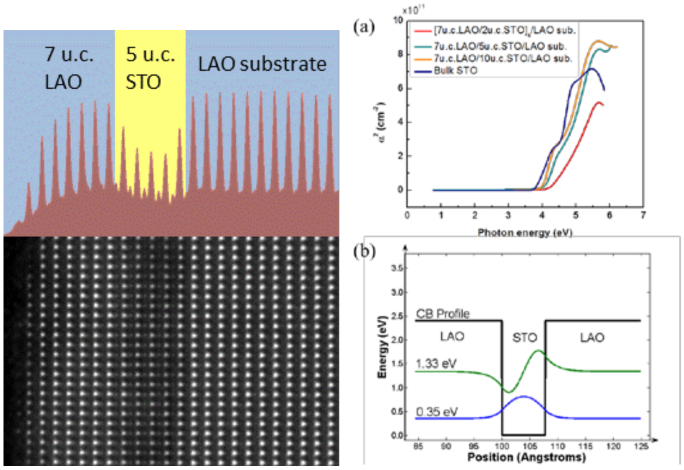

Figure 1. left: STEM image of the oxide quantum well; right: (a) The square of absorption coefficient of STO QW *vs* photon energy for bulk STO and for STO QW structures. (b) Calculated ground and first excited states of a two unit cell thick STO QW using a Poisson-Schrödinger solver.

We0950

Influence of Structural Order on the Properties of ALD VO_2 Films

Virginia Wheeler, Marko Tadjer, Marc Curie, Zachary Robinson, Jordan Greenlee, Neeraj Nepal, Tim Nunney, Fritz Kub, and Charles Eddy Jr.

U.S. Naval Research Laboratory, Washington, DC 20375
ThermoFisher Scientific, West Sussex, UK

Vanadium oxides are thermochromic materials which exhibit large, abrupt changes in thermal emittance, optical transmittance and reflectance, and intrinsic electrical properties due to a metal-insulator phase transition (MIT). Thus, these functional materials offer great advantages in a variety of applications including electrochemical applications, energy storage and conversion processes, thermoelectric devices, Mott transistors, and smart windows. In this work, atomic layer deposition (ALD) was used to produce thin, highly uniform, amorphous VO_2 films which enabled the investigation of the impact structure (amorphous vs. crystalline) has on the rate of change of intrinsic properties due to the MIT.

Amorphous vanadium oxide films (5-45nm) were deposited by ALD at 150°C using tetrakis(ethylmethyl)amido vanadium and ozone precursors. X-ray photoelectron spectroscopy (XPS) was used to verify the quality, stoichiometry, and depth uniformity of the films. All as-grown films exhibited carbon surface contamination due to atmospheric transfer from the ALD to XPS chambers. Moreover, the top ~1nm of the film exhibited V*2p* peaks at 517.7 and 516.3eV correlating to V_2O_5 or vanadium oxycarbide and VO_2 components, respectively. XPS depth profiles using gas cluster ions, to prevent selective etching, were conducted to determine the stoichiometry throughout the thickness of the films. At depths >~1nm, no residual carbon contamination and only a single VO_2 peak was detected. The FWHM of the VO_2 peak ranged from 2-2.7 eV, which is similar to crystalline films and indicative of the high uniformity and quality of these films. Additionally, the depth profiles revealed the presence of a low binding energy shoulder at 513.5 eV near the VO_x/Si interface, suggesting that initially the films were very oxygen deficient.

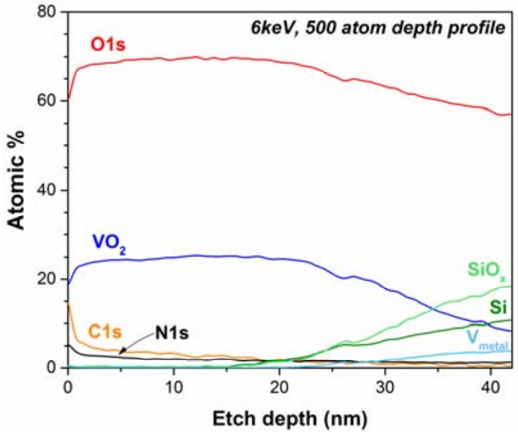

Ex situ anneals were employed in to induce crystallinity in these as-deposited amorphous ALD films. The influence of temperature (200-550°C), time (0.17-3hr), and gas environment (Ar/H_2, Ar, and O_2) on the ability to obtain single phase VO_2 films was investigated. Initial results indicate that only O_2 anneals produce crystalline VO_2, but other critical factors including gas partial pressure and temperature must be optimized to inhibit multiple orientations or multiphase films.

Electrical and optical performance of amorphous and crystalline ALD films was assessed as a function of temperature. Unlike crystalline VO_2 films that exhibit an abrupt, up to five orders of magnitude change in resistance around the MIT point at 68°C, amorphous VO_2 films had an exponential change in resistance of ten orders of magnitude over the entire temperature range studied (77-500K). The larger, more gradual electrical change could be useful for some devices such as bolometers. Initial optical measurements showed that amorphous films had a gradual ~2% increase in transmittance from 30-90ºC, while optimized crystalline films had >40% decrease in transmittance over the same temperature range. These variations show the importance of structural order on the exhibited properties of VO2 films and define the limits for different applications of interest.

We0955

Structural variations of epitaxial $PbVO_3$ thin films on $LaAlO_3$(001), $SrTiO_3$(001), and MgO(001) crystal substrates

Seol Hee Oh[1], Hye-Jin Jin[1], Hae-Young Shin[1], Seokhyun Yoon[1], Sung Jin Kang[2], Miyoung Kim[2], Jai-Seok Ahn[3], Janghwan Cha[4], Suklyun Hong[4], Sukgeun Choi[5], and William Jo[1,*]

[1]Department of Physics, Ewha Womans University, Seoul, Korea
[2]Department of Materials Science and Engineering, Seoul National University, Seoul, Korea
[3]Department of Physics, Pusan National University, Busan, Korea
[4]Department of Physics and Graphene Research Institute, Sejong University, Seoul Korea
[5]National Renewable Energy Laboratory, Golden, Colorado, USA
*E-mail: wmjo@ewha.ac.kr

Layered perovskite $PbVO_3$ (PVO) is an intriguing polar magnetic material because its strong tetragonal distortion allows VO_5 square-pyramidal structure rather than VO_6 octahedron [1]. Its unique feature exhibits the 2-dimensional antiferromagnetic ordering and large pyroelectric polarization [2]. It is notable that the c-axis of the PVO films is abnormally elongated more than 5% on the well-lattice matched $LaAlO_3$ substrates [3]. Phase formation of the tetragonal PVO thin films deposited under various Ar:O_2 gas and laser fluence on $LaAlO_3$ (001) substrates was investigated. In this study, structural properties of the PVO thin films were investigated by applying mechanical and chemical strain using lattice mismatch with substrates and Pb-deficiency. Substitution of vanadium ions to Pb sites in PVO thin films was demonstrated by X-ray diffraction and energy dispersive X-ray analysis. Phase formation with local structure and dielectric functions of the PVO thin films were investigated by Raman scattering spectroscopy and spectroscopic ellipsometry, respectively. In addition to, interfacial layer between PVO thin film and substrate was investigated by high resolution transmission electron microscopy.

[1] A. A. Belik *et al.*, Chem. Mater. 17, 269 (2005).

[2] A. Kumar *et al.*, Phys. Rev. B 75, 060101 (2007).

[3] S. H. Oh *et al.*, J. Phys. D: Appl. Phys. **47**, 245302 (2014).

We1000

Atomic structure and intrinsic electronic states of the In_2O_3(111) surface

Holger Eisele,[1] Robert Zielinski,[1] Andrea Lenz,[1] Zbigniew Galazka,[2]
and M. Dähne[1]
[1]Institut für Festkörperphysik, Technische Universität Berlin, Hardenbergstraße 36, 10623 Berlin, Germany
[2]Leibniz Institute for Crystal Growth, Max-Born-Str. 2, 12489 Berlin, Germany
Email Address: ak@physik.tu-berlin.de

Indium oxide as transparent semiconductor is one of the most promising materials for contact layers in photovoltaic applications. Nevertheless, due to the delicate fabrication process for single crystals only a few intrinsic properties are known about In_2O_3, yet. Especially the storage under air conditions may influence the surface properties. Even from excellent experimental results it is hence hard to decide, which properties are intrinsic and which ones are influenced by physisorbed and/or chemisorbed atoms and molecules from the ambient air.

In this contribution for the first time we studied high quality single crystals at their freshly UHV-cleaved (111) surfaces by scanning tunneling microscopy (STM) and spectroscopy (STS). Using freshly from bulk material cleaved surfaces is the only possibility to receive stoichiometric conditions. From these investigations we achieve knowledge about the atomic configuration at the surface. The found configuration fits well with recent density functional theory calculations, and indicates a local charge enhancement within the surface unit cell. Furthermore, STS reveals intrinsic electronic surface states within the fundamental band gap. The Fermi level is energetically located within the fundamental bulk band gap, which leads to the assumption that previously reported electron accumulation at this surface is not an intrinsic property, but related to extrinsic effects, such as e.g., non-stoichiometric material reorganization. After oxidation of the In_2O_3(111) surfaces outside the UHV their structural as well as their electronic properties look quite different: astonishingly both show a much more metallic behavior as the freshly cleaved ones kept under UHV-conditions. The processes leading to such a behavior are still under discussions, but the data of the oxidized surface fits much better to previous observations not using the cleavage technique for surface preparation.

InAs Based Heterostructures

We1105 Invited

Engineering 2D Topological Insulators from InAs/GaSb Semiconductors

Rui-Rui Du

Department of Physics and Astronomy
Rice University

Topological insulators (TIs) are a novel class of materials with nontrivial surface or edge states. Time-reversal symmetry (TRS) protected TIs are characterized by the Z_2 topological invariant. We have engineered a TI made of electron-hole bilayers from indium arsenide-gallium antimonide (InAs/GaSb) semiconductors, and observed robust helical liquid edge states with wide conductance plateaus precisely quantized to $2e^2/h$ in a broad temperature range. We found an unexpectedly long scattering-time of the edge states due to Z_2 protection. Remarkably, the quantized plateaus persist to 10T applied in-plane field before transitioning to a trivial semimetal. In a perpendicular field, broken TRS leads to a spatial separation of the movers in the Kramers pair and consequently the intra-pair backscattering phase space vanishes, *i.e.*, the conductance increases from $2e^2/h$ in strong fields manifesting chiral edge transport. In addition, since the helical liquid edge states have a small Fermi velocity (in the order of $2x10^4$ m/s), electron interaction effects play important roles in transport properties. We will discuss the surprising observations that the edge conductance is independent of temperatures down to the millikelvin regime, and possible relevance to the helical Luttinger liquids and other correlated 1D electronic states. Finally, we will mention the experimental approaches in engineering proximity-induced superconductivity on the helical edge devices that hosting Majorana zero-modes.

Reference

1. H. Kroemer, The 6.1Å family (InAs, GaSb, AlSb) and its heterostructures: a selective review. *Physica* E 20 196 – 203 (2004).
2. Ivan Knez, R.R. Du, and G. Sullivan, Evidence for Helical Edge Modes in Inverted InAs/ GaSb Quantum Wells, *Phys. Rev. Lett*. **107**, 136603 (2011).
3. J.C.Y. Teo and C.L. Kane, Critical Behavior of a Point Contact in a Quantum Spin Hall Insulator, Phys. Rev. B **79**, 235321/1-22 (2009).

InAs heterostructures with superconducting contacts

J. Shabani[1], B. Shojaei[2], S. Das Sarma[3], K. Shtengel[4], R. Lutchyn[5], C. Nayak[5,6] and C.J. Palmstrøm[1,2,7]

[1] California NanoSystems Institute, University of California, Santa Barbara
[2] Materials Department, University of California, Santa Barbara
[3] Physics Department, University of Maryland, College Park
[4] Physics Department, University of California, Riverside
[5] Microsoft Station Q, Santa Barbara
[6] Physics Department, University of California, Santa Barbara
[7] Department of Electrical Engineering, University of California, Santa Barbara

The hybrid devices based on superconductor-semiconductor interface combine the macroscopic superconducting properties of the superconducting leads with the microscopic degrees of freedom of the semiconductor. The semiconducting part allows tuning these degrees of freedom using gate voltages which gives access to a variety of exotic transport regimes and new device functionalities. Recently theory and experiment suggest that new quasiparticles, Majorana zero-mode, can emerge under certain conditions at a superconductor/semiconductor interface. It has been predicted that even richer physics emerge at an interface between superconductors and semiconductors in the quantum Hall regime. Quantum Hall systems host a variety of novel states of matter that can be controlled by magnetic fields, electrical gating and doping. In addition, excitations in quantum Hall systems carry electrical charge, which allows for their control and utilization in quantum circuit elements. Although techniques for semiconductor and superconductor growth are individually well established, combining them experimentally is a formidable task. The magnetic fields needed for the quantum Hall effect are generally deleterious to superconductivity, but some superconductors can tolerate such fields.

We have studied different ways of making superconducting contacts to several III-V high mobility 2DESs including GaAs and InAs. The advantage of the GaAs system is that quantum Hall physics are well-studied and many fractional quantum Hall states have been observed, however, it is difficult to achieve a good interface with superconductors due to depletion of electrons near surface. Another approach is to explore InAs where due to their surface Fermi level pinning good interfaces can be made to superconductors. One of the current challenges lies in understanding InAs material properties and limitations in quantum Hall studies. For example no fractional quantum Hall state has been observed in narrow bandgap semiconductors so far. We have studied for the, first time, metal insulator transition and mobility vs density dependence of several InAs samples and have extracted dominant scattering mechanisms. A comparison of these scatterings with the Landau level broadening calculated from the onset of Shubnikov de Haas indicates that there is a substantial gap (between the numbers) as opposed to GaAs material systems.

Part of this work is funded by Microsoft Station Q, University of California, Santa Barbara. A portion of this work was performed at the National High Magnetic Field Laboratory, which is supported by National Science Foundation Cooperative Agreement No. DMR-1157490, the State of Florida, and the U.S. Department of Energy.

We1145

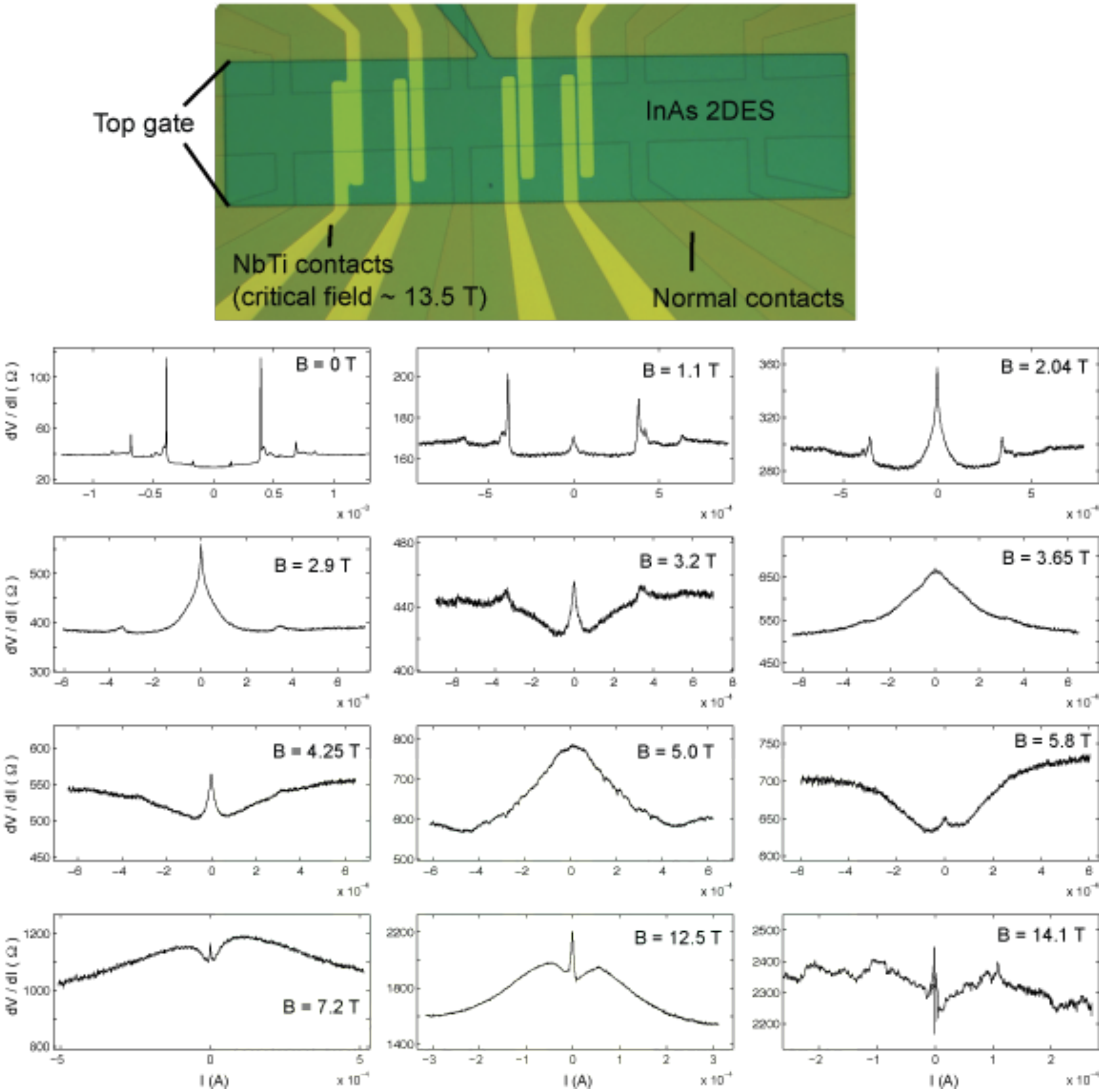

Fig. 1 : (Top) Optical image of devices measured. A standard Hall bar is patterned with NbTi contacts in S-N-S and S-N geometries. dV/dI vs current bias taken at different magnetic field.

We1145

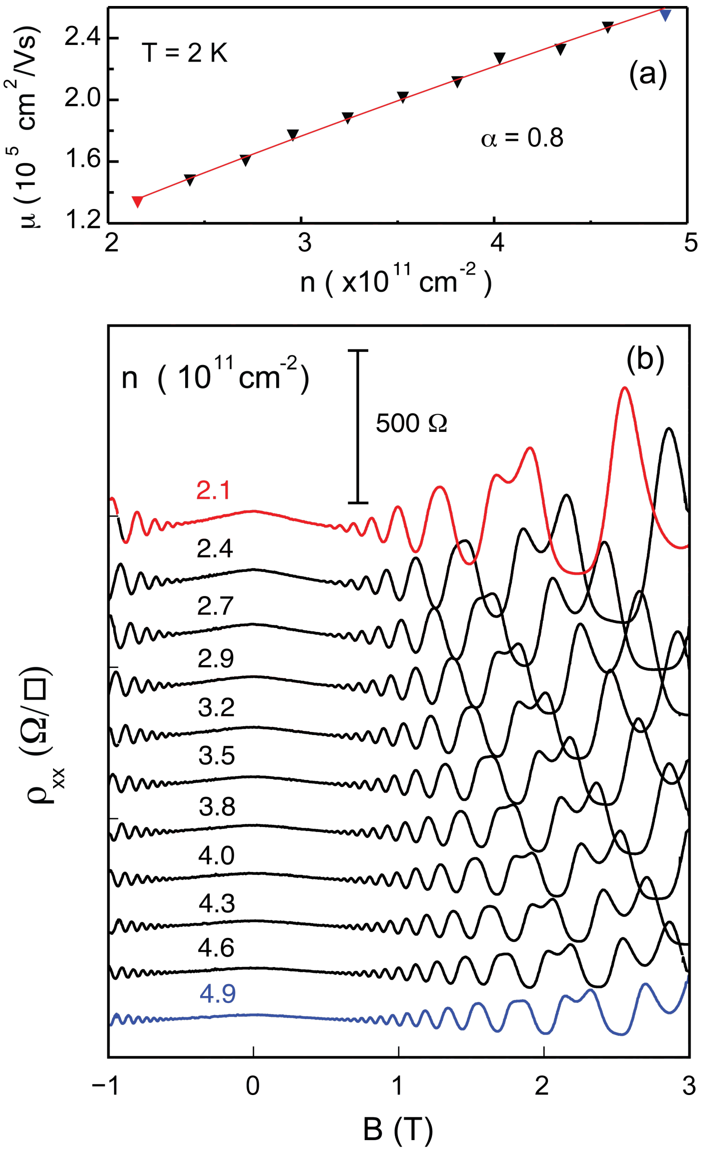

Fig. 2 : (a) Electron mobility plotted as a function of density (by varying the top gate bias). An exponent of 0.8 is derived from fitting the data at 2 K. (b) Corresponding magneto-resistance data measured at different densities from top to bottom: n = 2.1 (red), 2.4, 2.7, 2.9, 3.2, 3.5, 3.8, 4.0, 4.3, 4.6 and 4.9 (blue) $\times 10^{11}$ cm^{-2}. The lowest (and highest) density are marked in red (and blue) in (a) and (b).

We1150

Tuning the emission wavelength from self-assembled InAs quantum dots on GaAs(001) to over 1.55 µm by controlling the cap and barrier layers

K. Shimomura and I. Kamiya*
Toyota Technological Institute
2-12-1 Hisakata, Tempaku, Nagoya 468-8511, Japan
E-mail: sd12502@toyota-ti.ac.jp, *Corresponding author: kamiya@toyota-ti.ac.jp

Tuning the emission wavelength of InAs quantum dots (QDs) grown on GaAs(001) by molecular beam epitaxy (MBE) to 1.55 µm has attracted great attention for telecommunication applications. Typically, the emission wavelength of InAs QDs on GaAs(001) with GaAs cap remains between 1.0 and 1.2 µm. To redshift the emission, capping with InGaAs which has a lower bandgap has been proposed [1]. However, the lattice mismatch between the buffer and the cap layers increases with increasing In content, and results in three dimensional growth of the cap layer. According to our study on the growth of InGaAs thin film on GaAs(001), it was found that the strain in the InGaAs layer increases with increasing thickness [2]. Therefore, we deduced that reducing the cap thickness should reduce the strain of InAs QDs on GaAs(001), and result in further redshift in the PL emission wavelength of the QDs. In addition, it has been reported that the strain in the QDs is also controlled by the barrier layer allowing us to tune the emission to longer wavelengths [3].

The samples are grown by MBE. After oxide removal at 600°C, a 100 nm-thick undoped (u.d.) GaAs buffer layer is grown on semi-insulating (s.i.) GaAs(001) at a substrate temperature of 590°C. Following 600°C annealing of the u.d. GaAs buffer layer, the structures comprising of InAs are grown at substrate temperature of 480°C. photoluminescence (PL) measurements are carried out at 4K and RT using 780 nm light from a Ti:sapphire laser as excitation source at a power density of 5 W/cm^2.

Figure 1 shows the PL spectra obtained from a 2.5 ML InAs QD layer covered by GaAs cap with varied thickness of 4, 9, 20, and 30 nm. The PL peak is redshifted with decreasing GaAs cap thickness. This result indicates that strain in the QDs can be controlled not only by the lattice constant of the capping layer but also by the cap thickness in the case of thin cap. In particular, a strong peak shift is observed between 9 nm and 4 nm caps. Figure 2 shows the PL spectra obtained at 4K and RT from the sample using thin cap and controlled barrier layer. PL with emission peaks exceeding 1.6 and 1.7 µm are observed at 4K and room temperature (RT), respectively. The sample structure and strain variation by cap and barrier layers will be discussed in detail

This work was supported by the Strategic Research Infrastructure Project, MEXT, Japan.

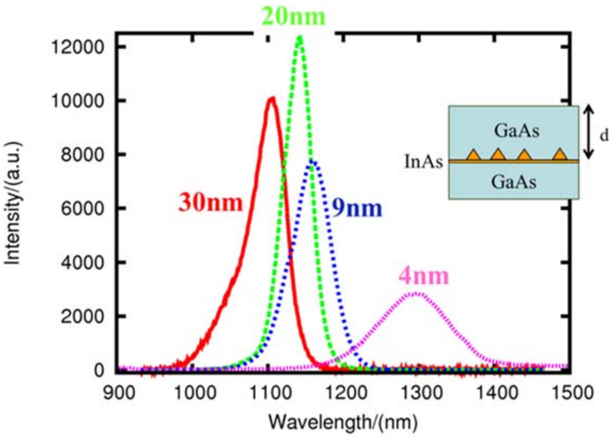

Figure 1. 4 K PL spectra of InAs QDs grown on GaAs and capped by GaAs of various thickness (4 nm, 9nm, 20 nm and 30 nm).

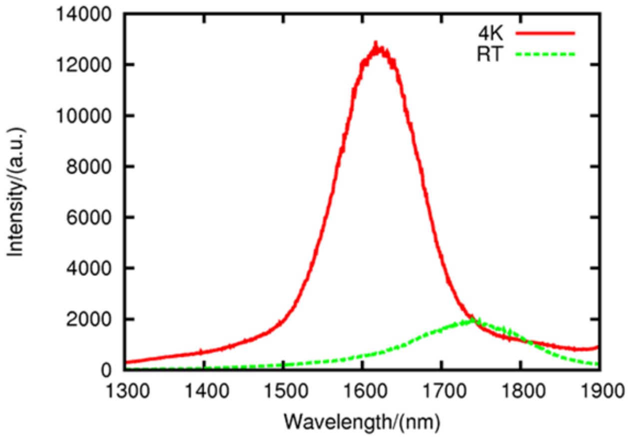

Figure 2. 4 K and RT PL spectra. Emission peaks exceeding 1.6 and 1.7 µm are observed at 4K and RT, respectively.

[1] K. Nishi, *et al.*, Appl. Phys. Lett. **74**, 1111 (1999).
[2] T. Sasaki, *et al.*, Appl. Phys. Express **2**, 085501 (2009).
[3] Z. Z. Sun, *et al.*, Appl. Phys. Lett. **88**, 203114 (2006).

Novel Heterostructures

We1400 Invited

Metal Oxides-Organic Semiconductor Interfaces

Z.H. Lu
Department of Materials Science and Engineering
University of Toronto
184 College Street, Toronto, Canada M5S 3E4

Thin-film metal oxides are among the key materials used in organic semiconductor devices. As there are no intrinsic charge carriers in organic molecules, all charges in the device must be injected from electrode/organic interfaces, whose energetic structure consequentially dictates the performance of devices. The energy barrier at the interface depends critically on the work function of the electrode. For this reason, various types of thin-film metal oxides have been experimented to modify the electrode work function. This talk will discuss recent progress in metal oxide/organic interface energetics, oxide valence structure and work function, as well as the impact of defects and interfacial reactions on oxide work functions. The talk will also review applications of some of these metal oxides-organic semiconductor interfaces in fabricating organic light-emitting diodes with record breaking performances.

New Frontiers in Thin Film Organic-Based Magnets

Howard Yu[1], M. Harberts[1], R. Adur[1], I. Froning[1], Y. Lu[2], G. Schmidt[3], P. Chris Hammel[1], A.J. Epstein[1,2], and E. Johnston-Halperin[1]

[1]*Department of Physics, The Ohio State University, Columbus, OH 43210-1117, USA*

[2]*Department of Chemistry, The Ohio State University, Columbus, OH 43210-1173, USA*

[3]*Institute für Physik, Martin-Luther-Universität Halle-Wittenberg, Halle, Germany*

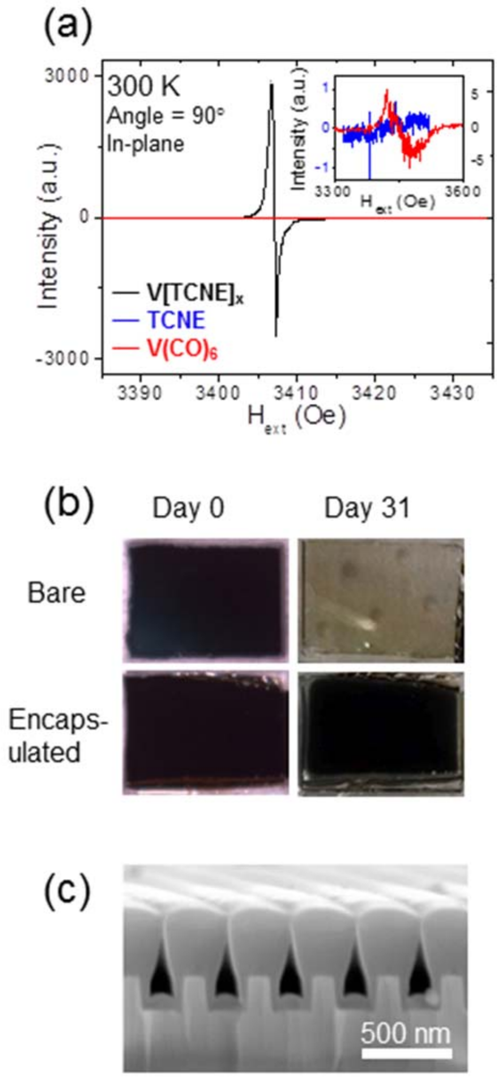

We present three recent advances in the development of vanadium tetracyanoethylene (V[TCNE]$_{x\sim2}$) thin films that signal a new paradigm for organic spintronics. Organic materials have long been attractive for their low temperature and conformal deposition on a wide variety of substrates, and have seen applications that take advantage of their optical and electronic properties, such as in organic LEDs. The inclusion of magnetic functionality within this existing framework of organic electronics has the potential to enable novel applications in memory, high frequency electronics, sensing, and spintronics. First, through optimization of the sample deposition process we have achieved materials with a dramatic increase in Curie temperature and extremely narrow ferromagnetic resonance (FMR) linewidths. Specifically, we observe a single peak with linewidth comparable to yttrium iron garnet (roughly 1 G). Recent developments in spintronics suggest that the high frequency response of ferromagnetic materials is an attractive path to generating pure spin currents, and that the linewidth is an important metric for FMR-driven spin injection. Second, the development of an epoxy-based encapsulation technique has extended sample lifetime in air by orders of magnitude, from under an hour to over a month. This removes the single largest barrier to incorporating magnetic materials into functional organic electronic circuits and heterostructures. Third, the deposition of V[TCNE]$_{x\sim2}$ on patterned substrates has enabled the formation of V[TCNE]$_{x\sim2}$ "nanowires" that induce magnetic anisotropy. Many applications depend on anisotropy, such as memory, sensing, and spin valves, so the ability to induce anisotropy in a nominally isotropic material represents a significant advance in materials control. Taken together these three technical achievements lay the foundation for a myriad of new applications and provide the materials basis for increasingly sophisticated investigation of spin transport and magnetism in organic materials.

We1445

Growth of AlN/Pt Heterostructures on Amorphous Substrates at Low Temperatures via Atomic Layer Epitaxy

N. Nepal, R. Goswami, S.B. Qadri, N.A. Mahadik, F. J. Kub, and C.R. Eddy, Jr.*
U.S. Naval Research Laboratory, Washington, DC 20375, USA
*chip.eddy@nrl.navy.mil

Atomic Layer Epitaxy at low temperatures (< 500°C) offers an interesting alternative to conventional crystalline growth techniques where the limitations of miscibility gaps and substrates can be largely mitigated if not eliminated. This promise enables a wider range of bandgap engineering and the creation of novel structures on non-conventional substrates.

Here we report on recent results on the atomic layer epitaxy (ALE) of crystalline (0001) aluminum nitride (AlN) thin films on highly-oriented (111) platinum (Pt) layers grown by atomic layer deposition (ALD) on amorphous ALD hafniuim oxide (HfO_2) on silicon (Si) (100) substrates. HfO_2 was deposited by ALD on Si(100) at 200°C followed by ALE growth of 15 nm Pt at 200°C and, subsequently, 60 nm AlN at 500°C, a temperature previously shown to result in crystalline films on conventional gallium nitride (GaN) substrates[1]. After growth of each layer, the substrate was characterized *ex situ* before being re-inserted into the reactor for subsequent layer growth. The resulting AlN/Pt/HfO_2 stacks were characterized using spectroscopic ellipsometery (SE), x-ray photoelectron spectroscopy, x-ray diffraction (XRD), atomic force microscopy, and transmission electron microscopy (TEM). The SE measurements indicate that the thickness of AlN layer is about 60 nm indicating a growth rate of 1Å per ALE cycle. Based on the XRD and TEM measurements, the Pt and are highly oriented along (111) and the AlN layers are preferentially oriented in the (0001) direction. High resolution TEM analyses have shown that these Pt and AlN films have a fine columnar texture and sharp interfaces. Successful demonstrations of AlN/Pt heterostructures grown by ALE open up the possibilities of new state-of-the-art microelectromechanical devices.

References:

[1]. N. Nepal, S.B. Qadri, J.K. Hite, N.A. Mahadik, M.A. Mastro and C.R. Eddy, Jr., Appl. Phys. Lett. **103**, 082110 – 082110-5 (2013).

We1445

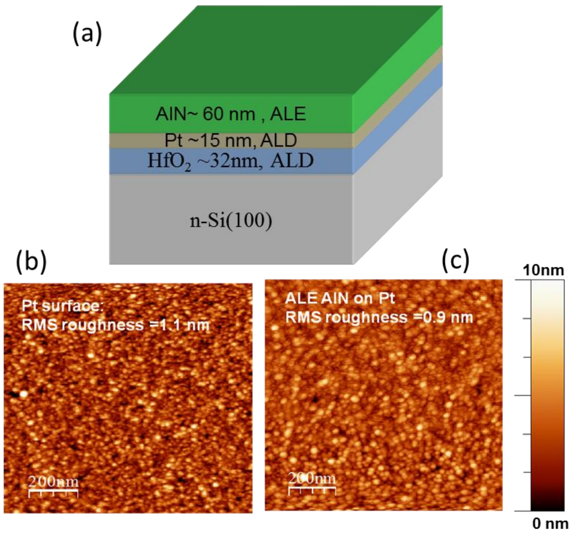

Figure 1. (a) A schematic of the layer structure of ALD/E grown AlN/Pt/HfO$_2$ stack on Si(100), (b) AFM image of Pt on the HfO$_2$/Si(100) surface (c) AFM image of ALE grown AlN on the Pt surface. Both the Pt and AlN surfaces are uniform.

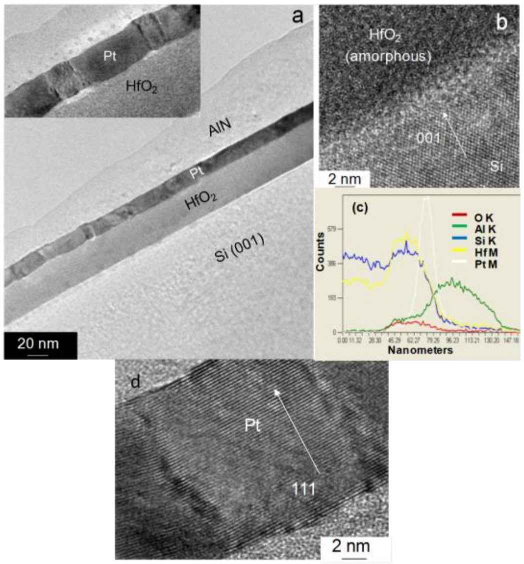

Figure 3. (a) Cross-sectional transmission electron microscograph of ALD/E grown AlN/Pt/HfO$_2$ stack on Si(100). (b) High resolution TEM micrograph of Si/HfO$_2$ interface. (c) TEM-EDS line scan across the interfaces as shown in Fig. 3(a). (d) High resolution phase contrast TEM micrograph of HfO$_2$/Pt interface.

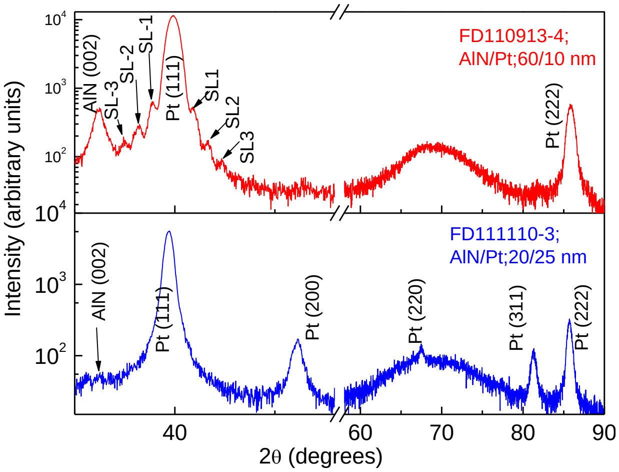

Figure 2. X-ray diffraction θ-2θ scan of (a) ALE AlN on the thin ALD grown highly oriented Pt surface (b) AlN on the ALD grown polycrystalline Pt surface. AlN on highly oriented Pt is (0002) oriented.

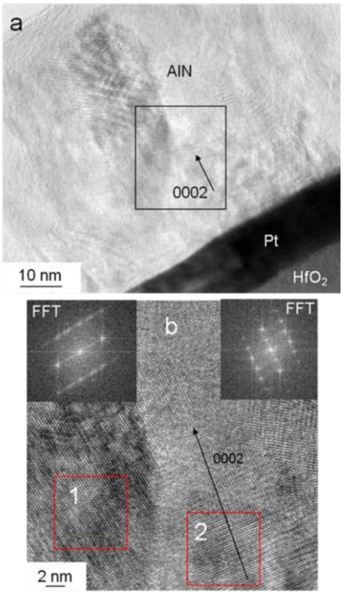

Figure 4. (a) Cross-sectional TEM image of the AlN/Pt interface. (b) High-resolution TEM image of boxed area of 4(a). Insets in 4(b) are inverse fast Fourier transforms (IFFTs) of regions (1) and (2).

We1450

Detection of Inhomogeneous Regions in Yttrium Iron Garnet Films Deposited by Aerosol Deposition

Scooter D. Johnson, E. R. Glaser, Shu-Fan Cheng, Jennifer K. Hite, Fritz J. Kub, and Charles R. Eddy, Jr.
U.S. Naval Research Laboratory, Washington, D.C., 20375, U.S.A.

Aerosol deposition (AD) is a thick-film deposition process that can produce films of up to several hundred micrometers thick with densities greater than 95% of the bulk and be performed at moderate vacuum conditions of 1–20 Torr in the deposition chamber. The primary advantage of AD is that the deposition takes place entirely at room temperature; thereby enabling high melting temperature film growth onto a substrate with a much lower melting temperature[1]. There have been many reports on using AD for applications to improve electronics components. Such areas include piezoelectrics, multiferroics, magnetoelectrics, thermoelectrics, and flexible dielectrics. The low-cost operation, flexibility, high deposition rate, and simplicity of AD has spurred interest by researchers in Germany, France, Japan, Korea, and now in the United States.

While AD has found wide-spread application, there has been few reports elucidating structural details within the film itself. In this work, we report structural variations within the film by analyzing the ferromagnetic resonance (FMR) linewidth of yttrium iron garnet $Y_3Fe_5O_{12}$ (YIG) films on sapphire formed by AD at varying thicknesses between about 1–40 μm. The FMR linewidth profile can provide information on the relaxation mechanisms within the film and thereby give insight into the structural profile of the film[2]. We complement FMR results with scanning electron microscopy (SEM) results of the top surface and cross-section of the films along with x-ray diffraction data to determine the crystal structure and an estimate of the crystallite size.

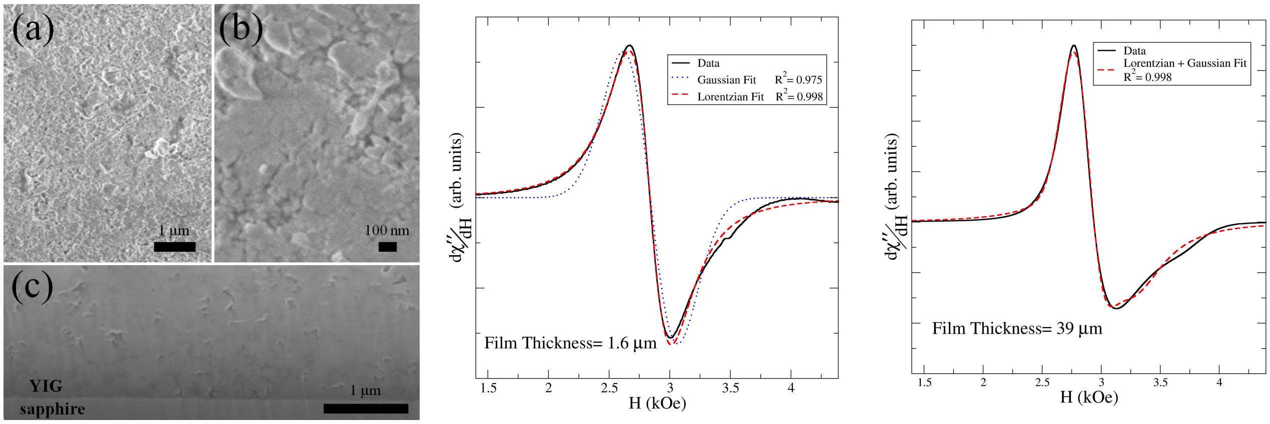

The left-hand side of the figure in insets (a) and (b) show SEM images of the top surface of an as-deposited 1.6 μm-thick film of YIG at two magnifications. In the image, consolidation and densification of the 0.5 μm starting particles is apparent. The figure inset (c) shows a cross-section prepared by a focused ion beam mill, which shows the void content, compact nature of the film, and the YIG-sapphire interface. Estimates of film density are between 90%–96% of the theoretical density for YIG. The FMR absorption derivative curve of these dense films is shown at center of the figure. We attempted fits to these data using a Gaussian or a Lorentzian function as shown overlaid in the plot. The poor fit by the Gaussian suggests that the relaxation is not due to inhomogeneous regions within the film. The good fit by the Lorentzian suggests instead that the relaxation mechanisms in the film are primarily Gilbert and/or two-magnon scattering[2]. On the right-hand side of the figure is an FMR absorption derivative of a 50% dense 39 μm-thick YIG film. The best fit to these data were found by forming a fit from a sum of a Gaussian (centered at 2891 Oe) and a Lorentzian (centered at 3117 Oe) indicating that in the thicker films a film density gradient develops causing larger contributions to the inhomogeneous scattering. Note also that the asymmetry between the peak and valley hints at the need for a additional fit functions. These results suggest that while AD can form very thick films, there may be an upper limit to the thickness where homogeneous films can be formed.

---

[1] J. Akedo, "Room temperature impact consolidation (RTIC) of fine ceramic powder by aerosol deposition method and applications to microdevices," *J. of Thermal Spray Technology* **17**, p. 181, 2008.

[2] S. S. Kalarickal, P. Krivosik, J. Das, K. S. Kim, and C. E. Patton, "Microwave damping in polycrystalline Fe-Ti-N films: Physical mechanisms and correlations with composition and structure," *Phys. Rev. B* **77**, p. 054427, Feb 2008.

We1455

The study of trapping states and their correlation to gate hysteresis and $1/f$ noise on the Al_2O_3 and HfO_2 atomic layer deposited epitaxial graphene field effect transistor.

H. K. Chan[1], V. D. Wheeler[2], L. O. Nyakiti[3], R. L. Myers-Ward[2], N. Y. Garces[2],
J. P. Goss[1], N.G. Wright[1], C. R. Eddy Jr.[2], D. K. Gaskill[2]and A. B. Horsfall[1]

[1]School of Electrical and Electronic Engineering, Newcastle University, Newcastle, NE1 7RU, UK
[2]U.S. Naval Research Laboratory, 4555 Overlook Ave SW, Washington DC 20375 USA
3Department of Material Science and Engineering, Texas A&M University, TX 77553, USA

The superior carrier mobility, surface-to-volume ratio and thermal conductivity of graphene position it as a prospective candidate for the realization of many interesting applications such as the next generation high electron mobility transistor (HEMT), parts per billion grade sensor and terahertz photonics. In practice, however, the material growth and device fabrication process are the major limiting factors that deteriorate the synthesized graphene properties from those predicted theoretically. This abstract presents the properties of graphene-dielectric interface states and their correlation to the gate hysteresis and $1/f$ noise performance of a graphene field effect transistor (GFET) that employs epitaxial graphene (EG) synthesized using low pressure sublimation of Si in an Ar ambient on the Si-face of SiC.[1] These transistors were fabricated by subjecting the EG to a fluorine pre-treatment prior to gate dielectric formation using atomic layer deposition (ALD).[2, 3] In general, the presence of gate bias sensitive dielectric/graphene interface states demonstrate deleterious impact on the electrical and noise characteristics of these devices, which can render the graphene electronics inoperable.

Figure 1 illustrates the current normalized noise power spectral density ($S_{I_{CH}}/I_{DS}^2$) for a) Al_2O_3 and b) HfO_2 top-gated GFET as a function of gate source voltage (V_{GS}) swept from -3.0V to 2.0V and back to -3.0V continuously (denoted as forward and reverse sweep, respectively). Inset in the figure shows the corresponding drain-source current $(I_{DS}) - V_{GS}$ relation. It can be clearly observed that the Al_2O_3 gated GFET demonstrate a weak V_{GS} dependence throughout the investigated biases, where both $S_{I_{CH}}/I_{DS}^2 - V_{GS}$ and the $I_{DS} - V_{GS}$ relations illustrate a minimal gate hysteresis. In contrast, the $S_{I_{CH}}/I_{DS}^2$ behavior of the HfO_2 gated GFET is strongly modulated by V_{GS}, demonstrating almost an order of magnitude change across the examined V_{GS} range. The observation of these noise behaviours implies a strong interaction between graphene channel and dielectric charges, indicating the strong presence of interfacial trapping states on the HfO_2 gated transistor.

To further investigate the interfacial charge characteristics of the two dielectrics, the capacitance-voltage (C-V) characteristics were correlated with the noise results. C-V data were acquired by first holding the V_{GS} at -3.5V up to an accumulative hold time (τ_{hold}) of 400s prior the measurement and a post-recovery C-V characteristics was obtained by stressing V_{GS} at +3.5V for 100s. The results in Figure 2 shows that the C-V behavior of the HfO_2 gated GFET decreases monotonically with increasing τ_{hold} and the transistor Dirac voltage (V_{Dirac}) appears to be positive shifted gradually. Furthermore, the altered C-V characteristics can be successfully reverted to the initial value using positive V_{GS} stress. In contrast, the C-V data of the Al_2O_3 GFET illustrate a negligible shift throughout the stressing period. These results indicate that the polarity of V_{GS} on the HfO_2 gated transistor behaves as the populating/de-populating mechanism that modify the interfacial charge species, ultimately modulating the electronic properties of the underlying graphene channel.

Figure 3 shows a similar C-V data for the HfO_2 devices under forward and reverse V_{GS} sweep. The results illustrate the impact of interfacial charges that cause the deformity of the C-V curve near V_{Dirac} under reverse gate sweep (red). Moreover, the C-V curve (filled dashed line) without undergoing the positive V_{GS} stress appears to settle at the shifted behavior, supporting the hypothesis that V_{GS} is regulating the interfacial charge. Furthermore, the rate of change in gate-source capacitance (C_{GS}) relative to the V_{GS} between the forward and reverse V_{GS} sweep show a significant deviation as shown in Figure 3b. This observation may be related to the deformed C-V curve, where the gate capacitance is superimposed with additional capacitive components generated by the trapped interface charge.

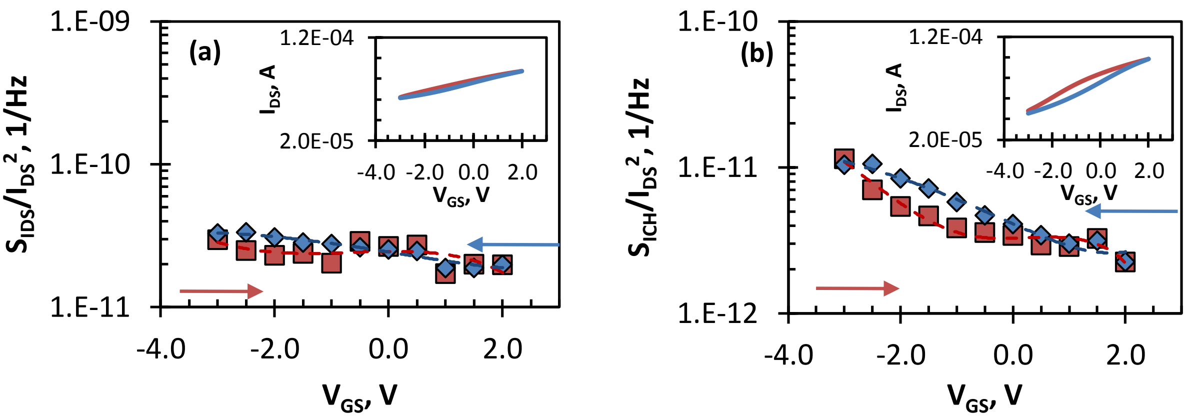

Figure 1: $S_{I_{CH}}/I_{DS}^2$ as a function of V_{GS} under forward and reverse gate bias sweep on a) Al_2O_3 and b) HfO_2 gated GFET at V_{DS} = 1 V at 10 Hz. Inset shows the $I_{DS} - \boldsymbol{V_{GS}}$ for each corresponding GFET.

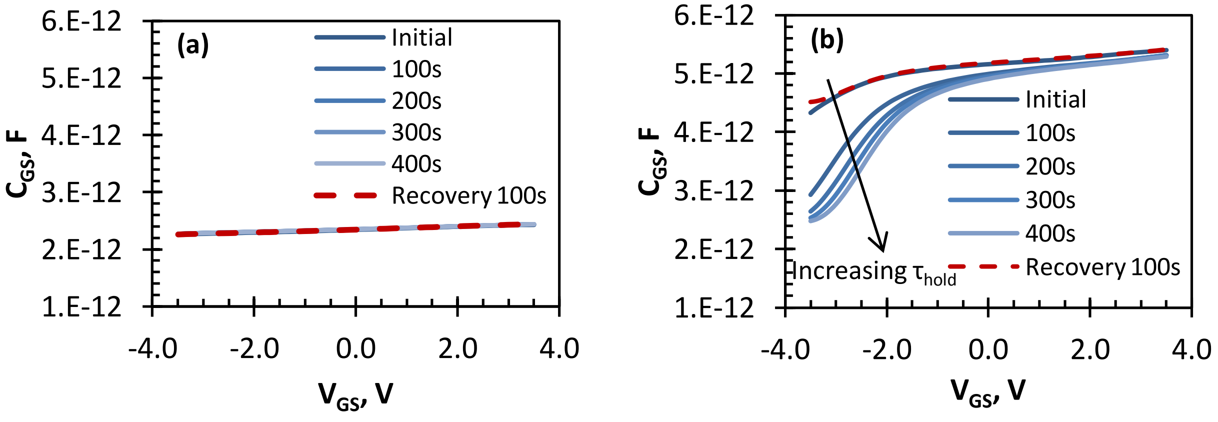

Figure 2: Comparison of C-V curve for the a) Al_2O_3 and b) HfO_2 gated GFET under forward $\boldsymbol{V_{GS}}$ sweep up to an accumulative τ_{hold} of 400s at -3.5V and a post-recovery $\boldsymbol{V_{GS}}$ stress at 3.5V for 100s.

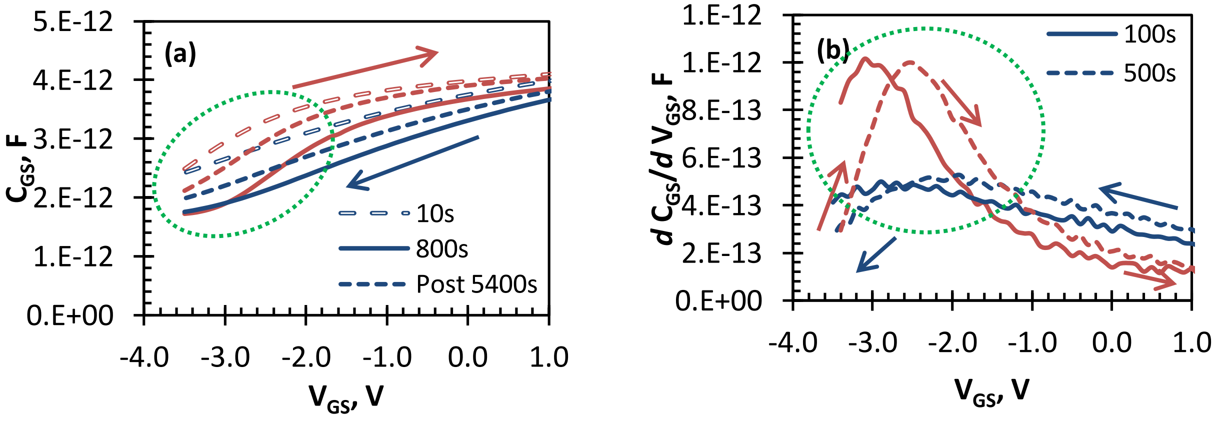

Figure 3: a) Comparison of C-V characteristics for the HfO_2 gated GFET between forward and reverse $\boldsymbol{V_{GS}}$ sweep. b) Rate of change of $\boldsymbol{C_{GS}}$ relative to $\boldsymbol{V_{GS}}$ as a function of $\boldsymbol{V_{GS}}$.

1. L. Nyakiti, R. Myers-Ward, et. al., *Nano Lett.*, vol. 12, no. 4, pp. 1749–56, 2012.
2. V. Wheeler, N. Garces, et. al., *Carbon N. Y.*, vol. 50, no. 6, pp. 2307–2314, May 2012.
3. A. Balandin, *Nat. Nanotechnol.*, vol. 8, no. 8, pp. 549–55, Aug. 2013.
4. Y. Lin, P. Avouris, "*Nano Lett.*, vol. 8, no. 8, pp. 2119–25, Aug. 2008.
5. Y. Zhang, E. E. Mendez, et. al., *ACS Nano*, vol. 5, no. 10, pp. 8124–30, Oct. 2011.

Interface Bonding Characteristics of Graphene with Metal and Dielectric Substrates

Santanu Das [a], Debrupa Lahiri [b], Arvind Agarwal [c], and Wonbong Choi [a*]

[a] Department of Materials Science and Engineering, University of North Texas, Denton, Texas 76203 USA.
[b] Department of Metallurgical and Materials Engineering, Indian Institute of Technology—Roorkee, Uttarakhand, India
[c] Nanomechanics and Nanotribology Laboratory, Mechanical and Materials Engineering Department, Florida International University, Miami, FL 33174, USA

*Corresponding authors: Wonbong Choi, Email: Wonbong.Choi@unt.edu

Recently, 2D graphene have created an immense research interests due to its extraordinary physical, chemical, and physiochemical properties including high electron mobility, wide range of optical transparency, excellent mechanical properties, and chemical inertness. We developed large scale graphene using chemical vapor deposition (CVD) process and transferred it to different substrates for applications in electronic/optoelectronic devices including, solar cells. However, achieving strong adhesion between the graphene and the corresponding metal or dielectric substrates is crucial to fabricate reliable graphene based electronics and electro-optic devices. Here, we report the measurement of the adhesion energy between the graphene and different metals and dielectric substrates. In addition, we demonstrate the improvement of the adhesion energy of graphene-SiO_x/Si dielectric substrate adhesion energy by using the nano-scratch technique coupled with Raman spectroscopy and x-ray photoelectron spectroscopy (XPS). The adhesion energy of graphene on Cu, Ni and Si substrates was measured to be 12.8, 72.7 Jm^{-2}, and ~2.978 J m^{-2} respectively. Furthermore, by applying different annealing protocols of rapid thermal annealing and vacuum annealing, the adhesion energy of graphene-SiO_x/Si is increased to 10.09 and 20.64 J m^{-2}, respectively. The XPS depth profiling confirms that C–O and C=O chemical bond formation occur at the graphene/SiO_x interface, which specifically improve the adhesion energy. These finding could be further applied for the enhancement of graphene and other 2D materials substrate bonding characteristics and this will further open up a pathway towards producing reliable solid state devices.

We1505

The Impact of GaN and AlN Nucleation by Metalorganic Chemical Vapor Deposition on Epitaxial Graphene

Zakaria Y. Al Balushi[a,c], Takahira Miyagi[a,c,d], Yu-Chuan Lin[a,c], Ke Wang[b], Lazaro Calderin[b,c], Ganesh Bhimanapati[a,c], Joan M. Redwing[a,b,c] and Joshua A. Robinson[a,b,c]

[a] Department of Materials Science and Engineering, The Pennsylvania State University, University Park, Pennsylvania 16802, USA.

[b] Materials Research Institute, The Pennsylvania State University, University Park, Pennsylvania 16802, USA

[c] Center for Two-Dimensional and Layered Materials, The Pennsylvania State University, University Park, Pennsylvania 16802, USA

[d] Research Center, Asahi Glass Co., Ltd., 1150 Hazawa-cho, Kanagawa-ku, Yokohama, Kanagawa, 221-8755, Japan

The growth of GaN and AlN by metalorganic chemical vapor deposition (MOCVD) for optoelectronic (visible and ultraviolet) devices and high-frequency power electronics has relied primarily on buffer assisted epitaxy on a variety of foreign substrates (Si, SiC and sapphire). The use of graphene as a pseudo-substrate has gained interest due to the hexagonal arrangement of the sp^2 hybridized carbon atoms being similar to the (0001) c-plane of wurtzite GaN. However, most studies on the use of graphene for the heteroepitaxy of III-nitrides (GaN and AlN) have produced layers with surface morphologies and structural qualities inferior to those produced on SiC and sapphire. This is due to the challenges associated with heteroepitaxy on the basal plane of pristine graphene which has few dangling bonds and is therefore chemically inert. Despite the growing interest in the heteroepitaxy of GaN and AlN layers on graphene, there have been limited studies aimed at understanding the nucleation process.

In this study, the nucleation of GaN and AlN by MOCVD on quasi-free standing epitaxial graphene was investigated. Epitaxial graphene (EG) was produced via sublimation of Si from the (0001) surface of 6H-SiC. The surface of EG follows the morphology of the underlying SiC substrate, consisting of $(1\bar{1}0n)$ step edges with wide (0001) terraces, which provides large areas of pristine and highly oriented graphene. Using a combination of growth experiments and structural and chemical analysis, we investigated the effect of growth temperature, the influence of the number of graphene layers and the role of step edges and defects on the nucleation process. We observed that the nucleation of AlN and GaN was preferential along the periodic $(1\bar{1}0n)$ EG coated step edges and at defects sites due to the enhanced chemical reactivity at those regions. In the case of AlN, the density of nuclei on the (0001) terraces of EG increased with the introduction of intentional defects into graphene via O_2 plasma treatment or unintentional nitrogen incorporation into the graphene lattice via NH_3 exposure during the nucleation process. Aberration corrected scanning/TEM confirmed that AlN grown on EG was polycrystalline with large grains and produced no disorder to the underlying EG. In the case of GaN nucleation, high-resolution TEM revealed that the GaN nuclei were single crystalline, [0002] oriented and free of threading dislocations. However, high-resolution TEM also revealed that the graphene underlayers were highly defective at the (0001) terrace regions of EG. Raman spectral mapping showed that GaN selectively nucleates on regions of few-layered EG as opposed to regions of multi-layered EG, where the regions of few-layered EG were observed to be highly defective as confirmed from the $I(\mathrm{D})/I(\mathrm{G})$ ratio. As was evident from surface chemical analysis by X-ray photoelectron spectroscopy, strong sp^2 and sp^3 C-N bonding at the III-nitide/EG interface was observed. The chemical bonding at the interface may contribute to the observed disordering of the EG underlayer in addition to enhanced strain energy due to the large in-plane lattice mismatch between GaN and graphene, which is a focus of current studies. This nucleation study provides insight into the initial stages of group-III nitride (GaN, AlN) growth on van der Waal surfaces such as graphene and the impact of the nucleation process on the structural properties of EG, which is important for the growth of high quality III-nitride films on graphene.

Graphene and
Other 2D Materials

We1615 Invited

Probing the valley Hall effect in MoS_2 transistors

Kin Fai Mak, Penn State University

Two-dimensional (2D) atomic layers of molybdenum disulfide (MoS_2) have attracted much recent attention due to their unique electronic properties. In addition to charge and spin, electrons in MoS_2 monolayers possess a new valley degree of freedom (DOF) that has finite Berry curvatures. As a result, not only optical control of the valley DOF is allowed, but each valley is also predicted to exhibit an anomalous Hall effect whose sign depends on the valley index. In this talk, we will discuss our recent observation of this new valley Hall effect (VHE) in monolayer MoS_2 transistors. This is manifested experimentally as a finite anomalous Hall effect when circularly polarized light is used to preferentially excite electrons into a specific valley. We will describe the dependence of the anomalous Hall conductivity on photon helicity, photon energy, doping levels and crystal symmetry, and will compare these observations with theoretical predictions. Possibilities of using the valley DOF as an information carrier in next-generation electronics and optoelectronics will also be discussed.

We1655

Band structure, band gap opening and topological edge states in clean bilayer graphene

Jun Zhu, Department of Physics, Penn State University

Bernal-stacked bilayer graphene possesses a unique electronic band structure that is tunable by a perpendicular electric field and multiple quantum degrees of freedom (spin, valley, layer) that lead to complex interplay and symmetry breaking in a magnetic field. Using high-quality h-BN encapsulated bilayer graphene, we have made precise measurements of the effective mass of electrons and holes and determined the E-field controlled band gap up to 0.2 eV using transport and magneto-transport measurements. These information allow us to accurately construct the band structure of bilayer graphene, capturing its hyperbolicity, large electron-hole asymmetry, and the effect of interaction-induced renormalization of m* at low carrier densities. Experiments in split dual-gated bilayer graphene show evidence of topological edge states at the line junction of two oppositely biased bilayer graphene.

We1700

Optoelectronic and Spin Dependent Properties of Transition Metal Dichalcogenides

Yunqiu (Kelly) Luo[1], Elizabeth Bushong[1], Patrick Odenthal[2], Roland Kawakami[1,2]
[1]Department of Physics, The Ohio State University, Columbus OH 43210
[2]Department of Physics and Astronomy, University of California, Riverside, CA 92521

Two-dimensional semiconductors are an exciting class of materials for novel physics and nanoelectronics. Among the two-dimensional semiconductors, transition metal dichalcogenides (TMD) have received tremendous interest due to its native band gap and strong spin orbit coupling. In monolayer molybdenum disulfide (MoS_2) and tungsten diselenide (WSe_2) specifically, the inversion symmetry breaking produces strong spin splittings in the valence band that have opposite polarity for the K and K' valleys. This produces a strong coupling of spin and valley degrees of freedom for holes, leading to novel valley-dependent and spin-dependent properties. These include the valley-selective optical selection rules for optical excitation and detection of valley- and spin-polarization, enhanced spin lifetimes for holes, valley Hall effect, and spin Hall effect.

We follow two approaches to investigate the spin-dependent properties of TMD. The first approach is to develop hybrid graphene/TMD devices, in which the established methods for detecting spin accumulation in graphene (i.e. graphene spin valves) can be exploited to investigate spin-dependent properties of TMD. The important initial step is to understand the properties of the graphene/TMD junction. Our studies find that graphene makes excellent low resistance contacts to MoS_2, as quantified by comparing I-V curves on Ti-MoS_2-Ti, Ti-MoS_2-graphene, and graphene-MoS_2-graphene lateral devices. Photoconductivity microscopy studies also provide insight into the electrical properties of the junctions. Photoconductivity is strongest near Ti/MoS_2 junctions which indicates the formation of strong Schottky barriers, while photoconductivity is suppressed at the graphene/MoS_2 junctions. Further studies focus on the transport of spins across the graphene/MoS_2 junction. The second approach is to directly probe spin and valley-polarization using optical probes by taking advantage of the optical selection rules. These methods include Kerr rotation and circular-polarization resolved photoluminescence. We will report our progress in these efforts.

We1700

Two-probe DC IV measurements across graphene/MoS_2 junction:

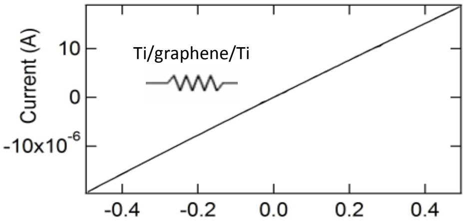

- Ti/graphene: Ohmic contacts
- Highly conductive (~25KΩ)

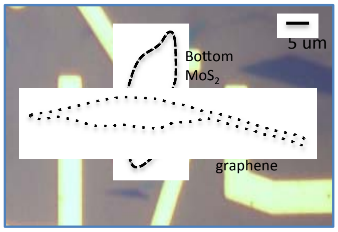

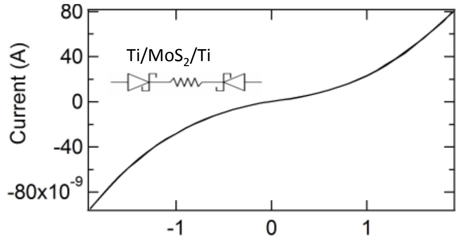

- Ti/MoS_2/Ti: highly resistive back-to-back Schottky diodes
- $R_{+/-}$ ~ 20 MΩ

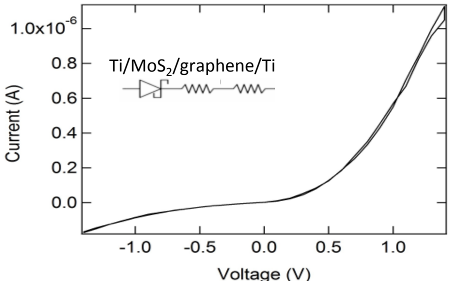

- Ti/MoS_2/graphene/Ti: diode like, one side less resistive than the other
- R_+ ~ 1 MΩ
- **Data suggests that graphene/MoS_2 junction is less resistive than Ti/MoS_2 junction.**

Scanning Photocurrent microscopy measurement mapping the device:

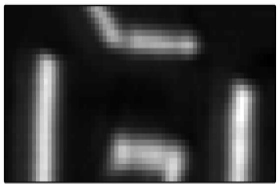

Reflection

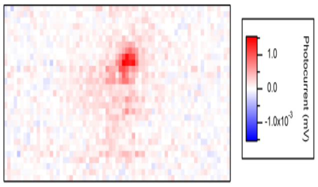

Photocurrent

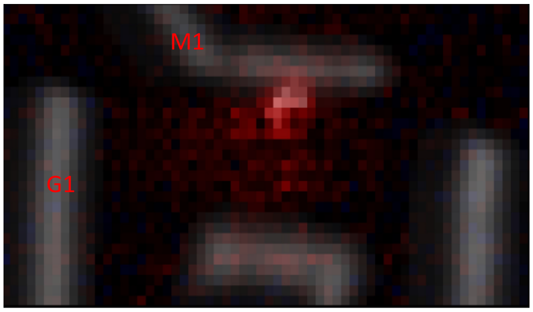

- 595nm OPO laser scanned across device area
- Small drain-source bias (−0.2V) is applied across Ti/MoS_2/graphene/Ti (M1-G1) junctions
- Reflection signal and photocurrent signal are mapped simultaneously
- Strong photocurrent detected at the edge of MoS_2/Ti junction
- Data suggests that MoS_2/Ti junction is the dominate Schottky barrier in this system.

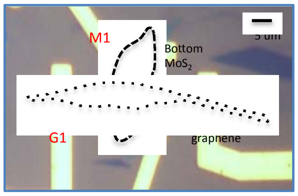

We1705

Impact of the Direct Growth of MoS_2 on Graphene for Tunneling Applications

Corey Joiner, Philip Campbell, and Eric M. Vogel
School of Material Science and Engineering, Georgia Institute of Technology, Atlanta, GA 30332, USA
Phone: (985) 2591807, Email: cojoiner@gatech.edu

Graphene (Gr) based 2D heterostructures are promising candidates for future electronic devices due to the resonance in tunneling when the Dirac points of the two graphene layers are aligned which gives rise to negative differential resistance (NDR). Britnell *et al.* first demonstrated gate controlled resonant tunneling for exfoliated graphene – hexagonal boron nitride (hBN) – graphene heterostructures with an on-off ratio of 10^4 [1]. A larger on-off ratio can be achieved by incorporating 2D materials with reduced band gaps such as Molybdenum disulfide (MoS_2) as demonstrated in the literature [2]. The present work seeks to fabricate 2D heterostructures devices consisting of Gr-MoS_2-Gr by utilizing scalable fabrication methods such as CVD synthesis for the 2D materials and assess the impact of the fabrication process on the layers of the heterostructure and their interfaces.

The 2D heterostructures were fabricated using CVD grown materials. CVD graphene was transferred as the electrodes using a wet transfer technique [3], and Ni/Au contacts were deposited via e-beam evaporation. CVD trilayer MoS_2 was transferred using the wet transfer technique followed by the top CVD graphene electrode. This transferred 2D heterostructure stack was compared to a 2D stack consisting of transferred CVD graphene with a MoS_2 interlayer directly grown on the transferred graphene. Raman spectroscopy and electrical characterization were performed on the heterostructures in order to assess the impact of the direct growth of MoS_2 in terms of material quality and device performance.

The Raman spectrum of the graphene for the transferred MoS_2 heterostructures compared to the grown MoS_2 heterostructures shows that the direct growth of MoS_2 on graphene results in a large increase in the D peak (1350 cm^{-1}) intensity suggesting the graphene is damaged from the growth process. Broadening of the 2D peak (2700 cm^{-1}) and G peak (1580 cm^{-1}) occurs for both the transferred and grown MoS_2 structures, though the broadening for the grown MoS_2 is much greater. A slight shift in the 2D peak position is seen, consistent with van der Waal's interactions between the graphene and MoS_2 shown in the literature for exfoliated structures [4]. A much larger shift in the 2D peak position is seen in the grown MoS_2 structures suggesting doping effects stemming from the excess sulfur used during the growth process. The Raman spectrum of the MoS_2 shows a shifting in the MoS_2 peak positions for both transferred and grown MoS_2 heterostructures. The A_{1g} peak shows a blue shift of 2 cm^{-1}, consistent with results in the literature [4], showing a van der Waal's interaction between the graphene and the MoS_2 layers.

Electrical characterization on the individual graphene electrodes as well as the tunneling current between electrodes was performed. A positive voltage shift in the charge neutral point is seen for both the transferred MoS_2 and the grown MoS_2 structures suggesting charge inhomogeneity resulting from the addition of the MoS_2 layer. A much larger shift is seen for the grown MoS_2 structure due to the excess sulfur used during the growth process introducing additional charge inhomogeneity in the underlying SiO_2 substrate. The addition of the MoS_2 layer further results in reduced electron conductivity consistent with literature results [5]. Tunneling measurements of the grown and transferred MoS_2 structures were comparable to results in the literature for exfoliated devices [2].

While several reports have been made for exfoliated Gr/MoS_2/Gr structures, few reports of the impact of CVD based fabrication methods exist despite the impact of scalable fabrication methods on the heterostructure layers and interfaces being crucial to the viability of 2D materials for future electronics. In the present work, we have compared 2D tunneling heterostructures fabricated with a direct synthesis technique to an indirect transfer technique in order to assess the impact of the fabrication process. Raman spectroscopy and electrical measurements showed that the direct growth of the MoS_2 on the underlying graphene introduces additional defects as well as additional charge inhomogeneity, reduces the electron conductivity of the graphene, and introduces p-type doping in the graphene. Similar characterization of the MoS_2 layer shows comparable results as exfoliated MoS_2 used in the literature in terms of the Raman peak positions and device tunneling currents.

[1] L. Britnell, et al., *Science*, vol. 335, pp. 947, Feb 2012
[2] L. Britnell, *et al.*, *Nano Letters*. vol. 12, pp. 1707, 2012
[3] J. Chan, et al., *ACS Nano*, vol. 6, pp. 3224, Apr 2012.
[4] K. Zhou *et al*. *ACS Nano*, Article ASAP DOI**:** 10.1021/nn5042703
[5] J. Tan *et al*. *Applied Physcis Letters*. vol. 104, pp. 183504, 2014.

We1705

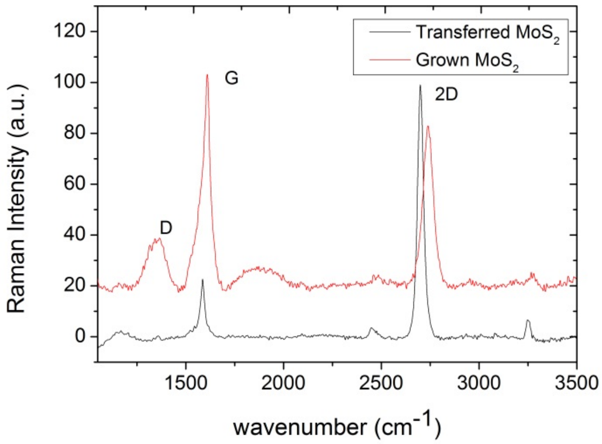

Figure 1 Raman spectra of graphene with a transferred MoS_2 layer and a grown MoS_2 layer. The growth of the MoS_2 layer results in peak broadening of the G and 2D peaks, an increase in D peak intensity, and a blue shift in the 2D peak position.

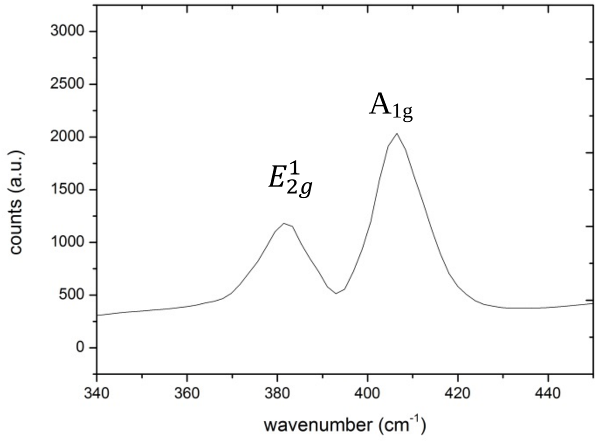

Figure 2 Raman spectra of the MoS_2 interlayer. The MoS_2 spectra is identical for transferred and grown samples. The A_{1g} peak blue shifts from 404 cm^{-1} to 406 cm^{-1}.

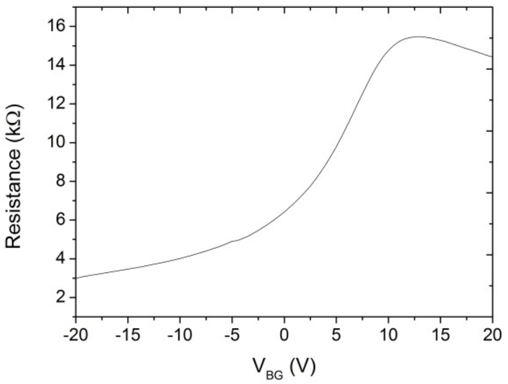

Figure 3 I_DV_G for the individual graphene electrodes show reduced electron conductivity and a positive voltage shift in the charge neutral point. The reduced electron conductivity is caused by the MoS_2 layer while the voltage shift is due to charge inhomogeneity from the substrate and MoS_2 layer.

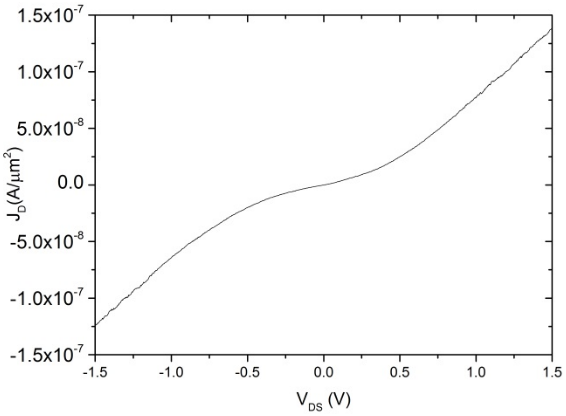

Figure 4 A sample tunneling current density for the MoS_2 heterostructures. The current densities for the transferred and grown MoS_2 interlayers are comparable.

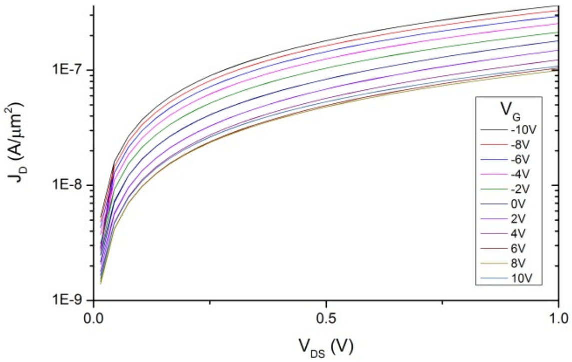

Figure 5 Tunneling current density as a function of the back gate. The 2D heterostructures can be modulated with the application of an electric field showing transistor behavior for the tunneling based devices.

We1710 Upgraded

Conductance Fluctuations in Graphene Nanoribbons

B. Liu, R. Akis, and D. K. Ferry
School of Electrical, Computer, and Energy Engineering, Arizona State University
Tempe, AZ 85287-5706

Over the past few years, fluctuations have been observed in the conductance through nanoribbons of graphene at low temperature. These fluctuations arise from the presence of a random potential in the semiconductor, which arises from e.g. impurities present in the material structure, and are observed when one varies the Fermi energy, applies a magnetic field, or moves from one sample to another. Contrary to most prior studies of such conductance fluctuations in normal semiconductors, these fluctuations are observed to violate the principal of ergodicity (independence of the results on the source of perturbation) and to violate the universal nature that has been predicted. Here, we study the conductance fluctuation in a graphene strip using a numerical approach based upon an atomistic tight-binding basis [1] for a nanoribbon with arm-chair edges and short-range scattering. The atomistic Hamiltonian can be integrated into the recursive scattering matrix method, and has good numerical stability. The calculation of conductance is studied for both a Fermi energy sweep and a magnetic field. In this way, the dependence of the variation of conductance on amplitude of disorder can be determined. We find that there is no general universality in the fluctuations, as their amplitude depends upon the amplitude of the random short-range potential. For a magnetic field variation, we find that the fluctuations are significantly weaker than for a Fermi energy variation, for comparable amplitude of the scattering potential. Surprisingly, however, the presence of a magnetic field does not affect the fluctuations for a Fermi energy variation, and no reduction in the amplitude is found as the magnetic field is increased. This is contrary to published measurements [2], which show a reduction for the presence of a magnetic field. The source of this reduction remains unknown at present.

---

1. B. Liu, R. Akis, and D. K. Ferry, J. Comp. Electr. 13, *in press*, DOI 10.1007/s10825-014-0613-9.
2. G. Bohra, R. Somphonsane, R. Aoki, Y. Ochiai, R. Akis, D. K. Ferry, and J. P. Bird, Phys. Rev. B **86**, 161405 (2012).

We1710 Upgraded

Liu-Akis-Ferry: Conductance Fluctuations in Graphene Nanoribbons

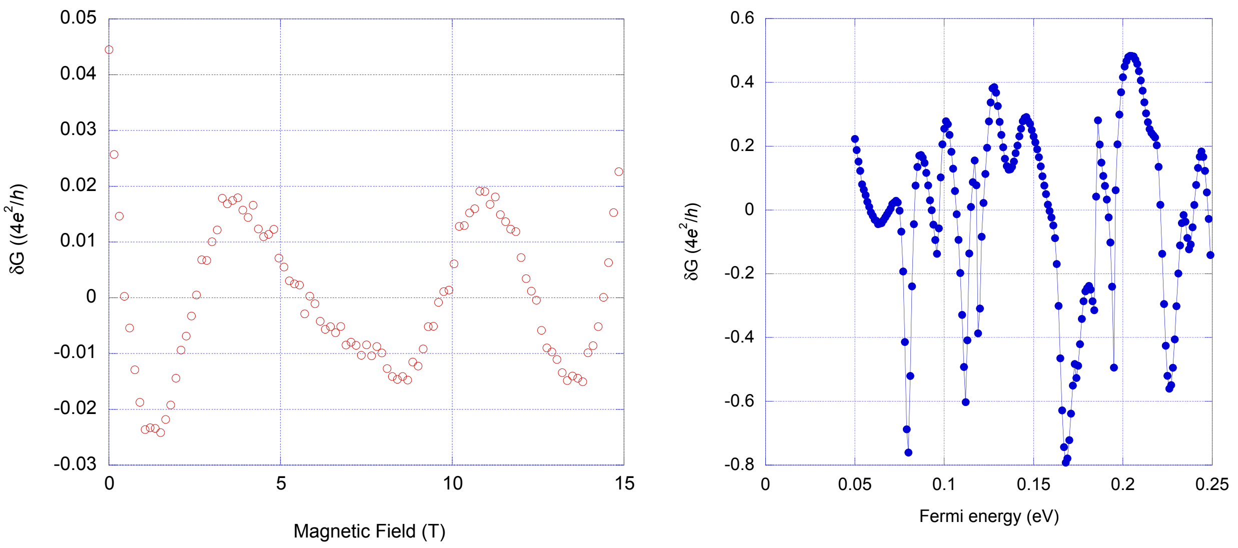

Left panel: conductance fluctuations as a function of the magnetic field. Right panel: Conductance fluctuation as a function of the Fermi energy. Both sets are for a random potential of 2.8 eV peak-to-peak. It is clear that the fluctuations in the right panel are much larger in amplitude.

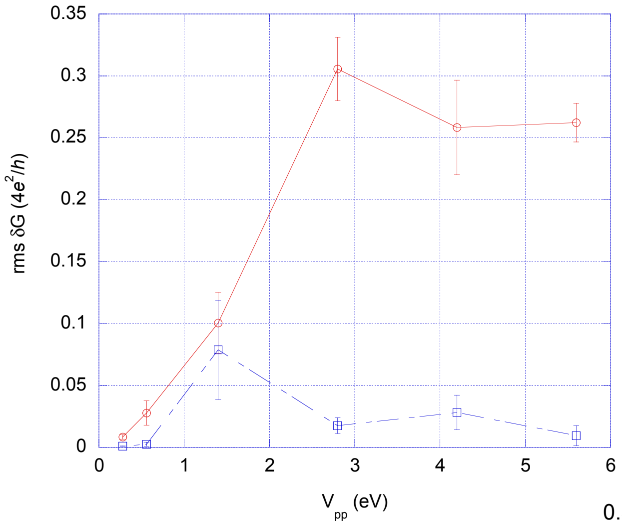

Dependence of the fluctuation rms amplitude on the peak-to-peak value of the random potential used in the problem (left). Adapting the results of Kechedzhi *et al.*, Phys. Rev. B **77**, 193403 (2008), to our data would give a value of ~0.36 on this plot. The red curve is for a sweep of the Fermi energy, while the blue curve is for a sweep of the magnetic field.

The magnetic field has almost no effect on the fluctuations seen for a sweep of the Fermi energy, as can be seen in the figure at the right.

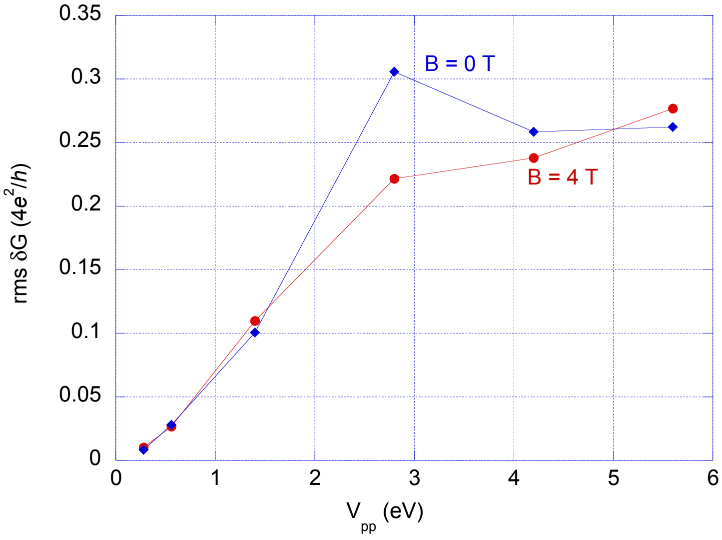

Direct growth of hexagonal boron nitride on epitaxial graphene by high-vacuum-CVD

Patrick C. Mende, Jun Li, Randall M. Feenstra
Carnegie Mellon University, Department of Physics – Pittsburgh, PA 15213

Despite the great excitement surrounding graphene in the years following its discovery, useful, scalable device-centered applications have yet to be realized, mostly owing to graphene's lack of a band gap. One of the most promising routes for novel graphene-based devices is its incorporation into heterostructures with other two-dimensional (2D) materials. Among the various 2D materials, hexagonal boron nitride (h-BN) is the most promising in terms of its compatibility with graphene owing to the low lattice mismatch between the two (< 2%), and its atomically flat structure. Indeed, graphene/h-BN based vertical heterostructures with unique tunneling characteristics have been demonstrated,[1] consistent with earlier theoretical predictions.[2] Presently, all such devices have been fabricated using transferred materials (whether exfoliated, or grown by CVD on metal foils), whereas it would be preferable to grow and pattern these devices directly. In this work, we demonstrate our recent attempts at achieving such a direct growth. By exposing our graphene samples (grown on Si-face SiC) to a low-pressure (~ 1×10^{-4} Torr) background of borazine at temperatures exceeding 1000°C, we obtain *in-situ* low-energy electron diffraction patterns consistent with the presence of many randomly oriented grains of h-BN. We find that increasing the growth temperature leads to the development of a preferential orientation, with the h-BN aligning with the underlying SiC substrate. Atomic-force microscopy and low-energy electron microscopy (LEEM) show triangular crystals exceeding 1 μm in extent. Additionally, using a first-principles method for examining low-energy electron reflectivity spectra,[3] we are capable of determining the coverage of h-BN on our samples. We show that our method is sufficiently robust to discriminate between various combinations of numbers of h-BN monolayers (MLs) and graphene MLs based on unique features in their spectra. Prospects for improvement of the h-BN crystallinity, as well as the controlled growth of a specific number of MLs are discussed.

Acknowledgements: This work was supported in part by the Center for Low Energy Systems Technology (LEAST), one of the six SRC STARnet Centers, sponsored by MARCO and DARPA.

References

1) L. Britnell *et al.*, Nat. Comm. **4**, 1794 (2013).
2) R. M. Feenstra *et al.*, J. Appl. Phys. **111**, 043711 (2012).
3) R. M. Feenstra *et al.*, Phys. Rev. B **87**, 041406(R) (2013).

We1730

Direct growth of hexagonal boron nitride on epitaxial graphene by high-vacuum-CVD (extended abstract)

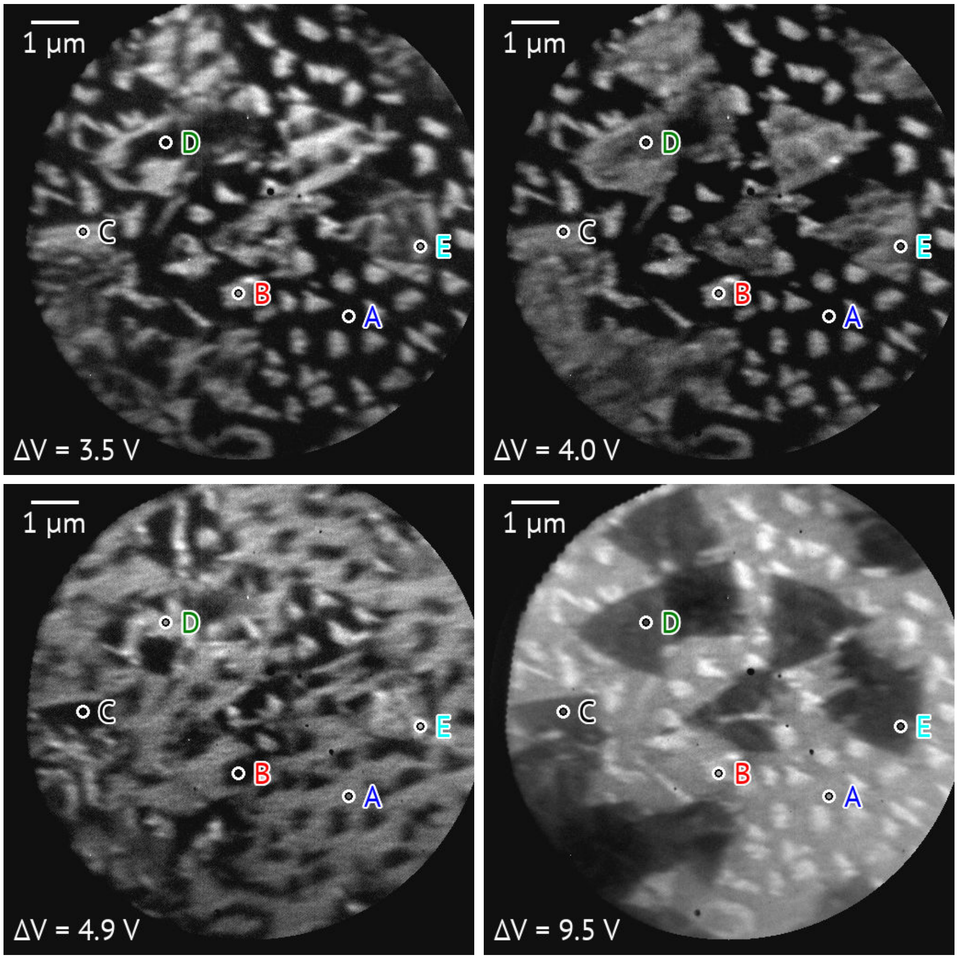

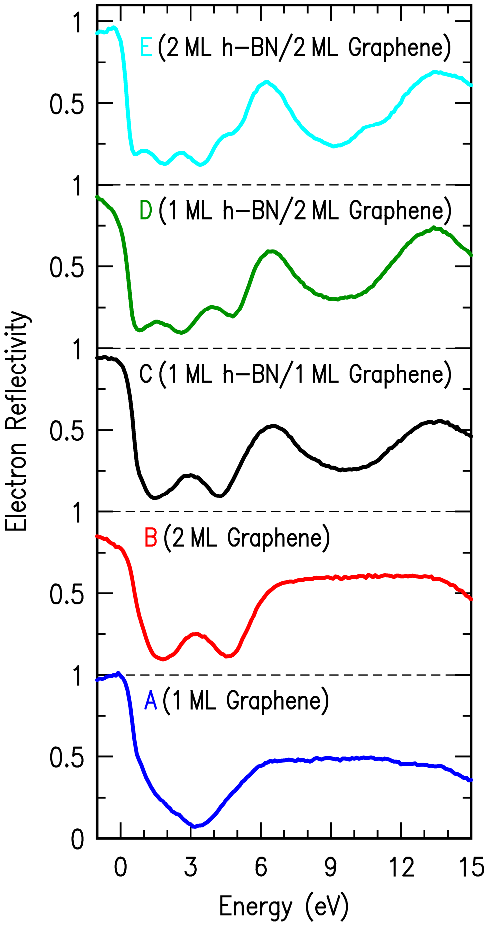

The above left and middle columns show a series of low-energy electron microscopy (LEEM) images of the same location acquired at various biases between the electron gun and the sample surface. The plot to the right of the images shows the low-energy electron reflectivity from the points indicated in the LEEM images. The darker areas seen at a bias of 9.5 V (e.g. points C, D, and E) are covered by hexagonal boron nitride (h-BN). Examining the reflectivity spectra of the various points, we can see that the surface is dominated by bare graphene of either 1 or 2 monolayers (MLs) in thickness. When determining the number of 2D MLs of either material on the surface, we focus on the energy range from 0 to 6 eV. By simply counting the number of reflectivity minima, we directly obtain this information: 1 minimum implies 1 ML of h-BN or graphene; 2 minima implies 2 MLs of a combination of h-BN and graphene; etc. When we want to discriminate between the presence of h-BN or graphene, however, we examine the rest of the spectrum. Comparing the spectra of points B and C, we see 2 minima in the energy range from 0 to 6 eV. However, in the spectrum of point C, we see a broad minimum at 10 eV whereas there is a plateau in the case of point B. Additionally, comparing the spectra of points D and E, we see that the broad minimum at 10 eV in the case of point D is replaced by a sharper minimum in point E at 9 eV with a small plateau at 11 eV. This small plateau feature is indicative of the formation of more than 1 ML of h-BN.

We1735

Large Area Transfer and Optoelectronic Properties of Multilayer Epitaxial Germanane

W. Amamou[1], P. M. Odenthal[1], D. J. O'Hara[1], E. Bushong[2], Y. Luo[2], J. van Baren[1], I. V. Pinchuk[2], Y. Wu[1], M. Bockrath[1], H. Tom[1], J. E. Goldberger[3], R. K. Kawakami[1,2,*]

[1]*Department of Physics and Astronomy, University of California, Riverside,*
[2]*Department of Physics, The Ohio State University,*
[3]*Department of Chemistry, The Ohio State University*

[*]kawakami.15@osu.edu

Abstract:

Two-dimensional crystals are an important class of materials for novel physics, chemistry, and engineering. Germanane (GeH), the germanium-based analog of graphane (CH), is of particular interest due to its direct band gap and surface covalent functionalization. Furthermore, its large spin orbit coupling makes it possible to explore novel physical phenomena such as quantum spin hall effect at room temperature.

Currently, large area GeH films are synthesized on Ge(111) wafers using substrate reaction or molecular beam epitaxy combined with chemical processing.
This results in a high quality GeH film that is left on top of the germanium substrate. In order to perform the electrical characterization of GeH, it is required to transfer the film to an insulating substrate. This will enable fundamental studies of the electronic and optoelectronic properties of epitaxial GeH.

Transfer to insulating substrates can be achieved through mechanical exfoliation by tape or polymer stamp, however the resulting flakes are small and of low quality. Here, we demonstrate a highly efficient, nondestructive electrochemical route for the transfer of molecular beam epitaxy (MBE) GeH film from Ge(111) surfaces. The electrochemically transferred films are continuous over 95% of the surface and this process affords the advantages of high efficiency and large area transfer. This technique enables us to characterize the optoelectronic properties of epitaxial GeH after transfer such as I-V characteristics and photoconductivity wavelength dependence. These results are an important step towards the realization of electronic and optoelectronic devices in this emerging 2D material.

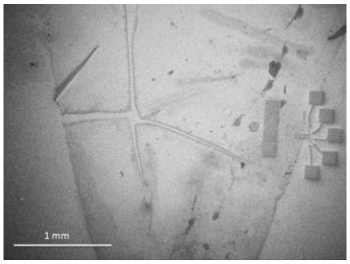

Figure: SEM image of transferred GeH film

We1740

COMPUTER SIMULATION LINEAR DEFECTS IN GRAPHENE AND NANOGRAPHENE

Yadgarov I.[1], Stelmakh V.[1], Dzhurakhalov A.A.[2]

[1]Institute of Ion-Plasma and Laser Technologies, 33, Do’rmon yo’li Street, 100125 Tashkent,
Uzbekistan, iyadgarov@mail.ru
[2]Dept. of Mathematics and Computer Sciences, University of Antwerp, Antwerp, Belgium,
dzhurakhalov@mail.ru

The ideal structure of graphene is a two-dimensional hexagonal lattice. The presence of defects in graphene leads to a disruption of this structure and to changes in physical and chemical properties of graphene. Using Metropolis Monte Carlo method, the formation of linear defects and stable configurations of graphene and nanographene (which has a small finite size with free boundary atoms) have been studied. The interatomic interactions have been described by the Brenner's reactive empirical bond order potential which was parametrized specifically for carbon and hydrocarbon systems [1].
Nanographene has been modeled by 112 carbon atoms arranged in a flat plane and in the appropriate configuration for graphene with a lattice constant of 2.46 Å. To simulate a graphene the periodic conditions were superimposed on the boundary atoms of nanographene along its plane. The presence of linear defects has been modeled as point vacancies, which is located along the same line in the lattice. We studied their effects on changes in the lattice structure and binding (cohesive) energy of atoms. In particular, it was found that linear defects results in decreasing the cohesive energy of studied systems. Figure 1 shows how the energy of cohesive varies on the number of point vacancies in a linear defect for graphene and nanographene.

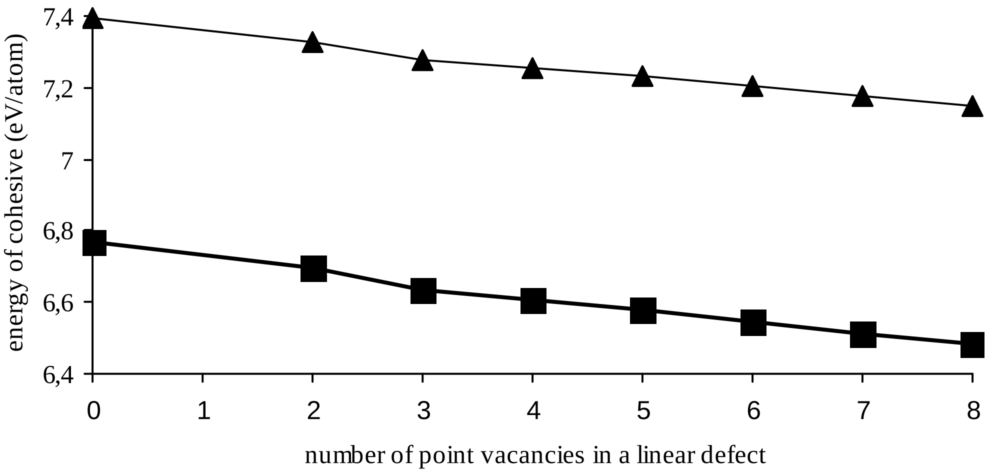

Fig.1 The dependence of the cohesive energy of the number of point vacancies in a linear defect for graphene (marked by triangles) and for nanographene (marked by squares)

[1] D.W. Brenner, O.A. Shenderova, J.A. Harrison, S.J. Stuart, B. Ni, S.B. Sinnot. “A second-generation reactive empirical bond order (REBO) potential energy expression for hydrocarbons”, J.Phys: Condens. Matter, **14**, pp.783-802 (2002)

We1745

Step flow like graphene growth controlled by crystallographic step alignment during thermal decomposition of 4H-SiC(000-1) C-face

Y. Kutsuma, D. Dojima, H. Shigemasa, K. Ashida, N. Ohtani, N. Tamai, and T. Kaneko
Gakuen 2-1, Sanda, Hyogo, 669-1337, Japan, E-mail: Kaneko@kwansei.ac.jp

The graphene layer grown on the C-face of 4H-SiC(000-1) substrates by a thermal decomposition process in the range of 1500-2000°C is known to exhibit excellent electrical conductivity without any transferring process [1]. This is attributed to the process associated unique electrical isolation characteristics of the C-face between graphene and SiC due to the absence of interplaying buffer layer, which should play a critical role to control the graphene quality by suppressing random nucleation and rotation of graphene islands during the decomposition process[2,3]. Therefore, in order to control the C-face graphene, it is required to find a new interplaying mechanism, in place of the role of the buffer layer, to suppress a disordered Volmer-Weber (VW)-like growth mode and guarantee an ordered step-flow-like decomposition mode.

To overcome this critical issue, firstly we designed a new graphene growth environment in the form of a confinement configuration using a refractory TaC/Ta enclosure for precisely controlling C/Si partial pressures during SiC thermal decomposition. While main function to suppress the fast thermal decomposition rate of C-face SiC surface was provided by introducing Ar ambient pressure up to 10kPa, the C/Si partial pressures also contributed to remove the excess carbon remaining at the graphene growth front.

As a result, the carbon adatom density on the growth front was intentionally controlled at 1400-1800°C. Secondary, various kinds of step-terrace structures of C-face 4H-SiC(000-1) were prepared as a template to be decomposed using Si-vapor thermal etching [4]. So far, the decomposition rate of the C-face was so fast that the growth kinetics associated with the difference in step-terrace structures was not clear. We have successfully found an ideal condition to initiate a step-flow-like growth mode, for the first time on the C-face, by fully suppressing the VW-like growth manner. The step flow-like mode can be only preserved when the basal plane of (000-1) terrace is spatially confined by facetted steps in the <1-100> direction, not by any facets in the <11-20> direction. Furthermore, it is revealed that as far as the step-flow mode maintaining, the rotational disorder of nucleated graphene islands does not seem to happen. It seems to be due to a site controlled graphene nucleation effect from {1-100} step edges. This growth mechanism considered here is a new step for controlling the uniform graphene on the C-face.

This research was financially supported by Adaptable & Seamless Technology Transfer Program through Target-driven R&D from Japan Science and Technology Agency.

[1] C. Berger et al., *Science* Vol. 312 no. 5777 (2006) 1191-1196
[2] J. L. Tedesco et al., *Applied Physics Letters* 96 (2010) 222103
[3] R. Zhang et al., *Journal of Applied Physics* 112 (2012) 104307
[4] S. Ushio et al., *Material Science Forum*, 717-720 (2012) 573

Application of LEEM, PEEM and STM/ncAFM techniques to Graphene on Metal Surfaces

A. Thissen, Y. Dedkov, A. Kaiser, S. Schmitt, T. Schulmeyer*, S. Bahr, O. Schaff

SPECS Surface Nano Analysis Inc., 20 Cabot Blvd STE 300, Mansfield, MA 02048
*Corresponding author: Thomas.Schulmeyer@specs.com

Abstract Summary: We present recently obtained results in graphene-based systems as measured with LEEM / PEEM and STM / NC-AFM techniques. We highlight the latest state-of-the-art developments in these two techniques and show how these techniques are applied in the latest graphene research as well in other experimental systems.

Introduction: Eighty years ago, Ernst Brueche developed the first photoemission electron microscope (PEEM) in the AEG laboratories in Berlin. Today, the state-of-the-art Low Energy Electron Microscope (LEEM) is produced just a few kilometers away from Brueche's former laboratory carrying forward these groundbreaking developments into the SPECS FE-LEEM P90. This instrument - based on the sophisticated electron-optical design by Ruud Tromp - combines user friendly operation with highest stability and ultimate resolution measurements. Graphene monolayer step edges on Si-sublimated SiC, measured using the aberration corrector, show a spatial resolution of 1.6 nm, closely approaching theoretical limits.

One of the advantages of SPECS systems is their interconnect ability, in this case, by combining the LEEM / PEEM with a SPECS SPM Aarhus 150 with KolibriSensor. The SPM is an ideal system for investigating lattice mismatched surfaces, with a focus in the present talk of SPM measurements on the graphene/Ir(111) system. Microscopy experiments were performed in constant current / constant frequency shift (CC/CFS) and constant height (CH) modes, exploiting a combination of the STM and NC-AFM capabilities of the system. We found that in STM imaging the electronic contribution is prevailing compared to the topographic one and the inversion of the contrast can be assigned to the particular features in the electronic structure of graphene on Ir(111). Contrast changes observed in constant height AFM measurements are analyzed on the basis of the energy, force, and frequency shift curves, obtained in DFT calculations, reflecting the interaction of the W-tip with the surface and are attributed to the difference in the height and the different interaction strength for high-symmetry cites within the moirè unit cell of graphene on Ir(111).The presented findings are of general importance for the understanding of the properties of the lattice-mismatched graphene/metal systems especially with regard to possible applications as templates for molecules or clusters.

Thursday

Th0745	Continental Breakfast
Th0845	Thursday Morning Session: *Spintronics*
Th0955	Coffee Break and Poster Viewing
Th1045	Thursday Morning Session: *Topological Insulators II*
Th1130	Poster Viewing
Th1200	Conference Ends

Spintronics

Optically-Induced Persistent Magnetization in Strontium Titanate

W. D. Rice[1], P. Ambwani[2], J. D. Thompson[1], G. Haugstad[2], C. Leighton[2] & S. A. Crooker[1]
[1]*Los Alamos National Laboratory, Los Alamos, NM 87545* *crooker@lanl.gov
[2]*Dept. of Chemical Engineering & Materials Science, U. Minnesota, Minneapolis, MN 55455*

Interest in electronics and spintronics based on complex oxide materials has exploded in recent years, fueled by the ability to grow atomically-precise heterostructures of various oxides [1]. One of the most important and foundational materials in this burgeoning field is strontium titanate, a (nominally) non-magnetic wide-bandgap semiconductor. Owing to its ubiquity in oxide materials science, studies of $SrTiO_3$'s interesting dielectric, lattice, and optical properties represent mature research areas. However, considerable renewed interest in $SrTiO_3$ [1] was recently sparked by observations of unexpected and emergent *magnetization* and *spin phenomena* at interfaces between $SrTiO_3$ and other nonmagnetic oxides such as $LaAlO_3$, first revealed through hysteretic magnetoresistance studies and subsequently via magnetization, various transport methods, torque and scanning-SQUID magnetometry, and X-ray measurements. The formation and distribution of oxygen vacancies (V_O) in $SrTiO_3$ are widely thought to play an essential but as-yet-incompletely understood role in these magnetic and spin phenomena.

Here [2] we demonstrate a surprising new aspect to the phenomenology of magnetism in $SrTiO_3$ by reporting the observation of an *optically-induced* and *persistent* magnetization in slightly oxygen-deficient $SrTiO_{3-\delta}$ bulk crystals, using magnetic circular dichroism (MCD) spectroscopy and optically-coupled SQUID studies. This magnetization appears below 18K, persists for *hours* below 10K, and is tunable via the polarization and wavelength of sub-bandgap (400-500 nm) light. As such, magnetic patterns can be 'written' into $SrTiO_{3-\delta}$, and subsequently read out, using light alone (see Fig. 1.) This magnetism occurs only in crystals containing oxygen vacancies, and is consistent with a metastable spin polarization of V_O-related defect complexes. These data reveal a detailed interplay between magnetism, lattice defects, and light in an archetypal complex oxide material, pointing to applications for complex oxide materials in spintronics and which may yield new insights into the recent exciting spin physics observed at oxide interfaces.

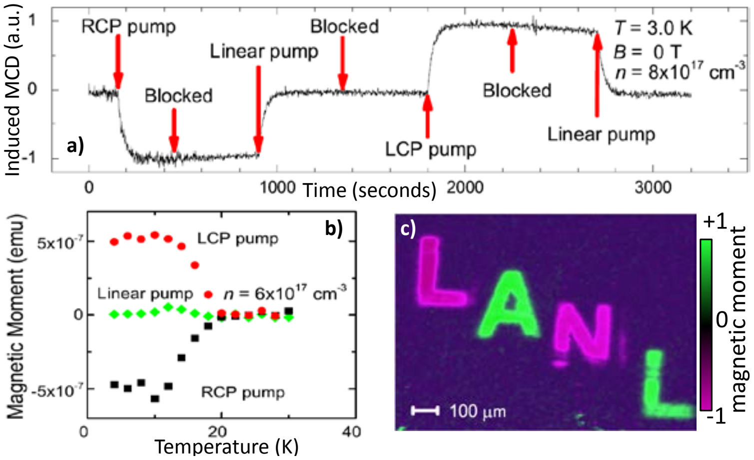

Fig. 1: a) Persistent magnetization in $SrTiO_{3-\delta}$, induced by circularly polarized light (detected by MCD). b) Persistent effects appear <18K (measured here by SQUID). c) Writing, storing, and reading magnetic patterns using light alone in $SrTiO_{3-\delta}$. Here, the circular polarization and therefore the magnetization direction were reversed at each letter.

[1] see, *e.g.*: H.Y. Hwang *et al.*, Nature Materials **11**, 103 (2012); J. Mannhart & D. G. Schlom, Science **327**, 1607 (2010); MRS Bulletin "Functional oxide interfaces" **38**, 1017-1063 (2013).

[2] W.D. Rice, P. Ambwani, M. Bombeck, J.D. Thompson, G. Haugstad, C. Leighton, SAC, *Nat. Mater.* **13**, 481 (2014); *ibid, J.Vac. Sci. Tech.B* **32**, 04E102 (2014).

Th0925 Upgraded

Barrier dependence of spin-dependent transport across FM/I/$SrTiO_3$ heterostructures

Adrian G. Swartz,[1,*] Hisashi Inoue,[1] Satoshi Harashima,[2,3] Takashi Tachikawa,[2,4] Yanwu Xie,[1,2] Di Lu,[5] Bongju Kim,[1,2] Christopher Bell,[2,6] Yasuyuki Hikita,[2] and Harold Y. Hwang[1,2]
[1] *Geballe Laboratory for Advanced Materials, Department of Applied Physics,*
Stanford University, Stanford, California 94305, USA
[2] *Stanford Institute for Materials and Energy Sciences,*
SLAC National Accelerator Laboratory, Menlo Park, California 94025, USA
[3] *Department of Applied Physics, The University of Tokyo, Bunkyo-ku, Tokyo 113-8656, Japan*
[4] *Department of Advanced Materials Science, The University of Tokyo, Kashiwa, Chiba 277-8561, Japan*
[5] *Department of Physics, Stanford University, Stanford, California 94305, USA*
[6] *School of Physics, University of Bristol, Tyndall Avenue, Bristol, BS8 1TL, United Kingdom*

(Dated: October 9, 2014)

Abstract

Electron-doped $SrTiO_3$ is an emerging material for the transportation of spin information [1–3]. Recent theoretical calculations have predicted long spin coherence times [4] and high mobilities have been observed in the quasi-2D conducting interface formed at the $LaAlO_3/SrTiO_3$ (LAO/STO) interface, as well as in 3D and 2D Nb-doped $SrTiO_3$ thin films [5]. Such high mobilities and the potential for long spin coherence times could lead to the realization of long spin transport lengths. A perovskite oxide spin channel is particularly attractive because of the ease of epitaxial integration with other functional complex oxides which are tunable by strain, electric, or magnetic fields. Before all-oxide spin field-effect transistors can be realized, spin injection and the creation of non-equilibrium spin populations in candidate materials must be explored. Towards this goal, we have performed experiments on spin-dependent transport from traditional *d*-orbital ferromagnets through tunnel barriers with polar and non-polar surfaces into electron-doped $SrTiO_3$.

Single crystal $LaAlO_3$ is deposited on TiO_2-terminated $SrTiO_3(001)$ substrate by pulsed laser deposition (PLD) at a substrate temperature of 650 °C and the thickness is monitored *in situ* by reflection high-energy electron diffraction (RHEED) oscillations (see Fig. 1a). This heterostructure of two band insulators forms a low dimensional conducting interface with mobilities exceeding 1000 cm^2/Vs at low temperature. We have investigated spin-dependent transport across Co/LAO/STO heterostructures using an all electrical three terminal (3T) geometry and observed Lorenzian magnetoresistance typically associated with Hanle spin dephasing (see Figs. 1b and 1e) [1]. However, such a picture fails to explain all the experimentally observed behavior as is commonly observed in many 3T experiments. Therefore, we have interpreted the data in terms of defect mediated spin-dependent transport (see Figs. 1c and 1d) as recently proposed by Song and Dery [6]. This picture is supported by control experiments with Au spin-unpolarized metallic contacts (Fig. 1f).

Despite development in our understanding of spin-polarized transport from FM into $SrTiO_3$, there are still fundamental limitations in scaling down the size of these FM/I/$SrTiO_3$ junctions in order to realize nano or micron-scale spin-valve devices. By examining both Co/LAO/STO (quasi-2DEG) and junctions with semiconducting $SrTi_{0.999}Nb_{0.001}O_3/SrTiO_3(001)$, we have identified the critical limiting problem as the large contact resistance ($R_C > 10^9\,\Omega\,\mu m^2$). In order to solve this problem, we have taken advantage of the polar nature of the $LaAlO_3$ (001) surface. By inserting $LaAlO_3$ between Nb-doped $SrTiO_3$ thin films and Cobalt electrodes, we have successfully tuned the contact resistance-area product (R_CA) product over 3 orders of magnitude (see fig. 2). We will discuss the underlying mechanism involved and the effect of such drastic changes in the electron transport on the three-terminal magnetoresistance.

This work is supported in part by FAME, one of six centers of STARnet, a Semiconductor Research Corporation program sponsored by MARCO and DARPA. We also acknowledge partial support by the Department of Energy, Office of Basic Energy Sciences, Division of Materials Sciences and Engineering, under contract DE-AC02-76SF00515.

---

[*] aswartz@stanford.edu

[1] A. G. Swartz, S. Harashima, Y. Xie, D. Lu, B. Kim, C. Bell, Y. Hikita, and H. Y. Hwang, Applied Physics Letters **105**, 032406 (2014).

[2] N. Reyren, M. Bibes, E. Lesne, J.-M. George, C. Deranlot, S. Collin, A. Barthélémy, and H. Jaffrès, Physical Review Letters **108**, 186802 (2012).

[3] W. Han, X. Jiang, A. Kajdos, S.-H. Yang, S. Stemmer, and S. S. Parkin, Nature Communications **4** (2013).

[4] C. Şahin, G. Vignale, and M. E. Flatté, Physical Review B **89**, 155402 (2014).

[5] H. Y. Hwang, Y. Iwasa, M. Kawasaki, B. Keimer, N. Nagaosa, and Y. Tokura, Nature Materials **11**, 103 (2012).

[6] Y. Song and H. Dery, Phys. Rev. Lett. **113**, 047205 (2014).

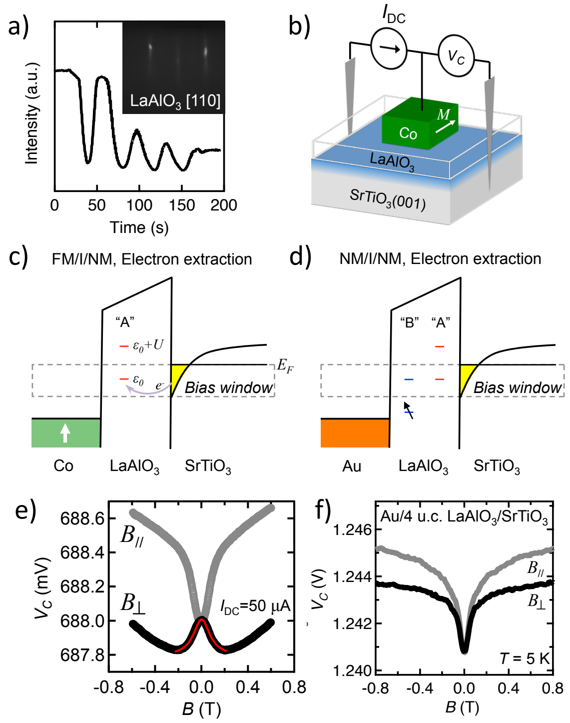

FIG. 1. a) RHEED intensity oscillations and image for 4 u.c. LaAlO$_3$ deposited by pulsed laser deposition onto SrTiO$_3$(001) substrate. b) Schematic of a Co/LAO/STO junction in a three-terminal geometry. c) and d) Band diagram for Co/LAO/STO (FM/I/NM) and Au/LAO/STO (NM/I/NM) under positive V_C (electron extraction) with type "A" and "B" defect states located in the barrier region. Such defects can generate a spin-blockade effect which modulates the resistance under an applied magnetic field. e) Field dependence of the contact voltage, V_C, for Co/LAO/STO under out-of-plane ($B_\perp$) applied field (black) and in-plane ($B_{//}$) applied field (grey) at T=10 K. Red line is a Lorentzian fit. f) Corresponding magnetic field modulation of V_C for Au/LAO/STO.

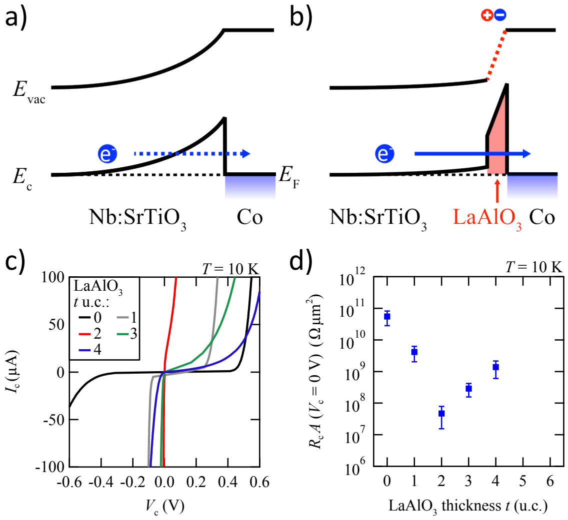

FIG. 2. a) Band diagram for metallic contacts to SrTi$_{0.999}$Nb$_{0.001}$O$_3$ and the formation of a Schottky junction. b) Lowering of the Schottky barrier height by insertion of LaAlO$_3$ which introduces an interfacial dipole. c) Effect on the junction I-V_C characteristics by insertion of various thicknesses of LAO. d) $R_C A$ vs. LaAlO$_3$ thickness and the effect of dipole tuning.

Th0945

Optically enhanced NMR studies of semiconductors

Zayd Ma, Matt Willmering, and Sophia Hayes
Washington University in St. Louis

Nuclear Magnetic Resonance (NMR) remains unparalleled in its ability to give non-invasive atomic scale information about chemical bonding, lattice structure, spin-spin interactions, and molecular motions. However, even with the wealth of potential information it is rarely applied to the study of films and interfaces due to typically weak signal, long acquisition times, and the need for very high magnetic fields. These difficulties can be alleviated to some extent with the ability to **enhance** the nuclear magnetization to several orders of magnitude higher than thermal equilibrium, and this enhancement can be realized in semiconductors with optical pumping. Optical pumping is a well-known technique in which polarized laser light, resonant at or above the band gap, excites spin-polarized electrons into the conduction band which, in turn, can spin-exchange with surrounding nuclei. Thus, the nuclear magnetization will build up to a point where detection can be achieved with traditional NMR techniques (OPNMR[1]). In addition to enhancing nuclear magnetization for detection, the ability to optically control (the sign of) electronic spin states that are coupled to surrounding nuclear spins which are easily manipulated with radio frequency irradiation has potential application in the preparation and control of desired spin states.

We present a series of OPNMR studies on poly, and single crystal CdTe, and GaAs quantum wells from 1.45 to 1.7eV (850-729nm). OPNMR energy profiles reveal an unexpected formation of a new cadmium resonance at super gap excitation energies where the light penetration into the sample is most likely only a few microns. In addition, CdTe sample to sample variability is shown, opening the possibility of using OPNMR as a probe into impurity characterization. Lastly, GaAs quantum well results demonstrate OPNMR's ability to separate signal from bulk GaAs substrate and GaAs quantum wells[2].

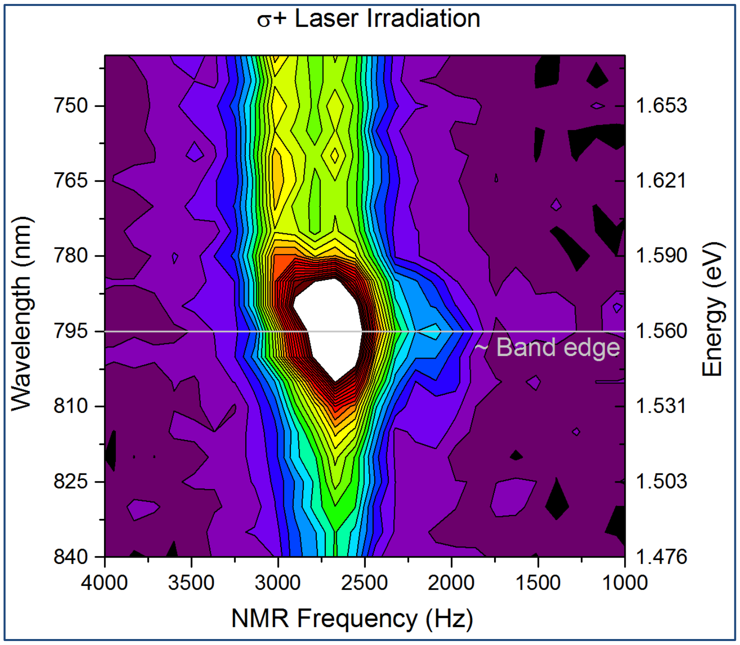

Figure 1 ^{113}**Cd OPNMR profile on CdTe. Laser excitation energy on vertical access and NMR frequency along horizontal**

1. Hayes, S. E. *et al.*, *J. Chem. Phys.*, **128**, 052203 (2008)
2. Sesti, E. L.; Wheeler, D. D.; Saha, D.; Sanders, G.; Hayes, S. E.; Stanton, C. J., *Phys. Rev. B*, **90**,125301 (2014)

Th0950

Dynamic-nuclear-polarization-induced anisotropic spin relaxation in *n*-GaAs

Nicholas J. Harmon[1], Timothy Peterson[2], Chad Geppert[2], Michael E. Flatté[1], and Paul Crowell[2]
[1]*Department of Physics and Astronomy and Optical Science and Technology Center, University of Iowa, Iowa City, Iowa 52242, USA*
[2]*School of Physics and Astronomy, University of Minnesota, Minneapolis, MN 55455, USA*

Observation of a new anisotropic spin-relaxation mechanism in bulk n-GaAs due to the presence of dynamically polarized nuclei is reported. Since the resulting hyperfine field is strongly inhomogeneous, electron spins traversing the sample experience fluctuations in precession rate which is a hallmark for spin relaxation as shown in the Figure below. To explain the phenomenon, a theory of spin relaxation based on the theory of random walks is presented. From this theory, the precise form of the spin relaxation can be analytically derived where it is demonstrated that this mechanism introduces a source of (unequal) longitudinal and transverse spin relaxation.

To investigate this effect, electrical three-terminal Hanle measurements were performed on epitaxially grown Co_2MnSi/n-GaAs and Fe/n-GaAs heterostructures fabricated into electrical spin injection devices. By modeling the resulting Hanle lineshapes including the effects of dynamic nuclear polarization, experiments are found to be in quantitative agreement with theoretical predictions.

Supported by C-SPIN, one of the six centers of STARnet, a SRC program sponsored by MARCO and DARPA.

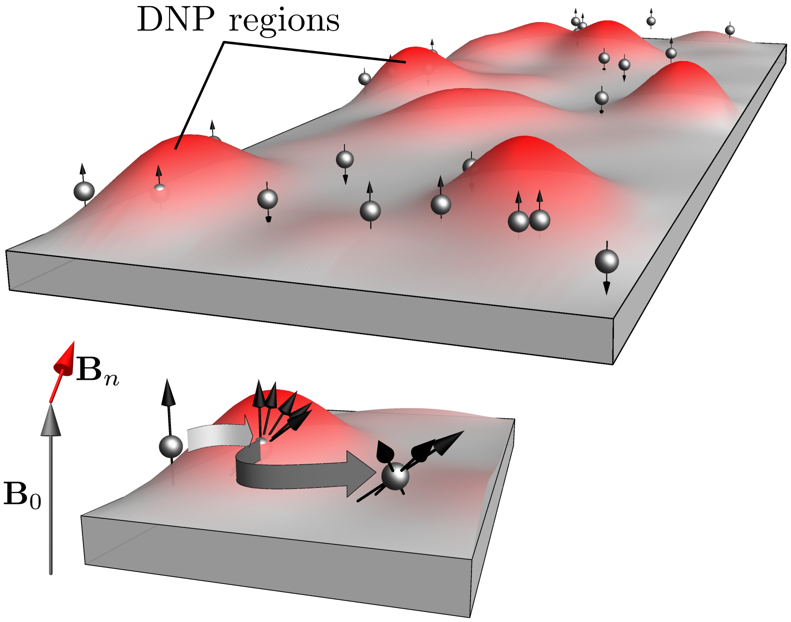

Figure. The mechanism of spin relaxation from dynamically polarized nuclei in *n*-GaAs. Red ‘bumps’ denote regions with donors that have polarized nuclei (shade of red depicts magnitude of the nuclear field). Smaller spheres are electrons. Bottom figure shows how an electron spin is relaxed by passing through a “DNP region”.

Topological Insulators II

Th1045 Invited

Direct electrical detection of spin-momentum locking in the topological insulator Bi_2Se_3

C. H. Li, O. M. J. van 't Erve, J. T. Robinson, Y. Liu, L. Li, and B. T. Jonker
Naval Research Laboratory, Washington DC 20375, USA

Topological insulators (TIs) are a new quantum state of matter [1] characterized by metallic surface states populated by massless Dirac fermions. TIs are expected to exhibit new behaviors and open horizons for science previously inaccessible with "conventional" materials. One of the most striking properties is that *of spin-momentum locking* -- the spin of the TI surface state lies in-plane, and is locked at right angle to the carrier momentum. An unpolarized charge current should thus create a net spin polarization whose amplitude and orientation are controlled by the charge current. This remarkable property has been anticipated by theory [2], but never accessed in a simple transport structure. Here we show that a bias current indeed produces a net surface state spin polarization *via* spin-momentum locking in molecular beam epitaxially grown Bi_2Se_3 films, and this polarization is directly manifested as a voltage on a ferromagnetic metal contact [3]. This voltage is proportional to the projection of the TI spin polarization onto the contact magnetization, is determined by the direction and magnitude of the bias current, scales inversely with Bi_2Se_3 film thickness, and its sign is that expected from spin-momentum locking rather than a Rashba effect [4]. Similar data are obtained for structures with two different ferromagnet/tunnel barrier contacts, demonstrating that these behaviors are independent of the details of the detector contact. These results demonstrate direct electrical access to the TI surface state spin system and enable utilization of its remarkable properties for future technological applications.

[1] J. E. Moore, Nature **464**, 194 (2010); M. Z. Hasan et. al., Rev. Mod. Phys. **82,** 3045 (2010); L. Fu et. al., PRL **98**, 106803 (2007); D. Hsieh et. al., Nature **452**, 970 (2008).

[2] A. A. Burkov et. al. PRL **105**, 066802 (2010); D. Culcer et. al., PRB **82**, 155457 (2010); V. Yazyev et. al., PRL **105**, 266806 (2010).

[3] C. H. Li, et. al., Nat. Nanotech. **9**, 218 (2014).

[4] S. Hong et. al., PRB **86**, 085131 (2012).

Th1125 Upgraded

Dirac mass generation and unconventional orbital texture in topological crystalline insulators

The newly discovered topological crystalline insulators (TCIs) harbor a complex band structure involving multiple Dirac cones with distinct orbital character [1]. One of the unique characteristics of these systems is that crystalline symmetry breaking is theoretically predicted to impart mass to otherwise massless surface state (SS) Dirac fermions. In this talk, I will discuss our progress in exploring these exotic phenomena in a prototypical TCI $Pb_{1-x}Sn_xSe$. In our experiments, we utilize two different spectroscopy methods: Fourier transform (FT) scanning tunneling spectroscopy (STS) and Landau level (LL) spectroscopy. First, by using FT-STS, we measure the interference patterns produced by the scattering of SS electrons. We discover that the intensity and energy dependences of FT conductance images show distinct characteristics, which can be directly attributed to the proposed unconventional orbital texture [2]. Second, by using LL spectroscopy, we observe a spontaneous Dirac gap opening in two out of the four Dirac cones within the first Brillouin zone [3]. Furthermore, STM topographs directly reveal a symmetry-breaking distortion on the surface which imparts mass to the otherwise massless Dirac electrons — a mechanism analogous to the long sought-after Higgs mechanism in particle physics [4]. Remarkably, our measurements show that the Dirac gap scales with alloy composition, while the magnitude of the distortion remains nearly constant. Based on theoretical calculations, we find that the Dirac mass in TCIs is controlled by the composition-dependent SS penetration depth, which determines the weight of the SS in the distorted region that is confined to the surface [4]. Finally, I will discuss recent experimental progress towards strain engineering of the SS band structure in TCI thin films.

[1] T. H. Hsieh *et al.*, Topological crystalline insulators in the SnTe material class, *Nat. Commun.* **3**, 982 (2012).

[2] I. Zeljkovic *et al.*, Mapping the unconventional orbital texture in topological crystalline insulators, *Nat. Phys.* **10**, 572–577 (2014).

[3] Y. Okada *et al.*, Observation of Dirac node formation and mass acquisition in a topological crystalline insulator, *Science* **341**, 1496–9 (2013).

[4] I. Zeljkovic *et al.*, Dirac mass generation from crystal symmetry breaking on the surfaces of topological crystalline insulators, *ArXiv*:1403.4906 (2014).

Author Index